The role of the endocannabinoid system in stress-related disorders and neuroimmune communication

Dissertation

zur

Erlangung des Doktorgrades (Dr. rer. nat.)

der

Mathematisch-Naturwissenschaftlichen Fakultät

der

Rheinischen Friedrich-Wilhelms-Universität Bonn

vorgelegt von

Eva Carolina Beins

aus

Bergisch Gladbach

Bonn, August 2019

Angefertigt mit der Genehmigung der Mathematisch-Naturwissenschaftlichen Fakultät der Rheinischen Friedrich-Wilhelms-Universität Bonn

1. Gutachter: Prof. Dr. Andreas Zimmer
2. Gutachter: Prof. Dr. Joachim Schultze

Tag der Promotion: 17.02.2020
Erscheinungsjahr: 2020

Für Gustav Beins

Abbreviations

2-AG	2-arachidonoylglycerol
3D	Three-dimensional
AA	Arachidonic acid
AC	Adenylyl cyclase
ACh	Acetylcholine
ACTH	Adrenocorticotropin hormone
AEA	Arachidonoylethanolamine (AEA)
ANOVA	Analysis of variance
APD	Avalanche photo-diode
ATP	Adenosine triphosphate
AU	Arbitrary unit
AV	Atrioventricular
BCP	1-bromo-3-chloropropane
BDNF	Brain-derived neurotrophic factor
BLA	Basolateral amygdala
BM	Bone marrow
BNST	Bed nucleus of the stria terminalis
bp	Base pair
BSA	Bovine serum albumin
CA1	Cornu Ammonis area 1
CAM	Cell adhesion molecule
cAMP	Cyclic adenosine monophosphate
CB1	Cannabinoid receptor 1 (protein)
CB2	Cannabinoid receptor 2 (protein)
CBD	Cannabidiol
CCL2 (MCP-1)	Chemokine C-C motif ligand 2 (monocyte chemoattractant protein 1)
CCR2	C-C chemokine receptor type 2
CD	Cluster of differentiation
cDNA	Complementary DNA
cm	Centimeter
Cnr1	Cannabinoid receptor 1 (gene)
CNS	Central nervous system
CORT	Corticosterone
COX	Cyclooxygenase
C_q	Quantification cycle
CR3	Complement receptor 3
CRH	Corticotropin-releasing hormone
CRHR1	Corticotropin-releasing hormone receptor 1
CSDS	Chronic social defeat stress
CX3CR1	CX3C chemokine receptor 1 (fractalkine receptor)
CXCL12	Stromal cell-derived factor 1; C-X-C motif chemokine 12
CYP	Cytochrome P450
DAG	Diacylglycerol
DAGL	Diacylglycerol lipase
DAPI	4',6-diamidino-2-phenylindole

DC	Dendritic cell
DG	Dentate gyrus
dH_2O	Deionised H_2O
DMEM	Dulbecco's Modified Eagle Medium
DMSO	Dimethyl sulfoxide
DNA	Deoxyribonucleic acid
dNTP	Deoxyribose nucleoside triphosphate
DPSS	Diode-pumped solid-state
DSE	Depolarisation-induced suppression of excitation
DSI	Depolarisation-induced suppression of inhibition
DSM-V	Diagnostic and Statistical Manual of Mental Disorders - Fifth Edition
DTT	Dithiothreitol
eCB	Endocannabinoid
ECG	Electrocardiogram
ECS	Endocannabinoid system
EDTA	Ethylenediaminetetraacetic acid
e.g.	For example (exempli gratia)
EIA	Enzyme Immunoassay
ELISA	Enzyme-linked immunosorbent assay
EtOH	Ethanol
FAAH	Fatty acid amid hydrolase
FACS	Fluorescence-activated cell sorting
FAM	6-carboxyfluorescein
FCS	Fetal calf serum
FITC	Fluorescein isothiocyanate
FRET	Fluorescence resonance energy transfer
FSC	Forward scatter
x g	Gravity
g	Gram
GABA	γ-aminobutyric acid
GC	Glucocorticoid
gMFI	Geometric mean fluorescence intensity
GPCR	G-protein coupled receptor
GR	Glucocorticoid receptor
h	Hour
H_2O	Water
HBSS	Hank's buffered salt solution
HCl	Hydrochloric acid
HeNe	Helium-neon
HPA axis	Hypothalamic–pituitary–adrenal axis
Hprt	Hypoxanthine-guanine phosphoribosyltransferase
HRP	Horseradish peroxidase
HSC	Hematopoietic stem cell
HyD	Hybrid photodetectors
i.p.	Intraperitoneal
IBA1	Ionized calcium-binding adapter molecule 1
ICAM-1	Intercellular adhesion molecule 1

IFNα	Interferon alpha
IHC	Immunohistochemistry
IL	Interleukin
kb	Kilobase
kg	Kilogram
LOX	Lipooxygenase
LPS	Lipopolysaccharide
LTD	Long-term depression
Ly6	Lymphocyte antigen 6
M	Molar
m	Meter
M-CSF	Macrophage colony-stimulating factor
mA	Milliampere
MAGL	Monoacyl glycerol lipase
MAPK	Mitogen-activated protein kinase
MDD	Major depressive disorder
MeOH	Methanol
MGB	Minor groove binder
MHC	Major histocompatibility complex
min	Minutes
mM	Millimolar
mPFC	Medial prefrontal cortex
mRNA	Messenger RNA
ms	Milliseconds
mtCB1	Mitochondrial cannabinoid receptor 1
n	Number (sample size)
n.s.	Not significant
NA	Numerical aperture
NAc	Nucleus accumbens
NaCl	Sodium chloride
NAPE	N-acyl-phosphatidylethanolamine
NAPE-PLD	NAPE-phospholipase D
NDS	Normal donkey serum
NeuN	Neuronal nuclear antigen
NFκB	Nuclear factor kappa-light-chain-enhancer of activated B cells
ng	Nanogram
NK	Natural killer (cell)
nm	Nanomolar
NO	Nitric oxide
Nr3c1	Glucocorticoid receptor (gene)
OD	Optical density
PBS	Phosphate-buffered saline
PCR	Polymerase chain reaction
PE	Phosphatidylethanolamine
PFA	Paraformaldehyde
PFC	Prefrontal cortex
PI3K	Phosphatidylinositide 3-kinase

PKA	Protein kinase A
PKC	Protein kinase C
PLC	Phospholipase C
PMT	Photomultiplier tube
PPAR	Peroxisome proliferator-activated receptor
PNS	Parasympathetic nervous system
PTSD	Posttraumatic stress disorder
PVN	Paraventricular nucleus
qPCR	Real time quantitative PCR
RBC	Red blood cell
RNA	Ribonucleic acid
ROI	Region of interest
ROS	Reactive oxygen species
RT	Room temperature
s	Second
SAM axis	Sympathetic-adrenal-medullary axis
SD	Standard deviation
SDS	Sodium dodecyl sulfate
SEM	Standard error of the mean
SI ratio	Social interaction ratio
SIP	Stock isotonic Percoll
SNS	Sympathetic nervous system
SPF	Specific pathogen-free
SSC	Side scatter
SSRI	Selective serotonin re-uptake inhibitors
TAE	Tris-acetate-EDTA
TBS	Tris-buffered saline
TE	Tris EDTA
TH	Tyrosine hydroxylase
THC	Δ^9-tetrahydrocannabinol
TMEM119	Transmembrane protein 119
TNFα	Tumor necrosis factor alpha
Tris	Tris (hydroxymethyl) aminomethane
TRPV1	Transient receptor potential vanilloid type-1
U	Unit
UV	Ultraviolet
VTA	Ventral tegmental area
WHO	World Health Organization
WT	Wild type
µl	Microliter
µM	Micromolar

Summary

In the last decades, increasing evidence suggests that inflammatory processes play an important role in the development of psychiatric disorders, such as anxiety and depression. Psychosocial stress – one of the main environmental factors contributing to these disorders – affects immune system activity through neuronal and endocrine signals. The endocannabinoid system (ECS) is a neuromodulatory system that regulates stress responses via the cannabinoid receptor 1 (CB1). Blockade of CB1 signalling, either pharmacologically or genetically, increases the sensitivity to stress and the risk to develop stress-related psychiatric pathologies. Whether this is based on a purely neuronal mechanism or whether it is accompanied or mediated by altered immune system regulation is, however, not known. The aim of this study was therefore to analyse how CB1 signalling modulates behavioural, neuroendocrine, and immunological responses in a mouse model of chronic social defeat stress (CSDS).

CB1-deficient (*Cnr1*$^{-/-}$) mice were extremely sensitive to a standard protocol of CSDS, indicated by an increased mortality rate. Therefore, a mild CSDS protocol was established, which still induced a behavioural phenotype in highly susceptible *Cnr1*$^{-/-}$ mice. Molecular analysis showed that lack of CB1 receptors alters glucocorticoid levels after mild CSDS, supporting the hypothesis that CB1 signalling regulates hypothalamic–pituitary–adrenal (HPA) axis activity and its adaptation during repeated stress exposure.

In both humans and rodents, chronic stress is associated with elevated inflammatory signalling. This is indicated by increased numbers of circulating myeloid cells, which possibly infiltrate the brain, and the activation of microglia – the brain-resident immune cells. Mild CSDS induced weak myelopoiesis in the periphery, but did not induce recruitment of myeloid cells to the brain. In contrast, mild CSDS did affect microglial function in *Cnr1*$^{-/-}$ mice, indicated by increased surface expression of activation markers and altered morphology. Furthermore, microglial parameters were correlated with the severity of the behavioural phenotype in *Cnr1*$^{-/-}$ mice, thus implicating endocannabinoid-mediated modulation of microglia in the development of stress-related pathologies.

In summary, the present study indicates that ECS/CB1 signalling is indeed essential to protect the organism from the physical and emotional harms of chronic stress. These protective mechanisms involve modulation of the HPA axis and microglial function.

Contents

1 Introduction

1.1 Stress and stress-related disorders

1.1.1 Concepts of stress

The concept of stress known today is largely based on observations of Claude Bernard, Walter B. Cannon, and Hans Selye in the late 19th and early 20th century (Goldstein and Kopin, 2007). Today, stress is defined as any threat to an organism's homeostasis, a term introduced by Cannon to describe the maintenance of various physiological functions within an acceptable range. The threat, or stressor, can be external (e.g. exposure to cold, social conflicts) or internal (e.g. hypoglycaemia, infection) and can be consciously or unconsciously perceived. The body is equipped with mechanisms that can sense disturbances and activate effector systems that respond to the stressor and eventually restore homeostasis (Chrousos, 2009). These effector systems include the sympathetic nervous system (SNS), with noradrenaline as the main neurotransmitter, and the hypothalamic-pituitary-adrenal (HPA) axis, with glucocorticoids (GCs) as end product and main effector (see Figure 1). Based on Selye's theories, it was long postulated that stress responses are nonspecific, meaning that stressors of different nature elicit the same set of responses. Today it is known that the responses can vary, at least to some degree, depending on the type, duration, intensity, and individual perception of the stressor (Childs et al., 2014; Natelson et al., 1988; Sgoifo and Papi, 1995). It was also Selye, who postulated that severe or prolonged stress can cause physical and mental disorders – a concept widely accepted and scientifically proven today.

1.1.2 Hypothalamic-pituitary-adrenal axis

The main neuroendocrine stress response system is constituted by the HPA axis (Godoy et al., 2018). Its activation is initiated by corticotrophin-releasing hormone (CRH)-expressing neurons in the paraventricular nucleus (PVN) of the hypothalamus. Release of CRH stimulates the production of adreno-corticotropic hormone (ACTH) by the pituitary gland and its release into circulation. ACTH then stimulates cells in the adrenal cortex to synthesise GCs (mainly cortisol in humans, corticosterone (CORT) in rodents). Circulating GCs in turn act on glucocorticoid receptors (GRs) in the hypothalamus and pituitary to inhibit further CRH and ACTH synthesis in a negative feedback loop. GCs are responsible for many of the physiological and psychological effects of stress by activating GRs in various target organs. Among others, GCs regulate immune system activity, metabolism, and cognitive functions (Kadmiel and Cidlowski, 2013). In the brain, GRs are not only expressed in the hypothalamus, but also in brain stem nuclei and limbic brain areas, such as the amygdala, hippocampus and prefrontal cortex (PFC). These brain regions also provide input to the PVN and can thereby modulate activity of the HPA axis (Godoy et al., 2018).

1.1.3 Sympathetic nervous system

Along with the parasympathetic nervous system (PNS), the SNS is part of the autonomic nervous system that regulates unconscious body functions (McCorry, 2007). Sympathetic nerves arise in the spinal cord and innervate a variety of target organs, in most cases via two neurons that are connected within ganglia (pre- and postganglionic neuron). With a few exceptions (e.g. neurons innervating sweat glands), postganglionic neurons use catecholamines adrenaline or noradrenaline as neurotransmitter, which activate adrenergic receptors in the target organ. Both SNS and PSNS are active at baseline to maintain homeostasis, however, the SNS is also rapidly activated under stressful conditions (Ziegler, 2004). Activation of the SNS during stress leads, among others, to increased heart rate and contractile force, increased glucose production by the liver, and increased blood flow to muscles – all functions to prime the body for action and enhance the probability of survival. Sympathetic nerves also directly innervate the adrenal glands in a monosynaptic connection, also referred to as the sympathetic-adrenal-medullary (SAM) axis (McCorry, 2007). Release of acetylcholine (ACh) from preganglionic sympathetic fibres innervating the adrenal medulla stimulates the secretion of adrenaline, noradrenaline, and dopamine from chromaffin cells and thereby can potentiate stress effects.

Furthermore, GCs and catecholamines are not only released in response to stress, but also under basal conditions, where their secretion follows a circadian rhythm (Dibner et al., 2010; Son et al., 2011). Levels increase at the onset of an organism's active phase (light phase in humans, dark phase in nocturnal animals, e.g. rodents). This provides a rhythmic signal to mobilise energy, increase alertness, and prime the immune system – all mechanisms to prepare the organism for potential challenges during the day (or night in nocturnal animals).

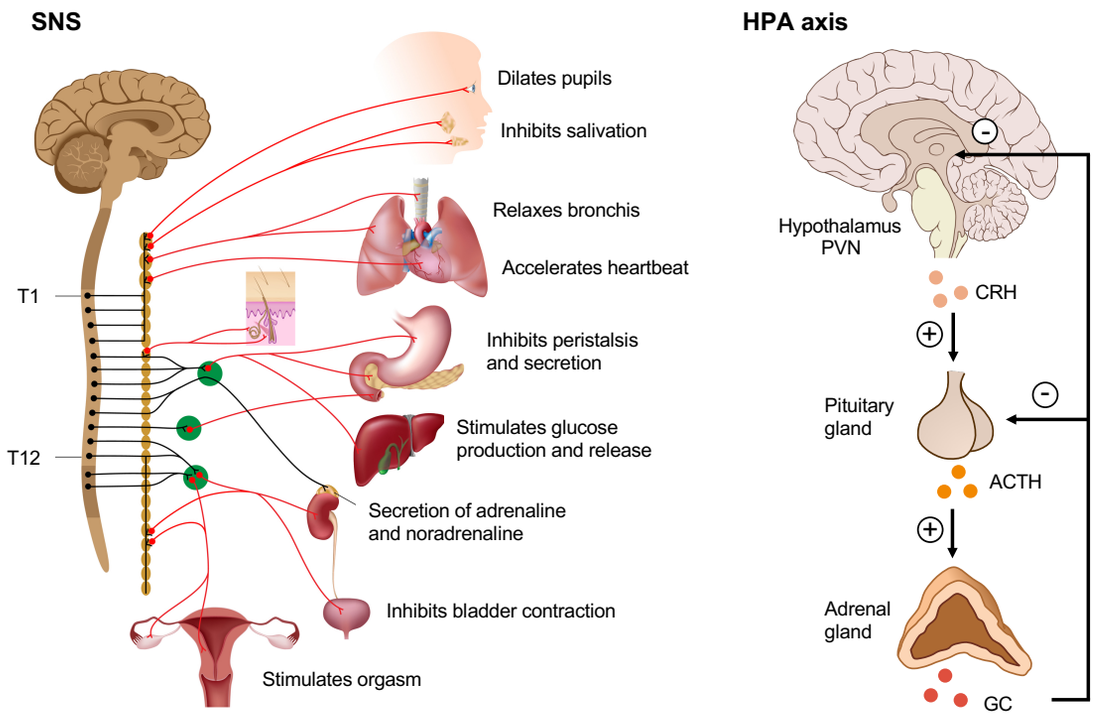

Figure 1. Overview of the two main stress response systems. Left panel: sympathetic nervous system (SNS). Sympathetic nerves arise in the spinal cord and innervate a variety of target organs, in most cases via two neurons that are connected within ganglia (pre- and postganglionic neurons are depicted in black and red, respectively). Most postganglionic neurons use adrenaline or noradrenaline as neurotransmitter, which activate adrenergic receptors in the target organ. Activation of the SNS has diverse functions, depending on the target organ. Right panel: hypothalamic-pituitary-adrenal (HPA) axis. Activation of the HPA axis is elicited in the paraventricular nucleus (PVN) of the hypothalamus. Release of corticotrophin-releasing hormone (CRH) from PVN neurons stimulates the production of adreno-corticotropic hormone (ACTH) by the pituitary gland and its release into circulation. ACTH then stimulates cells in the adrenal cortex to synthesise glucocorticoids (GCs). Circulating GCs in turn act on glucocorticoid receptors (GRs) in the hypothalamus and pituitary to inhibit further CRH and ACTH synthesis in a negative feedback loop.

1.1.4 Chronic stress and stress-related disorders

While the activation of stress response systems provides an important benefit in situations of acute threat, prolonged or disturbed activity of these systems can have detrimental effects. Indeed, chronic stress is a major risk factor for various pathologies, ranging from psychiatric, to metabolic, cardiovascular, inflammatory, and autoimmune disorders (De Kloet et al., 2005; Yaribeygi et al., 2017). Among the most common consequences of chronic stress are negative emotional states and the development of affective disorders, including depression, anxiety, and posttraumatic stress disorder (PTSD). Symptoms of these disorders show considerable overlap, suggesting some common underlying pathology. The following section will exemplarily summarise the aetiology of depression, as one of the most common affective disorders.

Depression, or major depressive disorder (MDD), affects up to 20% of the population throughout life. With more than 300 million people affected worldwide, depression is the leading cause of disability and substantially contributes to the overall disease burden (World Health Organization (WHO), 2018). Like other psychiatric disorders, depressive disorders are diagnosed according to

"The Diagnostic and Statistical Manual of Mental Disorders - Fifth Edition" (DSM-V) (American Psychiatric Association, 2013). For MDD diagnosis, patients must present at least five of the symptoms listed below over a period of at least two weeks (Table 1). Among those, one of the symptoms must be depressed mood or anhedonia (loss of interest or pleasure). Depression is caused by a complex interplay between biological (e.g. genetics, physical health) and external factors (e.g. social environment, adverse life events, trauma) (Lesch, 2004). And while there has been substantial research into the pathology of depression for many years, the underlying mechanisms still remain largely unknown. Classical pharmacological treatments are mainly based on the so-called monoamine hypothesis of depression, which postulates that depression is caused by a lack of monoamine neurotransmitters, such as serotonin, dopamine, and noradrenalin (Coppen, 1967; Schildkraut, 1995). However, anti-depressants that increase neurotransmitter levels in the brain (e.g. selective serotonin re-uptake inhibitors (SSRIs)) are ineffective in up to 30% of patients (Nemeroff, 2007). Another hypothesis that has recently been receiving increasing interest is the inflammatory hypothesis of depression, which will be discussed in chapter 1.2.4.

Table 1. DSM-V criteria for diagnosis of major depressive disorder

Symptoms (≥ 5 have to be present for at least two weeks, one of them depressed mood or anhedonia)
Depressed mood – most of the day
Anhedonia: diminished interest or pleasure in all or most activities – most of the day
Significant (> 5%) weight gain or loss, or reduced or increased appetite
Insomnia or hypersomnia
Psychomotor agitation or retardation (noticed by others)
Fatigue or lack of energy
Feelings of worthlessness or excessive or inappropriate guilt
Diminished ability to think or concentrate, or indecisiveness
Recurrent thoughts of death or suicide, suicide attempt or specific intention to commit suicide

Next to psychiatric disorders, there is strong evidence linking chronic stress to an increased risk of metabolic and cardiovascular diseases (Dimsdale, 2008; Tamashiro et al., 2011). One major function of stress responses is the rapid mobilisation of energy and an increase in heart activity, which enables the organism to cope with the immediate threat (e.g. fleeing a predator). However, prolonged exposure to stressors will persistently disrupt metabolic homeostasis and eventually override regulatory systems (Ryan, 2014). Accordingly, chronic stress alters feeding behaviour and promotes obesity, which in turn is a known risk factor for diseases like type-2 diabetes and cardiovascular disease. Additionally, direct cardiovascular effects of elevated SNS activity (e.g. increased blood pressure) further increase the risk of cardiovascular complications like sudden death, myocardial infarction and ischemia (Dimsdale, 2008; Kivimaki and Steptoe, 2018). Finally, chronic stress is associated with an increased risk and exacerbated disease progression of inflammatory and autoimmune diseases, including inflammatory bowel disease, arthritis, and asthma (Evers et al., 2014; Mawdsley and Rampton, 2005; Wright, 2005). The connection between stress and immunity will be described in more detail in the following section.

1.2 Stress and the immune system

One of the target systems of the HPA axis and SNS is the immune system. Peripheral immune cells are generally assigned to either the innate or the adaptive immune system (Parkin and Cohen, 2001). The innate immune system is considered the first line of defence against any pathogen or insult and mounts a rapid, but rather unspecific, immune response. It is comprised of myeloid cells, such as monocytes, macrophages, dendritic cells (DCs), and granulocytes as well as innate lymphocytes, such as natural killer (NK) cells. Adaptive immunity refers to the acquired, highly specific response to particular pathogens that is carried out by T- and B-lymphocytes, which also provide long-term protection against the encountered pathogen by developing immunological memory. Both cells of the innate and adaptive immune system are mainly generated from hematopoietic stem cell (HSC)-derived precursors in the bone marrow (Ng and Alexander, 2017).

1.2.1 Myeloid cells: monocytes and microglia

With regard to stress and stress-related disorders, a lot of research has been focused on myeloid cells, especially peripheral monocytes and microglia – the brain-resident immune cells.

Monocytes are generated from myeloid progenitor cells in the bone marrow and are released into the circulation to eventually migrate to tissues throughout the body (Geissmann et al., 2010). This release is increased in response to inflammation or insults, such as injury. Monocytes can be differentiated into subsets of classical inflammatory and non-classical monocytes, which are characterized by differential expression of surface proteins, such as lymphocyte antigen 6 complex (Ly6C), C-C chemokine receptor type 2 (CCR2), and fractalkine receptor (CX3CR1) (Gordon and Taylor, 2005). In the bone marrow, the vast majority of monocytes express high levels of Ly6C (Ly6C^{hi}). Commonly, they are released into the circulation as Ly6C^{hi} cells, where they either retain high Ly6C expression or differentiate into non-classical Ly6C low-expressing (Ly6C^{lo}) monocytes that patrol the circulation. In tissues, monocytes usually differentiate into resident macrophages or DCs. The spleen serves as a reservoir for undifferentiated monocytes that can be rapidly mobilized in response to insults (Swirski et al., 2009). Monocytes fulfil several functions in innate immunity, including antigen presentation, phagocytosis, cytokine production, and tissue repair (Yang et al., 2014). Importantly, stress is associated with an increased blood monocyte count in both humans and animal models (see chapter 1.2.5).

Microglia are the resident immune cells of the central nervous system (CNS) and fulfil various functions in both homeostasis and under pathological conditions (Gomez-Nicola and Perry, 2015). Microglia are derived from yolk-sac erythromyeloid progenitors that colonize the developing CNS early during embryogenesis (Ginhoux et al., 2013; Hoeffel and Ginhoux, 2015). This pool of microglia persists throughout life and maintains itself by proliferation, without substantial (or any)

replacement by infiltrating peripheral cells under normal circumstances (Askew et al., 2017). Microglia were long thought to remain in a resting state in the healthy brain and only become activated in response to pathological stimuli. By now it is known that "resting" microglia are highly dynamic cells that constantly scan their environment with many fine, mobile processes (Nimmerjahn et al., 2005). When brain homeostasis is disturbed (e.g. by injury, infection, or neurodegeneration) microglia undergo functional and morphological changes that aim at tissue defence and elimination of the insult – often termed "activation" (Colton and Wilcock, 2010; Kierdorf and Prinz, 2013). This state of "classical activation" is typically characterised by retraction of processes (amoeboid shape), increased phagocytic activity, increased surface expression of major histocompatibility complex (MHC) and costimulatory proteins (e.g. cluster of differentiation (CD)40, CD86) for antigen presentation, production of pro-inflammatory cytokines and chemokines (e.g. interleukin (IL)-6, IL-1β, tumor necrosis factor alpha (TNFα), chemokine C-C motif ligand 2 (CCL2)) and other inflammatory mediators, such as nitric oxide (NO) (Beins et al., 2016; Boche et al., 2013). In order to restore homeostasis once the insult has been eliminated, microglia also contribute to the resolution of inflammation and tissue regeneration by acquiring an "alternative", anti-inflammatory activation state. These activation states, however, are not a black or white situation but should rather be seen as a continuum (Martinez and Gordon, 2014; Murray et al., 2014).

Next to those typical immune-related functions, microglia play important roles during brain development and homeostasis. In recent years, the interaction between microglia and neurons has been focus of many studies. As the major phagocyte of the brain, microglia are involved in phagocytosis of apoptotic cells (Sierra et al., 2010) as well as synaptogenesis and synaptic pruning (the elimination of unnecessary or non-functional synapses) and thus refinement of neuronal connections (Kettenmann et al., 2013; Tremblay, 2011; Wake et al., 2013). These processes are very important during development, when neuronal networks are generated, but also in the mature brain, where they play important roles in neuronal plasticity – the ability of neuronal connections to change over time in an activity-dependent manner.

1.2.2 Glucocorticoid effects on the immune system

Most immune cells express both GRs and adrenergic receptors and thus can sense and respond to the main signalling molecules released during stress (Miller et al., 1998; Scanzano and Cosentino, 2015). GCs are one of the body's most potent immunosuppressants and are also commonly used as anti-inflammatory agents in the treatment of inflammatory or autoimmune diseases (Coutinho and Chapman, 2011). However, the mechanisms underlying the immunosuppressive actions are still not fully understood. Classically, the effects are mediated by cytoplasmic GRs expressed by immune cells. Upon GC binding, GRs are translocated to the

nucleus to induce or repress transcription of target genes, or to interact with other transcription factors (Coutinho and Chapman, 2011). One important target of GRs is the inflammation-related transcription factor nuclear factor kappa-light-chain-enhancer of activated B cells (NFκB) (Bekhbat et al., 2017). The transcriptional activity of NFκB is inhibited upon interaction with GRs, which suppresses the expression of several pro-inflammatory genes. Pro-inflammatory cytokines, such as IL-1β, IL-6, and TNFα can further directly stimulate the HPA axis (Dunn, 2000). The release of GCs then suppresses the excessive expression of pro-inflammatory genes in a negative feedback loop. Thus, interaction between stress-response systems and the immune system is bidirectional. Additionally, GCs can differentially modulate other immune cell functions in a cell type-dependent manner, such as migration, adhesion, phagocytosis, antigen-presentation, differentiation, and survival (Oppong and Cato, 2015). For example, GCs have apoptotic actions on T-cells, but are anti-apoptotic in neutrophils (Brunetti et al., 1995; Liles et al., 1995).

While GCs are generally powerful immunosuppressants, they can become pro-inflammatory under certain conditions. For example, it was repeatedly demonstrated that stress-induced GC production prior to an inflammatory stimulus increases pro-inflammatory responses of microglia (Fonken et al., 2016; Frank et al., 2010). Chronic stress is also associated with increased inflammation, both in the periphery and the brain. One explanation for this phenomenon is the development of GC resistance, i.e. the insufficient responsiveness of cells to GCs, both at the level of the HPA axis and of immune cells themselves (Pace et al., 2007; Raison and Miller, 2003). The lack of proper GC signalling may in turn lead to HPA axis hyperactivity and excessive inflammation. Thus, GC resistance can explain the seemingly paradox finding that many stress-related disorders are associated with HPA axis hyperactivity (hypersecretion of CRH and GCs) and a lack of GC-mediated signalling at the same time. In fact, GC resistance at the level of the HPA axis is observed in up to 80% of depressed patients, as determined in the dexamethasone/CRH suppression test (Raison and Miller, 2003). Furthermore, peripheral immune cells isolated from the blood of depressed patients exhibit reduced responsiveness to the immunosuppressant actions of GCs (Carvalho et al., 2010, 2014; Pariante, 2017). Consistent with that, meta-analyses repeatedly showed that subsets of depressed patients exhibit higher levels of circulating pro-inflammatory cytokines, such as TNFα and IL-6 (Dowlati et al., 2010; Liu et al., 2012). Finally, both PTSD and MDD symptom severity is positively correlated with increased pro-inflammatory cytokine production and NFκB signalling in monocytes (Carvalho et al., 2014; Gola et al., 2013; Pace et al., 2007).

1.2.3 Interaction between sympathetic nervous system and immune system

Next to the HPA axis, the SNS provides the second important communication pathway between the brain and the immune system. Already in the early 20th century, it was found that a single injection of adrenaline into healthy human volunteers rapidly increases the number of circulating leukocytes (Loeper and Crouzon, 1904). These initial observations are supported by several studies showing that both acute and chronic psychological stress can increase HSC mobilisation from the bone marrow (Dhabhar et al., 2012; Heidt et al., 2014; Mckim et al., 2018). The bone marrow and other lymphoid organs, such as thymus and spleen, are heavily innervated by sympathetic nerve fibres that terminate in close proximity to stem cell niches (Katayama et al., 2006; Yamazaki and Allen, 1990). In response to stress, release of noradrenaline and its interaction with adrenergic receptors on bone marrow stromal cells increases HSC proliferation and differentiation towards the myeloid cell lineage (Heidt et al., 2014). Furthermore, since most immune cells express adrenergic receptors, adrenaline and noradrenaline can also directly affect immune cell function (Scanzano and Cosentino, 2015).

1.2.4 Inflammation and depression

Already over two decades ago, the "inflammatory hypothesis of depression" was postulated by Michael Maes and has since received increasing interest in the scientific community (Maes, 1995). Indeed, there are several lines of evidence suggesting that inflammatory responses contribute to the pathology of depression: 1) As mentioned above, depression is associated with elevated levels of pro-inflammatory cytokines in the blood, along with increased numbers of circulating leukocytes. 2) Many of the symptoms of depression resemble what is known as sickness behaviour – a generalised response to illness that includes low mood, lethargy, decreased appetite, social withdrawal, impaired concentration, pain, and fever (Dantzer, 2009). 3) Chronic inflammatory disorders, such as cardiovascular disease, have a high co-morbidity with depression (Marrie et al., 2017). 4) Administration of pro-inflammatory mediators, such as interferon-α (IFNα) treatment in hepatitis C patients, induces depression in many patients (Dieperink et al., 2000). Furthermore, many studies using laboratory animals have by now confirmed the relevance of aberrant inflammatory signalling in depressive disorders.

1.2.5 Animal models of depression and inflammation

Exposure to psychosocial stress is one of the most reliable predictors of developing depression in humans and is a common experimental procedure to induce depressive-like behaviour in rodents (Björkqvist, 2001). Chronic social defeat stress (CSDS), the model applied in this study, is a resident-intruder paradigm, where the experimental mouse – the intruder – is exposed to repeated bouts of social defeat by a dominant aggressor mouse – the resident) (Golden et al., 2011). This or similar models recapitulate many of the behavioural, endocrine, and immunological

responses that are observed in patients suffering from stress-related disorders, such as MDD, PTSD, and anxiety disorders. Mice that underwent CSDS typically show GC resistance, elevated plasma cytokines, and increased production and mobilization of myeloid cells from the bone marrow. In the brain, CSDS increases neuronal and microglial activity in stress-responsive regions and increases cell adhesion molecule expression on neurovascular endothelial cells. This in turn recruits inflammatory monocytes to the brain, which are said to play a causative role in the development of stress-related behavioural pathology (Weber et al., 2017; Wohleb et al., 2015).

So while there is increasing evidence for a role of neuroimmune mechanisms in the pathology of depression and other stress-related disorders, the treatment is still largely based on directly modulating neurotransmitter systems in the brain. However, the low efficacy of available anti-depressant treatments prompts the need for more research and identification of other drug targets. One such potential target is the so-called endocannabinoid system (ECS), which will be discussed in the following sections. It is well known for its role in regulating neuronal signalling, stress responses, and inflammation and thus constitutes a promising target for the treatment of stress-related disorders.

1.3 The endocannabinoid system

Preparations of the plant *Cannabis sativa*, commonly known as cannabis, have been used for medicinal and recreational purposes for centuries and are well known for their mood-elevating and stress-relieving properties (Murray et al., 2007). Its main psychoactive ingredient, Δ^9-tetrahydrocannabinol (THC), was discovered in 1964 by Raphael Mechoulam and colleagues (Gaoni and Mechoulam, 1964), who is today considered the “father of cannabinoid research”. It then took over two decades until THC’s molecular target – the first cannabinoid receptor (CB1) – was identified in the late 1980s (Devane et al., 1988; Matsuda et al., 1990), followed by the second cannabinoid receptor (CB2) (Munro et al., 1993) and their two main endogenous ligands N-arachidonoylethanolamine (anandamide, AEA) and 2-arachidonoylglycerol (2-AG) (Devane et al., 1992; Mechoulam et al., 1995). These discoveries initiated extensive research into the ECS and its role in health and disease. Today, it is known that the ECS is widely expressed in mammalian tissues and is involved in a multitude of physiological and pathological processes (Pacher et al., 2006). The following section will briefly describe the main components of the ECS and its signalling mechanisms in the CNS, where it is best characterised.

1.3.1 Endocannabinoid system components: receptors, ligands, and enzymes

Both of the two main cannabinoid receptors, CB1 and CB2, are G protein-coupled receptors (GPCR), but their expression pattern varies substantially. CB1 receptors are highly expressed in the CNS (Matsuda et al., 1990), while CB2 receptors are mainly found in the periphery, with high expression on immune cells (Galiegue et al., 1995; Munro et al., 1993). In recent years, this segregation of the "central" and "peripheral" cannabinoid receptor was, however, challenged by the identification of CB2 expression by different brain cells, including neurons (Li and Kim, 2015; Onaivi et al., 2006; Stempel et al., 2016) and studies showing that CB1 receptors also act in peripheral, non-neuronal cells (Cota et al., 2003; Teixeira-Clerc et al., 2006). Next to CB1 and CB2, several other receptors (e.g. GPR55, GPR18) are considered cannabinoid or cannabinoid-like receptors, since they can be activated by cannabinoid compounds, be it endogenous, plant-derived, or synthetic (McHugh, 2012; Stella, 2010).

The main functions of CB1 and CB2 are attributed to the two well-documented endocannabinoids (eCBs), 2-AG and AEA. Although AEA and 2-AG possess distinct properties and binding affinities for the receptors, both are derived from lipid precursors and are produced on-demand in response to increased intracellular calcium (Ca^{2+}) concentrations. Due to their lipophilic nature, eCBs cannot be stored in intracellular vesicles like neurotransmitters. The synthesis and degradation of 2-AG and AEA are catalysed by a set of specific enzymes that complete the main components of the ECS. In brief, 2-AG is primarily produced by the hydrolysis of diacylglycerol (DAG) by the enzyme DAG lipase (DAGL) (Prescott and Majerus, 1983; Sugiura et al., 1995). DAGL exists in two isoforms – DAGLα and DAGLβ, which display distinct expression patterns with respect to the type of tissue and developmental stage (Bisogno et al., 2003). In the adult brain, DAGLα seems to be the main source of 2-AG. Degradation of 2-AG is mainly mediated by monoacylglycerol lipase (MAGL) that cleaves 2-AG into arachidonic acid (AA) and glycerol (Sugiura et al., 2006). While DAGLα and MAGL constitute the primary metabolic pathways for 2-AG, other less abundant pathways have been described, such as hydrolysis by the enzymes ABHD6 and ABHD12 (Blankman et al., 2007). For AEA, several pathways have been described for its synthesis. The most direct one involves the hydrolysis of N-acyl-phosphatidylethanolamine (NAPE) by NAPE-specific phospholipase D (NAPE-PLD) (Hansen et al., 2000; Okamoto et al., 2007). Degradation of AEA is mediated by fatty acid amino hydrolase (FAAH), which hydrolyses AEA into AA and ethanolamine (Cravatt et al., 1996). AEA and 2-AG can further both be metabolised by several other enzymes, including cyclooxygenase-2 (COX-2), lipoxygenases (LOX), and cytochrome P450 (CYPs) enzymes (Zelasko et al., 2015).

1.3.2 Retrograde endocannabinoid signalling in the central nervous system

In the brain, CB1 receptors are one of the most widely-expressed receptors from the GPCR family, suggesting an essential role of CB1 signalling in brain function (Herkenham et al., 1991; Kano et al., 2009; Mackie, 2005). CB1 receptors are localized at the presynaptic neuron of both excitatory and inhibitory synapses and are activated by eCBs produced by the postsynaptic neuron (Katona et al., 1999, 2006). CB1 signalling thus acts as a retrograde feedback system. Since 2-AG concentrations are approximately 800 times higher than AEA in the brain, 2-AG is considered the primary mediator of eCB signalling in the CNS (Sugiura et al., 1995). Therefore, the following section will exemplify CB1 signalling via 2-AG (see Figure 2). Nonetheless, it should be noted that AEA also contributes to eCB signalling.

The classical eCB retrograde signalling usually starts with excessive neurotransmitter release from the presynaptic neuron (Kano et al., 2009). The consequent strong depolarization of the postsynaptic neuron causes increased cytoplasmic Ca^{2+} concentrations and/or activated $G_{q/11}$ protein-coupled receptors, which induces the production of 2-AG by DAGLα. Subsequently, 2-AG is released into the synaptic cleft and activates presynaptic CB1 receptors. $G_{i/o}$ proteins coupled to the CB1 receptor then suppress further release of neurotransmitter from the presynaptic neuron by inhibiting Ca^{2+} influx through voltage-gated Ca^{2+} channels. CB1 signalling is terminated by the rapid uptake and subsequent degradation of 2-AG primarily by presynaptic MAGL (Murataeva et al., 2014). Depending on whether the synapse uses glutamate (excitatory) or γ-aminobutyric acid (GABA) (inhibitory), retrograde CB1 signalling thus mediates depolarisation-induced suppression of excitation (DSE) or inhibition (DSI), respectively (Kreitzer and Regehr, 2001a, 2001b; Ohno-Shosaku et al., 2001; Wilson et al., 2001).

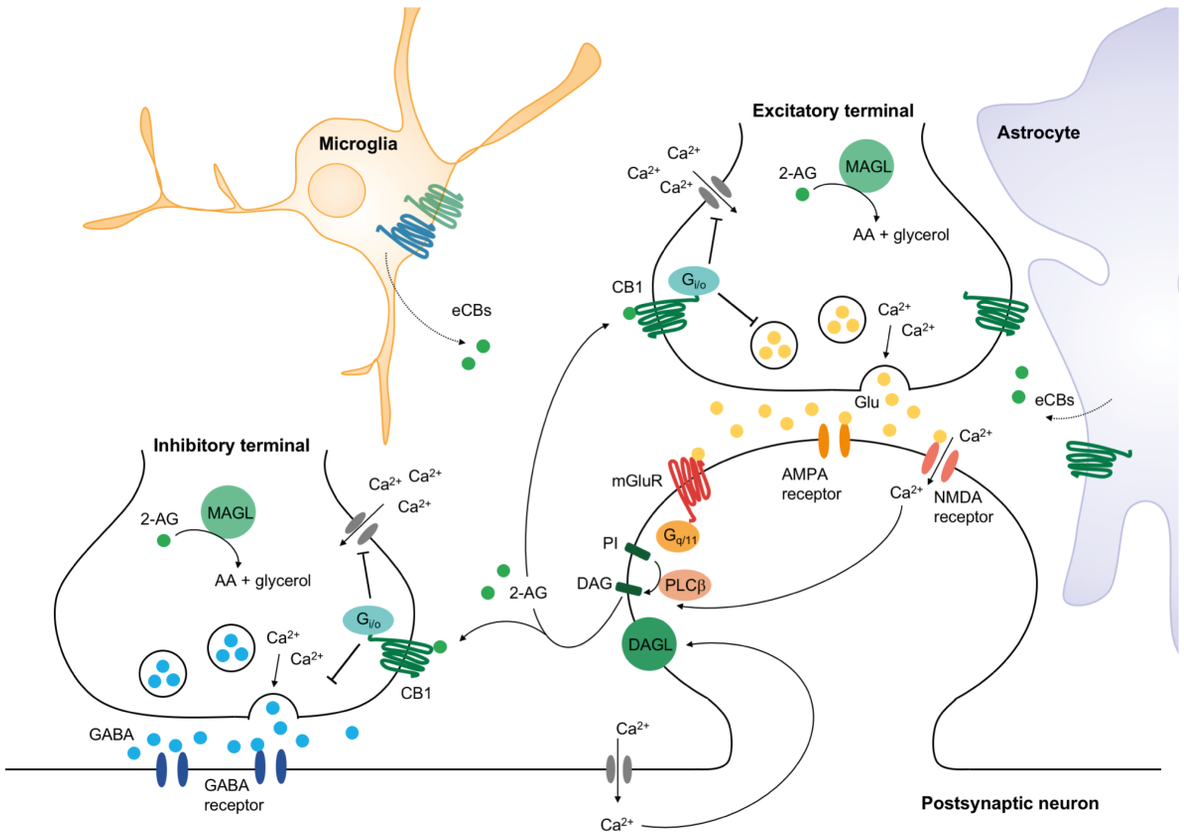

Figure 2. Retrograde signalling of the endocannabinoid system in the brain. Exemplarily illustrated for 2-AG, the most abundant brain eCB. Left: inhibitory, GABAergic synapse; right: excitatory, glutamatergic synapse. High frequency stimulation of a presynaptic neuron leads to influx of Ca2+ into the presynaptic terminal, triggering the release of neurotransmitter into the synaptic cleft (GABA or glutamate, respectively), which activate postsynaptic receptors. Strong depolarization of the postsynaptic neuron causes influx of Ca2+ through voltage-gated Ca2+ channels (and/or NMDA receptors in glutamatergic synapses). The increase in Ca2+ induces the production of 2-AG from DAG through DAGL activity. In glutamatergic synapses, 2-AG production can further be triggered via activation of metabotropic glutamate receptors (mGluR5) coupled to $G_{q/11}$ proteins, which induce DAG production from membrane phosphatidylinositol (PI) by phospholipase Cβ (PLCβ). 2-AG is released into the synaptic cleft and activates presynaptic CB1 receptors. Associated $G_{i/o}$ proteins suppress the influx of Ca2+ through voltage-gated Ca2+ channels – among others – thus inhibiting further neurotransmitter release. 2-AG is taken up into the presynaptic terminal and degraded by MAGL. Additionally, astrocytes close to the synapse can actively contribute to synaptic transmission and endocannabinoid (eCB) signalling, since they are able to detect and produce both neurotransmitters and eCBs. Microglia, the resident immune cells of the brain, are equipped with components of the ECS as well and thus can respond to or modulate eCB signalling. Abbreviations: AA: arachidonic acid, AMPA: a-amino-3-hydroxy-5-methyl-4-isoxazolepropionic acid receptor (ionotropic glutamate receptor), Ca2+: calcium ion, DAG: diacylglycerol, DAGL: DAG lipase, GABA: γ-aminobutyric acid (inhibitory neurotransmitter), Glu: glutamate (excitatory neurotransmitter), NMDA receptor: N-methyl-D-aspartate receptor (ionotropic glutamate receptor).

1.3.3 CB1 receptors – beyond retrograde signalling

While this retrograde signalling at synapses is the best described mechanism of endocannabinoid actions, recent years have provided evidence that eCB/CB1 signalling is much more diverse. CB1 activation can modulate several intracellular signalling cascades, such as the adenylyl cyclase (AC)/cyclic adenosine monophosphate (cAMP)/protein kinase A (PKA) pathway, or several mitogen-activated protein kinases (MAPKs) (Turu and Hunyady, 2010). Thereby, CB1 signalling can also have other, longer-lasting effects on synaptic transmission - one example being long-term

depression (LTD), a process crucially involved in neuronal plasticity. Furthermore, CB1 receptors are also located on mitochondrial membranes (mtCB1), where they can regulate mitochondrial activity and thus energy supply of the cell (Bénard et al., 2012; Hebert-Chatelain et al., 2014). In the brain, mtCB1 signalling was shown to regulate cannabinoid effects on memory formation, a process long-thought solely dependent on presynaptic plasma membrane CB1 receptors (Hebert-Chatelain et al., 2016). So far, mtCB1 expression has been demonstrated for neurons and astrocytes in the brain. CB1 receptors, as well as other components of the ECS, are thus not only expressed by neurons, but also other cell types within the CNS, including astrocytes and microglia (Metna-Laurent and Marsicano, 2015; Stella, 2010). The ECS can therefore act as a communication system between the different cells of the CNS.

1.3.4 CB1 signalling in the periphery

Next to its well-described functions in the CNS, the ECS regulates a plethora of peripheral processes, ranging from reproductive-, gastrointestinal-, and cardiovascular-function to bone metabolism, immunity and the endocrine system (Chiurchiu et al., 2015; Idris and Ralston, 2012; Izzo and Sharkey, 2010; Meccariello et al., 2014; Montecucco and Di Marzo, 2012). The next section will briefly outline how CB1 signalling can regulate peripheral systems relevant to this study.

1.3.4.1 Sympathetic nervous system

CB1 receptors are expressed on adrenergic and noradrenergic neurons both in the brain and peripheral nerves that innervate various target organs (Lowin and Straub, 2015; Mackie, 2005; Oropeza et al., 2007; Sanudo-Pena et al., 1999). Similar to the retrograde feedback signalling described above, activation of CB1 receptors on sympathetic nerve terminals inhibits the release of noradrenaline (Ishac et al., 1996; Pfitzer et al., 2005; Szabo et al., 2001). For example, it was demonstrated that the lack of CB1 signalling increases noradrenaline levels in the bone and thereby influences bone formation and absorption (Bab and Zimmer, 2008; Tam et al., 2008). Similarly, blocking CB1 receptors on sympathetic nerves that innervate the spleen can increase adrenergic signalling and thereby modulate immune processes (Mnich et al., 2010).

1.3.4.2 Hypothalamic-pituitary-adrenal axis

CB1 receptors are also found at all levels of the HPA axis, namely within the hypothalamus, the pituitary, and the adrenal glands (Hillard et al., 2017). In fact, CB1 signalling is essential for the GC-mediated fast feedback inhibition of the HPA axis. *In vitro* and *in vivo* studies showed that GCs can rapidly induce the production of 2-AG by CRH neurons in the hypothalamus via non-genomic GR signalling (Di et al., 2003; Evanson et al., 2010; Hill et al., 2010b). Activation of CB1 receptors

on presynaptic glutamatergic neurons by 2-AG then suppresses the excitatory input onto CRH neurons and thus inhibits HPA axis activity. Furthermore, GCs can modulate eCB levels and CB1 signalling in other brain regions that provide input to the PVN (hippocampus, PFC, amygdala) (Hill et al., 2010a, 2011; Rademacher et al., 2008; Sumislawski et al., 2011; Wang et al., 2012; Zoppi et al., 2011). For example, CB1 signalling via AEA and 2-AG in the basolateral amygdala (BLA) appears to be important for HPA axis initiation during acute stress exposure and its habituation to repeated stress, respectively. Since CB1 receptors are also expressed by cells of the pituitary and adrenal gland, they can also directly regulate HPA axis activity at these levels (Cota et al., 2007).

1.3.5 CB1 signalling and depression

As described above, CB1 signalling is involved in the regulation of many aspects that are affected in psychiatric disorders, such as mood, stress responses, and cognitive function. Accordingly, lack of CB1 signalling is associated with an increased risk to develop these disorders. A prominent example is the drug rimonabant (SR141716), an inverse agonist selective for CB1 receptors (Rinaldi-Carmona et al., 1994). It was developed by Sanofi-Aventis and approved as an anorectic drug for obese patients in Europe in 2006. However, its approval was eventually withdrawn worldwide in 2008 due to serious psychiatric side effects. In about 10% of subjects, blocking CB1 receptors with rimonabant caused mood alterations or depressive symptoms and even suicidal ideation in about 1% (Christensen et al., 2007). Other side effects included anxiety, irritability, sleep disorders, fatigue, gastrointestinal problems (nausea, diarrhoea, vomiting), spasms, respiratory tract infections and flu-like symptoms (Aagaard, 2014; Christensen et al., 2007). Similarly, mice with a genetic deletion of the gene encoding CB1 (*Cnr1*) show phenotypes similar to clinical symptoms of depressive disorders (see Table 2) (Valverde and Torrens, 2012).

Table 2. Phenotype of CB1 knockout (*Cnr1*$^{-/-}$) mice and symptoms of depression (from Valverde & Torrens, 2012)

Phenotype of *Cnr1*$^{-/-}$ mice	Clinical symptoms of depressive disorders
Increased anxiety-like behaviour	Increased anxiety
Higher sensitivity to develop depressive-like symptoms after stress	Impaired stress-coping
Cognitive impairments, e.g. in the extinction of aversive memories	Cognitive dysfunction in MDD, impaired extinction of traumatic experiences in PTSD
Decreased rewarding effects of natural rewards and altered responses to drugs of abuse	Anhedonia; co-morbidity with substance use disorders
Decreased locomotor activity	Low energy and psychomotor retardation
Changes in baseline and higher stress-induced CORT levels	Enhanced cortisol response to stress, hyperactivity of HPA axis in depression

1.3.6 ECS/CB1 signalling and inflammation

Most of the studies on CB1 and its role in depressive disorders have focused on CB1-mediated regulation of neuronal function, such as serotonergic signalling or neurogenesis (Aso et al., 2008a, 2009; Steiner et al., 2008). However, the ECS in general also has well-documented immunomodulatory functions (Chiurchiu et al., 2015). These are mainly attributed to CB2 receptors, which are expressed by most immune cells, including microglia (Galiegue et al., 1995; Munro et al., 1993). In microglia, eCBs can reduce the production of pro-inflammatory mediators and increase anti-inflammatory cytokine production via CB2 receptors (Correa et al., 2010; Eljaschewitsch et al., 2006; Puffenbarger et al., 2000). Furthermore, 2-AG stimulates microglial proliferation and migration, which seems to be mediated by both CB1 and CB2 (Carrier et al., 2004; Eljaschewitsch et al., 2006; Walter et al., 2003). Furthermore, there are a few studies showing that also CB1 receptors can regulate immune function. For example, blocking CB1 signalling in peripheral organs appears to be protective under inflammatory conditions (e.g. liver fibrosis), mediated by reducing macrophage migration, reactive oxygen species (ROS) production, and pro-inflammatory activation (Mai et al., 2015; Mnich et al., 2010; Tian et al., 2017). In the CNS, lack of CB1 receptors on GABAergic forebrain neurons alters neuroinflammatory processes and microglial activation at baseline and in response to pro-inflammatory stimuli as well as during ageing (Albayram et al., 2011; Ativie et al., 2018).

However, the contribution of CB1 signalling to immune function has never been studied in the context of stress. In a recent study, it was shown that pharmacological treatment with a cannabinoid agonist can reverse social stress-induced myelopoiesis, neuroinflammation, and anxiety (Lisboa et al., 2018). Whether these effects were mediated by CB1 or CB2 receptors is, however, not known, since a non-selective agonist was used. Considering the prominent role of CB1 in stress-related pathologies, its presence in most – if not all – systems that are involved in neuroimmune communication, and the increasing evidence linking inflammation to psychiatric disorders, it is tempting to speculate that CB1 signalling provides a connection between behavioural, neuroendocrine, and immunological responses to stress (see Figure 3).

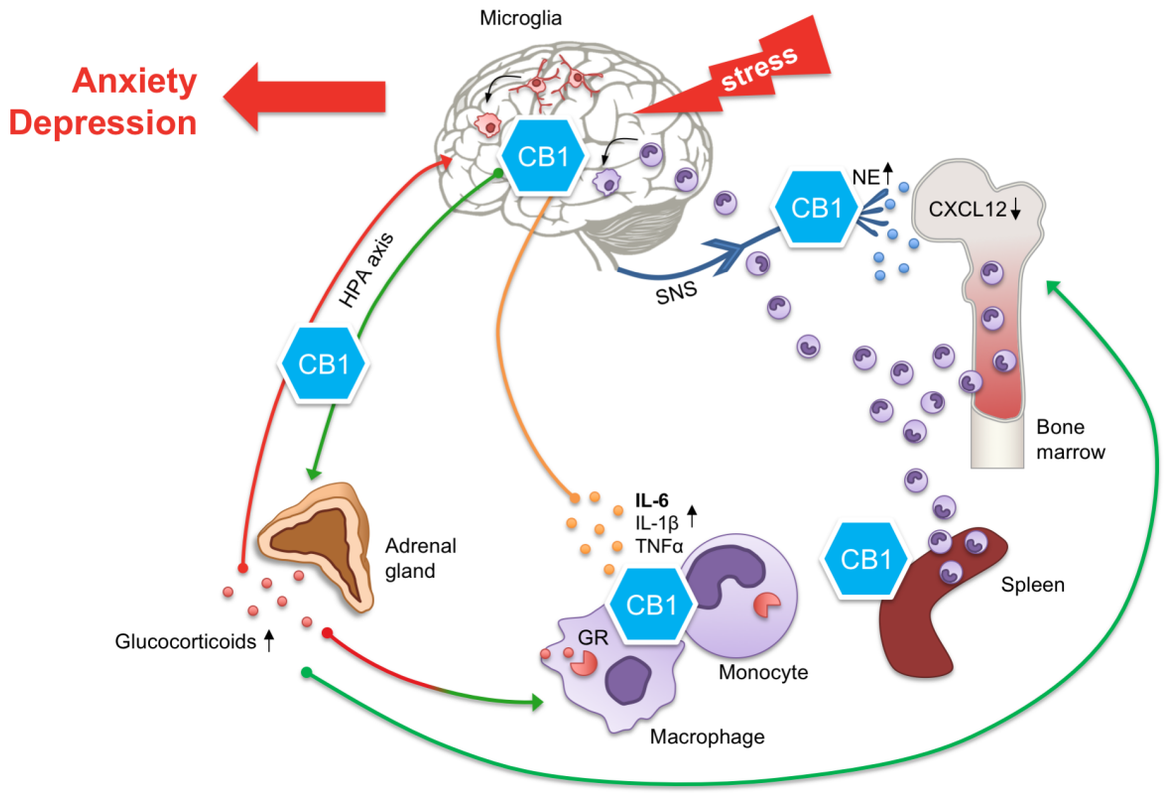

Figure 3. Neuroimmune communication systems during chronic stress and their possible regulation by CB1 signalling. Stress activates stress responses, including the hypothalamic–pituitary–adrenal (HPA) axis, which leads to the secretion of glucocorticoids (GCs) by the adrenal glands. GC acting via glucocorticoid receptors (GR) expressed by immune cells (e.g. macrophages, monocytes) usually exert strong immunosuppressant functions. During chronic stress, this immunosuppressive function is often lost, eventually leading to enhanced production of inflammatory mediators (e.g. pro-inflammatory cytokines) and thus chronic low-grade inflammation. Cytokines, such as interleukin 6 (IL-6), IL-1β, or tumor necrosis factor alpha (TNFα) can signal to the brain and act on microglia – the resident immune cells of the brain. High levels of pro-inflammatory cytokines and microglial activation trigger neuroinflammation, which can affect neuronal function. A second system activated by stress is the sympathetic nervous system (SNS). During chronic stress, increased release of noradrenaline (norepinephrine, NE) from nerves innervating the bone marrow induces the production of myeloid cells (monocytes, neutrophils). Downregulation of retention factor C-X-C motif chemokine 12 (CXCL12), mediated by NE and GCs, increases the release of myeloid cells into the circulation and subsequent trafficking to different organs, including the spleen and possibly the brain. In the brain, infiltrated monocytes are thought to contribute to neuroinflammatory processes and thereby drive the development of stress-related pathologies, such as depression and anxiety. The CB1 receptor is expressed in all systems involved in this neuroimmune communication during stress and known to regulate them in different contexts. Whether CB1 signalling also regulates these processes during chronic stress and whether they contribute to the increased stress-susceptibility in the absence of CB1 signalling is however not known.

1.4 Aim of this study

As described above, there is increasing evidence linking inflammatory processes to psychiatric disorders. Chronic stress, a major environmental factor contributing to the development of these disorders, affects immune system activity through neuronal and endocrine signals. The link between CB1 signalling, stress-reactivity, and psychiatric disorders is well established. However, it is not known whether this is a purely neuronal effect or whether it is accompanied or mediated by altered immune system regulation. The aim of this study was therefore to analyse how CB1 signalling modulates behavioural, neuroendocrine, and immunological responses in a mouse model of chronic social defeat stress (CSDS). The model recapitulates many of the symptoms that are observed in patients suffering from stress-related disorders, such as depression, PTSD, and anxiety disorders and previous studies suggest that these stress effects are driven by altered myeloid cell function. To elucidate the role of CB1 signalling in these processes, CSDS was performed in mice with a genetic deletion of CB1 receptors (*Cnr1*$^{-/-}$).

2 Materials and methods

2.1 Equipment

Technical instrument	Identifier, company
Analytical balance	BP 121 S, Sartorius
Liquid handling platform	Janus®, Perkin Elmer
Cell culture incubator	Binder GmbH
Centrifuges	Biofuge fresco, Heraeus Instruments
	Megafuge 1.0R, Heraeus Instruments
	Multifuge 3 S-R, Heraeus Instruments
Cryostat	CM3050S, Leica
Digital gel documentation	ChemiDoc MP imaging system, Bio-Rad Laboratories
Electrophoresis chamber	Sub-Cell GT System, Bio-Rad Laboratories
Flow cytometer	FACS Canto II, BD Bioscience
Home cage activity measurement	Mouse-E-Motion, Infra-e-motion
Laminar flow hood	Herasafe, Kendro
Magnetic stirrer	MR 3001 K, Heidolph, Fisher
Microplate reader	MRX TC II, Dynex Technologies
Microscope	Leica TCS SP8, Leica
Animal video-tracking-system	EthoVision XT, Noldus Information Technology
PCR cycler	iCycler, Bio-Rad Laboratories
pH meter	inoLab, WTW
Real-time PCR cycler	LightCycler 480, Roche
Spectrophotometer	NanoDrop 1000, Thermo Scientific
Sterilizing oven	Varioklav 25T, H+P Labortechnik
Tissue homogeniser	Precellys 24, Bertin Technologies
Vacuum concentrator	SpeedVac SPD111V, Thermo Fisher
Vortexer	Vortex-Genie 2, Scientific Industries
Mouse telemetry implants	Data Science International

2.2 Chemicals and reagents

2.2.1 Chemicals/enzymes

Chemical/enzyme	Company (catalog #)
1-bromo-3-chloropropane (BCP)	Sigma-Aldrich (B9673)
100 bp DNA ladder	Life Technologies (15628-050)
10x red blood cell (RBC) lysis buffer	BioLegend (420301)
2-Methylbutan/isopentane	Sigma-Aldrich (320404)
2-Propanol/isopropanol	Carl Roth (6752.4)
4',6-diamidino-2-phenylindole (DAPI)	Sigma-Aldrich (10236276001)
Ammonium hydroxide	Sigma-Aldrich (221228)
Carprofen (Rimadyl®)	Pfizer (30601241)
Citric acid	Promega (H526a)
Collagenase/Dispase (for brain tissue)	Roche (11097113001)
Collagenase type VIII (for spleen tissue)	Sigma-Aldrich (C2139-1g)
DNase I from bovine pancreas (for spleen tissue)	Sigma-Aldrich (DN-25-100mg)
DNase I from bovine pancreas (for brain tissue)	Roche (11284932001)
DNase I recombinant, RNase-free (+ 10x incubation buffer)	Sigma-Aldrich (4716728001)
DNase/RNase-free distilled water	Gibco (10977015)
dNTP mix (10 mM)	Sigma-Aldrich (D7295)
Dulbecco's Modified Eagle Medium (DMEM), high glucose	Gibco (11965-092)
Ethanol (EtOH) absolute	VWR (20821.330)
Ethidium bromide solution (10 mg/ml)	Sigma-Aldrich (E1510)
Ethylenediaminetetraacetic acid (EDTA), disodium salt	Calbiochem (324503)
Fetal calf serum (FCS)	PAA (A15-108)
Fluoromount-G®	SouthernBiotech (0100-01)
Hydrochloric acid (HCl) 37%	Carl Roth (X942.1)
Isoflurane	Piramal (30372.00.00)
Ketamine hydrochloride	Inresa Arzneimittel GmbH (30101021)
L-glutamine (200 mM)	Gibco (25030081)
Lipopolysaccharide (LPS) from *E. coli 0127:B8*	Sigma-Aldrich (L4516)
Normal donkey serum	Abcam (ab7475)
Normal goat serum	Abcam (ab7481)
Oligo(dT) primer (50 µM)	Invitrogen (18418012)
Paraformaldehyde (PFA)	Sigma-Aldrich (P6148)
Penicillin-Streptomycin (10,000 U/ml)	Gibco (15140122)
Percoll™	GE Healthcare (17-0891-01)
Phosphate-buffered saline (PBS) tablets	Gibco (18912014)
Phosphoric acid (H_3PO_4)	Sigma Aldrich (43.808)
Proteinase K	NEB (P8107S)

Chemical/enzyme	Company (catalog #)
RPMI 1640 medium	Gibco (21875-034)
Sodium azide	Sigma-Aldrich (S8032)
Sodium chloride (NaCl)	Carl Roth (9265)
Sodium dodecyl sulphate (SDS)	Carl Roth (2326)
Sucrose, for microbiology	Sigma-Aldrich (84100)
SuperScript™ II reverse transcriptase	Invitrogen (18064014)
(+ 5x first-strand buffer and DTT (0.1M))	
Taq Polymerase (+ 10x ThermoPol buffer)	NEB (M0267X)
TaqMan® Gene Expression Assays	Applied Biosystems (4331182)
TaqMan® Gene Expression Master Mix	Applied Biosystems (4370074)
Tissue-Tek® O.C.T. Compound	VWR (4583)
Tris-(hydroxymethyl)aminomethane (Tris)	Carl Roth (5429)
Tris-HCl	Carl Roth (9090.3)
Triton™ X-100 detergent	Sigma-Aldrich (T9284)
TRIzol® reagent	Life technologies (15596026)
TWEEN® 20	Sigma-Aldrich (P9416)
UltraPure™ agarose	Invitrogen (15510-027)
Xylazin hydrochloride (Rompun®)	Bayer (03406)

2.2.2 Solutions and buffers (general)

If not stated otherwise, solutions were prepared with ultrapure distilled water (MilliQ H_2O).

Solution/buffer	Composition
Phosphate-buffered saline (PBS), pH 7.4	500 ml MilliQ H_2O + 1 PBS tablet
Tris-buffered saline (TBS), pH 7.5	MilliQ H_2O + 50 mM Tris-HCl + 150 mM NaCl
Tris-EDTA (TE) buffer, pH 7.4	MilliQ H_2O + 10 mM Tris + 1 mM EDTA, pH 8.0
Tris-acetate-EDTA (TAE) buffer	MilliQ H_2O + 40 mM Tris-acetate + 1 mM EDTA pH 8.0

2.2.3 Genotyping

Solution/buffer	Composition
Mouse tail lysis buffer	MilliQ H_2O + 100 mM Tris/HCl pH 8.0 + 5 mM EDTA + 200 mM NaCl + 0.2% (w/v) SDS + Proteinase K (1 mg/ml) (added later)
Ethidium bromide bath solution	TAE buffer + 1.5 µg/ml ethidium bromide

2.2.4 Immunohistochemistry

Solution/buffer	Composition
4% Paraformaldehyde (PFA)	PBS + 4% (w/v) PFA, sterile filtered
Decalcification solution for bone tissue	PBS + 14% (w/v) EDTA + 3% (v/v) ammonium hydroxide
Cryoprotection solution	PBS + 30% (w/v) sucrose
Citrate buffer pH 6.0 for antigen retrieval	MilliQ H_2O + 10 mM citric acid + 0.05% (v/v) Tween 20
PBS-Triton X-100 (PBS-T)/ TBS-Triton X-100 (TBS-T)	PBS/TBS + 0.025 – 0.5% (v/v) Triton X 100
Blocking solution	PBS-T 0.5% or TBS-T 0.5% + 5 – 10% (v/v) normal serum (of host species of 2nd antibody)
Antibody solution	PBS-T 0.025 – 0.1% or TBS-T 0.25% + 2.5 – 5% (v/v) normal serum (of host species of 2nd antibody)

2.2.5 Cell culture

Solution/buffer	Composition
Culture medium for splenocytes	RPMI 1640 + 10% (v/v) FCS + 1% (v/v) Penicillin-Streptomycin (10,000 U/ml) + 1% (v/v) L-glutamine (200 mM)
Lipopolysaccharide (LPS)	Stock: 5 mg/ml LPS from *Escherichia coli 0127:B8* in sterile dH_2O

2.2.6 Flow cytometry

Solution buffer	Composition
FACS buffer	PBS + 2% (v/v) FCS
Red blood cell (RBC) lysis buffer	MilliQ H_2O + 10% (v/v) 10x RBC lysis buffer
Medium CNS mononuclear cells	DMEM, high glucose + 10% (v/v) FCS
Digestion mix for brain tissue	Medium + 1 mg/ml Collagenase/Dispase + 1 mg/ml DNase I
Stock isotonic Percoll (SIP)	Percoll™ + 10% (v/v) PBS (10X)
Digestion mix for spleen tissue	PBS + 1 mg/ml Collagenase type VIII + 120 KU/ml DNase I

2.2.7 Enzyme-linked Immunosorbent Assay (ELISA) Kits

Assay	Company	Solutions prepared (not provided by Kit)
Mouse IL-1β Ready-SET-Go!	eBioscience	Wash buffer (0.05% TWEEN® 20 in PBS) Stop solution (1 M H_3PO_4)
Mouse IL-6 Ready-SET-Go!	eBioscience	Wash buffer (0.05% TWEEN® 20 in PBS) Stop solution (1 M H_3PO_4)
Mouse TNFα Ready-SET-Go!	eBioscience	Wash buffer (0.05% TWEEN® 20 in PBS) Stop solution (1 M H_3PO_4)
Mouse CCL2 (MCP-1) Ready-SET-Go!	eBioscience	Wash buffer (0.05% TWEEN® 20 in PBS) Stop solution (1 M H_3PO_4)
DetectX® Corticosterone Enzyme Immunoassay Kit	Arbor Assays	

2.3 Methods

2.3.1 Mice

In this study, the following mouse lines were used for behavioural and molecular analysis: C57BL/6J wild type (WT) and B6.cg*Cnr1*tm1Zim (constitutive CB1 knockout). C57BL/6J mice were originally obtained from a commercial breeder (Charles River) and bred at the animal facility of the University of Bonn. B6.cg*Cnr1*tm1Zim mice were generated by disrupting the *Cnr1* coding region with a neomycin cassette, using homologous recombination in embryonic stem cells (Zimmer et al., 1999). Mutant mice were backcrossed to C57BL6/J mice for more than ten generations. For this study, B6.cg*Cnr1*tm1Zim mice were bred mainly using heterozygous breeding pairs (*Cnr1*$^{+/-}$ x *Cnr1*$^{+/-}$) that generate offspring with the following genotypes: homozygous wild type (*Cnr1*$^{+/+}$), heterozygous CB1 knockout (*Cnr1*$^{+/-}$), and homozygous CB1 knockout (*Cnr1*$^{-/-}$). *Cnr1*$^{+/+}$ and *Cnr1*$^{-/-}$ littermates were used for most experiments. In early experiments (standard CSDS), WT and *Cnr1*$^{-/-}$mice were derived from separate homozygous breeding pairs. For clarity, WT mice will be referred to as *Cnr1*$^{+/+}$ in this case as well. If not stated otherwise, mice were group-housed (3-5 animals per cage) in standard laboratory cages under specific-pathogen-free (SFP) conditions, with a normal light-dark cycle (lights on from 07:00 am to 07:00 pm) with *ad libitum* access to food and water. Male CD1 mice (6 months old retired breeders), used as aggressor mice for CSDS, were obtained from a commercial breeder (Janvier) and single-housed in standard laboratory cages with a reversed light-dark cycle (lights on from 09:00 pm to 09:00 am) with *ad libitum* access to food and water. All experiments followed the guidelines of the German Animal Protection Law and the Local Committee for Animal Health, LANUV NRW, approved the experiments (84-02.04.2015.A192).

2.3.1.1 Genotyping – DNA isolation

For mouse genotyping, DNA was isolated from mouse tail biopsies. The tissue was incubated overnight in 200 µl mouse tail lysis buffer and proteinase K (1 mg/ml) at 50°C with shaking (550 rpm). After lysis, samples were centrifuged (12000 *x g*, 10 min, 4°C) and the supernatant transferred to a fresh tube. DNA was precipitated by adding 200 µl isopropanol and inverting the tube several times. Afterwards, the DNA pellet was washed twice with 70% ethanol, air-dried and dissolved in 100 µl TE buffer.

2.3.1.2 Genotyping – DNA amplification by polymerase-chain reaction

Sequence specific amplification of DNA fragments for genotyping was performed using polymerase-chain reaction (PCR). Each PCR reaction was specifically adapted to the temperature requirements of the oligonucleotides (primer) and the length of the desired PCR product. PCR was performed using Taq Polymerase, 10x ThermoPol buffer, dNTPs, and respective primer pairs. Established PCR conditions and corresponding primer sequences are listed below.

PCR reaction for B6.cgCnr1tm1Zim genotyping	
15.4 µl	Sterile water
2.1 µl	10x ThermoPol buffer
0.5 µl	dNTP mix (10mM)
0.3 µl	Primer WT: 5´-TGT GTC TCC TGC TGG AAC CAA CGG-3´
0.7 µl	Primer KO: 5´-TCT CTC GTG GGA TCA TTG TTT TTC TCT TGA-3´
0.5 µl	Primer COM: 5'-CTC CTG GCA CCT CTT TCT CAG TCA-3'
0.5 µl	Taq Polymerase
1 µl	Mouse tail DNA (100 - 150 ng/µl)

Cycling parameter		Temp.	Time
1 x	Initial denaturation	94°C	4 min
	Denaturation	94°C	45 s
35 x	Annealing	65°C	45 s
	Elongation	68°C	60 s
1 x	Final elongation	68°C	7 min
	Cooling	4°C	∞

2.3.1.3 Genotyping – agarose gel electrophoresis

DNA fragments from PCR reactions were separated using agarose gel electrophoresis. Gels were prepared by dissolving 1 - 2% agarose in TAE buffer. Electrophoresis was run in chambers filled with TAE buffer at 120 V for 60 - 120 min. A 100 bp DNA ladder was used for estimating the size of the DNA fragments. DNA fragments in the gel were stained in an ethidium bromide bath for 10 – 20 min and visualised using a ChemiDoc MP imaging system.

2.3.2 Chronic social defeat stress (CSDS)

Chronic stress is a main cause of depression in humans (De Kloet et al., 2005; Lupien et al., 2009). Several chronic stress models have been established to investigate stress-induced depressive-like behaviour and molecular changes in rodents, including CSDS. In humans, chronic social defeat, like bullying in schools or workplaces, can lead to sociophobia, the loss of self-esteem, anxiety and depression (Björkqvist, 2001). The animal model CSDS is based on a resident-intruder paradigm, in which a young male C57BL6/J mouse (intruder) is placed into the home cage of an older, more aggressive male CD1 mouse (resident). The defeated animal is considered to experience social stress.

2.3.2.1 Screening for aggressive CD1 mice

Reproducible and successful application of CSDS is strongly dependent on consistent levels of aggressive behaviour of the CD1 mice. Single-housed, male retired breeders exhibit the strongest territoriality and aggressiveness against foreign males and are therefore the most recommended aggressors. Nevertheless, aggression levels can vary greatly between individuals and a screening procedure is essential. In this study, a screening procedure described by Golden et al. (2011) was

applied. Screening was performed on three consecutive days in the home cage of the CD1 mouse. Each day, a novel 7-9 weeks old C57BL6/J mouse was placed into the home cage of the aggressor for up to 5 min and the latency until the first aggression was recorded. Only CD1 mice that attacked within 60 s in at least two of the three screening days were selected.

2.3.2.2 Chronic social defeat stress protocol

At least one week before starting the CSDS paradigm, male C57BL6/J mice were habituated to a reversed light-dark cycle (lights on from 09:00 pm to 09:00 am). Depending on the experiment, mice were single- or group-housed before CSDS, with *ad libitum* access to food and water. Social defeat sessions were carried out during the active phase of the animals (lights off), between 10:00 am – 01:00 pm. In the standard CSDS paradigm, 8 - 10 weeks old male C57BL6/J mice were subjected to repeated bouts of social defeat by a CD1 aggressor mouse for 5 - 10 min daily on 10 consecutive days (Golden et al., 2011). A mild CSDS paradigm was established later, with only 1 - 2 min defeat per day. After the daily defeat session, animals were separated by a perforated plastic glass wall, which allowed sensory but no physical contact for the following 24 h. In order to prevent habituation between resident and intruder, C57BL6/J mice were exposed to a novel CD1 aggressor every day. Subsequent to the last defeat session, animals were single-housed and tested in different anxiety- and depression-related behavioural tests. Control C57BL6/J mice were housed with two unfamiliar mice per cage, constantly separated by a perforated wall.

2.3.3 Behavioural tests

If not stated otherwise, all behavioural tests were performed during the animal's active phase (lights off).

2.3.3.1 Social avoidance test

Social avoidance behaviour was analysed after CSDS. A metal grid cage containing a foreign CD1 mouse (male retired breeder) was placed close to one wall of an open field box. The test mouse was placed into a corner of the box and its movement recorded for 5 min using the EthoVision XT software. Interaction was measured as the time spent in close proximity to the cage (nose-point). The less time the test mouse spent interacting with the CD1 mouse, the higher the social avoidance behaviour. In later experiments, the test was divided into two trials. During the first half (2.5 min), the metal cage was empty and then replaced by a cage containing a CD1 mouse for the second half (2.5 min). Test mice were shortly removed from the open field box in between trials. The social interaction (SI) ratio was calculated as the interaction with the CD1 mouse divided by the interaction with the empty cage. Thereby, changes in exploratory behaviour can be excluded from the social avoidance behaviour. The lower the ratio, the higher the social avoidance behaviour.

2.3.3.2 Open field test

Anxiety behaviour and locomotor activity were analysed using the open field test. Animals were tested in a sound-isolated room in an open field box (44 cm x 44 cm). Depending on the experiment, the room was differently illuminated (20 or 150 lux for a non-aversive or aversive environment, respectively). The mice were allowed to explore the box freely and their behaviour was recorded for 10 min, using the EthoVision XT software. The time spent in the centre of the open field box (25% of the whole area) is considered a measure of anxiety. Rodents usually avoid open lit-up areas and increased anxiety is associated with decreased time spent in the centre of the open field. Additionally, locomotor activity and exploratory behaviour were determined as the total distance travelled.

2.3.3.3 Sucrose preference test

Anhedonia, the inability to experience pleasure, is a common symptom of affective disorders, such as depression. In rodents, anhedonia can be analysed using the sucrose preference test. Rodents generally prefer sweet solutions to water with a preference up to 95% in C57BL/6 mice (Pothion et al., 2004) and a reduction of this preference is considered a measure of depressive-like behaviour (Katz, 1981). Mice were single-housed and had free access to two bottles, one containing water and the other one containing 1% sucrose solution. Consumption of each solution was measured by weighing the bottles before and after the test. During the test, positions of the bottles were changed at least once to avoid side-bias. Preference was calculated as the percentage of sucrose consumption of the total fluid consumption.

2.3.3.4 Nestlet test

When provided with suitable material, mice build a nest that provides shelter and camouflage from predators and helps conserving body temperature (Bult and Lynch, 1997). In laboratory mice, nest building is further considered a home-cage activity related to social behaviour (Moretti et al., 2005). In the nestlet test, single-housed mice were provided with a pre-weighed nestlet made of compressed cotton. After 1 h, the remaining intact nestlet was removed and weighed to calculate the amount of nesting material used.

2.3.3.5 Home cage activity measurements

Home cage activity was recorded for four days using an infrared system (Mouse-E-Motion, Infra-e-motion GmbH). An infrared sensor was attached to the cage lid to record movements in the home cage every 30 s. Movements were sampled and averaged over 1 h.

2.3.3.6 Zero-maze test

Anxiety-related behaviour was also tested in the zero-maze (height 40 cm, internal diameter 46 cm, width 5.6 cm) in a sound-isolated room. The maze was divided into four equal quadrants, with non-transparent walls enclosing the two opposite quadrants. Animals were placed in the open area of the zero-maze and their movements were recorded for 5 min with 600 - 700 lux illumination. Time spent in the different areas and distance travelled was analysed using EthoVision XT software.

2.3.3.7 Forced swim test

Mice were tested for behavioural despair in the forced swim test. This test is based on the assumption that mice try to escape an aversive (stressful) stimulus, such as water. Mice were placed individually into a glass cylinder (height 28 cm, diameter 20 cm) containing water (height 14 cm, 24 - 25°C) and their movements observed and videotaped for 6 min. Immobility, i.e. the lack of any movements other than those necessary to balance the body and keep the head above the water, was recorded during the last 4 min of the 6 min testing period and is considered a measure of helpless behaviour (Porsolt et al., 1977).

2.3.4 Telemetric measurement of heart activity

To record cardiac activity of mice during CSDS, electrocardiograms were recorded in cooperation with Prof. Dr. med. J. Schrickel and Dr. med. T. Beiert (Department of Internal Medicine II, University Hospital Bonn). Two weeks before starting the CSDS paradigm, mice were implanted with telemetric ECG-transmitters specifically made for small rodents. For implantation, mice were anaesthetised by i.p. injection of xylazin hydrochloride (16 mg/kg) and ketamin hydrochloride (100 mg/kg) and received s.c. injections of the analgesic carprofen (5 mg/kg) once during and for 3 days after the surgery. Anaesthetised mice were fixed on a warming plate (37°C) and eyes were protected from drying with eye ointment (Bepanthen®). After shaving the fur, a small incision of the skin was prepared between the scapulae and the transmitter implanted subcutaneously. Additionally, two electrode wires were implanted subcutaneously at the left-lateral and anterior thoracic wall. The wound was closed with prolene threads. After this type of surgery, mice behave normally with respect to circadian rhythm, feeding, and grooming. The wound is usually healed after approximately one week, but since mice were exposed to physical contact with CD1 aggressor mice during CSDS, a recovery period of two weeks was applied in this study. Mice were subjected to the standard CSDS paradigm and heart activity was recorded during the 10-day period (no recording during the 10 min of stress exposure). Measurements were performed by telemetric recording plates that are placed below the cages of the mice and thus do not require any further manipulation on the animal. The ECG recordings were analysed by Dr. med. Beiert. In ECG traces, ventricular and atrial depolarisation are represented by the QRS-complex and P-wave, respectively (see Figure 4).

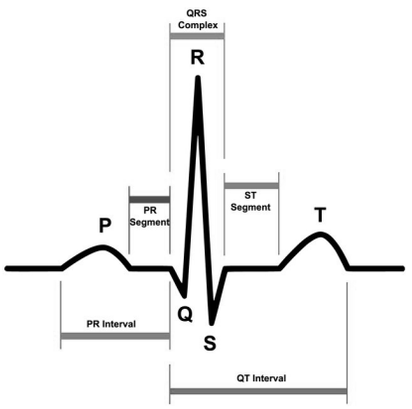

Figure 4. A typical electrocardiogram (ECG) trace of the cardiac cycle. The signal of one cardiac cycle (heartbeat) consists of three events: atrial depolarisation (P wave), ventricular depolarization (QRS complex), and repolarisation of ventricles (T wave). In a healthy heart, these events follow each other in an orderly progression. Figure from Elgendi et al. (2014).

2.3.5 Transcardial perfusion and tissue processing

For organ isolation, mice were deeply anaesthetised by isoflurane inhalation. Abdomen and thorax were opened and mice were transcardially perfused through the left ventricle with approximately 25 ml of ice-cold PBS at a flow rate of approximately 4 ml per min. In some cases, blood was withdrawn from the right ventricle before starting the perfusion. Organs were isolated and processed depending on the subsequent analysis.

For flow cytometric analysis, organs were transferred into PBS, FACS buffer, or corresponding medium and kept on ice until further processing. For RNA or protein isolation, organs were snap-frozen in isopentane on dry ice and stored at -80 °C until use. For immunohistochemistry, organs were post-fixed overnight in 4% paraformaldehyde (PFA) at 4 °C, followed by 2 - 3 days incubation in 30% (w/v) sucrose solution for cryoprotection. Organs were then snap-frozen in isopentane on dry ice and stored at -80 °C until use. For immunohistochemistry of bone marrow, tibias were post-fixed in 4% PFA for 3 days at 4 °C, decalcified for 4 days at 4 °C in EDTA solution (14% EDTA, 3% ammonium hydroxide, pH = 7.1), cryoprotected in 30% sucrose solution for 24 h at 4 °C, embedded in TissueTek, and stored at-80 °C until further processing.

2.3.6 Preparation of blood plasma

Blood was collected from the heart or the submandibular vein into EDTA-treated micro tubes (red caps) to prevent coagulation. Blood was centrifuged at 1000 - 2000 *x g* for 30 min at 4 °C. Plasma (supernatant) was transferred into a fresh tube, snap-frozen in liquid nitrogen and stored at -80 °C until analysis.

2.3.7 Isolation of cells for flow cytometry

2.3.7.1 Bone marrow

Bone marrow cells were isolated from tibias and/or femurs. The bone was cleared from surrounding tissue using scissors and gauze. The bone was opened on both ends and the bone

marrow flushed out into a fresh petri dish, using a 10 ml syringe with 27G cannula filled with 10 ml ice-cold PBS or FACS buffer. Single cell suspensions were prepared by pipetting cells up and down and transferring them into 50 ml tubes through a cell strainer (70 µm pore size). Petri dish and cell strainer were rinsed with FACS buffer to harvest all remaining cells. Cells were centrifuged (300 *x g*, 7 min, 4°C) and resuspended in FACS buffer. For gene expression analysis of bone marrow, cells were stored at-80°C as a pellet or dissolved in 500 µl TRIzol® reagent.

2.3.7.2 Brain

For isolation of CNS mononuclear cells (resident microglia and infiltrating peripheral cells), brains were harvested and stored in medium (DMEM, high glucose + 10% FCS) on ice. Brains (or one hemisphere) were placed in a petri dish, the cerebellum removed and the remaining tissue cut into small pieces using a scalpel. Tissue was further homogenised in 4 ml medium using a syringe with 20G cannula. When all samples were homogenised, 1 ml digestion mix (DNase I/Collagenase/Dispase) was added and samples incubated at 37°C for 45 min. Single cell suspensions were prepared and filtered through a cell strainer (70 µm pore size) into a 50 ml tube. Petri dish and cell strainer were rinsed with medium. Tubes were filled up to 50 ml with medium and centrifuged (300 *x g*, 7 min, 4°C). Separation of leukocytes from other cells and debris was performed using Percoll gradient centrifugation. Stock isotonic Percoll (SIP) was prepared by diluting 9 parts of Percoll with one part of 10x PBS. 40% and 80% Percoll solutions were prepared by diluting SIP with either medium (40%) or FACS buffer (80%). Cell pellets were resuspended in 8 ml of 40% Percoll, transferred to a 15 ml tube and carefully sublayered with 5 ml 80% Percoll using a Pasteur pipette. Cells were then centrifuged (2100 rpm, 25 min, RT, slow acceleration, without break). After centrifugation, myelin accumulated at the surface was carefully aspirated before collecting the leukocytes at the interface between 40% and 80% Percoll. Approximately 2 ml were collected, transferred into a 50 ml tube, washed with 20 ml medium, and centrifuged (300 *x g*, 7 min, 4°C). Cells were resuspended in 1 ml medium and transferred into FACS tubes through gauze to remove remaining fat and cell doublets. Cells were washed once more with medium.

2.3.7.3 Spleen

Spleens (or half spleens) were placed in a petri dish and cells flushed out by injecting 1 ml digestion mix (DNase I/Collagenase type VIII). Tissue was cut into small pieces before adding additional 4 ml or 8 ml digestion mix for one half or one full spleen, respectively. Tissue was digested at 37°C for 45 min and then homogenised with a syringe to prepare a single cell suspension. Homogenates were filtered through a cell strainer (70 µm pore size) into a 50 ml tube and petri dish and cell strainer were rinsed with FACS buffer. The cell suspension was filled up to 25 or 50 ml with FACS buffer, centrifuged (300 *x g*, 7 min, 4°C), and washed once more with FACS buffer. Alternatively, cells were isolated from spleens without digestion by directly mincing the tissue through the cell strainer using the back of a 10 ml syringe.

2.3.8 Cell culture of splenocytes

Isolated splenocytes were resuspended in splenocyte culture medium (RPMI 1640, supplemented with 10% FCS, 1% penicillin/streptomycin, 1% L-glutamine), counted in a Neubauer chamber, and seeded in 12-well plates at a density of 1 x 10^6 cells/ml. Cells were either untreated or stimulated with 100 – 1000 ng/ml lipopolysaccharide (LPS) from *Escherichia coli O127:B8* overnight. After overnight culture, cells and medium were collected and centrifuged (300 *x g*, 5 min, 4°C). Supernatants were transferred to a fresh tube, snap-frozen in liquid nitrogen and stored at -20°C. Cells were resuspended in FACS buffer and stained for flow cytometric analysis.

2.3.9 Flow cytometry/fluorescence-activated cell sorting (FACS)

Flow cytometry is a technique to measure physical and chemical properties of thousands of individual cells or particles, commonly used for the analysis of immune cells. The technique is based on three components – fluidics, optics, and electronics. Cells are suspended in a fluid and hydrodynamically focused in a stream that allows cells to pass a laser beam one at a time. The light scattered by the cell passing the laser is detected by specific detectors and corresponds to physical properties of the cell, such as cell size (detected by forward scatter, FSC) and internal complexity/granularity (detected by side scatter, SSC). Furthermore, fluorescent staining of cell surface markers is used to identify cells based on their specific pattern of marker expression or to quantify the expression of surface proteins. By using fluorophores with different excitation/emission spectra and appropriate lasers and detectors, many markers can be measured simultaneously. In this study, the flow cytometer (BD FACSCanto II) was equipped with three lasers for excitation and eight filters for detection of different emission wavelengths.

Flow cytometry was used to analyse cell surface marker expression on immune cells from whole blood or cells isolated from bone marrow, spleen, and brain. To ensure cell viability, cells were kept at 4°C during the whole procedure. Cells were transferred to FACS tubes and filtered through gauze to exclude cell aggregates. Cells were centrifuged (300 *x g*, 7 min, 4°C) and supernatants removed. Cell pellets were resuspended in 50 µl Fc-block (anti-mouse CD16/32), diluted 1:100 in FACS buffer, to block unspecific binding of antibodies to Fc-receptors. After 5 min incubation, 50 µl primary antibody solution was added and incubated for 30 min in the dark. Antibodies and corresponding dilutions are listed in the table below. Cells were washed with 3 ml FACS buffer, followed by centrifugation. Cells were then incubated with 100 µl secondary antibody solution for 15 min. After another washing step, erythrocytes were lysed in 1 - 3 ml 1x RBC-lysis buffer for 5 min at RT (depending on the tissue of origin). Cells were washed once more and dead cells stained using DAPI or DRAQ7™. To avoid fading of the fluorescent signal, cells were kept in the dark whenever possible. Flow cytometric analysis was performed using the BD FACSCanto II and the BD FACSDiva Software. Resulting files were analysed using FlowJo version 10.0.6 (Tree Star Inc.).

List of antibodies used for flow cytometry

Antigen	Conjugate	Host	Clone	Dilution	Company	Catalog #
CD115 (CSF-1R)	PerCP/Cy5.5	Rat	AFS98	1:100	BioLegend	135526
NK1.1	Biotin	Rat	PK136	1:200	BioLegend	108704
TER-119	Biotin	Rat	TER-119	1:200	BioLegend	116204
Ly-6G	Biotin	Rat	1A8	1:200	BioLegend	127604
Ly-6G	PE/Cy7	Rat	1A8	1:200	BD	560601
CD3	Biotin	Rat	17A2	1:200	BioLegend	100244
CD45	BV 510	Rat	30-F11	1:200	BioLegend	103137
CD11b	PE/Cy7	Rat	M1/70	1:200	BioLegend	101216
CD11b	FITC	Rat	M1/70	1:200	BD	553310
Ly-6C	APC	Rat	HK1.4	1:200	BioLegend	128016
CD19	APC/Cy7	Rat	1D3	1:200	BD	557655
CCR2 (CD192)	BV 421	Rat	SA203G11	1:200	BioLegend	150605
MERTK (Mer)	PE	Rat	2B10C42	1:400	BioLegend	151505
MHCII (I-A/I-E)	PerCP/Cy5.5	Rat	M5/114.15.2	1:200	BioLegend	107625
CD11c	FITC	Hamster	N418	1:200	BioLegend	117306
CD40	PE	Rat	1C10	1:200	eBioscience	12-0401
Streptavidin	APC/Cy7			1:200	BioLegend	405208

2.3.10 RNA-isolation

Total RNA from cells or frozen tissue was extracted using TRIzol® reagent. Cells were resuspended in 0.5 – 1 ml TRIzol® and homogenated by vortexing. Frozen tissue was transferred into 2 ml tubes containing 1.4 mm zirconium oxide beads and homogenised in TRIzol® (1 ml TRIzol®/100 mg tissue) by vigorous shaking in a tissue homogeniser. After centrifugation (12,000 *x g*, 10 min, 4°C), the homogenate was transferred into a fresh tube. For phase separation, 1-bromo-3-chloropropane (BCP) (1:5) was added. After vortexing for 30 s and 3 min incubation at RT, samples were centrifuged (12,000 *x g*, 10 min, 4°C) and the RNA containing aqueous phase transferred into a fresh tube. RNA was precipitated by isopropanol (1:1). Samples were mixed, incubated at RT for 10 min and centrifuged at 12,000 *x g*, 10 min, 4°C. The supernatant was discarded and the pellet was washed twice with 500 µl 75% EtOH. RNA was dried at 50°C for 5 – 10 min and dissolved in 15 – 50 µl RNase-free water. After dissolving, RNA was digested with approximately 1 U of recombinant DNase I per 1 µg of RNA at 37°C for 20 min to remove any remaining genomic DNA. The reaction was stopped by heat inactivation of DNase at 75°C for 10 min. Concentration and purity of RNA was determined by optical density (OD) measurements at 260 and 280 nm, using a NanoDrop 1000. The absorbance of 1 unit at 260 nm is equivalent to a RNA concentration of 40 µg/ml. Purity of RNA was confirmed by A_{260}/A_{280} values close to 2. RNA was stored at-80°C until further processing.

2.3.11 Reverse transcription PCR

Messenger RNA (mRNA) was reverse transcribed into complementary DNA (cDNA) using SuperScript™ II Reverse Transcriptase. Up to 3 µg of RNA in a total volume of 11 µl RNAse-free H_2O were used per sample. The reaction conditions and cycling parameters are summarised in the table below. After reverse transcription, cDNA was diluted appropriately and stored at -20°C.

Reaction and cycling parameters for cDNA synthesis

Reaction		Cycling parameters	
11 µl	RNA (0.5 – 3 µg)		
+ 1 µl	Oligo(dT) primers		
+ 1 µl	dNTP mix (10mM)		
		Temp.	**Time**
		65°C	5 min
		4°C	3 min
+ 4 µl	5 x first strand buffer		
+ 2 µl	DTT (0.1 M)		
		42°C	2 min
		4°C	3 min
+ 1 µl	SuperScript™ II		
		42°C	50 min
		70°C	15 min
		4°C	∞

2.3.12 Quantitative real-time PCR (qPCR)

Expression levels of mRNA were analysed using TaqMan® Gene Expression Master Mix and Gene Expression Assays. TaqMan® gene expression analysis is one option for real-time qPCR using the fluorescence resonance energy transfer (FRET) technology. FRET is based on an energy transfer between two fluorophores. For qPCR, a short gene-specific oligonucleotide probe, fluorescently labelled at the 5' end (FAM™ or VIC®) and quenched by a non-fluorescent tag (MGB = minor groove binder) at the 3' end, is added to the cDNA sample together with an unlabelled pair of primers. Due to sequence complementarity, the probe hybridises with the target cDNA and is cleaved during the PCR reaction through the 5' - 3' exonuclease activity of the polymerase. The fluorescent signal is therefore no longer quenched and increases with each PCR cycle, in proportion to the amount of available cDNA. For relative quantification of gene expression, the expression level of the target gene is normalised to the expression level of a constitutively expressed reference gene. In this study, hypoxanthine-guanine phosphoribosyltransferase (*Hprt*) was used as a reference gene. Expression of target and reference genes was either measured within the same reaction, using two different fluorescent dyes (VIC® + FAM™, dual colour analysis), or measured in separate reactions (FAM™, mono colour analysis). Reactions were pipetted in triplicates into 384-well plates by a JANUS® automated workstation. qPCR was performed using the LightCycler 480 and parameters listed in the table below. Data was analysed

using the $2^{-\Delta\Delta Cq}$ method (Livak and Schmittgen, 2001). The quantification cycle (C_q), i.e. the cycle at which fluorescence from amplification exceeds the background fluorescence, was determined for each gene and ΔC_q calculated as the difference between the C_q of the target gene and the C_q of the reference gene. Relative expression levels were calculated as $2^{-\Delta Cq}$. For calculating the fold change from control samples, data was normalised to the mean $2^{-\Delta Cq}$ of the respective control group.

Reaction and cycling parameters for qPCR

Reaction (dual colour analysis)				**Reaction (mono colour analysis)**			
4 µl	cDNA			4 µl	cDNA		
5 µl	TaqMan® Gene Expression Master Mix			5 µl	TaqMan® Gene Expression Master Mix		
0.5 µl	TaqMan® Assay for target gene (dye: FAM-MGB)			0.5 µl	TaqMan® Assay for target or reference gene (dye: FAM-MGB)		
0.5 µl	TaqMan® Assay for reference gene (dye: VIC-MGB)			0.5 µl	H_2O		
Cycling parameters				**Cycling parameters**			
	Temp.	**Time**	**Quantification**		**Temp.**	**Time**	**Quantification**
1x	95°C	10 min	None	1x	95°C	10 min	None
45x	95°C 60°C	15 s 1 min	Dual colour (FAM + VIC)	45x	95°C 60°C	15 s 1 min	Mono colour (FAM)
1x	4°C	∞	None	1x	4°C	∞	None

List of TaqMan® Gene Expression Assays used for qPCR

Target mRNA	**TaqMan® assay ID**	**Target mRNA**	**TaqMan® assay ID**
Arg1	Mm00475988_m1	Hprt	Mm00446968_m1
Ccl2	Mm00441242_m1	Il10	Mm99999062_m1
Cnr1	Mm00432621_s1	Il1b	Mm01336189_m1
Cnr2	Mm00438286_m1	Il6	Mm0446190_m1
Fkbp5	Mm00487406_m1	Mgll	Mm00449274_m1
Crh	Mm01293920_s1	Napepld	Mm00724596_m1
Crhr1	Mm00432670_m1	Nos2a	Mm00440485_m1
Faah	Mm00515684_m1	Nr3c1	Mm00433832_m1
Dagla	Mm00813830_m1	Ptgs2	Mm00478374_m1
Daglb	Mm00523381_m1	Tnf	Mm00443258_m1

2.3.13 Enzyme-linked immunosorbent assay (ELISA)

Levels of cytokines/chemokines IL-1β, IL-6, TNFα, and CCL2 in blood plasma or cell culture supernatants were determined using indirect sandwich ELISAs. ELISAs are antibody-based assays to detect and quantify proteins or other small molecules. In indirect sandwich ELISAs, the target protein is captured by antibodies immobilised on a plate and subsequently detected by a second

antibody. The detection antibody is then bound by a secondary antibody that is coupled to an enzyme that can catalyse a colour reaction, such as horseradish peroxidase (HRP). The amount of target protein thus correlates with the intensity of the colour reaction and can be quantified by applying appropriate standard curves. Respective ELISA assays were used according to the manufacturer's instructions. Briefly, Nunc MaxiSorp flat-bottom 96-well plates were coated with 50 µl corresponding capture antibodies, diluted 1:250 in coating buffer, overnight at 4°C. The next day, plates were washed 3 - 5 times with 200 µl wash buffer per well, followed by blocking with 100 µl assay diluent for 1 h at RT. After blocking, 50 µl of standard and samples were incubated for 2 h at RT. Samples were tested in duplicates and diluted in assay diluent, if necessary. After washing, 50 µl of corresponding detection antibodies (coupled to biotin), diluted 1:250 in assay diluent, were added and incubated for 1 h at RT. After another washing step, 50 µl of avidin-HRP, diluted 1:250 in assay diluent, were incubated for 30 min at RT. Plates were washed again, followed by 15 min incubation with 50 µl TMB substrate solution. The reaction was stopped by adding 25 µl 1 M H_3PO_4. Absorbance was measured at 450 nm using a microplate reader.

2.3.14 Measurement of corticosterone

Plasma and faecal CORT levels were measured using the DetectX® Corticosterone Enzyme Immunoassay (EIA) Kit. Plasma samples were incubated with dissociation reagent provided by the kit and diluted with assay buffer. To extract steroids from frozen faeces (stored at-80°C), samples were dried for 2 h at 37°C. Subsequently, 200 – 300 mg of dried faeces were transferred into a 5 ml microcentrifuge tube and 1 ml 100% EtOH per 100 mg of solid was added. For extraction, samples were incubated for 30 min at RT in a shaking incubator. Subsequently, samples were centrifuged at 4500 rpm for 15 min and 600 µl of the supernatant was transferred into a 1.5 ml microcentrifuge tube. Samples were evaporated to dryness in a SpeedVac for 1 h at 35°C. Extracted samples were kept at -20°C overnight. On the next day, samples were dissolved in 100 µl EtOH, followed by addition of 400 µl assay buffer, and vortexed and incubated for 5 min at RT. The vortexing and incubation steps were repeated for three times. Afterwards, samples were diluted 1:2 with assay buffer, since the final EtOH concentration should be lower than 5% for the measurements. The CORT immunoassay was performed according to the manufacturer´s protocol. After incubation of all kit reagents for 30 min at RT, the CORT standards were prepared with a concentration range of 78.128 pg/ml to 10000 pg/ml. Subsequently, 50 µl of diluted samples or standards were pipetted in duplicates into the wells of a clear microtiter plate coated with an antibody to capture sheep antibodies, followed by 25 µl DetectX® Corticosterone (Peroxidase-) Conjugate and 25 µl DetectX® Corticosterone Antibody. After 1 h shaking at RT, wells were aspirated and washed 4 times with 300 µl wash buffer, followed by 100 µl TMB substrate per well. After 30 min incubation at RT, 50 µl stop solution was added to each well. Absorbance was measured at 450 nm using a microplate reader.

2.3.15 Immunohistochemistry (IHC), image acquisition and analysis

2.3.15.1 Brain

2.3.15.1.1 IBA1, ICAM-1, CD45 staining

For microglia analysis, frozen brain hemispheres were cut into coronal 60 µm free-floating sections and stored in PBS + sodium-azide at 4°C. For immunohistochemical staining, sections were blocked in 10% normal donkey serum (NDS) in PBS-T 0.5% for 4 h, followed by overnight incubation at 4°C with primary antibodies, diluted in 5% NDS in PBS-T 0.1%. Antibodies used were rabbit anti-ionized calcium-binding adapter molecule 1 (IBA1) (1:1000), goat anti-intercellular adhesion molecule 1 (ICAM-1) (1:1000), and rat anti-CD45 (1:500). Negative controls were incubated in diluent without primary antibody. After antibody incubation, sections were washed three times in PBS for 10 min. After washing, sections were stained with secondary antibodies, diluted 1:1000 in 5% NDS in PBS-T 0.1%. Secondary antibodies used were donkey anti-rabbit AlexaFluor®594, donkey anti-goat AlexaFluor®647, and donkey anti-rat AlexaFluor®488. For details on antibodies, see table below. Nuclei were stained with DAPI (0.1 µg/ml in PBS) for 15 min at RT, followed by another washing step. Sections were shortly washed in MilliQ H_2O and embedded in Fluoromount-G®. Sections were covered by cover glasses of 170± µm (No. 1.5H) and edges closed with nail polish. Stained sections were stored at 4°C in the dark.

2.3.15.1.2 IBA1, TMEM119, CD68 staining

Free-floating sections (see above) were permeabilised in TBS-T 0.5% for 30 min, followed by two 10 min wash steps in TBS. Sections were then incubated in citrate buffer pH = 6 for 20 min at 65°C for heat-mediated antigen retrieval. Sections were washed again and blocked in 10% NDS in TBS-T 0.5% for 2 h, followed by 48 h incubation at 4°C with primary antibodies, diluted in 5% NDS in TBS-T 0.25%. Antibodies used were goat anti-IBA1 (1:1000), rabbit anti-Transmembrane protein 119 (TMEM119) (1:1000, 0.614 µg/ml), and rat anti-CD68 (1:1000). Negative controls were incubated in diluent without primary antibody. After antibody incubation, sections were washed three times in TBS-T 0.25% for 15 min. After washing, sections were stained with secondary antibodies, diluted 1:1000 in 5% NDS in TBS-T 0.25%. Secondary antibodies used were donkey anti-rabbit AlexaFluor®594, donkey anti-goat AlexaFluor®647, and donkey anti-rat AlexaFluor®488. For details on antibodies, see table below. Nuclei were stained with DAPI (0.1 µg/ml in PBS) for 15 min at RT, followed by another washing step. Sections were shortly washed in MilliQ H_2O and embedded in Fluoromount-G®. Sections were covered by cover glasses of 170± µm (No. 1.5H) and edges closed with nail polish. Stained sections were stored at 4°C in the dark.

List of antibodies used for immunohistochemistry

Antigen	Conjugate	Host	Clone	Dilution	Company	Catalog #
CD45	unconjugated	Rat	IBL-3/16	1:500	abcam	ab23910
CD68	unconjugated	Rat	FA-11	1:1000	AbD Serotec	MCA1957
IBA1	unconjugated	Rabbit	Polyclonal	1:1000	Wako	019-19741
IBA1	unconjugated	Goat	Polyclonal	1:1000	abcam	ab5076
ICAM-1/CD54	unconjugated	Goat	Polyclonal	1:1000	R&D systems	AF796
TH	unconjugated	Rabbit	Polyclonal	1:1000	abcam	ab112
TMEM119	unconjugated	Rabbit	28-3	1:1000	abcam	ab234501
Anti-rabbit IgG	Alexa Fluor® 594	Donkey		1:1000	Invitrogen	A21207
Anti-rat IgG	Alexa Fluor® 488	Donkey		1:1000	Invitrogen	A21208
Anti-goat IgG	Alexa Fluor® 647	Donkey		1:1000	Invitrogen	A21447

2.3.15.1.3 Image acquisition

Sections were imaged using a Leica TCS SP8 confocal microscope. For excitation of fluorophores, the microscope was equipped with a UV diode (405 nm), a pulsed argon ion laser with several wavelengths (458, 476, 488, 514 nm), a yellow-green diode-pumped solid-state (DPSS) laser (561 nm), a yellow helium-neon (HeNe) laser (594 nm), and a red HeNe laser (633 nm). For detection of emitted light, two photomultiplier tubes (PMT) and two hybrid photodetectors (HyD) were available. DAPI was excited at 405 nm, AlexaFluor®488 at 488 nm, AlexaFluor®594 at 594 nm, and AlexaFluor®647 at 633 nm.

For overview pictures, images were acquired with a 20x objective (numerical aperture (NA) = 0.75), pinhole = 1 AU, 0.28 µm/pixel. Z-stacks of 9 µm were acquired at a step size (voxel depth) of 3.0 µm. Two - three sections were imaged per animal for each region. For higher resolution, images were acquired with a 40x objective (NA = 1.1), pinhole = 1 AU, 0.19 µm/pixel. Five single plane images were acquired within the 60 µm section at a distance of 5 µm. Two - three sections were imaged per animal for each region. For three-dimensional (3D) morphological analysis of microglia, z-stacks of 40 - 50 µm were acquired using the 63x objective (NA = 1.2), pinhole = 1 AU, voxel depth 0.5 µm, 0.18 µm/pixel. Two z-stacks were acquired per animal per region.

2.3.15.1.4 Image analysis

Images were analysed using Fiji (ImageJ 2.0.0). For measurement of IBA1-positive (IBA1+) area, an appropriate threshold was applied to exclude background signal. IBA1+ area was quantified as area fraction of either the whole image or within a region of interest (ROI). In the same images, IBA1+ cells were manually counted and cell number normalised to the area of the ROI. Similarly, ICAM-1+ area was quantified. To determine neurovascular ICAM-1 expression, a threshold was applied that excluded ICAM-1 immunoreactivity on microglia, which was considerably lower than neurovascular ICAM-1. To measure ICAM-1, CD68, and TMEM119 immunoreactivity on microglia,

IBA1+ area was determined as described above and used as a ROI. ICAM-1+, CD68+, or TMEM119+ area and mean grey intensity were then measured within the IBA1+ ROI.

For 3D analysis of microglia, mages were pre-processed using ImageJ functions for smoothing and background subtraction (rolling ball). Images were then analysed using automated custom-written ImageJ plug-ins, written by Jan Niklas Hansen (Institute of Innate Immunity, University of Bonn) (Plescher et al., 2018). Binary images were obtained by application of an intensity threshold, which was determined in a 50% downscaled maximum projection of the original z-stack image using ImageJ's implemented threshold algorithm "MinError." Individual cells were automatically traced in the z-stack by overlap. Particles smaller than 12,000 voxel were removed from the image. Correct tracing of cells was visually verified and incorrectly traced cells (e.g. incomplete or clustered) excluded from analysis. Surface area, volume, convex hull, and ramification index were automatically reconstructed based on the size-filtered binary image. The microglial ramification index is the ratio of cell surface area and surface area of a perfect sphere with the same volume as the analysed cell and thus calculated using the equation: cell surface area/(4π x ((3 x cell volume)/(4π))$^{2/3}$. The ramification index is a unit-free parameter for the complexity of the cellular shape. A ramification index of 1 corresponds to a perfectly round cell without processes. The more the cell differs from a perfectly round shape, i.e. the more branches the cell possesses, the higher is its 3D ramification index. For quantification of branch number, junctions, and tree length, skeleton parameters were obtained by Gauss-filtering (sigma = 0.5) of the size-filtered binary image and subsequent skeleton generation and analysis using the plugins by Arganda-Carreras et al. (2010). On average, 10 cells were analysed per animal, giving a total of 60 – 90 cells per group.

2.3.15.2 Bone marrow

2.3.15.2.1Tissue preparation and IHC staining

Frozen, fixed and decalcified bones were cut into 10 µm sections using a cryostat and stored at -80°C until further processing. To analyse SNS innervation of the bone marrow, tyrosine hydroxylase (TH) positive (TH+) nerve endings were stained. Therefore, sections were washed in PBS for 5 min, permeabilised in PBS-T 0.5% for 30 min, followed by washing in PBS (3x 5 min) and incubation in blocking solution (5% NGS in PBS-T 0.025%) for 1 - 2 h. Sections were then incubated with primary antibody rabbit anti-TH (1:1000), diluted in antibody solution (2.5% NGS in PBS-T 0.025%), overnight at 4°C. On the next day, sections were washed (3x 10 min), followed by 2 h incubation with secondary antibody goat anti-rabbit AlexaFluor®594 (1:1000). Nuclei were stained with DAPI (0.1 µg/ml in PBS) for 10 min. After washing in PBS (3x 10 min), sections were washed in MilliQ H_2O once and embedded in Fluoromount-G®. Sections were covered by cover glasses of 170± µm (No. 1.5H) and edges closed with nail polish. Stained sections were stored at 4°C in the dark.

2.3.15.2.2 Image acquisition

Bone marrow sections, stained for TH+ nerve endings, were imaged using a Leica TCS SP8 confocal microscope. Z-stacks of 10 µm were acquired using the 63x objective (NA = 1.2), pinhole = 1 AU, voxel depth 1 µm, 0.10 µm/pixel). Next to TH and DAPI, a transmitted light picture was taken for identification of blood vessels within the bone. Five – seven images were acquired per animal.

2.3.15.2.3 Image analysis

Images were analysed using Fiji (ImageJ 2.0.0). For the analysis of bone marrow SNS innervation, maximum projections of z-stacks (TH channel) were used. Signal in the TH channel was thresholded to limit the analysis to TH+ nerve endings. Within this threshold, TH immunoreactivity was measured as mean grey intensity.

2.4 Statistical analysis

Statistical analysis was performed using the GraphPad Prism 6 software. Datasets with only two groups were analysed using unpaired Student's t-test. Datasets containing more than two groups, but only one independent variable (e.g. stress) were analysed by one-way analysis of variance (ANOVA). Datasets containing two independent variables (e.g. stress and genotype) were analysed using two-way ANOVA. The ANOVA was considered significant at a 95% confidence interval ($p < 0.05$). P-values between 0.05 and 0.1 were considered a tendency. Results for main effects and interactions in the two-way ANOVA are stated in the corresponding figure (significant effects are indicated by + for stress effect, * for genotype effect, # for stress x genotype interaction). Detailed results (F ratio and p-value) for relevant main effects are stated in the figure legends. The ANOVA was followed by Bonferroni *post-hoc* comparisons. Non-parametric datasets were analysed using the Kruskal-Wallis test, followed by Dunn's multiple comparisons. If not stated otherwise, data are presented as mean values ± standard error of the mean (SEM). Significances in *post-hoc* comparisons are depicted in the graphs (+ for $p < 0.05$ compared to controls of the same genotype; * for $p < 0.05$ compared to *Cnr1*$^{+/+}$ mice of the same group). Correlation analysis was performed either using Pearson correlation (parametric) or Spearman correlation (non-parametric). The correlation was considered significant at a 95% confidence interval ($p < 0.05$).

3 Results

3.1 Standard chronic social defeat stress (CSDS)

In the first sets of experiments, *Cnr1*$^{+/+}$ and *Cnr1*$^{-/-}$ mice were exposed to a standard protocol of CSDS – a common rodent model of social stress and based on a resident-intruder paradigm. In brief, male *Cnr1*$^{+/+}$ and *Cnr1*$^{-/-}$ mice were single-housed for two weeks before starting the CSDS paradigm, during which mice were exposed to 5 – 10 min of daily defeat sessions by a CD1 aggressor mouse on 10 consecutive days. Standard CSDS experiments were performed in four separate cohorts of mice, with slight adaptations to the experimental setup, such as a different timeline for behavioural tests and organ retrieval. For clarity, results of behavioural analysis will only be shown for the last two cohorts of mice, where the experimental setup most closely resembled later experiments with mild CSDS (see chapter 3.2). The respective experimental setup and timeline for behavioural analysis is shown below (Figure 5). Experimental setups and behavioural data for the other two cohorts can be found in the appendix. Results for physiological and molecular effects of standard CSDS shown here are derived from different cohorts of mice. When applicable, data was pooled from different cohorts (e.g. for body weight).

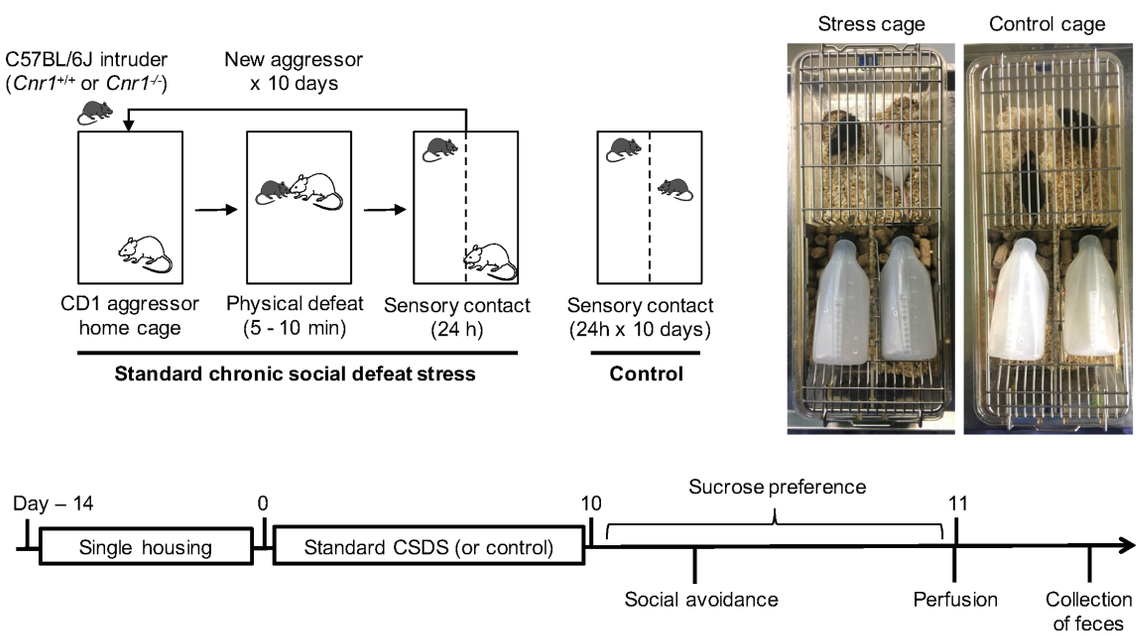

Figure 5. Experimental setup for standard CSDS. C57BL/6J intruder mice were single-housed for two weeks prior to stress exposure. During CSDS, male *Cnr1*$^{+/+}$ or *Cnr1*$^{-/-}$ mice were individually introduced into the home cage of a CD1 aggressor mouse. Mice were allowed to physically interact for 5 – 10 minutes, during which the intruder is exposed to repeated bouts of social defeat by the CD1 aggressor. After the physical defeat, mice were separated by a perforated Plexiglas wall to allow sensory, but not physical contact for the following 24 hours. C57BL/6J intruder mice were exposed to a new CD1 aggressor for 10 consecutive days. Control mice were housed in pairs of two, unfamiliar to each other and separated by a perforated Plexiglas wall. Combinations of control mice were not alternated during the 10-day period. After standard CSDS, social avoidance behaviour and sucrose preference was analysed. One day after the last stress exposure, mice were sacrificed and organs harvested for analysis.

3.1.1 Increased mortality of *Cnr1*$^{-/-}$ mice during standard CSDS

CSDS consists of physical defeat sessions that are highly demanding for the defeated mice. Occasionally, this protocol results in injuries due to physical attacks of the CD1 mouse, however this is rare and leads to the direct exclusion of the injured mouse. *Cnr1*$^{-/-}$ mice are known to be stress-sensitive and to have an increased spontaneous mortality rate (Zimmer et al., 1999). Surprisingly, nearly 50% of *Cnr1*$^{-/-}$ mice died during the first days of standard CSDS or had to be excluded from the experiments because they reached exclusion criteria (e.g. loss of more than 20% of body weight). In contrast, mortality rates of *Cnr1*$^{+/+}$ mice reached only 10%. Deaths usually occurred during the first days of stress exposure and mice died without any signs of injuries. In most, but not all cases the death was preceded by substantial body weight loss. Mice never died during the 10-minute stress exposure, but rather during the following period of sensory contact. Due to the high mortality rate, the group size of stressed *Cnr1*$^{-/-}$ for behavioural and molecular analysis after standard CSDS was lower than for *Cnr1*$^{+/+}$ mice (seven *Cnr1*$^{+/+}$, four *Cnr1*$^{-/-}$ mice).

3.1.2 Social avoidance after standard CSDS

The social avoidance test is commonly used to determine the susceptibility of mice to CSDS. In the first trial of the test, movements of mice are recorded in the presence of an empty metal cage (no target), while in the second trial the cage contains an unknown CD1 aggressor (target) (Figure 6A). Thereby, behavioural changes specifically induced by the presence of the CD1 mouse can be distinguished from generally altered exploratory behaviour. The social interaction (SI) ratio is calculated as the ratio between interaction time with a CD1 mouse and an empty cage. SI ratios higher than one are commonly used as a threshold for stress resilience (Golden et al., 2011).

After standard CSDS, all stressed mice showed SI ratios below 0.5 and were thus classified as stress susceptible (Figure 6B). Statistical analysis showed a clear stress effect that was significant in *post-hoc* comparisons for both genotypes. Detailed analysis of the mice's movement revealed that all mice behaved rather similarly when no CD1 target was present (Figure 6 left panel). There was no difference in the time spent in the interaction zone after stress, but a tendency for a genotype effect (Figure 6C). Furthermore, a tendency for a stress effect as well as stress x genotype interaction was detected for the time spent in corners (Figure 6D). *Post-hoc* comparison showed that these effects were due to stressed *Cnr1*$^{-/-}$ mice spending more time in corners compared to control *Cnr1*$^{-/-}$ mice. Stress had a significant effect on locomotion, slightly reducing total distances moved during the first trial (Figure 6E). In the second trial, movements of mice were traced in the presence of an CD1 target (Figure 6 right panel). Highly significant stress effects were seen for interaction time (Figure 6F) and time spent in corners (Figure 6G). For both genotypes, stress significantly reduced interaction with the CD1 target and increased the time spent in corners. Furthermore, stress caused a significant reduction of locomotion in *Cnr1*$^{-/-}$ mice (significant stress effect and stress x genotype interaction) (Figure 6H).

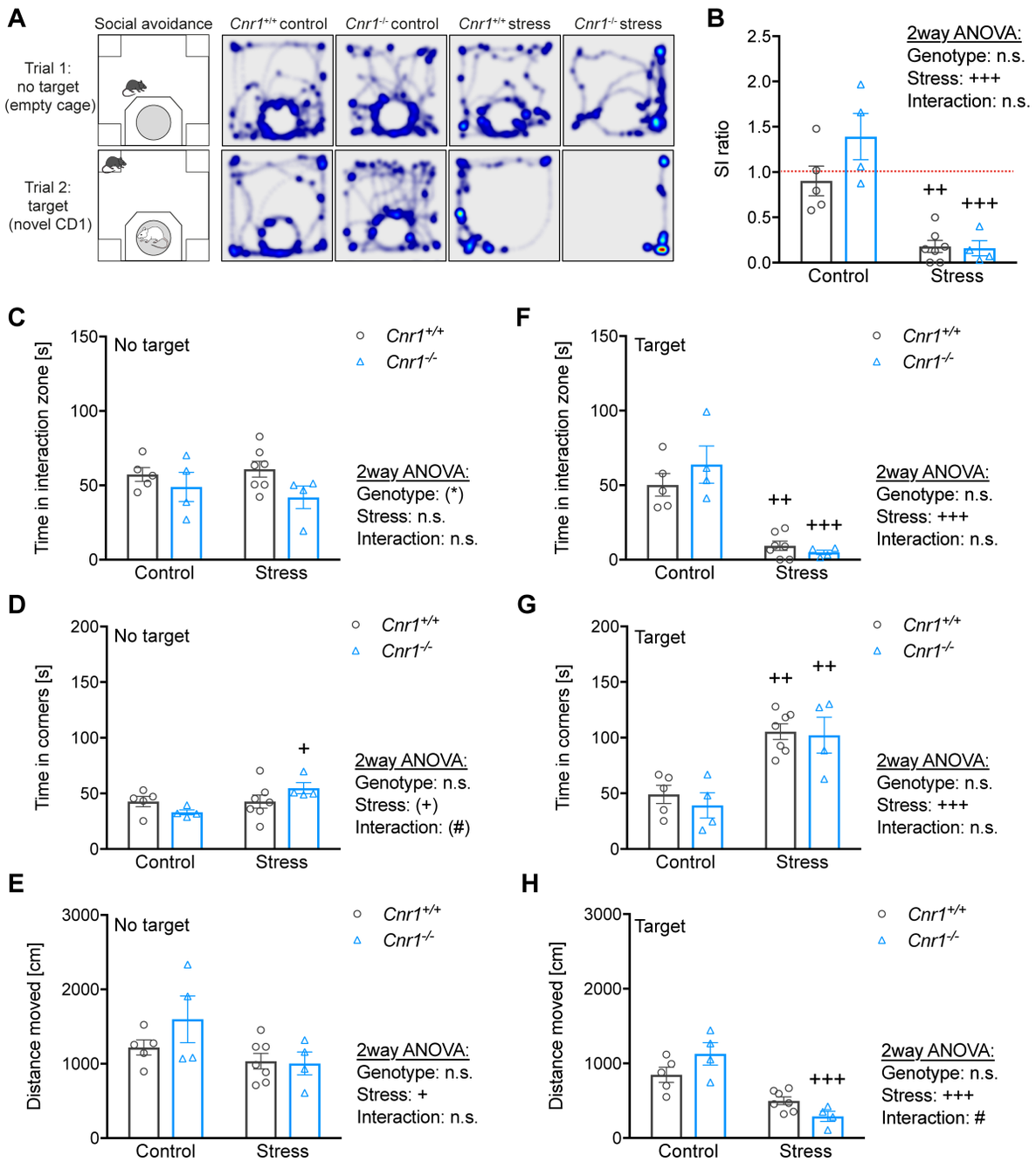

Figure 6. Standard CSDS induces strong social avoidance behaviour in both *Cnr1*$^{+/+}$ and *Cnr1*$^{-/-}$ mice. Mice were subjected to the social avoidance test after standard CSDS. **(A)** Experimental setup and representative heatmap visualization of movement of mice during the two trials of the test. First trial (no target): the cage on one side of the arena is empty. Second trial (target): cage containing an unfamiliar CD1 aggressor mouse. After all mice had completed the first trial, empty cages were replaced by cages with CD1 mice. **(B)** Social interaction (SI) ratio, calculated from the interaction time in the first (C) and second trial (F). A ratio > 1 (red line) is usually used to identify stress-resilient mice (stress: $F_{(1,16)} = 46.10$, $p < 0.0001$). **(C - E)** Quantification of the first trial of the test (no target). **(C)** Interaction with empty cage (genotype: $F_{(1,16)} = 4.09$, $p = 0.060$). **(D)** Time spent in any of the four corners (stress: $F_{(1,16)} = 3.93$, $p = 0.065$; stress x genotype interaction: $F_{(1,16)} = 4.02$, $p = 0.062$). **(E)** Locomotion, total distance moved (stress: $F_{(1,16)} = 5.39$, $p = 0.034$). **(F - H)** Quantification of the second trial (target). **(F)** Interaction with an unfamiliar CD1 aggressor (stress: $F_{(1,16)} = 54.43$, $p < 0.0001$). **(G)** Time spent in corners (stress: $F_{(1,16)} = 33.43$, $p < 0.0001$). **(H)** Total distance moved (stress: $F_{(1,16)} = 41.69$, $p < 0.0001$; stress x genotype interaction: $F_{(1,16)} = 7.07$, $p = 0.017$). Data was analysed by 2way ANOVA, followed by Bonferroni *post-hoc* comparisons. For genotype effects (compared to *Cnr1*$^{+/+}$ of the same group) * $p < 0.05$, ** $p < 0.01$, *** $p < 0.001$. For stress effects (compared to control of the same genotype) + $p < 0.05$, ++ $p < 0.01$, +++ $p < 0.001$.

3.1.3 Anhedonia after standard CSDS

After ten days of standard CSDS, hedonic behaviour was measured in the sucrose preference test. Mice usually prefer sweet solutions and a reduction in this preference is associated with anhedonia, the inability to experience pleasure. Quantification of the fluid consumption after standard CSDS showed that stress had a significant effect on sucrose preference, calculated as the percentage of sucrose consumed in relation to total fluid consumption (Figure 7A). A tendency for a genotype effect was observed as well. *Post-hoc* comparisons revealed no significant differences between the groups, probably due to small group sizes. Total fluid intake was significantly affected by stress, with stressed *Cnr1*$^{+/+}$ mice drinking significantly more compared to their control group (Figure 7B).

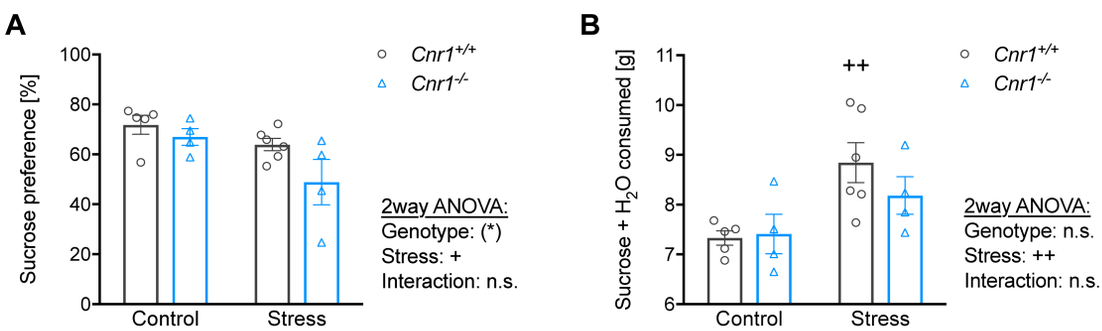

Figure 7. Standard CSDS induces mild anhedonia and increases fluid intake. Anhedonia was analysed after standard CSDS using the sucrose preference test. **(A)** Sucrose preference, i.e. the percentage of sucrose solution consumed in relation to the total fluid intake (stress: $F_{(1,15)}$ = 7.31, p = 0.016; genotype: $F_{(1,15)}$ = 4.31, p = 0.056). **(B)** Total fluid intake over 24 h (stress: $F_{(1,15)}$ = 10.27, p = 0.006). Data was analysed by 2way ANOVA, followed by Bonferroni *post-hoc* comparisons. For genotype effects (compared to *Cnr1*$^{+/+}$ of the same group) * p < 0.05, ** p < 0.01, *** p < 0.001. For stress effects (compared to control of the same genotype) + p < 0.05, ++ p < 0.01, +++ p < 0.001.

3.1.4 Physiological changes after standard CSDS

Body weight was monitored throughout the standard CSDS paradigm. Overall, *Cnr1*$^{-/-}$ mice were leaner than *Cnr1*$^{+/+}$ mice, which was independent from stress (Figure 8A). On average, stressed mice lost approximately 10 - 20% body weight (1 - 2 g) during the first days of stress exposure, but recovered completely within the remaining days. Over the 10-day period, stress had a significant effect on body weight change, with stressed animals of both genotypes gaining significantly more weight than control mice (Figure 8B).

After the CSDS paradigm, mice were sacrificed and organs isolated for further analysis. Adrenal glands were weighed as a measure for HPA axis activity, since continuous activation of the system is associated with enlargement of the adrenal glands. Indeed, stress increased adrenal weight (Figure 8C), reaching significance in *post-hoc* comparisons in *Cnr1*$^{+/+}$ mice. Chronic stress has also been reported to induce splenomegaly, which was also observed after standard CSDS (Figure 8D). *Post-hoc* comparison showed a significant stress-induced increase in spleen weight in *Cnr1*$^{-/-}$,

but not *Cnr1*$^{+/+}$ mice. To account for the reduced body weight of *Cnr1*$^{-/-}$ mice, adrenal and spleen weight was further normalised to body weight (Figure 8E - F). The main effect of stress remained significant in both cases. Additionally, a significant genotype effect and a tendency were found for adrenal glands and spleen, respectively.

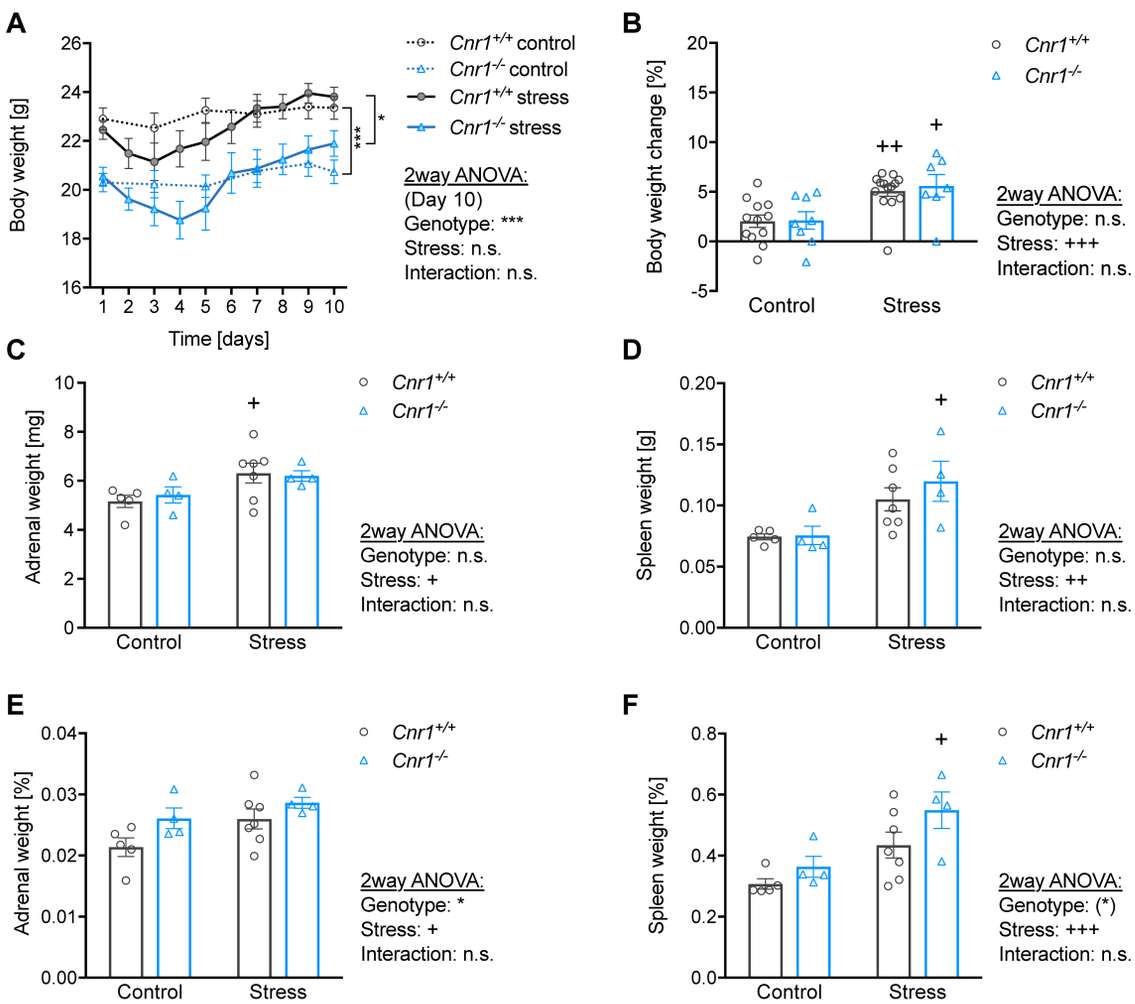

Figure 8. Standard CSDS affects body weight and leads to adrenal enlargement and splenomegaly. (A) During standard CSDS, body weight was monitored daily for stressed mice and every second day for control mice (analysis for day 10 - genotype: $F_{(1,38)} = 21.17$, $p < 0.0001$). **(B)** Body weight change after standard CSDS, compared to day one (stress: $F_{(1,37)} = 18.69$, $p = 0.0001$). **(C - F)** Organs were isolated and weighed approximately 24 h after the last stress exposure. Organ weight is shown as absolute weight and normalised to body weight, since *Cnr1*$^{-/-}$ mice weighed less than *Cnr1*$^{+/+}$ mice. **(C)** Absolute adrenal weight (stress: $F_{(1,16)} = 7.07$, $p = 0.017$). **(D)** Absolute spleen weight (stress: $F_{(1,16)} = 13.67$, $p = 0.002$). **(E)** Relative adrenal weight (stress: $F_{(1,16)} = 4.84$, $p = 0.043$; genotype: $F_{(1,16)} = 5.19$, $p = 0.037$). **(F)** Relative spleen weight (stress: $F_{(1,16)} = 13.34$, $p = 0.002$; genotype: $F_{(1,16)} = 3.96$, $p = 0.064$). Data was analysed by 2way ANOVA, followed by Bonferroni *post-hoc* comparisons. For genotype effects (compared to *Cnr1*$^{+/+}$ of the same group) * $p < 0.05$, ** $p < 0.01$, *** $p < 0.001$. For stress effects (compared to control of the same genotype) + $p < 0.05$, ++ $p < 0.01$, +++ $p < 0.001$.

3.1.5 Glucocorticoid signalling after standard CSDS

Corticosterone, the main GC in rodents, is produced by the adrenal glands at baseline and in response to stress. Basal CORT levels follow a diurnal rhythm, with a peak at the beginning of the active (dark) phase and low concentrations during the inactive (light) phase (Son et al., 2011). After standard CSDS, blood was collected at the beginning of the active phase, approximately 24 hours after the last stress exposure, and plasma CORT measured using an EIA kit. Although not statistically significant, there was a tendency for a genotype effect, with *Cnr1*$^{-/-}$ mice showing slightly increased plasma CORT levels (Figure 9A). In another cohort of mice (cohort 1), cumulative CORT was measured in faecal samples collected from a 24-hour period of single-housing after the last stress exposure, but no significant effects on faecal CORT levels were observed (Figure 9B).

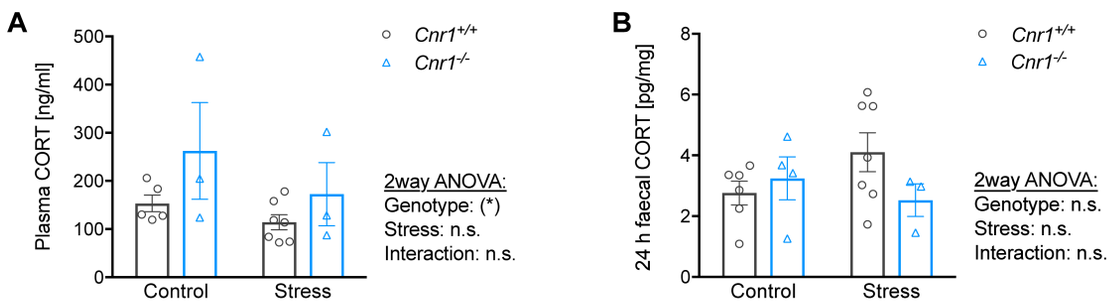

Figure 9. Corticosterone levels are not significantly altered after standard CSDS. Corticosterone (CORT) was measured after standard CSDS in blood plasma and faecal extracts using a CORT enzyme immunoassay (EIA). **(A)** Blood was collected approximately 24 h after the last stress exposure, at the beginning of the active phase (genotype: $F_{(1,18)}$ = 3.89, p = 0.064; stress x genotype interaction: $F_{(1,14)}$ = 3.78, p = 0.072). **(B)** In another cohort of mice, faeces were collected from a 24 h period after standard CSDS. Steroids were extracted from faecal samples using ethanol extraction and used for CORT measurements (no significant main effects). Data was analysed by 2way ANOVA, followed by Bonferroni *post-hoc* comparisons. For genotype effects (compared to *Cnr1*$^{+/+}$ of the same group) * p < 0.05, ** p < 0.01, *** p < 0.001. For stress effects (compared to control of the same genotype) + p < 0.05, ++ p < 0.01, +++ p < 0.001.

3.1.6 Effects of standard CSDS on peripheral myeloid cells

Chronic stress is associated with an increased production of myeloid cells in the bone marrow that are released into the circulation and migrate to different organs, including the spleen (Wohleb et al., 2015). Therefore, leukocytes from blood and spleen were isolated after standard CSDS approximately 24 hours after the last stress exposure and myeloid cell populations analysed by flow cytometry.

In the blood, a significant stress effect was detected for myeloid (CD11b^{+}) cells, with stressed mice of both genotypes showing elevated numbers (Figure 10B). Due to some variance and small group sizes, these differences did not reach significance in *post-hoc* comparisons. Separation of myeloid cells into neutrophils (Ly6G^{+}) and monocytes (Ly6G^{-}) revealed that this increase in myeloid cells was mainly driven by an increase in inflammatory, Ly6C^{hi} monocytes (Figure 10D). In contrast, there were no significant differences in neutrophil (Figure 10C) and Ly6C^{lo} monocytes (Figure 10E).

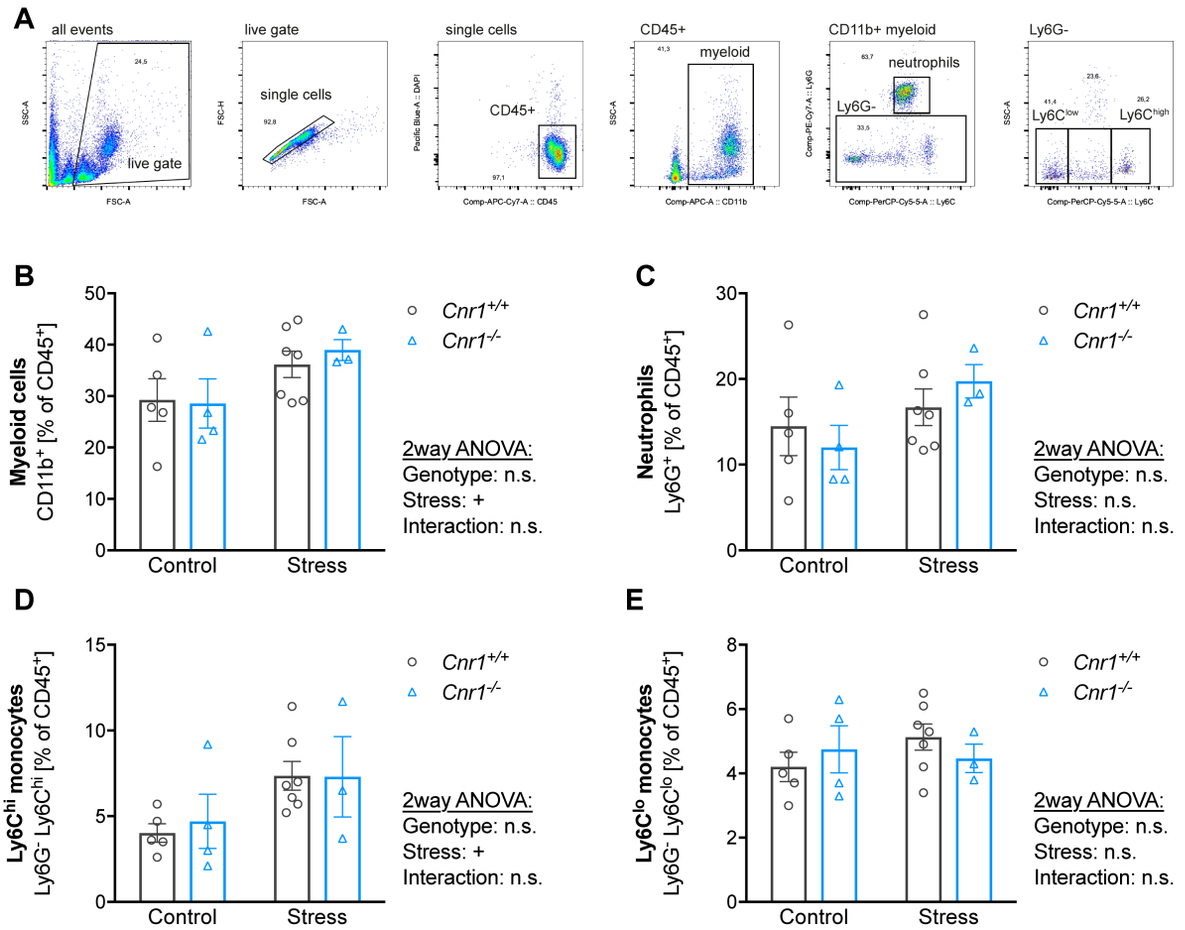

Figure 10. Standard CSDS increases circulating inflammatory monocyte frequencies. After standard CSDS, whole blood was collected by cardiac puncture and analysed by flow cytometry. **(A)** Gating strategy for blood cells. DAPI was used for staining dead cells. Neutrophils were identified as CD11b$^+$ Ly6G$^+$. Monocytes were identified as CD11b$^+$ Ly6G$^-$ and divided into Ly6C^{hi} and Ly6C^{lo} subsets. **(B)** Frequency of CD11b$^+$ myeloid cells (stress: $F_{(1,15)} = 5.24$, $p = 0.037$). **(C)** Neutrophil frequency (no significant main effects). **(D)** Ly6C^{hi} monocyte frequency (stress: $F_{(1,15)} = 5.81$, $p = 0.029$). **(E)** Ly6C^{lo} monocyte frequency (no significant main effects). Data was analysed by 2way ANOVA, followed by Bonferroni *post-hoc* comparisons. For genotype effects (compared to *Cnr1*$^{+/+}$ of the same group) * $p < 0.05$, ** $p < 0.01$, *** $p < 0.001$. For stress effects (compared to control of the same genotype) + $p < 0.05$, ++ $p < 0.01$, +++ $p < 0.001$.

In the same cohort of mice, spleen cells were isolated and cultured *ex vivo* overnight, with or without stimulation with LPS, which elicits a pro-inflammatory response. Flow cytometric analysis of unstimulated splenocytes revealed significant stress effects for overall myeloid cell frequencies (Figure 11B) and Ly6C^{hi} monocytes (Figure 11C). In both cases, stressed *Cnr1*$^{+/+}$ mice showed significantly higher values compared to their control group. For *Cnr1*$^{-/-}$ mice, only the increase in Ly6C^{hi} monocytes reached statistical significance.

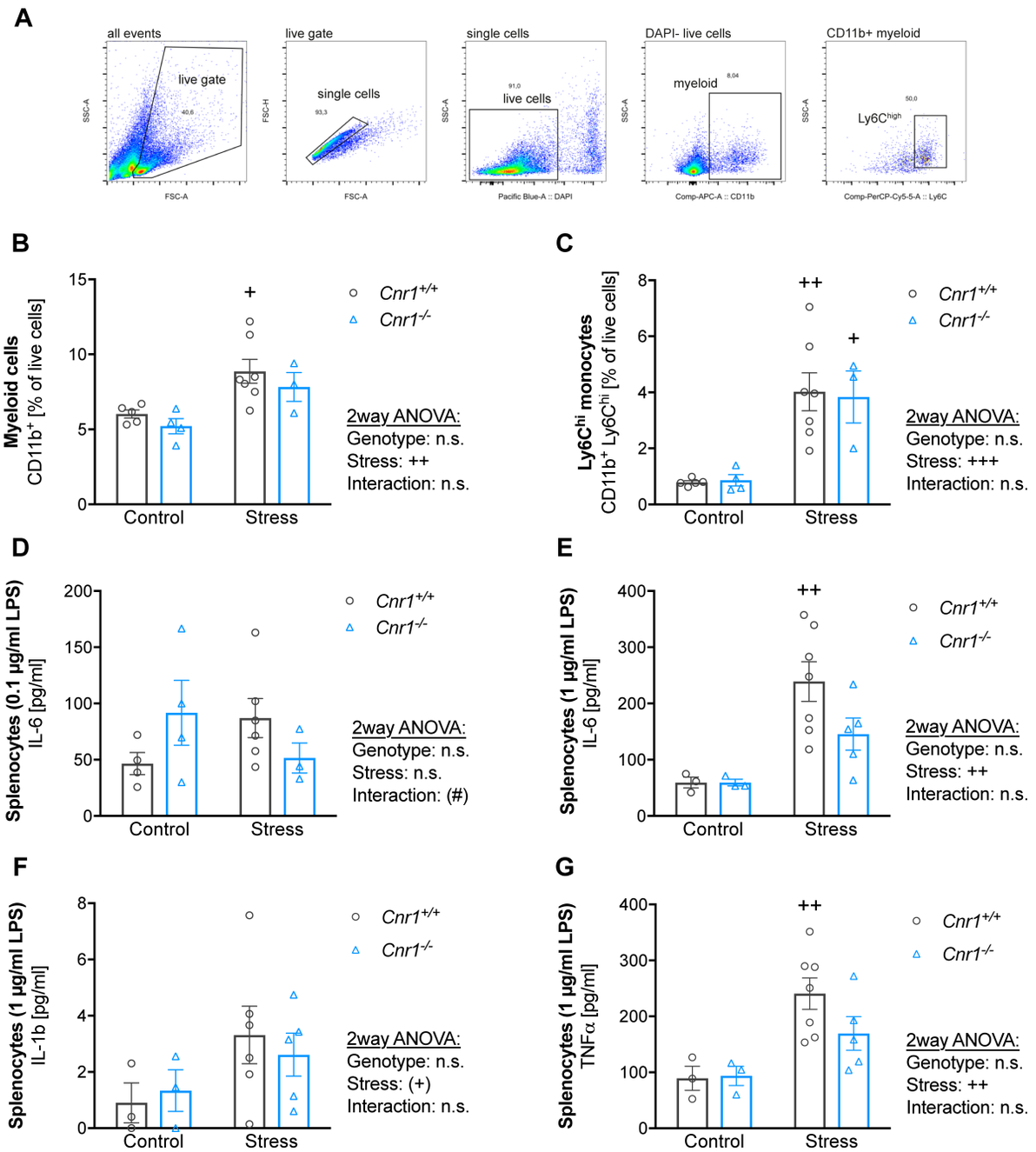

Figure 11. Standard CSDS increases splenic monocyte frequencies and increases pro-inflammatory responses to *ex vivo* stimulation. After standard CSDS, spleens were collected and isolated splenocytes cultured overnight and stimulated with LPS or vehicle (PBS). Afterwards, cells were harvested for flow cytometric analysis and supernatants collected for cytokine measurements. **(A)** Gating strategy for unstimulated splenocytes. DAPI was used for staining dead cells. **(B)** Frequency of CD11b$^+$ myeloid cells (stress: $F_{(1,15)} = 32.3$, $p = 0.003$). **(C)** Ly6C^{hi} monocyte frequency (stress: $F_{(1,15)} = 24.9$, $p = 0.0002$). **(D)** IL-6 released from splenocytes treated with 0.1 µg/ml LPS (stress x genotype interaction: $F_{(1,13)} = 3.99$, $p = 0.067$). **(E - G)** Cytokine measurements from another cohort of mice that underwent standard CSDS. Splenocytes were stimulated with 1 µg/ml LPS. **(E)** IL-6 (stress: $F_{(1,14)} = 14.12$, $p = 0.002$). **(F)** IL-1b (stress: $F_{(1,13)} = 3.46$, $p = 0.085$). **(G)** TNFα (stress: $F_{(1,14)} = 12.76$, $p = 0.003$). Data was analysed by 2way ANOVA, followed by Bonferroni *post-hoc* comparisons. For genotype effects (compared to *Cnr1*$^{+/+}$ of the same group) * $p < 0.05$, ** $p < 0.01$, *** $p < 0.001$. For stress effects (compared to control of the same genotype) + $p < 0.05$, ++ $p < 0.01$, +++ $p < 0.001$.

Supernatants from cultured splenocytes were collected for the measurement of cytokines released in response to LPS stimulation. Without LPS stimulation, cytokine levels were generally very low and mostly below the detection limit of the respective ELISA (data not shown). When cells were treated with 0.1 µg/ml LPS, IL-6 was detectable in the supernatant and a tendency for a stress x genotype interaction was observed (Figure 11D). In *Cnr1*$^{+/+}$ mice, stress slightly enhanced the release of IL-6, while this effect was not observed in *Cnr1*$^{-/-}$ mice. However, due to small group sizes and high variances between the samples, the differences did not reach significance. In another cohort of mice that underwent standard CSDS (cohort 2), splenocytes were stimulated with 1 µg/ml LPS. In this case, significant stress effects were detected for IL-6 and TNFα as well as a tendency for IL-1β (Figure 11E - G). Similar to the previous observation, prior stress exposure exaggerated the pro-inflammatory response of splenocytes to LPS stimulation. This effect was more pronounced in *Cnr1*$^{+/+}$ mice, where it reached significance in *post-hoc* comparisons for IL-6 and TNFα. In contrast, no significant differences were observed for splenocytes of *Cnr1*$^{-/-}$ mice.

3.1.7 Reduction of stress exposure during standard CSDS

In the following cohort of mice, defeat sessions were reduced to a maximum of 5 minutes daily and mice were not single-housed before CSDS to reduce baseline stress levels. Nonetheless, six out of nine *Cnr1*$^{-/-}$ mice died during the first four days of stress exposure. Therefore, all remaining *Cnr1*$^{-/-}$ mice were excluded and experiments were carried out only with *Cnr1*$^{+/+}$ mice. Behavioural analysis showed that this protocol was still sufficient to affect stress-related behaviours (Figure 12). Stressed mice displayed increased anxiety in the open field (Figure 12C) and a mild, albeit not significant, reduction in sucrose preference (Figure 12D). In the social avoidance test, stressed mice spent more time in the corners (Figure 12B). Furthermore, 8 out of 11 stressed mice showed an SI ratio below one and were thus classified as susceptible, while the remaining three mice with SI ratios above one were classified as resilient (Figure 12A). Separate analysis of behavioural data for these two sub-groups showed that this classification was able to differentiate mice in the social avoidance test, but not in other tests. In more detail, susceptible mice spent significantly more time in corners during the social avoidance test, compared to both control and resilient mice (Figure 12E). However, susceptible and resilient mice spent comparable amounts of time in the centre of the open field and the variance within the susceptible group was rather high (Figure 12F). In the sucrose preference test, resilient mice even seemed to have lower preferences than susceptible ones (Figure 12G). This suggests that the classification of mice into stress susceptible and resilient mice based on one behavioural readout (the SI ratio) does not reflect the overall stress-related phenotype.

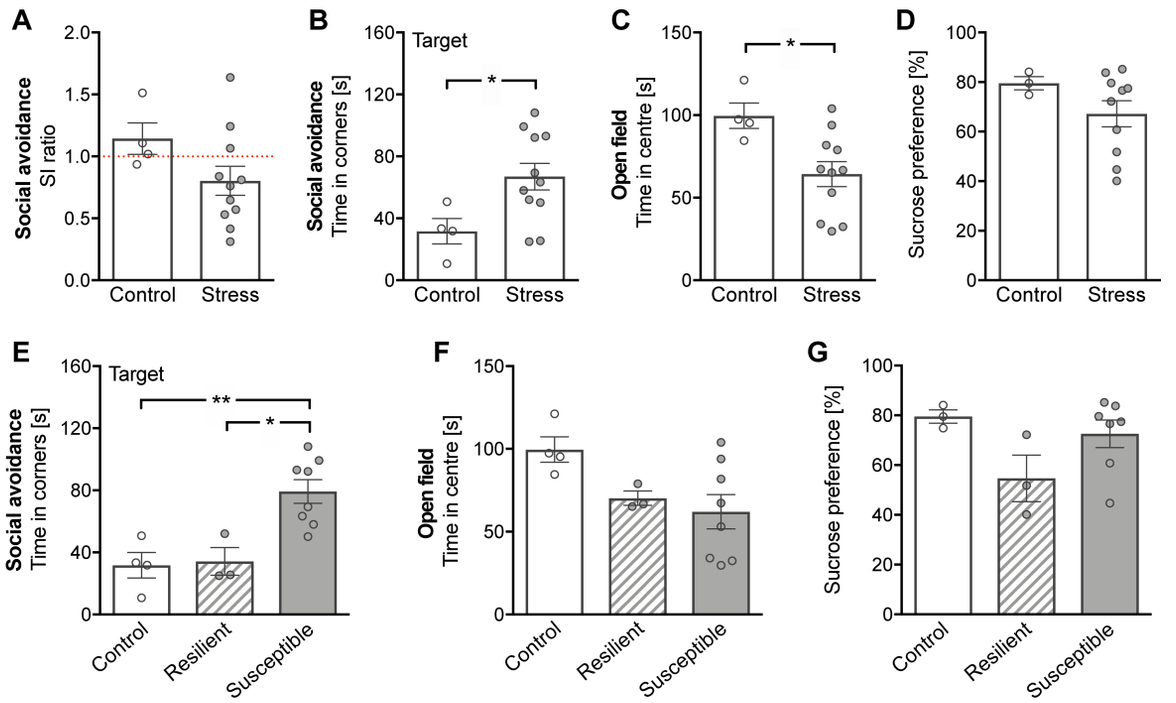

Figure 12. Social avoidance behaviour of *Cnr1*$^{+/+}$ mice does not correlate with other stress-related behaviour. Behavioural analysis of *Cnr1*$^{+/+}$ mice after standard CSDS with reduced stress exposure (max. 5 minutes daily). Due to substantial mortality, *Cnr1*$^{-/-}$ mice were completely excluded from the experiment after four days. **(A - D)** Quantification of behaviour of control versus all stressed mice. **(A)** Social interaction (SI) ratio, calculated from the interaction time during the two trials of the social avoidance test ($p = 0.13$, $t = 1.61$, $df = 13$). According to the SI ratio, stressed mice were classified as resilient (SI ratio > 1) or susceptible (SI ratio < 1). **(B)** Time spent in corners during trial two of the social avoidance test (CD1 target present) ($p = 0.04$, $t = 2.30$, $df = 13$). **(C)** Anxiety measured as time spent in the centre of the open field test ($p = 0.02$, $t = 2.61$, $df = 13$). **(D)** Anhedonia measured as sucrose preference ($p = 0.24$, $t = 1.23$, $df = 11$). **(E - G)** Analysis of the same data sets with separation of mice into stress resilient and susceptible. **(E)** Time spent in corners during the social avoidance test ($F = 10.71$, $p = 0.002$). **(F)** Time spent in the centre of the open field ($F = 3.35$, $p = 0.07$). **(G)** Sucrose preference ($F = 2.75$, $p = 0.11$). Data was analysed by unpaired Student's *t*-test (two groups) or 1way ANOVA, followed by Bonferroni *post-hoc* comparisons (three groups). Significant differences in the *t*-test or *post-hoc* comparisons are shown in the graph, * $p < 0.05$, ** $p < 0.01$.

3.1.8 Effect of standard CSDS on plasma interleukin-6

Stress-induced IL-6 release by circulating leukocytes has been shown to correlate with stress-susceptibility in social defeat models (Hodes et al., 2014). Therefore, blood was collected from submandibular veins one hour after the first stress exposure for quantification of plasma IL-6 levels. Stress significantly increased IL-6 concentrations in both genotypes (Figure 13A). Since *Cnr1*$^{-/-}$ mice had to be excluded from the experiment after four days, correlation of IL-6 with behavioural stress-susceptibility could only be performed in *Cnr1*$^{+/+}$ mice. However, there was no correlation of plasma IL-6 levels with later social avoidance behaviour (Figure 13B). Interestingly, one stressed *Cnr1*$^{-/-}$ mouse showed very high plasma IL-6 levels (608 pg/ml; mean = 191 pg/ml) and this particular animal was found dead on the following day (Figure 13A).

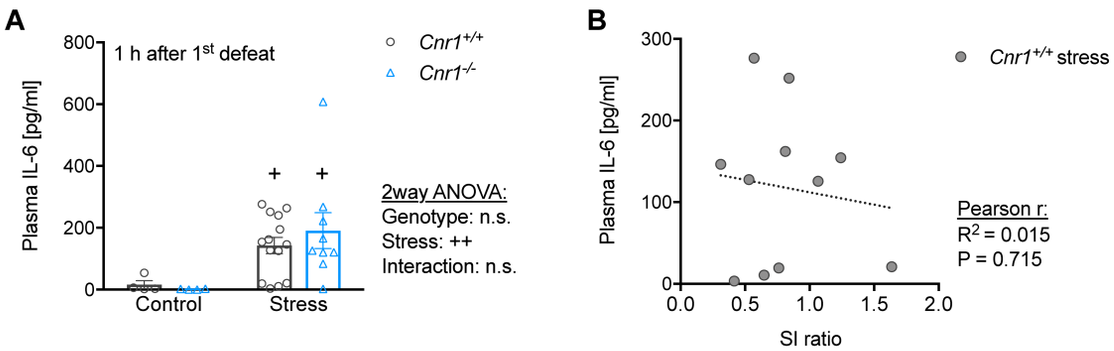

Figure 13. Circulating interleukin-6 is increased after the first exposure to standard CSDS. One hour after the first defeat session, blood was collected from submandibular veins. Plasma was prepared and levels of interleukin-6 (IL-6) measured by ELISA. **(A)** Plasma IL-6 levels (stress: $F_{(1,26)} = 14.98$, $p = 0.0007$). Data was analysed by 2way ANOVA, followed by Bonferroni *post-hoc* comparisons. For genotype effects (compared to *Cnr1*$^{+/+}$ of the same group) * $p < 0.05$, ** $p < 0.01$, *** $p < 0.001$. For stress effects (compared to control of the same genotype) + $p < 0.05$, ++ $p < 0.01$, +++ $p < 0.001$. **(B)** Pearson correlation analysis of plasma IL-6 levels in stressed *Cnr1*$^{+/+}$ with later social avoidance behaviour (SI ratio) ($R^2 = 0.014$, $p = 0.743$). For correlation, only *Cnr1*$^{+/+}$ mice could be used, since *Cnr1*$^{-/-}$ mice were excluded from the experiments due to a very high mortality rate.

3.1.9 Measurement of cardiac activity in *Cnr1*$^{-/-}$ mice during standard CSDS

In order to determine if the increased mortality of *Cnr1*$^{-/-}$ during standard CSDS was due to cardiovascular events, heart activity was monitored using ECG recordings. Therefore, *Cnr1*$^{-/-}$ mice were equipped with telemetric ECG chips that were implanted subcutaneously and did not require any further manipulation of the animal after surgery. Two weeks after the surgery, mice were subjected to 5 - 10 minutes of daily defeat sessions and cardiac activity was measured starting on the first day of stress exposure (Figure 14A). Out of seven *Cnr1*$^{-/-}$ mice analysed, three mice died during the recordings, on day three to five of CSDS exposure. All mice were bradycardic on the day of death (Figure 14B - C) and developed atrio-ventricular (AV) blocks (Figure 14C - F). In a healthy heart, depolarisation spreads from the atria to ventricles in a controlled sequence, which is visible as a 1:1 pattern in the ECG traces (one P wave followed by one QRS complex). An AV block of third degree indicates a complete dissociation of atrial and ventricular signal transmission, as seen for the examined *Cnr1*$^{-/-}$ mice (Figure 14D). Furthermore, mice might have had seizures or convulsions during the development of the AV block, indicated by high amplitude disturbances in the ECG trace, possibly caused by strong muscle contractions (Figure 14E - F).

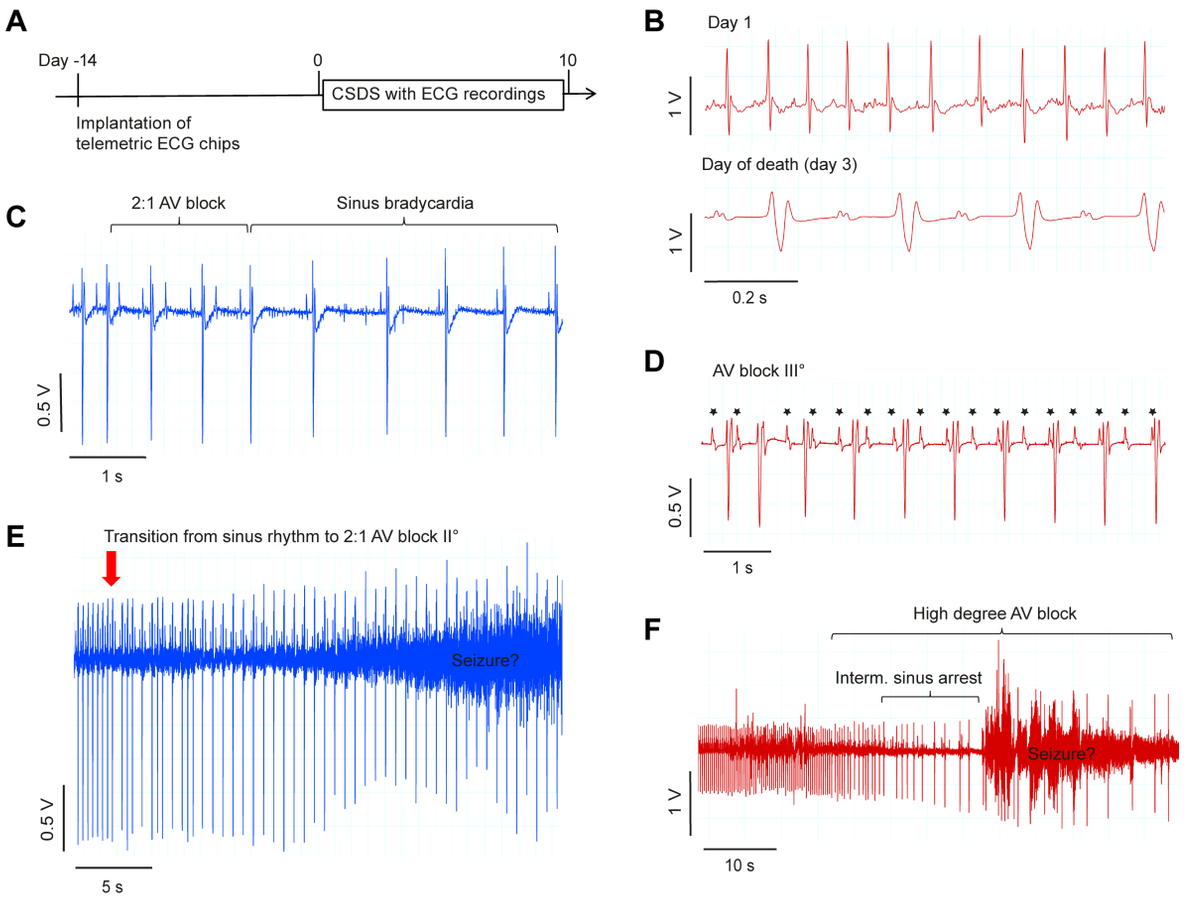

Figure 14. Signs of cardiac arrhythmias in *Cnr1*$^{-/-}$ mice that died during standard CSDS. Cardiac activity of *Cnr1*$^{-/-}$ mice was monitored during standard CSDS by long-term telemetric electrocardiogram (ECG) recording. Experiments were performed in cooperation with Dr. med. Thomas Beiert, Department of Internal Medicine II, University Hospital Bonn. **(A)** Timeline of experiments: ECG chips were implanted subcutaneously two weeks before starting the standard CSDS paradigm, to allow complete healing of the surgical wounds. **(B - F)** Representative ECG traces of two *Cnr1*$^{-/-}$ mice that died during the experiments (red and blue traces each correspond to one mouse). **(B)** Comparison of the heart beat on day one versus the day of death. **(C)** Example of a mouse with initial sinus rhythm (beat 1 - 2) with development of a short period of 2:1 atrio-ventricular (AV) block (beat 3 – 5), devolving into sinus bradycardia. **(D)** Example of a mouse developing total AV block (third degree, III°). Note the complete dissociation of atrial (P wave, indicated by stars) and ventricular (QRS complex) signals. **(E - F)** Extended time frames showing the development of persistent AV blocks of higher degree, with intermittent sinus arrest in one case and the possible occurrence of seizures or convulsions.

3.2 Mild chronic social defeat stress

In order to prevent mortality of *Cnr1*$^{-/-}$ mice during stress exposure, the CSDS paradigm was adapted to a much milder version, with only one - two minutes of daily defeat sessions (Figure 15). Thereby, survival rates could be increased to 100%. After mild CSDS, anxiety- and depressive-like behaviour was analysed in the open field, social avoidance, sucrose preference, and the nestlet test. Experiments were carried out in three separate cohorts of mice, with four - nine animals per group. In total, 29 *Cnr1*$^{+/+}$ mice (15 control, 14 stress) and 29 *Cnr1*$^{-/-}$ mice (12 control, 16 stress) were tested. All three cohorts were confronted with the same group of CD1 aggressor mice and experiments were performed within a time frame of eight weeks. Therefore, behavioural data was pooled from all cohorts. Two control cages (i.e. two *Cnr1*$^{+/+}$ and two *Cnr1*$^{-/-}$ mice) had to

be excluded from the analysis, due to highly deviant baseline behaviour. After completion of all behavioural tests, mice from the different cohorts where used for analysis of different cellular and molecular parameters. When applicable, data was pooled from two or all cohorts.

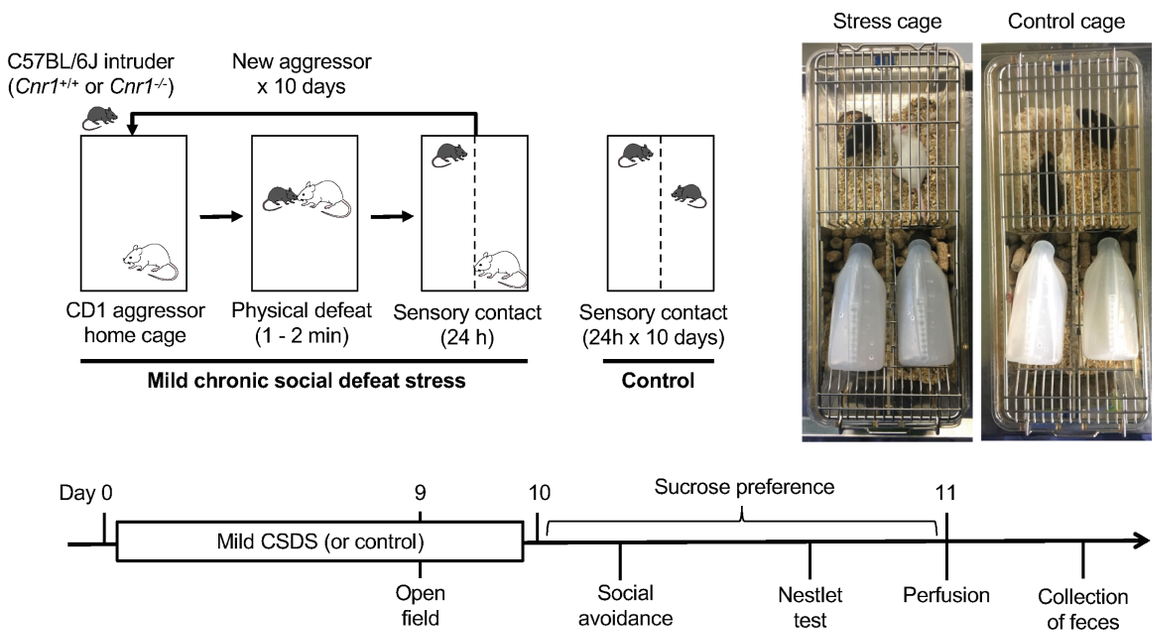

Figure 15. Experimental setup for mild CSDS. Male *Cnr1*$^{+/+}$ or *Cnr1*$^{-/-}$ mice were individually introduced into the home cage of a CD1 aggressor mouse. Mice were allowed to physically interact for 1 - 2 minutes, during which the intruder is exposed to repeated bouts of social defeat by the CD1 aggressor. After the physical defeat, mice were separated by perforated Plexiglas wall to allow sensory, but not physical contact for the following 24 h. C57BL/6J intruder mice were exposed to a new CD1 aggressor for 10 consecutive days. Control mice were housed in pairs of two, unfamiliar to each other and separated by a perforated Plexiglas wall. Combinations of control mice were not alternated during the 10-day period. After mild CSDS (starting on day 9), anxiety- and depressive-like behaviour was analysed in the open field, social avoidance, sucrose preference, and nestlet test. One day after the last stress exposure, mice were sacrificed and organs harvested for analysis. Faeces were collected from the 24 h period of single-housing after the last stress exposure.

3.2.1 Social avoidance after mild CSDS

Approximately three hours after the last stress exposure, social avoidance behaviour was analysed (Figure 16). In the first trial without a CD1 target, there was no difference in the time spent in the interaction or corner zones (Figure 16C - D). Locomotion during this trial was significantly affected by stress and genotype (Figure 16E). *Cnr1*$^{-/-}$ mice generally moved less and stress significantly reduced locomotion in *Cnr1*$^{+/+}$ mice. In the second trial, significant stress effects were detected for both interaction with the CD1 target and time spent in corners (Figure 16F - G). *Post-hoc* comparisons showed that stressed *Cnr1*$^{-/-}$ mice spent significantly less time in interaction zones and more time in corners compared to control *Cnr1*$^{-/-}$ mice. Similar directions were also seen in *Cnr1*$^{+/+}$ mice, however, they did not reach significance. Furthermore, both stress and genotype had a strong effect on locomotion in the presence of a CD1 target (Figure 16H), with stressed mice of both genotypes moving significantly less compared to their corresponding unstressed controls, and *Cnr1*$^{-/-}$ mice moving significantly less than *Cnr1*$^{+/+}$ mice.

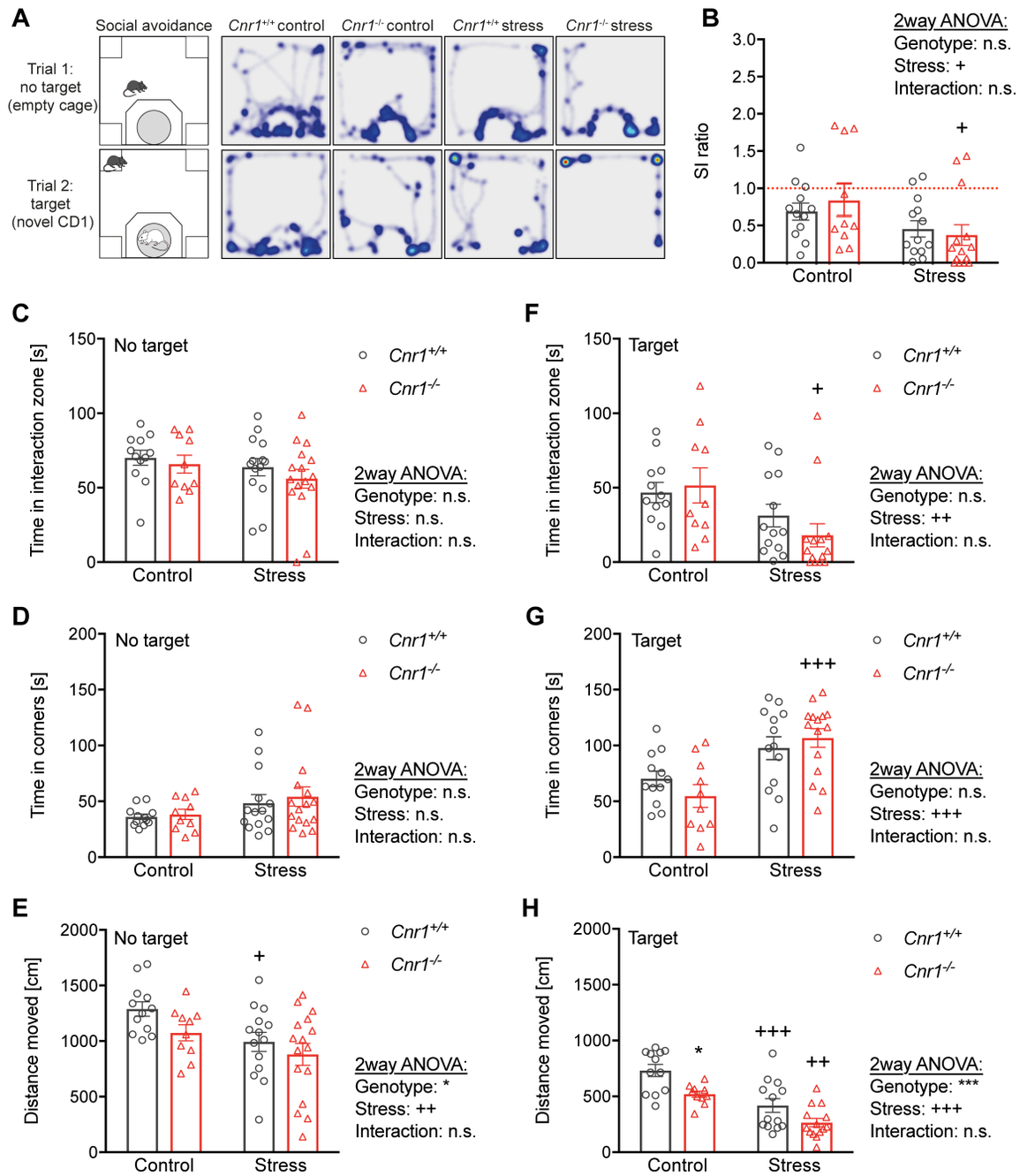

Figure 16. Mild CSDS induces social avoidance behaviour in *Cnr1*$^{-/-}$ mice. Mice were subjected to the social avoidance test after mild CSDS. **(A)** Experimental setup and representative heatmap visualization of movement of mice during the two trials of the test. First trial (no target): the cage located on one side of the arena is empty. Second trial (target): cage containing an unfamiliar CD1 aggressor mouse. In between trials, mice were briefly transferred to their home cage and the empty cages replaced by cages with CD1 mice. **(B)** Social interaction (SI) ratio, calculated from the interaction time in the first and second trial (stress: $F_{(1,45)} = 6.15$, $p = 0.017$). **(C - E)** Quantification of the first trial of the test (no target). **(C)** Interaction with empty cage (no significant main effects). **(D)** Time spent in any of the four corners (no significant main effects). **(E)** Locomotion, total distance moved (stress: $F_{(1,48)} = 7.68$, $p = 0.008$; genotype: $F_{(1,48)} = 3.42$, $p = 0.071$). **(F - H)** Quantification of the second trial of the test (target). **(F)** Interaction with an unfamiliar CD1 aggressor (stress: $F_{(1,45)} = 8.50$, $p = 0.006$). **(G)** Time spent in corners (stress: $F_{(1,46)} = 19.23$, $p < 0.0001$). **(H)** Total distance moved (stress: $F_{(1,45)} = 33.28$, $p < 0.0001$; genotype: $F_{(1,45)} = 13.73$, $p < 0.0006$). Data was analysed by 2way ANOVA, followed by Bonferroni *post-hoc* comparisons. For genotype effects (compared to *Cnr1*$^{+/+}$ of the same group) * $p < 0.05$, ** $p < 0.01$, *** $p < 0.001$. For stress effects (compared to control of the same genotype) + $p < 0.05$, ++ $p < 0.01$, +++ $p < 0.001$.

3.2.2 Locomotion and anxiety after mild CSDS

On day nine of the mild CSDS paradigm, exploratory and anxiety-like behaviour of mice was analysed in the open field test (Figure 17A). The test was performed under aversive, brightly illuminated conditions (150 lux). For all parameters analysed – locomotion (total distance moved) and anxiety (time spent in the centre and frequency to enter the centre) – a significant genotype effect was detected. Stress, on the other hand, only slightly reduced the frequency to enter the centre (Figure 17D). *Post-hoc* comparisons showed that control *Cnr1*$^{-/-}$ mice moved significantly less than control *Cnr1*$^{+/+}$ mice (Figure 17B). Furthermore, control and stressed *Cnr1*$^{-/-}$ mice entered the centre area less frequently and spent significantly less time in the centre of the open field compared to corresponding *Cnr1*$^{+/+}$ mice (Figure 17C - D), suggesting that *Cnr1*$^{-/-}$ mice were generally more anxious, independent from stress.

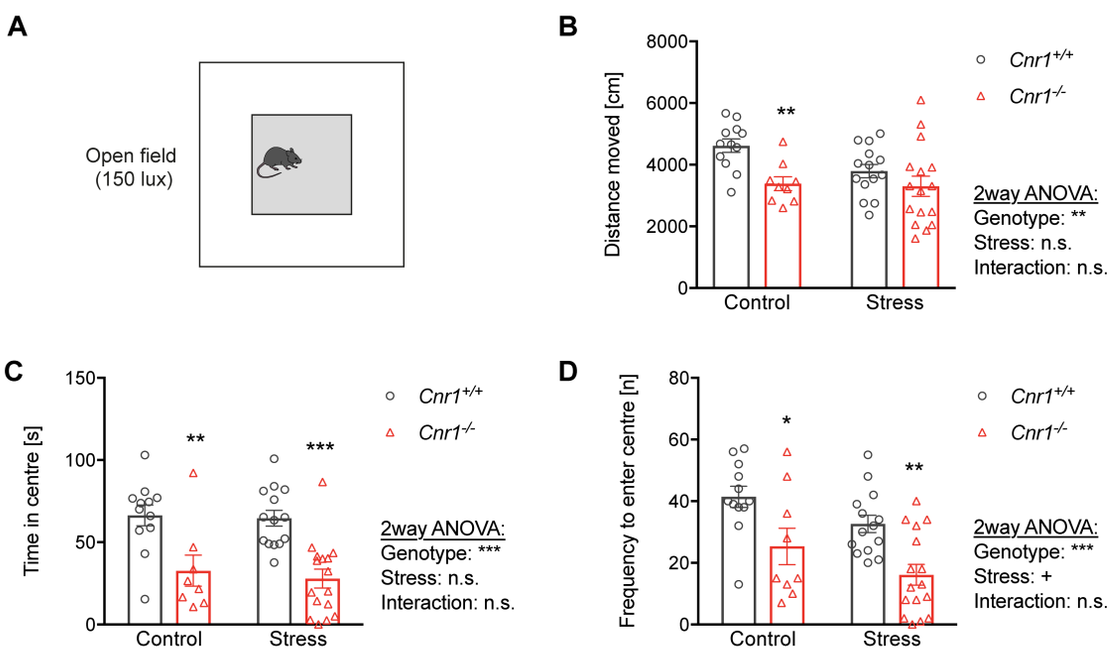

Figure 17. *Cnr1*$^{-/-}$ mice are hypoactive and more anxious in the open field test, independent from stress. Locomotion and anxiety-like behaviour was analysed on day nine of the mild CSDS paradigm in the open field test. **(A)** Mice were placed in a brightly illuminated open field arena and allowed to explore for 10 minutes. **(B)** Locomotion was measured as total distance moved (genotype: $F_{(1,47)} = 9.70$, $p = 0.003$). **(C)** Anxiety was measured as time spent in the centre area of the arena (genotype: $F_{(1,46)} = 29.96$, $p < 0.0001$) and **(D)** frequency to enter the centre (genotype: $F_{(1,47)} = 18.63$, $p < 0.0001$; stress: $F_{(1,47)} = 5.67$, $p < 0.021$). Data was analysed by 2way ANOVA, followed by Bonferroni *post-hoc* comparisons. For genotype effects (compared to *Cnr1*$^{+/+}$ of the same group) * $p < 0.05$, ** $p < 0.01$, *** $p < 0.001$. For stress effects (compared to control of the same genotype) + $p < 0.05$, ++ $p < 0.01$, +++ $p < 0.001$.

3.2.3 Anhedonia after mild CSDS

While standard CSDS slightly induced anhedonia in mice, mild CSDS had no effect on sucrose preference (Figure 18A). A significant genotype effect was detected, caused by a general reduction in sucrose preference in *Cnr1*$^{-/-}$ mice independent from stress. In *post-hoc* comparisons, the differences did not reach significance. Similar to standard CSDS, also mild CSDS increased fluid intake (Figure 18B), with stressed *Cnr1*$^{-/-}$ mice drinking significantly more than *Cnr1*$^{-/-}$ controls.

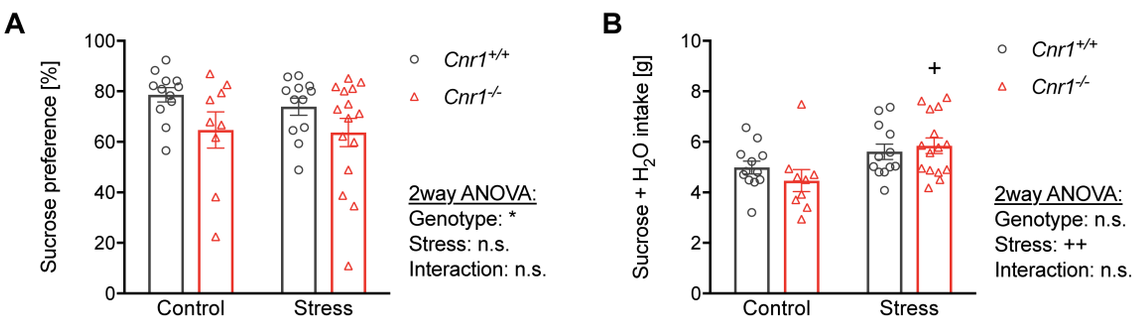

Figure 18. Mild CSDS has no effect on sucrose preference but increases fluid intake. Anhedonia was analysed after mild CSDS using the sucrose preference test. Mice had free access to two bottles, one containing H_2O and the other one 1% sucrose solution, and consumption of fluid was measured after 24 h. **(A)** Sucrose preference, i.e. the percentage of sucrose consumption in relation to the total fluid intake (genotype: $F_{(1,44)} = 5.82$, $p = 0.020$). **(B)** Total fluid intake over 24 h (stress: $F_{(1,44)} = 9.48$, $p = 0.004$). Data was analysed by 2way ANOVA, followed by Bonferroni *post-hoc* comparisons. For genotype effects (compared to *Cnr1*$^{+/+}$ of the same group) * $p < 0.05$, ** $p < 0.01$, *** $p < 0.001$. For stress effects (compared to control of the same genotype) + $p < 0.05$, ++ $p < 0.01$, +++ $p < 0.001$.

3.2.4 Nest building behaviour after mild CSDS

As a final behavioural readout for stress-sensitivity, nest building was analysed after mild CSDS. Therefore, mice were provided with pre-weighed nesting material and left undisturbed for one hour (Figure 19). Qualitatively, it was apparent that stressed mice did not build nests as well as control mice. Furthermore, *Cnr1*$^{-/-}$ mice generally had deficits in nest building behaviour and none of the stressed *Cnr1*$^{-/-}$ mice started using the nesting material at all (Figure 19A). Since the variability between individual mice was very high and data points were not distributed normally, data was analysed by a non-parametric Kruskal-Wallis test. The test revealed a significant variation of medians between the groups and Dunn's *post-hoc* comparisons showed that stressed *Cnr1*$^{-/-}$ mice used significantly less nesting material compared to *Cnr1*$^{-/-}$ control mice (Figure 19B).

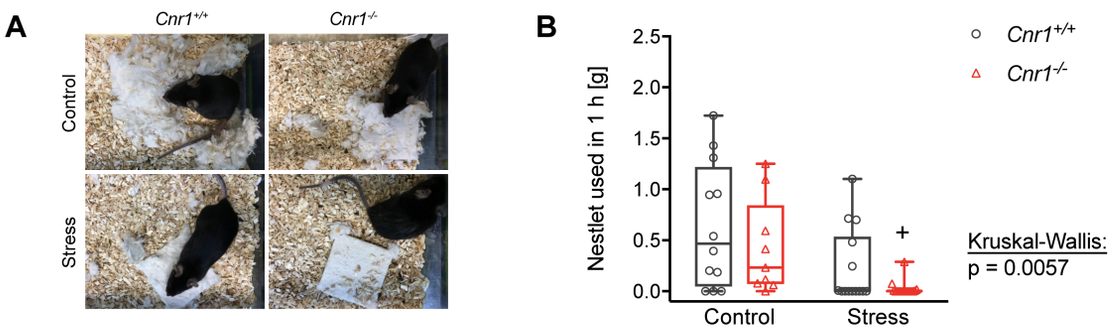

Figure 19. Mild CSDS reduces nest-building behaviour in *Cnr1*$^{-/-}$ mice. Nest-building behaviour was analysed as a measure of self-care after mild CSDS. Mice were provided with pre-weighed nestlet material and the amount of material used was measured after one hour. **(A)** Representative pictures of nests build by mice of the different groups. **(B)** Quantification of nestlet material used within one hour (Kruskal-Wallis statistic = 14.43, p = 0.006). Since data points were not normally distributed, data was analysed by non-parametric Kruskal-Wallis test, followed by Dunn's multiple comparisons and are presented as box and whiskers plots (Min to Max, line indicates median). For stress effects (compared to control of the same genotype) + $p < 0.05$.

3.2.5 Calculation of behavioural stress scores

To obtain an overall estimate of the stress-related behavioural phenotype, values from each behavioural test were transformed into a score ranging from zero (no phenotype) to three (strong phenotype). The score for each parameter was determined based on the deviation from the mean performance of *Cnr1*$^{+/+}$ control mice (within SD = score 0; > 1x SD = score 1; > 2x SD = score 2; > 3x SD = score 3). The overall stress score was then calculated as the mean of all individual parameters (Figure 20). Thereby, mice that had to be excluded from a certain test (e.g. due to a leaky bottle in the sucrose preference test) could still be assigned an overall stress score from the remaining tests. Non-parametric analysis confirmed that mild CSDS had a more pronounced effect in *Cnr1*$^{-/-}$ mice, with stressed *Cnr1*$^{-/-}$ mice showing significantly higher scores than both control *Cnr1*$^{-/-}$ mice and stressed *Cnr1*$^{+/+}$ mice. Mild CSDS increased the scores of *Cnr1*$^{+/+}$ mice to levels comparable to those of control *Cnr1*$^{-/-}$ mice, which were already increased under control conditions (not significant in *post-hoc* comparisons).

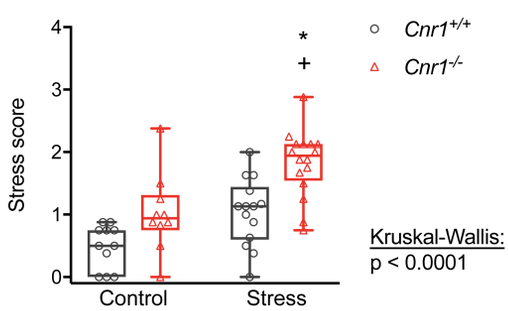

Figure 20. Mild CSDS increases overall stress-related behaviour in *Cnr1*$^{-/-}$ mice. Behavioural stress scores were calculated for individual mice based on their performance in all behavioural tests, ranging from zero (no phenotype) to three (strong phenotype), see text above for details (Kruskal-Wallis statistic = 25.1, $p < 0.0001$). Data was analysed by non-parametric Kruskal-Wallis test, followed by Dunn's multiple comparisons and are presented as box and whiskers plots (Min to Max, line indicates median). For genotype effects (compared to *Cnr1*$^{+/+}$ of the same group) * $p < 0.05$. For stress effects (compared to control of the same genotype) + $p < 0.05$.

3.2.6 Physiological effects of mild CSDS

During mild CSDS, body weight was monitored on a daily basis. Stress overall had no effect on body weight (Figure 21). In contrast, the genotype significantly affected body weight gain during mild CSDS, as control and stressed *Cnr1*$^{-/-}$ gained significantly less weight compared to the respective *Cnr1*$^{+/+}$ groups (Figure 21B). Unlike standard CSDS, which induced adrenomegaly and splenomegaly, mild CSDS had no effect on adrenal or spleen weight (Figure 21C - D). The genotype did also not influence these parameters. For adrenal glands, there was a significant stress x genotype interaction, however no differences between the groups in *post-hoc* comparisons.

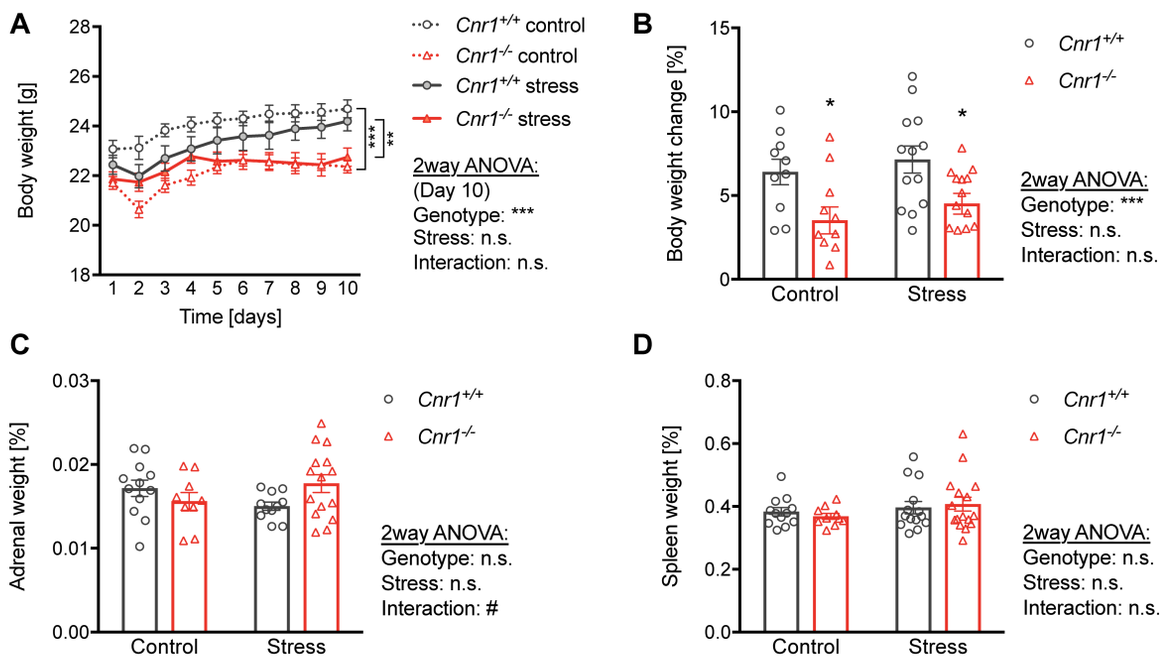

Figure 21. Mild CSDs has no effect on body weight, adrenal glands and spleen weight. (A) During mild CSDS, body weight was monitored daily for both stressed and control mice (analysis for day 10 – genotype: $F_{(1,47)} = 25.78$, $p < 0.0001$). **(B)** Body weight change after mild CSDS, compared to day one (genotype: $F_{(1,44)} = 13.51$, $p = 0.0006$). **(C - D)** Organs were isolated and weighed approximately 24 h after the last stress exposure. Organ weight was normalised to body weight, since *Cnr1*$^{-/-}$ mice generally weigh less than *Cnr1*$^{+/+}$ mice. **(C)** Relative adrenal weight (stress x genotype interaction: $F_{(1,43)} = 4.74$, $p = 0.035$). **(D)** Relative spleen weight (no significant main effects). Data was analysed by 2way ANOVA, followed by Bonferroni *post-hoc* comparisons. For genotype effects (compared to *Cnr1*$^{+/+}$ of the same group) * $p < 0.05$, ** $p < 0.01$, *** $p < 0.001$. For stress effects (compared to control of the same genotype) + $p < 0.05$, ++ $p < 0.01$, +++ $p < 0.001$.

3.2.7 Glucocorticoid signalling after mild CSDS

After mild CSDS, blood was collected at the beginning of the active phase approximately 24 hours after the last stress exposure and plasma CORT was measured using an EIA kit (Figure 22A). A significant stress x genotype interaction was detected and *post-hoc* comparisons showed that stressed *Cnr1*$^{-/-}$ mice had higher plasma levels compared to stressed *Cnr1*$^{+/+}$ mice. Additionally, cumulative CORT was measured in faecal samples collected from a 24-hour period of single-housing after the last defeat (Figure 22B). Faecal CORT was significantly affected by genotype and stress, and a tendency for a stress x genotype interaction was detected. In more detail, stress

induced a significant increase in 24-hour faecal CORT in *Cnr1*$^{+/+}$, but not in *Cnr1*$^{-/-}$ mice. Stressed *Cnr1*$^{-/-}$ mice thus had significantly lower CORT levels compared to stressed *Cnr1*$^{+/+}$ mice. To test whether CORT responses were associated with the individual behavioural susceptibility, data was correlated with the behavioural stress scores (see chapter 3.2.5). Only in *Cnr1*$^{+/+}$ mice, plasma CORT levels were negatively correlated with stress scores, as mice with high behavioural deficits showed the lowest CORT levels (Figure 22C). In contrast, there was no correlation in *Cnr1*$^{-/-}$ mice. For faecal CORT, no correlation was detected for any genotype (Figure 22D).

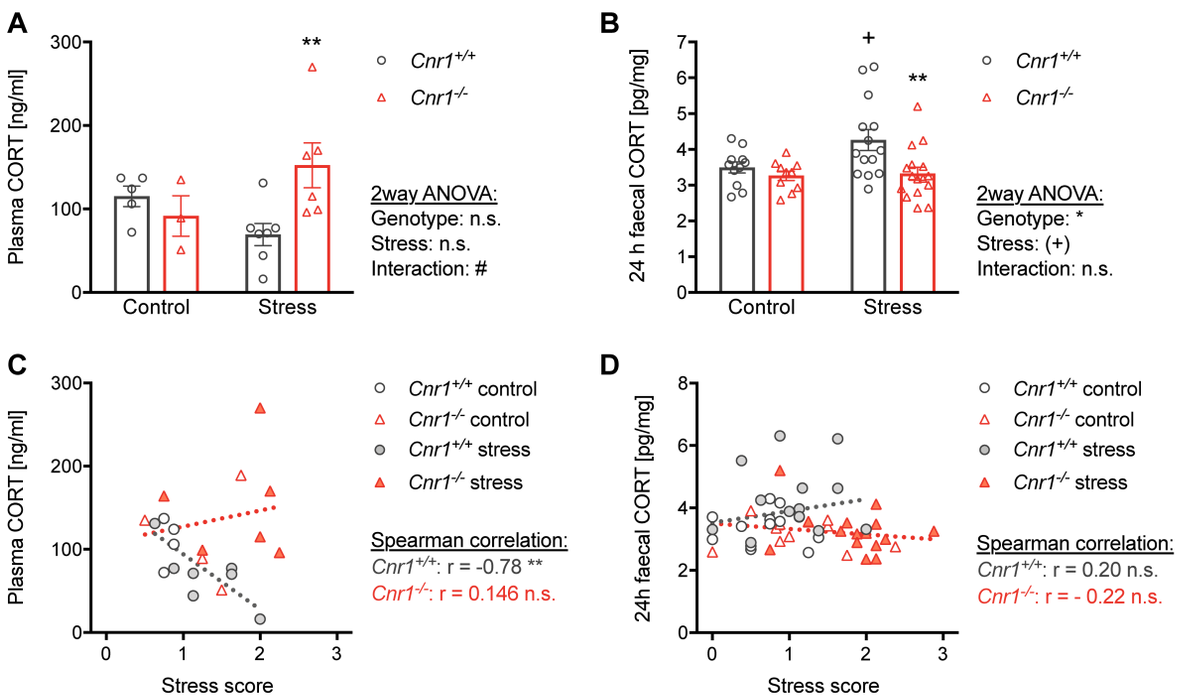

Figure 22. Mild CSDS increases cumulative corticosterone levels in *Cnr1*$^{+/+}$, but not in *Cnr1*$^{-/-}$ mice. Corticosterone (CORT) was measured after mild CSDS in blood plasma and faecal extracts using an enzyme immunoassay (EIA). **(A)** Blood was collected approximately 24 h after the last stress exposure. Measurement of CORT in plasma was performed for two cohorts of mice (stress x genotype interaction: $F_{(1,17)} = 6.41$, $p = 0.022$). **(B)** Faeces were collected from a 24 h period after mild CSDS in three cohorts of mice and steroids were extracted from faecal samples using ethanol extraction (stress: $F_{(1,47)} = 3.56$, $p = 0.065$; genotype: $F_{(1,47)} = 7.91$, $p = 0.010$). Data was analysed by 2way ANOVA, followed by Bonferroni *post-hoc* comparisons. For genotype effects (compared to *Cnr1*$^{+/+}$ of the same group) * $p < 0.05$, ** $p < 0.01$, *** $p < 0.001$. For stress effects (compared to control of the same genotype) + $p < 0.05$, ++ $p < 0.01$, +++ $p < 0.001$. **(C - D)** CORT levels were correlated to the behavioural stress scores. Spearman correlation was performed for each genotype. **(C)** Plasma CORT vs. stress scores (*Cnr1*$^{+/+}$: $r = -0.78$, $p = 0.004$; *Cnr1*$^{-/-}$: $r = 0.146$, $p = 0.686$). **(D)** Faecal CORT vs. stress scores (*Cnr1*$^{+/+}$: $r = 0.20$, $p = 0.317$; *Cnr1*$^{-/-}$: $r = -0.22$, $p = 0.276$).

GCs secreted by the adrenal glands give feedback to brain regions that regulate activity of the HPA axis directly or indirectly, such as the PVN, or the amygdala, hippocampus and mPFC (Godoy et al., 2018). To analyse whether the altered CORT levels after mild CSDS resulted in changes of HPA axis components in these brain regions, expression of the genes encoding GR (*Nr3c1*), CRH (*Crh)*, and CRHR1 (*Crhr1*) was analysed by qPCR in one cohort of mice (Figure 23). However, no significant differences were observed for *Nr3c1, Crh*, or *Crhr1* expression in any of the brain regions analysed.

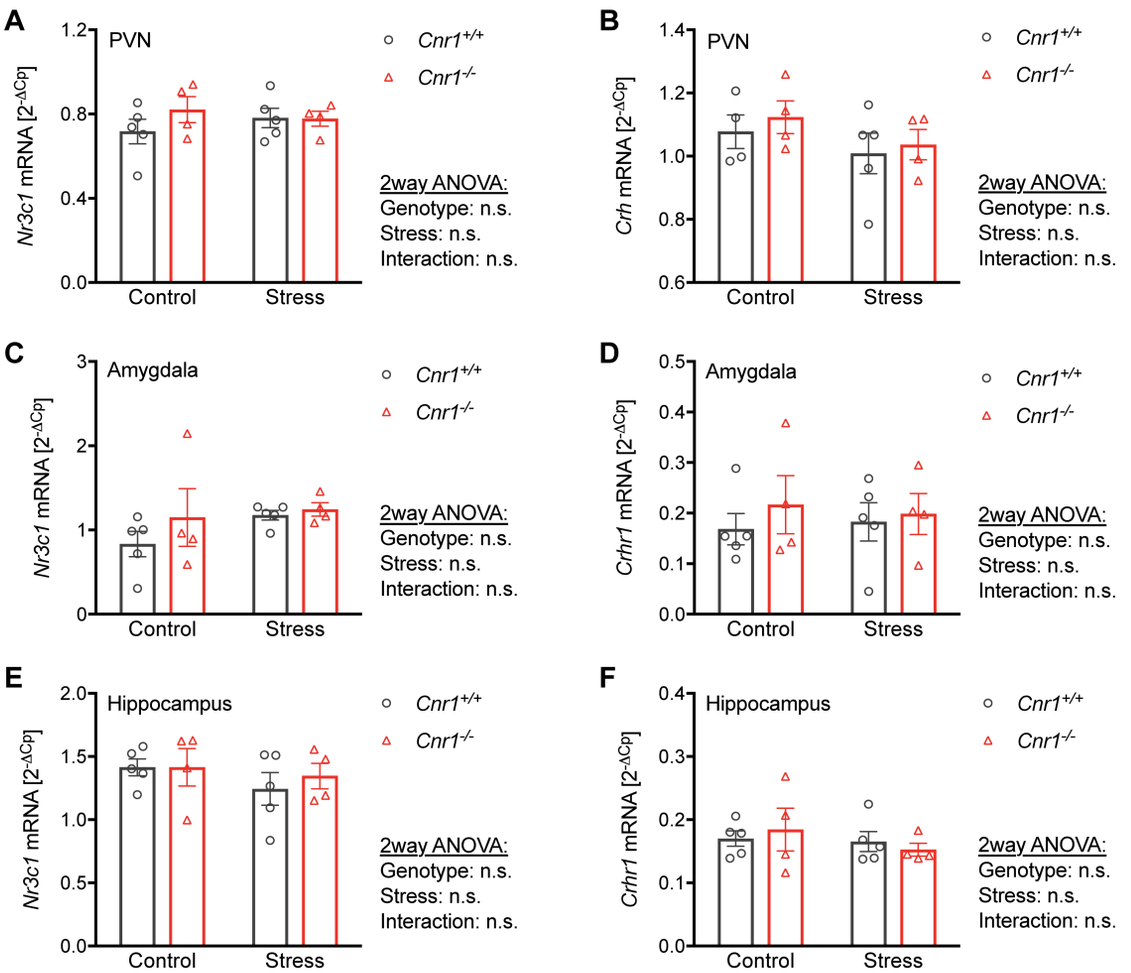

Figure 23. Gene expression of HPA axis-related genes is not altered in the brain after mild CSDS. Brain regions were isolated approximately 24 h after the last stress exposure in one cohort of mice. RNA was isolated, reverse transcribed into cDNA and gene expression analysed by qPCR. Expression of target genes was normalised to the expression of reference gene *Hprt* and is presented as $2^{-\Delta Cp}$. **(A - B)** *Nr3c1* and *Crh* mRNA levels in the PVN (no significant main effects). **(C - D)** *Nr3c1* and *Crhr1* mRNA levels in the amygdala (no significant main effects). **(E - F)** *Nr3c1* and *Crhr1* mRNA levels in the dorsal hippocampus (no significant main effects). Data was analysed by 2way ANOVA, followed by Bonferroni *post-hoc* comparisons.

3.2.8 Sympathetic innervation of the bone marrow after mild CSDS

Next to the HPA axis, another system activated by stress is the SNS. Sympathetic nerves innervate the bone marrow and release noradrenaline in response to stress (Ziegler, 2004). Noradrenaline is synthesised downstream of TH, the rate-limiting enzyme during catecholamines synthesis. To analyse whether mild CSDS altered sympathetic innervation of the bone marrow, tibia sections were stained for TH and imaged using confocal microscopy. TH+ nerve endings could clearly be identified in close proximity to blood vessels within the bone marrow (Figure 24A). Quantification of TH immunoreactivity within TH+ nerve endings showed that stress significantly increased TH levels in sympathetic nerve endings, indirectly suggesting increased production of noradrenaline (Figure 24B). It also seemed like the number of TH+ nerve endings was increased after stress, however this could not be reliably quantified, since the area of blood vessels varied strongly between samples, depending on the cutting angle of the sections.

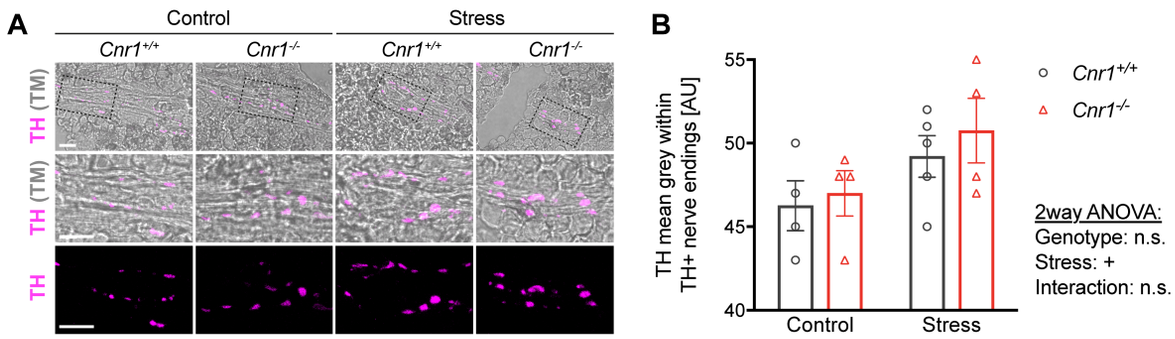

Figure 24. Mild CSDS increases tyrosine hydroxylase immunoreactivity in sympathetic nerves innervating the bone marrow. Tibias were collected after mild CSDS in one cohort of mice. Frozen, fixed and decalcified bones were cut into 10 µm longitudinal sections. Tyrosine hydroxylase (TH) was stained to identify noradrenergic nerve terminals innervating the bone marrow. Images were acquired using confocal microscopy using a 63x objective. Z-stacks of 10 µm were taken with a step size of 1 µm. **(A)** Representative images of maximum projections of z-stacks, showing TH-positive (TH+) nerve endings surrounding blood vessels within the bone marrow. Upper panels show overviews of a transmitted light (TM) image and TH signals (magenta). Black boxes indicate areas shown in higher magnification in the lower panels (middle: TM + TH signal; bottom: only TH signal for better visualisation); scale bar = 10 µm. **(B)** TH+ nerve endings were identified by applying an appropriate threshold and TH immunoreactivity (mean grey) was quantified within TH+ nerve endings (stress: $F_{(1,13)} = 4.94$, $p = 0.045$). AU = arbitrary unit. Data was analysed by 2way ANOVA, followed by Bonferroni *post-hoc* comparisons. For genotype effects (compared to *Cnr1*$^{+/+}$ of the same group) * $p < 0.05$, ** $p < 0.01$, *** $p < 0.001$. For stress effects (compared to control of the same genotype) + $p < 0.05$, ++ $p < 0.01$, +++ $p < 0.001$.

3.2.9 Regulation of CXCL12 in the bone marrow after mild CSDS

During chronic stress, both noradrenaline and GCs facilitate the egress of myeloid cells from the bone marrow into circulation via regulation of the chemokine stromal cell-derived factor 1, also known as C-X-C motif chemokine 12 (CXCL12) (Heidt et al., 2014; Niraula et al., 2018). CXCL12 is expressed by bone marrow stromal cells (among others) and functions as a retention factor for HSCs and myeloid cells within the bone marrow by interacting with its receptor CXCR4 expressed by those cells (Ding and Morrison, 2013; Eash et al., 2010). Therefore, *Cxcl12* gene expression was analysed in bone marrow cells isolated after mild CSDS using qPCR (Figure 25). A significant stress effect was detected, with stressed mice showing reduced *Cxcl12* expression. Although not significant in *post-hoc* comparisons for both genotypes, the reduction was slightly more pronounced in *Cnr1*$^{+/+}$ mice.

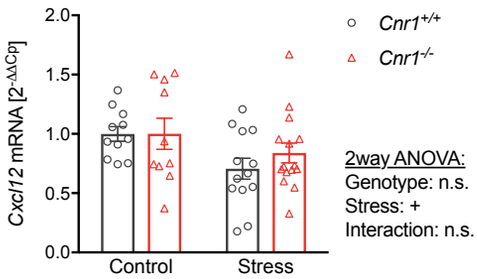

Figure 25. Mild CSDS reduces *Cxcl12* gene expression in the bone marrow. Bone marrow cells were isolated approximately 24 h after the last stress exposure in three cohorts of mice. RNA was isolated, reverse transcribed into cDNA and gene expression analysed by qPCR. Expression of target genes was normalised to the expression of reference gene *Hprt* and is presented as fold change from *Cnr1*$^{+/+}$ controls ($2^{-\Delta\Delta Cp}$). *Cxcl12* mRNA levels in the bone marrow (stress: $F_{(1,45)} = 5.97$, $p = 0.019$). Data was analysed by 2way ANOVA, followed by Bonferroni *post-hoc* comparisons. For genotype effects (compared to *Cnr1*$^{+/+}$ of the same group) * $p < 0.05$, ** $p < 0.01$, *** $p < 0.001$. For stress effects (compared to control of the same genotype) + $p < 0.05$, ++ $p < 0.01$, +++ $p < 0.001$.

3.2.10 Effects of mild CSDS on peripheral myeloid cells

As described above, chronic stress is associated with an increased production of myeloid cells in the bone marrow that are subsequently released into the circulation and migrate to different organs, including the spleen (Wohleb et al., 2015). In the spleen, they remain as a myelopoietic depot that provides persistent production of splenic monocytes even after cessation of the stressor (Mckim et al., 2018). Therefore, leukocytes from bone marrow, blood, and spleen were isolated after mild CSDS approximately 24 hours after the last stress exposure and myeloid cell populations analysed by flow cytometry.

3.2.10.1 Bone marrow

In the bone marrow, there was a clear stress effect on CD11b^{+} myeloid cells (Figure 26B). Separation of the myeloid cell population into neutrophils (Ly6G^{+} Ly6C^{int}) and monocytes (CD115^{+}) showed that the stress-induced increase in myeloid cells was mainly driven by neutrophils (Figure 26C). In *Cnr1*$^{-/-}$ mice, stress caused a significant increase in neutrophil frequencies compared to their control group and also compared to stressed *Cnr1*$^{+/+}$ mice. In contrast, mild CSDS had no significant effect on total CD115^{+} bone marrow monocytes (Figure 26D). However, there was a small tendency for *Cnr1*$^{-/-}$ mice showing higher monocyte frequencies. Similar to total monocytes, mild CSDS had no effect on bone marrow Ly6C^{hi} monocytes (Figure 26E), but *Cnr1*$^{-/-}$ mice had slightly higher frequencies (not significant). A significant stress effect was observed for Ly6C^{lo} monocytes, which were lower in stressed mice (Figure 26G), although the differences were not significant in *post-hoc* comparisons. Furthermore, *Cnr1*$^{-/-}$ mice showed slightly reduced CCR2 surface expression on Ly6C^{hi} monocytes (significant genotype effect) (Figure 26F).

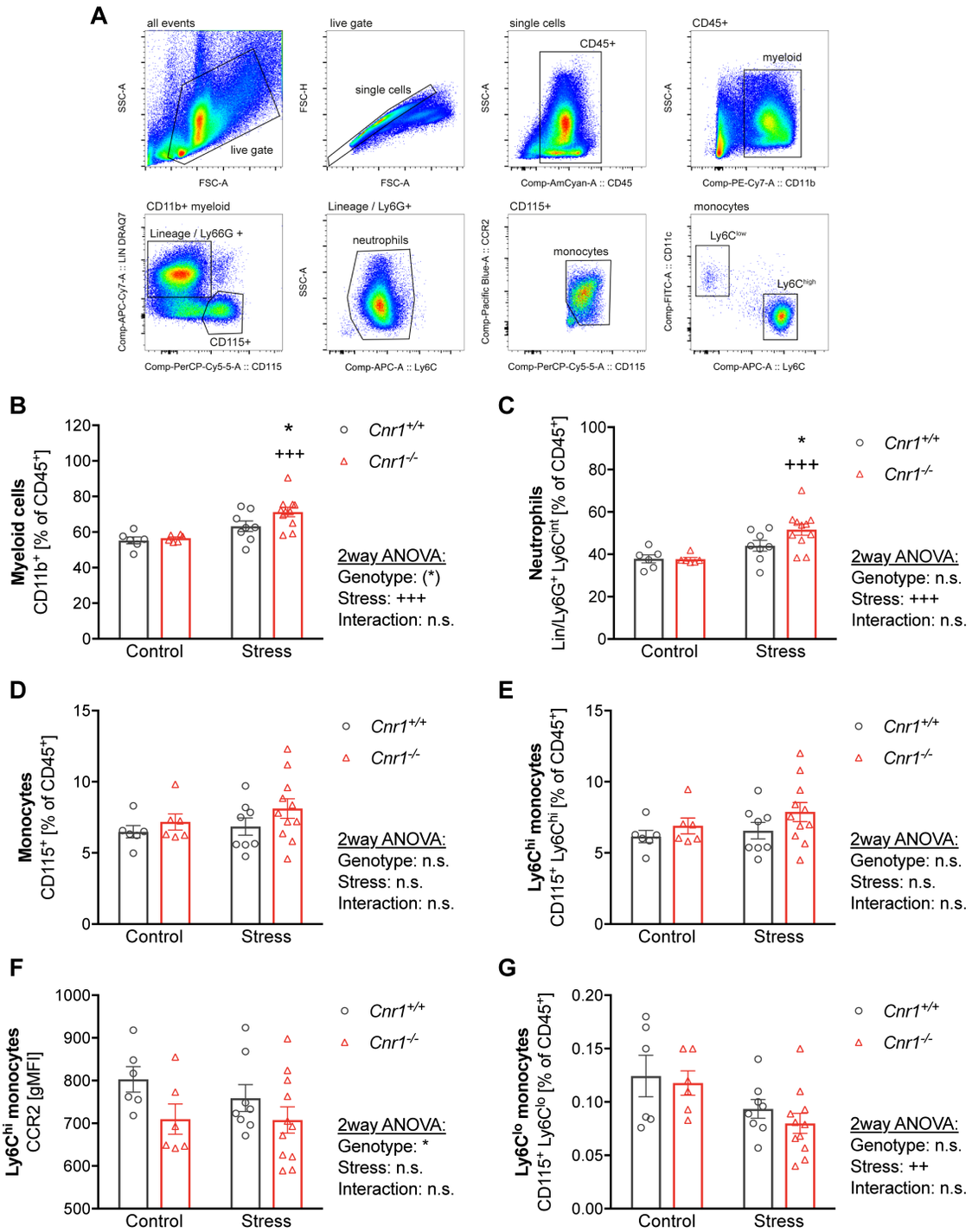

Figure 26. Mild CSDS increases neutrophil frequencies in the bone marrow of *Cnr1*$^{-/-}$ mice. After mild CSDS, bone marrow cells were isolated and analysed by flow cytometry in two cohorts of mice. **(A)** Gating strategy for bone marrow myeloid cells. Lineage stain included antibodies against CD3, CD19, NK1.1, TER-119, Ly6G, and DRAQ7™ for staining dead cells. Neutrophils were identified as CD11b^{+}, Lineage/Ly6G^{+}, Ly6C^{int}. Monocytes were identified as CD11b^{+}, Lineage/Ly6G^{neg}, CD115^{+} and divided into Ly6C^{hi} and Ly6C^{lo} subsets. A CD115$^{+/-}$ CCR2^{-} population was excluded from the CD115^{+} monocyte gate (possibly eosinophils). **(B)** Frequency of all CD11b^{+} myeloid cells (stress: $F_{(1,27)} = 18.2$, $p = 0.0002$; genotype: $F_{(1,27)} = 2.99$, $p = 0.095$). **(C)** Neutrophil frequency (stress: $F_{(1,27)} = 15.58$, $p < 0.0005$). **(D)** Total CD115^{+} monocyte frequency (genotype: $F_{(1,27)} = 2.12$, $p = 0.156$). **(E)** Ly6C^{hi} monocyte frequency (genotype: $F_{(1,27)} = 2.47$, $p = 0.128$). **(F)** CCR2 surface expression on Ly6C^{hi} monocytes, measured as geometric mean fluorescence intensity (gMFI) (genotype: $F_{(1,27)} = 4.57$, $p = 0.042$). **(G)** Ly6C^{lo} monocyte frequency (stress: $F_{(1,27)} = 7.91$, $p = 0.009$). Data was analysed by 2way ANOVA, followed by Bonferroni *post-hoc* comparisons. For genotype effects (compared to *Cnr1*$^{+/+}$ of the same group) * $p < 0.05$, ** $p < 0.01$, *** $p < 0.001$. For stress effects (compared to control of the same genotype) + $p < 0.05$, ++ $p < 0.01$, +++ $p < 0.001$.

3.2.10.2 Blood

In the same cohorts of mice, blood was collected for analysis of circulating leukocytes (Figure 27). Analysis of myeloid cell populations showed that stress had no significant effect on overall CD11b^{+} myeloid cells (Figure 27C), but slightly increased circulating neutrophils, with a tendency for a stress effect (Figure 27D). Mild CSDS did not significantly affect circulating monocytes, neither total CD115^{+} monocytes, nor the Ly6C^{hi} or Ly6C^{lo} subtypes (Figure 27F - G). In *Cnr1*$^{+/+}$ mice, stress increased the variance in Ly6C^{hi} monocytes, but did not overall increase their numbers. With the exception of two mice, stressed *Cnr1*$^{-/-}$ mice mostly showed lower Ly6C^{hi} frequencies than stressed *Cnr1*$^{+/+}$, however this was not significant (Figure 27F). In the blood, *Cnr1*$^{-/-}$ mice generally had less patrolling Ly6C^{lo} monocytes (significant genotype effect) (Figure 27G).

3.2.10.3 Spleen

After mild CSDS, overall CD11b^{+} myeloid cells were not changed in the spleen (Figure 28A), but a significant stress effect was observed for Ly6C^{hi} monocytes and Ly6C^{lo} monocytes/macrophages (Figure 28D - E). In *post-hoc* comparisons, this stress effect reached significance for Ly6C^{hi} monocytes in *Cnr1*$^{-/-}$ mice, where the amplitude of the stress effect was higher than in *Cnr1*$^{+/+}$ mice. Neutrophil frequencies were also significantly increased by stress in *Cnr1*$^{-/-}$ mice (significant stress x genotype interaction) (Figure 28C). Compared to the effects of standard CSDS on splenic myeloid cells (see Figure 11), the effects of mild CSDS were comparatively small. It should also be noted that the quality and quantity of splenocytes was not optimal for flow cytometry, possibly due to a rather long time-lag between cell isolation and analysis.

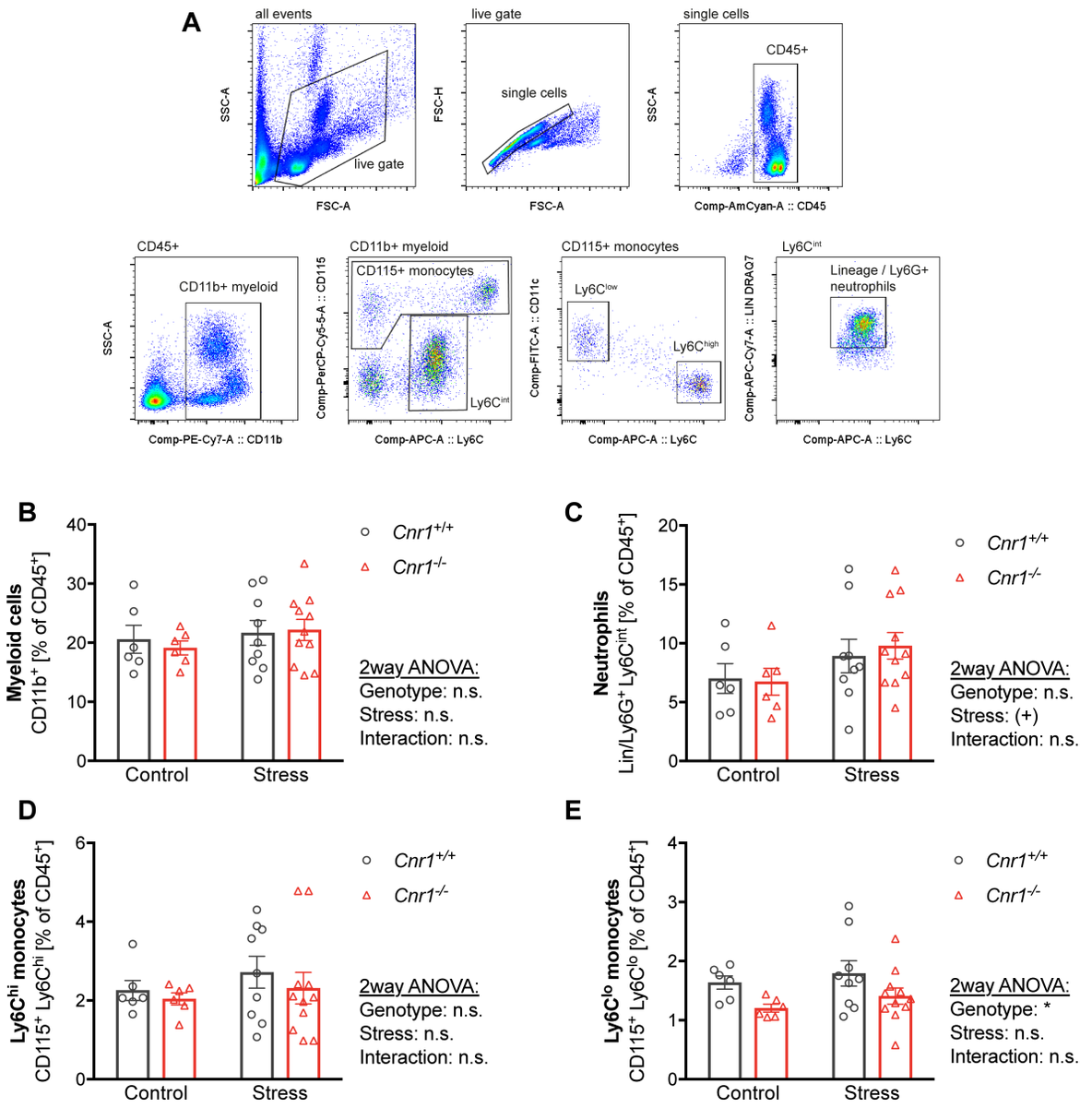

Figure 27. Mild CSDS has no major effect on circulating myeloid cell populations. After mild CSDS, whole blood was collected by cardiac puncture and analysed by flow cytometry in two cohorts of mice. **(A)** Gating strategy for blood cells. Lineage stain included antibodies against CD3, CD19, NK1.1, TER-119, Ly6G, and DRAQ7™ for staining dead cells. Neutrophils were identified as CD11b$^+$, Ly6C^{int,} Lineage/Ly6G$^+$. Monocytes were identified as CD11b$^+$ CD115$^+$ and divided into Ly6C^{hi} and Ly6C^{lo} subsets. **(B)** Frequency of CD11b$^+$ myeloid cells (no significant main effects). **(C)** Neutrophil frequency (stress: $F_{(1, 28)} = 3.08$, $p = 0.090$). **(D)** Ly6C^{hi} monocyte frequency (no significant main effects). **(E)** Ly6C^{lo} monocyte frequency (genotype: $F_{(1,28)} = 6.16$, $p = 0.019$). Data was analysed by 2way ANOVA, followed by Bonferroni *post-hoc* comparisons. For genotype effects (compared to *Cnr1*$^{+/+}$ of the same group) * $p < 0.05$, ** $p < 0.01$, *** $p < 0.001$. For stress effects (compared to control of the same genotype) + $p < 0.05$, ++ $p < 0.01$, +++ $p < 0.001$.

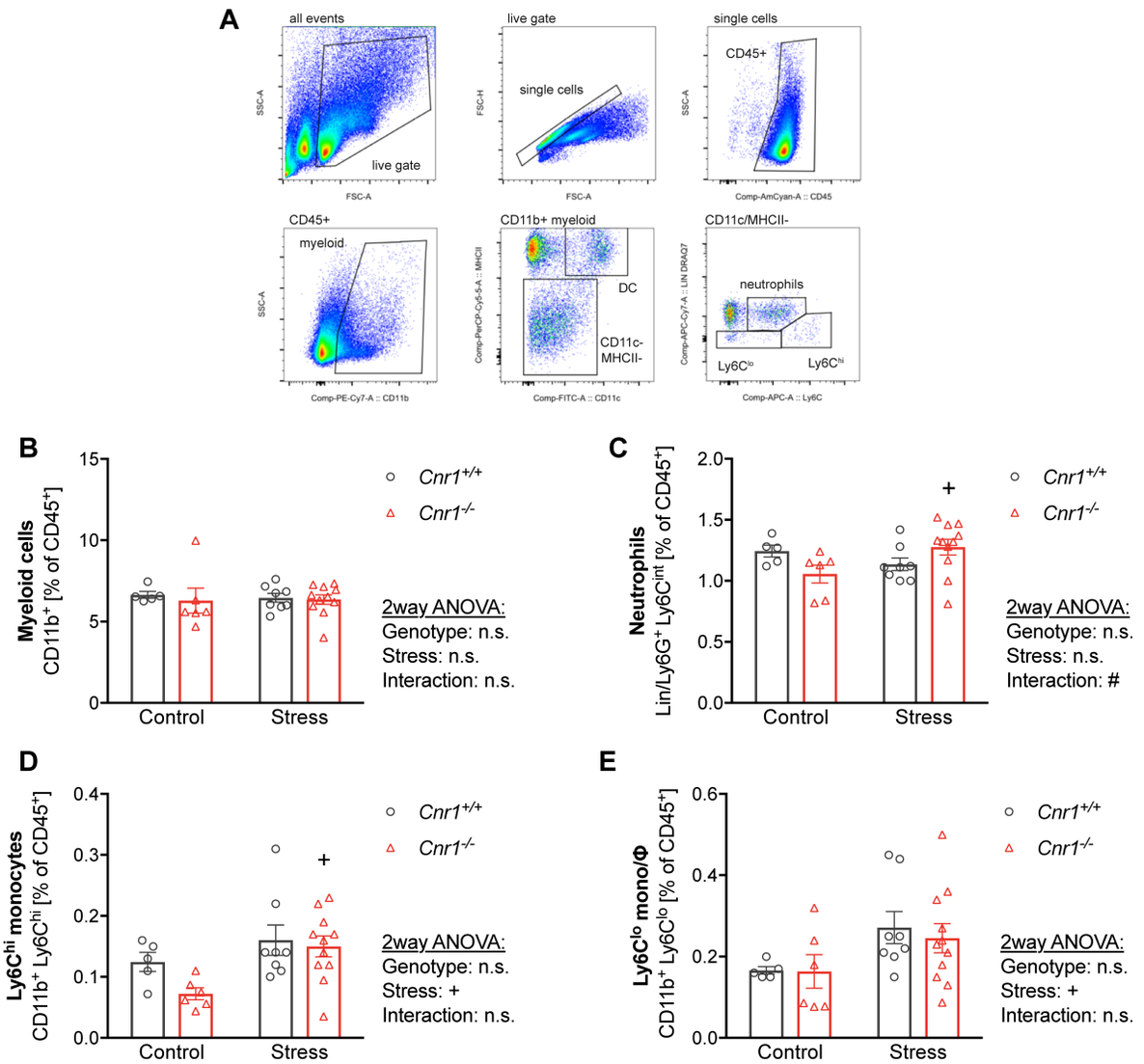

Figure 28. Mild CSDS slightly increases splenic myeloid cell frequencies in *Cnr1*$^{-/-}$ mice. After mild CSDS, spleens were collected and isolated splenocytes analysed by flow cytometry in two cohorts of mice. **(A)** Gating strategy for spleen cells. Lineage stain included antibodies against CD3, CD19, NK1.1, TER-119, Ly6G, and DRAQ7™ for staining dead cells. Neutrophils were identified as CD11b^{+}, CD11c/MHCII^{lo}, Ly6C^{int,} Lineage/Ly6G^{+}. Monocytes/macrophages were identified as CD11b^{+}, CD11c/MHCII^{lo} and divided into Ly6C^{hi} and Ly6C^{lo} subsets. **(B)** Frequency of CD11b^{+} myeloid cells (no significant main effects). **(C)** Neutrophil frequency (stress x genotype interaction: $F_{(1, 26)} = 5.97$, $p = 0.022$). **(D)** Ly6C^{hi} monocyte frequency (stress: $F_{(1,26)} = 7.67$, $p = 0.010$). **(G)** Ly6C^{lo} monocyte/macrophage frequency (stress: $F_{(1,26)} = 5.54$, $p = 0.026$). Data was analysed by 2way ANOVA, followed by Bonferroni *post-hoc* comparisons. For genotype effects (compared to *Cnr1*$^{+/+}$ of the same group) * $p < 0.05$, ** $p < 0.01$, *** $p < 0.001$. For stress effects (compared to control of the same genotype) + $p < 0.05$, ++ $p < 0.01$, +++ $p < 0.001$.

Correlation analysis of peripheral myeloid cell populations with the behavioural phenotype of mice showed that overall there was no clear association of myeloid cells with stress-susceptibility (Figure 29). The only significant correlation was found between splenic neutrophil frequencies and the stress score of *Cnr1*$^{+/+}$ mice (Figure 29E). However, neutrophil frequencies were generally not altered in these mice after mild CSDS, making it difficult to draw a valid conclusion. For Ly6C^{hi} monocytes, no significant correlations with the stress scores were found in any of the tissues analysed.

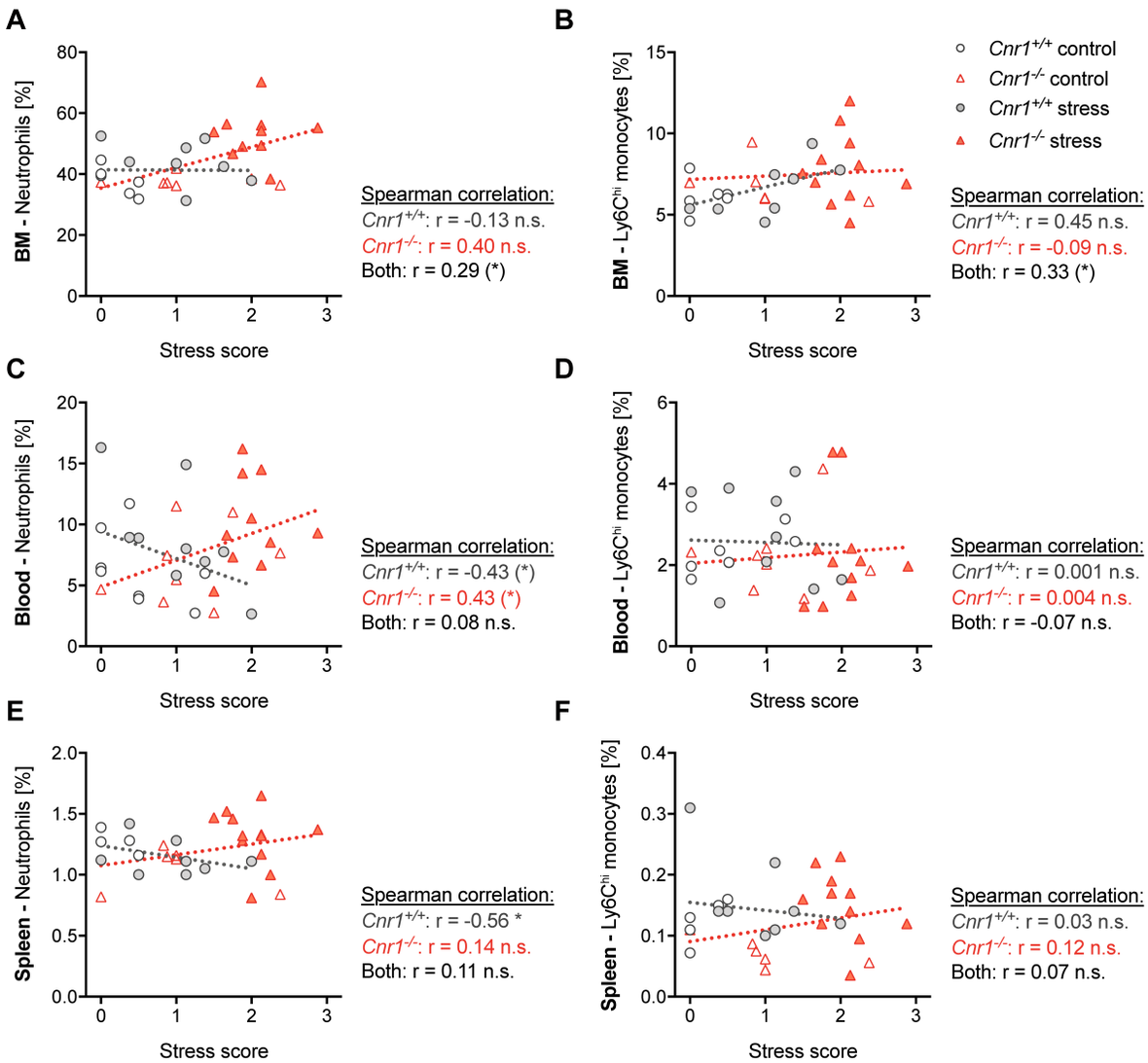

Figure 29. Overall, changes in peripheral myeloid cells do not correlate with behavioural susceptibility to mild CSDS. Results from flow cytometric analysis of peripheral myeloid cell populations were correlated to behavioural stress scores of individual mice. **(A)** Spearman correlation of bone marrow (BM) neutrophils vs. stress score (*Cnr1*$^{+/+}$: r = -0.23, p = 0.66; *Cnr1*$^{-/-}$: r = 0.40, p = 0.11; both genotypes: r = 0.29, p = 0.09). **(B)** BM Ly6C^{hi} monocytes vs. stress score (*Cnr1*$^{+/+}$: r = 0.45, p = 0.11; *Cnr1*$^{-/-}$: r = -0.09, p = 0.74; both genotypes: r = 0.33, p = 0.05). **(C)** Circulating neutrophils vs. stress score (*Cnr1*$^{+/+}$: r = -0.43, p = 0.08; *Cnr1*$^{-/-}$: r = 0.43, p = 0.07; both genotypes: r = 0.08, p = 0.66). **(B)** Circulating Ly6C^{hi} monocytes vs. stress score (*Cnr1*$^{+/+}$: r = 0.001, p = 0.99; *Cnr1*$^{-/-}$: r = -0.004, p = 0.99; both genotypes: r = -0.07, p = 0.70). **(D)** Splenic neutrophils vs. stress score (*Cnr1*$^{+/+}$: r = -0.56, p = 0.049; *Cnr1*$^{-/-}$: r = 0.14, p = 0.58; both genotypes: r = 0.11, p = 0.57). **(E)** Splenic Ly6C^{hi} monocytes vs. stress score (*Cnr1*$^{+/+}$: r = 0.03, p = 0.93; *Cnr1*$^{-/-}$: r = 0.12, p = 0.64; both genotypes: r = 0.07, p = 0.70).

Taken together, analysis of peripheral myeloid cell populations suggests that even mild CSDS induces myelopoiesis in the bone marrow (mainly neutrophils) and some accumulation of Ly6C^{hi} monocytes in the spleen. However, the effects were generally small and no significant differences were seen in circulating myeloid cells. In contrast, elevated blood Ly6C^{hi} monocytes were observed after standard CSDS (see Figure 11). Furthermore, lack of CB1 signalling seems to affect monocyte distribution in the periphery. Although the differences were minor, it seemed like *Cnr1*$^{-/-}$ mice generally had fewer circulating monocytes, especially of the Ly6C^{lo} subtype. This could possibly be related to reduced egress from the bone marrow, where monocyte frequencies were slightly higher in *Cnr1*$^{-/-}$ mice and CCR2 expression on monocytes was reduced.

3.2.11 Effects of mild CSDS on CNS myeloid cells

It has been reported in several studies that myeloid cells, especially inflammatory monocytes, are recruited to the brain during chronic stress, where they contribute to neuroinflammatory processes and the development of anxiety- and depressive-like behaviour (Reader et al., 2015; Wohleb et al., 2015). Therefore, brain mononuclear cells were isolated after mild CSDS from two cohorts of mice using Percoll density gradient centrifugation (Figure 30). In flow cytometric analysis, brain-resident microglia and infiltrated peripheral cells can be distinguished based on their expression of the leukocyte common antigen CD45 and the myeloid marker CD11b. While both microglia and peripheral myeloid cells are positive for CD11b, CD45 expression is higher on infiltrated cells (CD45^{hi}) than on microglia (CD45^{int}). Based on their expression of Ly6G and Ly6C, infiltrated cells can further be separated into neutrophils (Ly6G^{+}), inflammatory monocytes (Ly6G^{neg} Ly6C^{hi}), and macrophages/DCs (Ly6G^{neg} Ly6C^{lo}).

After mild CSDS, there was no apparent infiltration of peripheral cells into the brain parenchyma, irrespective of the cell type (Figure 30B - G). There was no change in microglia frequencies (CD45^{int} CD11b^{+}) and also no difference in total peripheral myeloid cells (CD45^{hi} CD11b^{+}). When separating those myeloid cells into neutrophils (Ly6G^{+}) and monocytes/macrophages/DCs (Ly6G^{-}), it seemed like *Cnr1*$^{-/-}$ mice had marginally reduced numbers of infiltrated monocytes/macrophages/DCs, but this did not reach significance. Further separation of cells into monocytes and macrophages/DCs did not provide any further information and cell numbers were overall too low to draw valid conclusions.

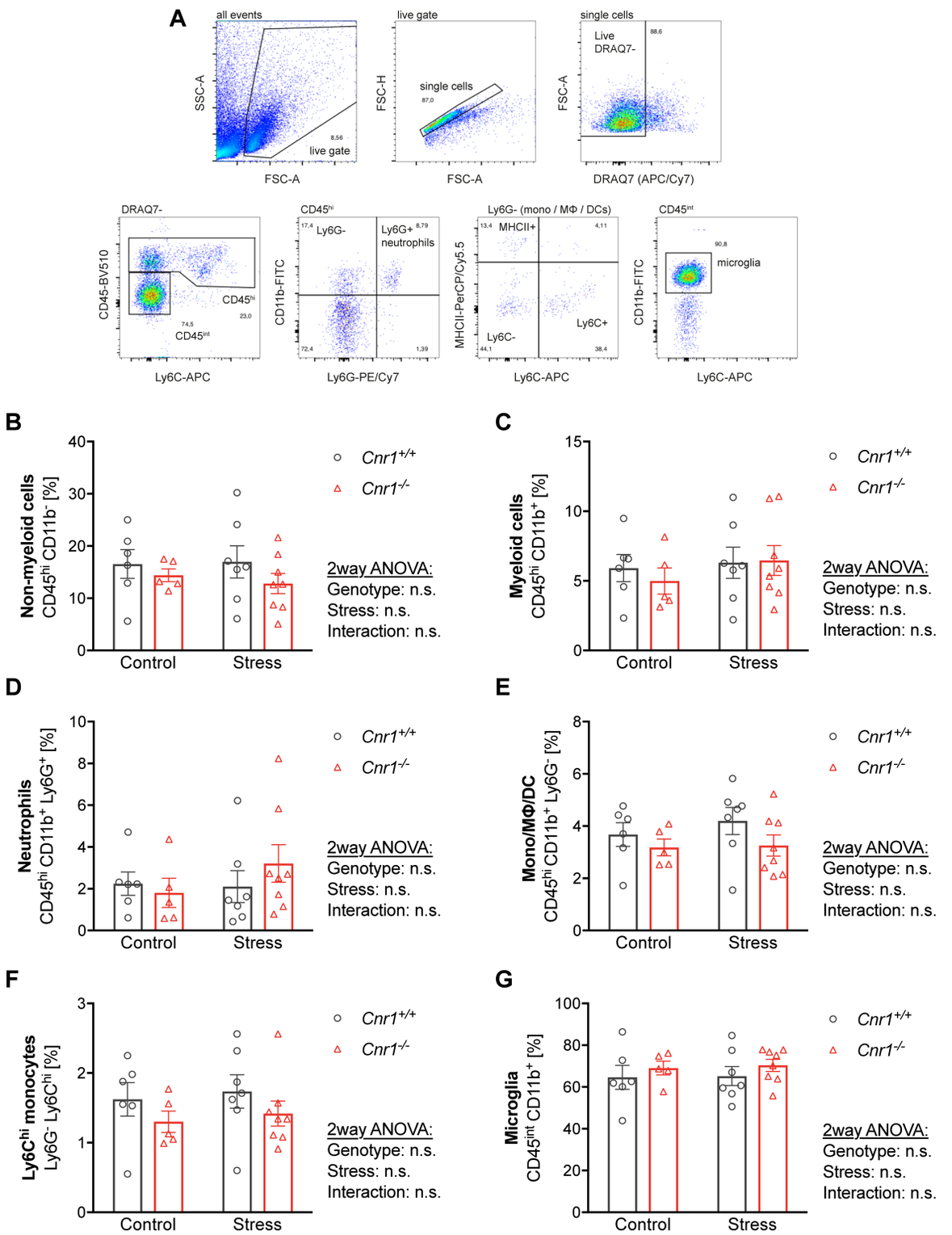

Figure 30. Mild CSDS does not cause infiltration of peripheral myeloid cells into the brain. After mild CSDS, brain mononuclear cells were isolated by Percoll gradient centrifugation and analysed by flow cytometry in two cohorts of mice. **(A)** Gating strategy for brain myeloid cells. Dead cells were stained with DRAQ7™. CD45 expression was used to differentiate between brain-resident microglia ($CD45^{int}$) and infiltrated peripheral cells ($CD45^{hi}$). Neutrophils were identified as $CD45^{hi}$ $CD11b^+$ $Ly6G^+$. Monocytes/macrophages/DCs were identified as $CD45^{hi}$ $CD11b^+$ $Ly6G^-$ and divided into $Ly6C^{hi}$ and $Ly6C^{lo}$ subsets. Microglia were identified as $CD45^{int}$ $CD11b^+$ **(B - C)** Frequency of infiltrated non-myeloid ($CD11b^-$) and myeloid ($CD11b^+$) cells (no significant main effects). **(D - F)** Myeloid cells were further separated into neutrophils, monocytes/macrophages/DCs and $Ly6C^{hi}$ monocytes (no significant main effects). **(G)** Frequency of brain-resident microglia (no significant main effects). Data was analysed by 2way ANOVA, followed by Bonferroni *post-hoc* comparisons.

Next to the infiltration of peripheral myeloid cells, activation of brain-resident microglia is commonly observed after chronic stress (Stein et al., 2017). Therefore, surface expression of activation markers CD11b, CD40, and MHCII was quantified on microglia, by measuring the gMFI or the percentage of microglia expressing the respective marker (Figure 31A). For all three markers, the highest values were measured on microglia of stressed *Cnr1*$^{-/-}$ mice. For CD11b, a significant stress effect was found that was driven by upregulation of CD11b gMFI after stress in *Cnr1*$^{-/-}$ mice (Figure 31B). For CD40 and MHCII, the percentage of positive cells was quantified, since these markers are not expressed by all microglia. Significant stress and genotype effects were detected for CD40, with stressed *Cnr1*$^{-/-}$ mice showing significantly more CD40^{+} microglia compared to their controls (Figure 31D), while the stress effect did not reach significance for *Cnr1*$^{+/+}$ mice. Similar results were also found for MHCII^{+} microglia (significant stress effect), but the differences did not reach significance in *post-hoc* comparisons (Figure 31F). Correlation analysis of microglial surface marker expression with the behavioural stress scores revealed a positive correlation for all three markers (Figure 31C, E and G). Thus, microglia activation marker expression was highest in those mice that showed the strongest stress-related behaviour. The directions of correlations were similar in both genotypes, however, they only reached significance in *Cnr1*$^{-/-}$ mice (for CD11b and CD40) or when mice of both genotypes were analysed together (for MHCII).

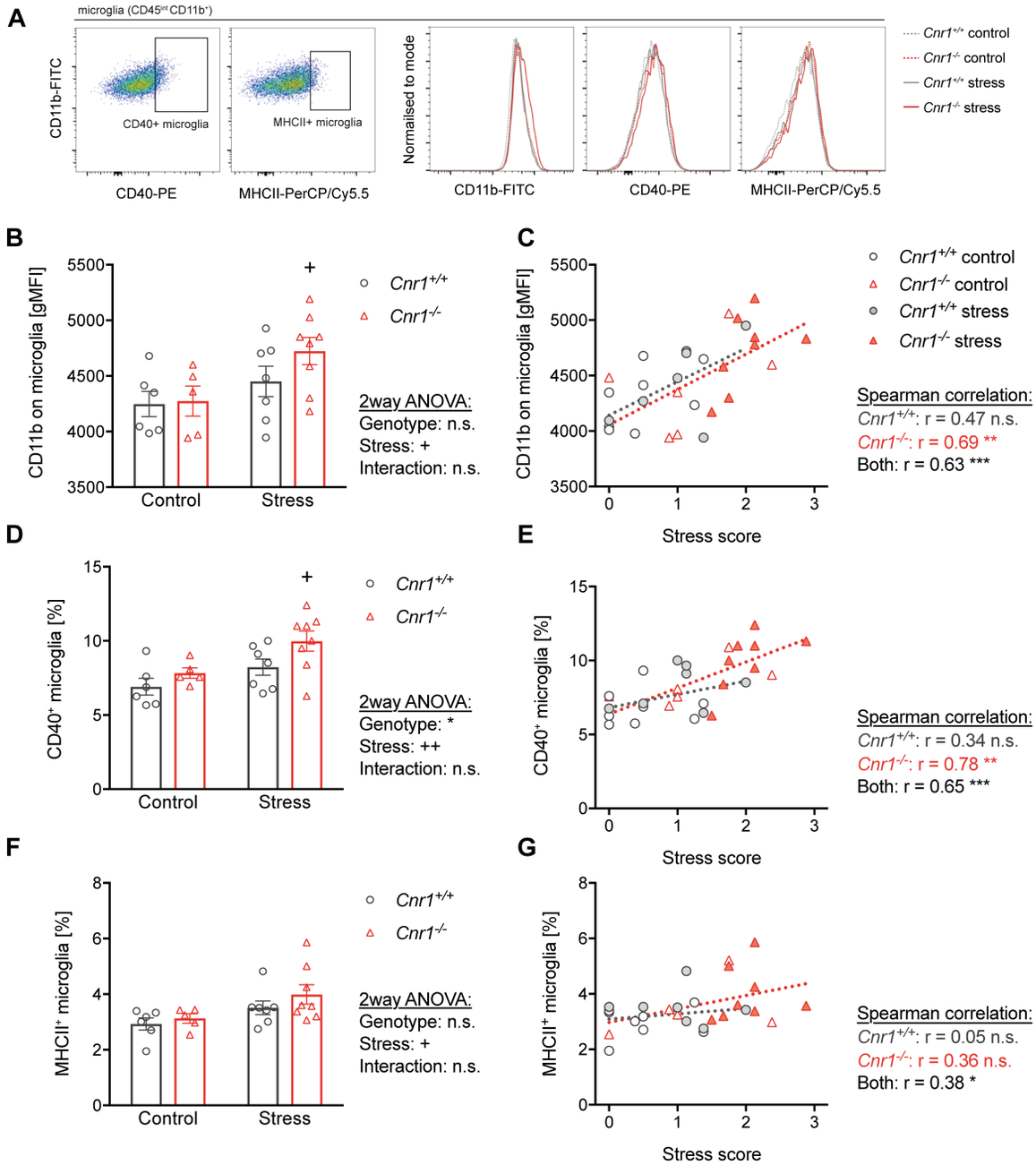

Figure 31. Surface expression of microglial activation markers is increased after mild CSDS in *Cnr1*$^{-/-}$ mice. After mild CSDS, brain mononuclear cells were isolated by Percoll gradient centrifugation and analysed by flow cytometry in two cohorts of mice. **(A)** Representative dot plots and histograms of surface marker expression on brain-resident microglia (CD45^{int} CD11b^{+} cells). **(B)** Geometric mean fluorescent intensity (gMFI) of CD11b on microglia (stress: $F_{(1, 22)} = 6.24$, $p = 0.021$). **(C)** Spearman correlation of CD11b gMFI vs. behavioural stress scores (*Cnr1*$^{+/+}$: $r = 0.47$, $p = 0.082$; *Cnr1*$^{-/-}$: $r = 0.69$, $p = 0.008$; both genotypes: $r = 0.63$, $p = 0.0002$). **(D)** Frequency of CD40^{+} microglia (stress: $F_{(1, 22)} = 8.21$, $p = 0.009$; genotype: $F_{(1, 22)} = 4.89$, $p = 0.038$). **(E)** Spearman correlation of CD40^{+} microglia vs. behavioural stress scores (*Cnr1*$^{+/+}$: $r = 0.34$, $p = 0.216$; *Cnr1*$^{-/-}$: $r = 0.78$, $p = 0.001$; both genotypes: $r = 0.65$, $p = 0.0001$). **(F)** Frequency of MHCII^{+} microglia (stress: $F_{(1, 22)} = 6.36$, $p = 0.019$). **(E)** Spearman correlation of MHCII^{+} microglia vs. behavioural stress scores (*Cnr1*$^{+/+}$: $r = 0.05$, $p = 0.851$; *Cnr1*$^{-/-}$: $r = 0.36$, $p = 0.207$; both genotypes: $r = 0.38$, $p = 0.04$). Data was analysed by 2way ANOVA, followed by Bonferroni *post-hoc* comparisons. For genotype effects (compared to *Cnr1*$^{+/+}$ of the same group) * $p < 0.05$, ** $p < 0.01$, *** $p < 0.001$. For stress effects (compared to control of the same genotype) + $p < 0.05$, ++ $p < 0.01$, +++ $p < 0.001$.

3.2.12 Effects of mild CSDS on microglia density and neurovascular ICAM-1 expression

Several studies showed that chronic stress leads to microglial rearrangements in stress-related brain areas, such as increased proliferation or altered morphology (Stein et al., 2017). It was also shown that chronic social stress increases neurovascular expression of adhesion molecule ICAM-1 in brain regions associated with stress-responses and emotional behaviour (Sawicki et al., 2015). Increased ICAM-1 enables adhesion of peripheral cells to blood vessels and thereby facilitates their interaction with the brain and possibly their entry into the brain parenchyma. Therefore, ICAM-1 and IBA1 (which stains microglia and macrophages/monocytes) immunoreactivity was analysed in the brain after mild CSDS using immunohistochemistry and confocal microscopy. IBA1+ area was quantified in thresholded images to determine the density of the microglial network in different brain regions. For quantification of neurovascular ICAM-1+ area, an appropriate threshold was applied to exclude ICAM-1 expression on microglia or macrophages, which was considerably lower than vascular ICAM-1.

3.2.12.1 Hippocampus

In the dentate gyrus (DG) of the hippocampus, IBA1+ area was significantly increased by stress in *Cnr1*$^{+/+}$, but not in *Cnr1*$^{-/-}$ mice (significant stress x genotype interaction) (Figure 32B). In contrast, the number of IBA1+ cells in the same area was not affected by stress or genotype (Figure 32C), suggesting that the difference in IBA1+ area was caused by altered morphology of microglia or altered expression levels of IBA1 itself. Similarly, a significant stress effect and a stress x genotype interaction was detected for neurovascular ICAM-1 expression in the DG, since ICAM-1+ area was significantly increased by stress in *Cnr1*$^{+/+}$ mice, but not in *Cnr1*$^{-/-}$ mice (Figure 32D). To further exclude that the observed changes in ICAM-1+ area were caused by altered ICAM-1 expression on microglia, ICAM-1 immunoreactivity was quantified in IBA1+ cells in images taken with higher resolution within the molecular layer of the DG (Figure 32A, right panel). No difference between the groups was observed for ICAM-1 mean grey intensity within the IBA1+ area (Figure 32E).

Correlation analysis with the behavioural stress score revealed a significant positive correlation in *Cnr1*$^{+/+}$ mice between stress score and IBA1+ area (Figure 33A) as well as ICAM-1+ area (Figure 33B). In contrast, there was no correlation for IBA1 in *Cnr1*$^{-/-}$ mice and only a tendency for a positive correlation for ICAM-1.

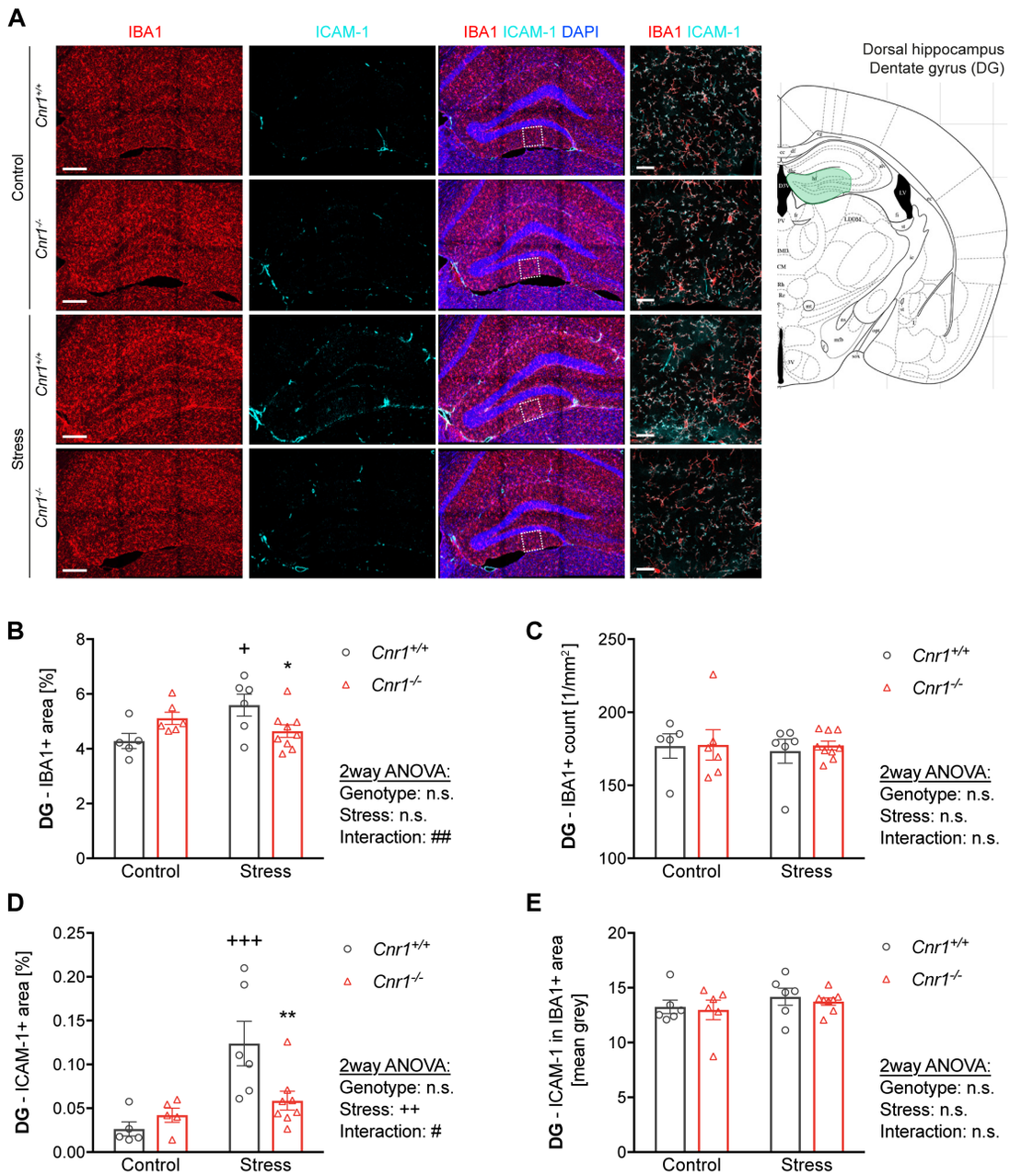

Figure 32. Hippocampal IBA1 and ICAM-1 immunoreactivity is increased by mild CSDS only in *Cnr1*$^{+/+}$ mice. Coronal brain sections of 60 µm were stained for IBA1 (red) and ICAM-1 (cyan), nuclei were stained with DAPI (blue). Sections were imaged using confocal microscopy. **(A)** Left panels: representative images of the dentate gyrus (DG) of the hippocampus, acquired with a 20x objective. Z-stacks of 9 µm were taken with a step size of 3 µm. Maximum projections are shown. Scale bar = 200 µm. Right panel: higher magnification images of the inferior molecular layer (indicated by white boxes in overview) were acquired using the 63x objective. Z-stacks of 40 – 50 µm were acquired with a step size of 0.5 µm. Maximum projections of 5 µm depth are shown. Scale bar = 25 µm. **(B)** Quantification of IBA1+ area in the DG in 20x overview images (stress x genotype interaction: $F_{(1,22)} = 9.23$, $p = 0.006$). **(C)** Microglia. **(E)** Quantification of ICAM-1 immunoreactivity on microglia, measured as ICAM-1 mean grey intensity within the IBA1+ area (no significant main effects). Data was analysed by 2way ANOVA, followed by Bonferroni *post-hoc* comparisons. For genotype effects (compared to *Cnr1*$^{+/+}$ of the same group) * $p < 0.05$, ** $p < 0.01$, *** $p < 0.001$. For stress effects (compared to control of the same genotype) + $p < 0.05$, ++ $p < 0.01$, +++ $p < 0.001$.

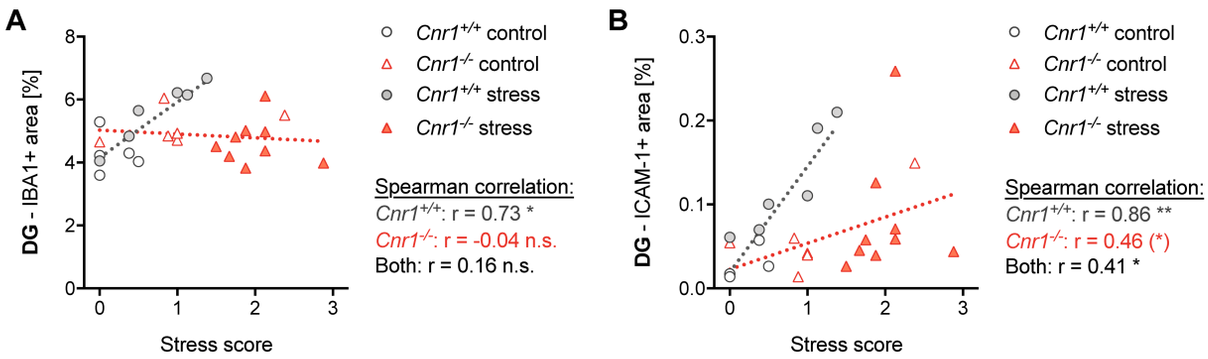

Figure 33. Changes in dentate gyrus IBA1 and ICAM-1 immunoreactivity are correlated with behavioural stress scores only in *Cnr1*$^{+/+}$ mice. Results from immunohistochemical staining of IBA1 and ICAM-1 in the dentate gyrus (DG) of the hippocampus were correlated to behavioural stress scores of individual mice. **(A)** Spearman correlation of IBA1+ area vs. stress score (*Cnr1*$^{+/+}$: r = 0.73, p = 0.014; *Cnr1*$^{-/-}$: r = -0.04, p = 0.88; both genotypes: r = 0.16, p = 0.429). (B) Spearman correlation of ICAM-1+ area vs. stress score (*Cnr1*$^{+/+}$: r = 0.86, p = 0.001; *Cnr1*$^{-/-}$: r = 0.46, p = 0.085; both genotypes: r = 0.41, p = 0.04).

Similar effects on IBA1 and ICAM-1 immunoreactivity were also observed in the CA1 region of the hippocampus (Figure 34). ICAM-1+ area was significantly increased by stress in *Cnr1*$^{+/+}$, but not in *Cnr1*$^{-/-}$ mice (significant stress effect, tendency for stress x genotype interaction) (Figure 34C). For IBA1+ area, the directions of the effects were the same, but did not reach significance (Figure 34B).

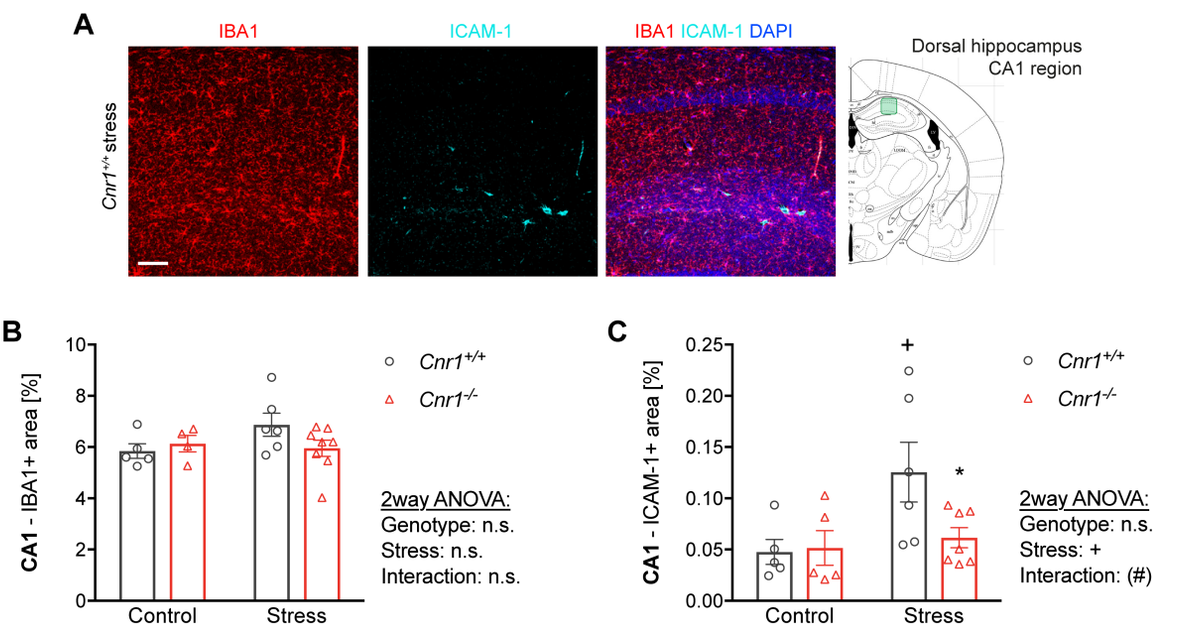

Figure 34. Hippocampal CA1 neurovascular ICAM-1 immunoreactivity is increased by mild CSDS only in *Cnr1*$^{+/+}$ mice. **(A)** Exemplary image of the CA1 region of the hippocampus of a stressed *Cnr1*$^{+/+}$ mouse, stained for IBA1 (red) and ICAM-1 (cyan), nuclei were stained with DAPI (blue). Scale bar = 50 µm. **(B)** Quantification of IBA1+ area in the CA1 region (no significant main effects). **(D)** Quantification of ICAM-1+ area in the CA1 region (stress: $F_{(1,19)}$ = 5.39, p = 0.032; stress x genotype interaction: $F_{(1,19)}$ = 3.21, p = 0.089). Data was analysed by 2way ANOVA, followed by Bonferroni *post-hoc* comparisons. For genotype effects (compared to *Cnr1*$^{+/+}$ of the same group) * p < 0.05, ** p < 0.01, *** p < 0.001. For stress effects (compared to control of the same genotype) + p < 0.05, ++ p < 0.01, +++ p < 0.001.

3.2.12.2 Amygdala and mPFC

Quantification of IBA1 immunoreactivity in the amygdala and mPFC revealed a similar pattern as observed in the hippocampus, although they were not as pronounced as in the DG (Figure 35). No difference was observed for the number of IBA1+ cells in the amygdala (Figure 35 C), but a significant stress x genotype interaction was found for IBA1+ area (Figure 35B). Stress slightly increased IBA1+ area in *Cnr1*$^{+/+}$ mice and had the opposite effect in *Cnr1*$^{-/-}$ mice. In contrast, stress or genotype had no significant effect on IBA1+ area in the mPFC (Figure 35E), but stress slightly increased the number of IBA1+ cells (not significant in *post-hoc* comparisons) (Figure 35F). Quantification of neurovascular ICAM-1 in the amygdala and mPFC revealed very similar effects as those observed in the hippocampus, with a stress-induced increase in ICAM-1+ area in *Cnr1*$^{+/+}$, but not in *Cnr1*$^{-/-}$ mice (Figure 35D and G). These effects reached statistical significance in the mPFC, but not in the amygdala.

To verify that the observed changes were indeed caused by microglia and not by infiltrated monocytes (which are also IBA1+), brain sections were co-labelled for IBA1 and TMEM119, a recently identified marker that is specific for brain-resident microglia and is not expressed by peripheral, meningeal and perivascular macrophages (Bennett et al., 2016). In the DG, changes in TMEM119+ area were very similar to those observed for IBA1, with a stress-induced increase in *Cnr1*$^{+/+}$, but not in *Cnr1*$^{-/-}$ mice (Figure 36B). However, the variance of the TMEM119 signal was rather high and the effects did not reach statistical significance (tendency for a stress x genotype interaction). Correlation analysis further showed a strong positive correlation between IBA1 and TMEM signals, supporting that the changes observed in IBA1+ area were caused by changes in brain-resident microglia (Figure 36C). Nonetheless, it should be noted that there were indeed a few IBA1+ TMEM119- cells. Mostly, those cells were found in proximity to blood vessels or meningeal regions and also displayed a round or rod-shaped morphology, rather different from the morphology of typical microglia (Figure 36A, white arrows). Only a very small number of IBA1+ TMEM119- cells with ramified morphology were found in the regions analysed. An interesting observation was that TMEM119 immunoreactivity was generally weaker in the granule cell layer and the subgranular zone of the DG, a region associated with neurogenesis. Although IBA1+ cells in this area had a faint TMEM119 signal, it was much weaker compared to other hippocampal regions (Figure 36A, arrow heads).

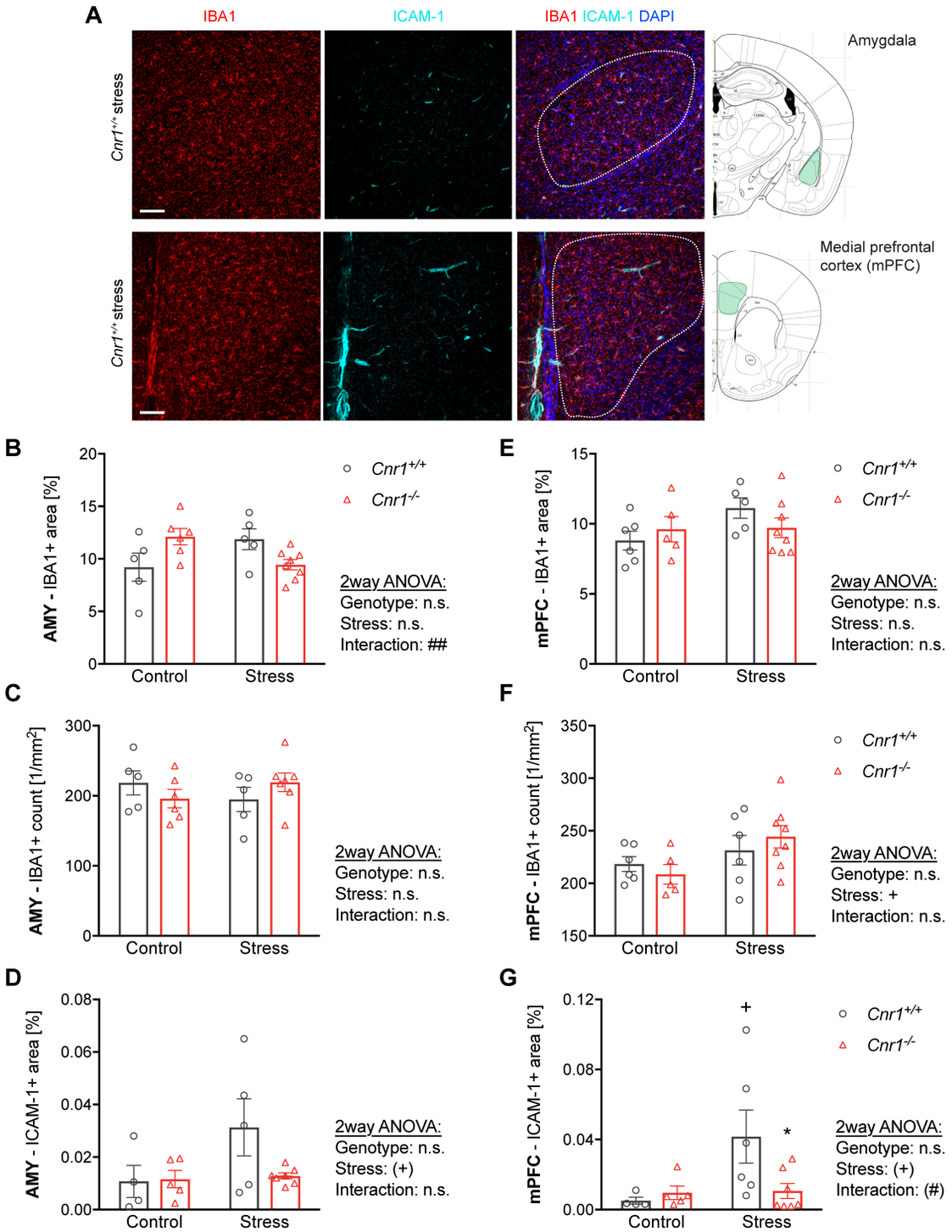

Figure 35. IBA1 and neurovascular ICAM-1 immunoreactivity in the amygdala and prefrontal cortex after mild CSDS. **(A)** Exemplary image of the amygdala (upper panel) and mPFC (lower panel) of a stressed *Cnr1*$^{+/+}$ mouse, stained for IBA1 (red) and ICAM-1 (cyan), nuclei were stained with DAPI (blue). White dashed lines indicate the region analysed. Scale bar = 50 µm. **(B)** Quantification of IBA1+ area in the amygdala (stress x genotype interaction: $F_{(1,20)} = 9.37$, $p = 0.006$). **(C)** Number of microglia (IBA1+ cells) in the amygdala (no significant main effects). **(D)** Quantification of ICAM-1+ area in the amygdala (stress: $F_{(1,17)} = 3.27$, $p = 0.088$). **(E)** Quantification of IBA1+ area in the mPFC (no significant main effects). **(F)** Number of IBA1+ cells in the mPFC (stress: $F_{(1,21)} = 4.89$, $p = 0.038$). **(G)** Quantification of ICAM-1+ area in the amygdala (stress: $F_{(1,18)} = 4.17$, $p = 0.056$; stress x genotype interaction: $F_{(1,18)} = 3.72$, $p = 0.070$). Data was analysed by 2way ANOVA, followed by Bonferroni *post-hoc* comparisons. For genotype effects (compared to *Cnr1*$^{+/+}$ of the same group) * $p < 0.05$, ** $p < 0.01$, *** $p < 0.001$. For stress effects (compared to control of the same genotype) + $p < 0.05$, ++ $p < 0.01$, +++ $p < 0.001$.

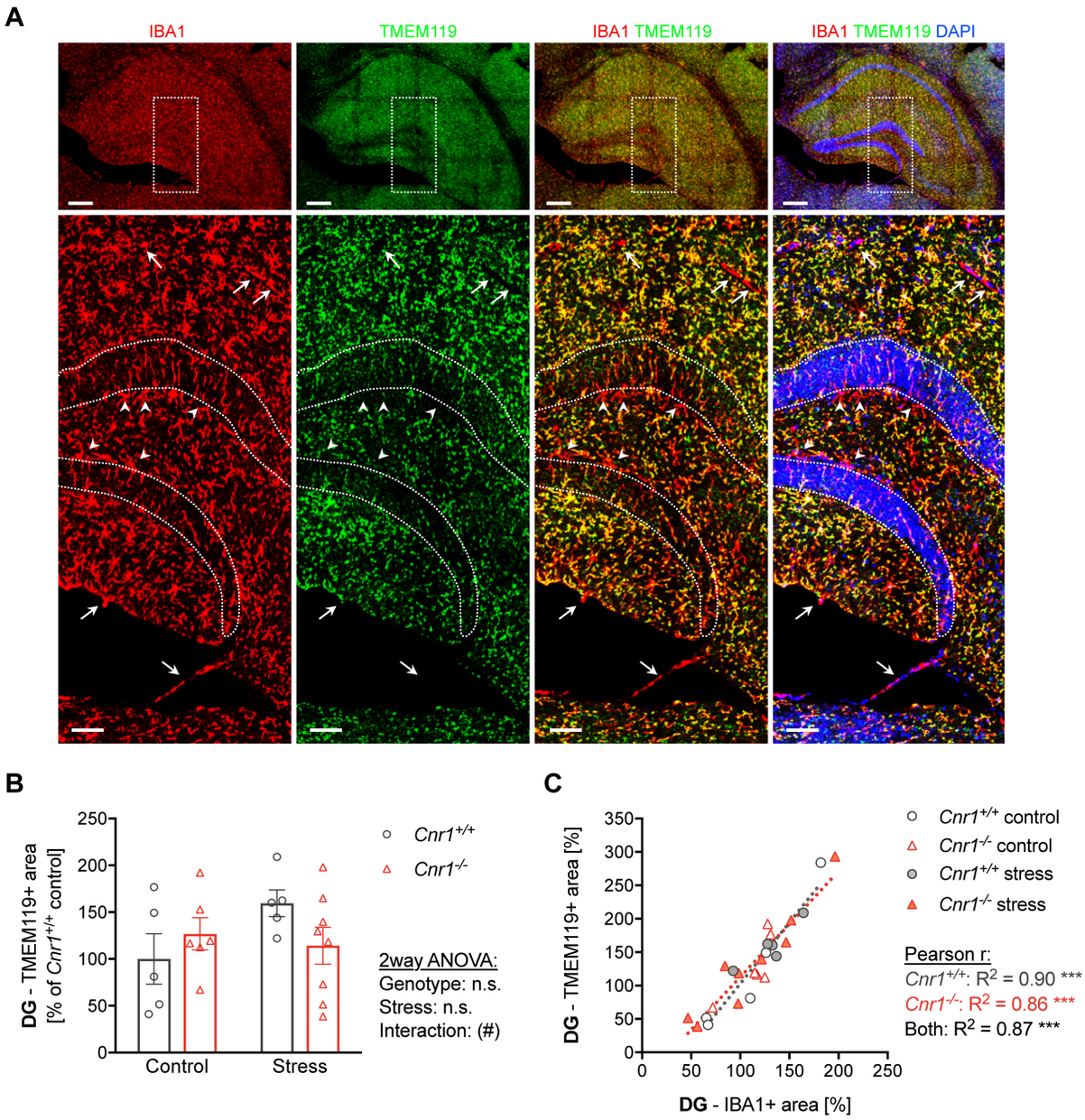

Figure 36. Stress-induced changes in IBA1 immunoreactivity are driven by brain-resident microglia. Coronal brain sections of 60 µm were stained with antibodies against IBA1 (red) and TMEM119 (green), nuclei were stained with DAPI (blue). Sections were imaged using confocal microscopy. **(A)** Upper panels: representative image of the hippocampus of a *Cnr1*$^{+/+}$ control mouse, acquired with a 20x objective, a single z-plane is shown. Scale bar = 200 µm. Bottom panel: higher magnification images of region of interest (indicated by white boxes in panel above). Arrows indicate IBA1+ TMEM119- cells, representing perivascular/meningeal macrophages, the arrow heads indicate IBA1+, TMEM119^{low} cells with ramified morphology in the subgranular zone of the DG. Scale bar = 50 µm. **(B)** Quantification of TMEM119+ area in the DG in 20x overview images (stress x genotype interaction: $F_{(1,20)} = 3.06$, $p = 0.096$). Data was analysed by 2way ANOVA, followed by Bonferroni *post-hoc* comparisons. For genotype effects (compared to *Cnr1*$^{+/+}$ of the same group) * $p < 0.05$, ** $p < 0.01$, *** $p < 0.001$. For stress effects (compared to control of the same genotype) + $p < 0.05$, ++ $p < 0.01$, +++ $p < 0.001$. **(C)** Pearson correlation analysis of IBA1+ vs. TMEM119+ area in the DG (for both genotypes: $R^2 = 0.87$, $p < 0.0001$).

3.2.13 Effects of mild CSDS on microglia morphology

To determine the cause for the differences in IBA1+ area, microglia morphology was analysed in more detail. Therefore, high resolution z-stack images of 40 – 50 µm depth were acquired and analysed using an ImageJ-based analysis tool that automatically traces cells through the z-stack to generate 3D reconstructions and skeletons of individual cells. Thereby, different morphological parameters, such as cell volume, number of branches, and many more can be determined.

3.2.13.1 Hippocampus: dentate gyrus

Analysis of microglia in the inferior molecular layer of the DG revealed that microglia morphology was differently affected by stress in *Cnr1*$^{+/+}$ and *Cnr1*$^{-/-}$ mice (Figure 37A). Firstly, IBA1 average intensity on individual microglia was significantly affected by both stress and genotype (Figure 37B). In both genotypes, IBA1 intensity was significantly increased by stress. Microglia of stressed *Cnr1*$^{+/+}$ mice showed highest IBA1 intensities, which were also significantly higher than those of stressed *Cnr1*$^{-/-}$ mice. For the cell soma size, a significant stress x genotype interaction was found, since microglial cell bodies were slightly enlarged after stress in *Cnr1*$^{+/+}$, but not in *Cnr1*$^{-/-}$ mice (Figure 37C). In contrast, a significant stress effect was observed for the number of branches per microglial cell, which was based on a stress-induced reduction in *Cnr1*$^{-/-}$ mice, while no significant differences were observed for *Cnr1*$^{+/+}$ mice (Figure 37D). Similar results were also observed for the number of junctions and the tree length, i.e. the total length of all processes (see Appendix). For both cell volume and cell surface area, significant stress effects and stress x genotype interactions were detected (Figure 37E - F). Under control conditions, microglia of *Cnr1*$^{-/-}$ mice had a slightly, albeit not significantly higher cell volume and surface than those of *Cnr1*$^{+/+}$ mice. Stress lead to a significant reduction of cell volume and surface area in *Cnr1*$^{-/-}$ mice, while it had no effect in *Cnr1*$^{+/+}$ mice. The ramification index, which is a measure for the complexity of the cellular shape, was also significantly affected by stress (Figure 37G). Although the effect was more pronounced in *Cnr1*$^{-/-}$ mice, stressed mice of both genotypes showed significantly lower ramification indexes compared to their respective control group. In *Cnr1*$^{+/+}$ mice, this reduction was probably caused by the increase in cell body size, while in *Cnr1*$^{-/-}$ mice it was based on reduced branching.

Overall, the results suggest that the stress-induced increase in IBA1+ area observed in the DG of *Cnr1*$^{+/+}$ mice (see Figure 32) was caused by increased cell soma size and higher expression of IBA1 on microglia. Since IBA1+ area was measured by applying a threshold, increased IBA1 expression would result in more particles falling within the IBA1+ threshold and thus increased IBA1+ area. In contrast, the lack of a stress effect on IBA1+ area in *Cnr1*$^{-/-}$ mice can be explained by morphological rearrangements of microglial processes. Microglia of stressed *Cnr1*$^{-/-}$ mice had less branches and were smaller than those of *Cnr1*$^{-/-}$ controls, which overall negated the increase in IBA1 expression.

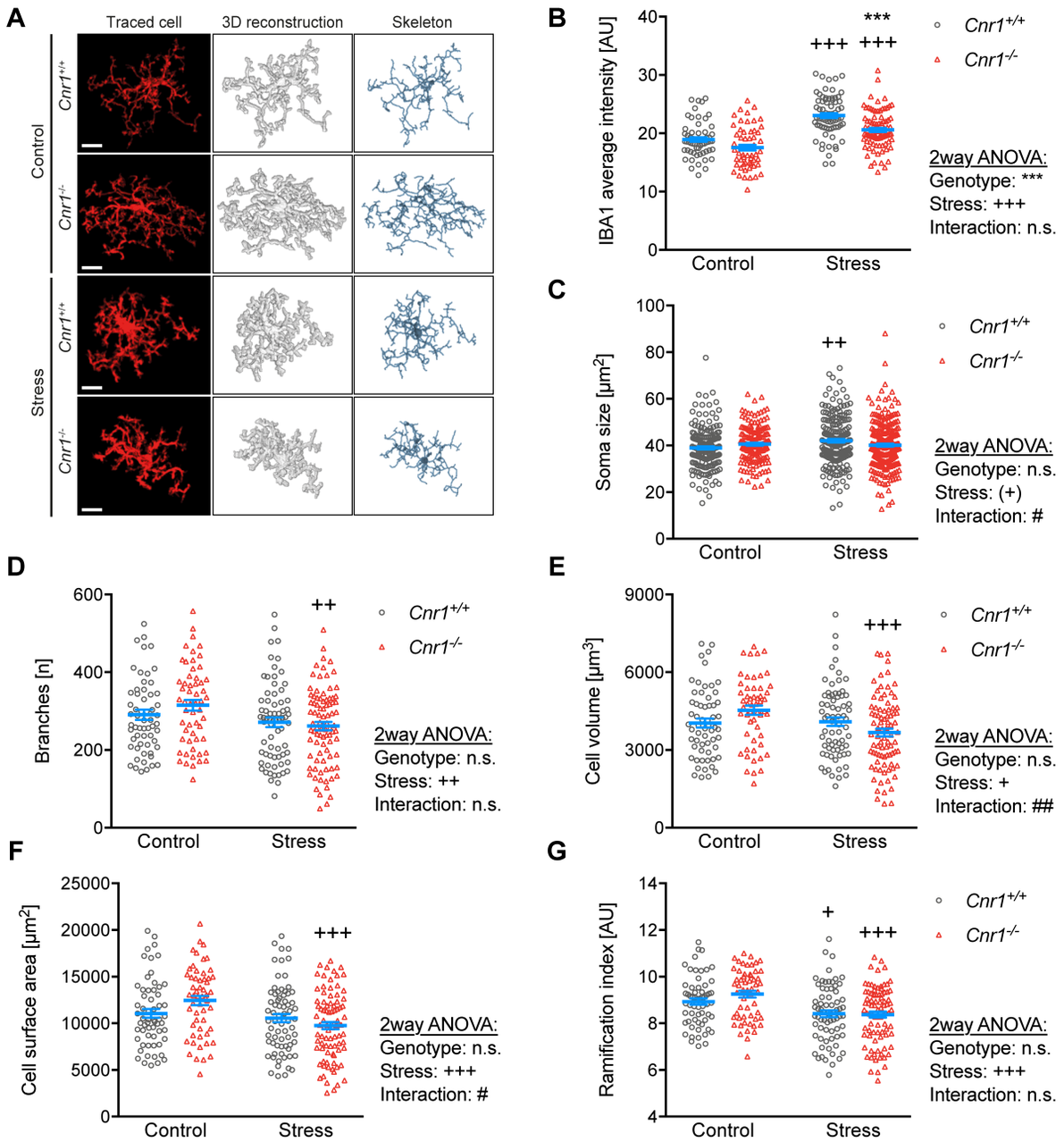

Figure 37. Mild CSDS alters microglia branching in the dentate gyrus of the hippocampus only in *Cnr1*$^{-/-}$ mice. Microglia morphology after mild CSDS was analysed in the inferior molecular layer of the dentate gyrus (DG) of the hippocampus. Coronal brain sections of 60 µm were stained for IBA1 and images acquired using confocal microscopy. Z-stack images were analysed using an automated ImageJ-based analysis tool that traces cells through the z-stack to generate 3D reconstructions and cell skeletons. A total of 56 – 87 cells were analysed per group. **(A)** Representative images of traced microglia and resulting 3D reconstructions and cell skeletons. Scale bar = 5 µm. **(B)** Average intensity (mean grey) of IBA1 immunoreactivity on traced cells (stress: $F_{(1,269)} = 76.4$, $p < 0.0001$; genotype: $F_{(1,269)} = 22.24$, $p < 0.0001$). **(C)** Cell soma size, analysed manually in z-projections (stress: $F_{(1,793)} = 3.61$, $p = 0.058$, stress x genotype interaction: $F_{(1,793)} = 6.66$, $p = 0.010$). **(D)** Number of branches per cell, determined from skeletons (stress: $F_{(1,269)} = 8.465$, $p = 0.0039$). **(E)** Cell volume determined from 3D reconstructed cells (stress: $F_{(1,265)} = 5.712$, $p = 0.0175$; stress x genotype interaction: $F_{(1,265)} = 7.282$, $p = 0.0074$). **(F)** Cell surface area determined from 3D reconstructed cells (stress: $F_{(1,266)} = 12.58$, $p = 0.0005$, stress x genotype interaction: $F_{(1,266)} = 5.932$, $p = 0.0155$). **(G)** Ramification index, determined from 3D reconstructed cells. The ramification index is a unit-free parameter describing the complexity of the cellular shape, a value of one corresponds to a perfectly round cell without processes (stress: $F_{(1,269)} = 24.0$, $p < 0.0001$). AU = arbitrary unit. Data was analysed by 2way ANOVA, followed by Bonferroni *post-hoc* comparisons. For genotype effects (compared to *Cnr1*$^{+/+}$ of the same group) * $p < 0.05$, ** $p < 0.01$, *** $p < 0.001$. For stress effects (compared to control of the same genotype) + $p < 0.05$, ++ $p < 0.01$, +++ $p < 0.001$.

To test whether changes in microglial morphology were associated with behavioural stress-susceptibility, mean values of each animal were correlated to the respective behavioural stress score (Figure 38). While IBA1 intensity and soma size were not correlated with stress scores in either genotype (Figure 38A - B), significant negative correlations were detected in *Cnr1*$^{-/-}$ mice for the number of branches (Figure 38C), cell volume (Figure 38D), surface area (Figure 38E), and the ramification index (Figure 38F). In contrast, these parameters were not correlated with the behaviour in *Cnr1*$^{+/+}$ mice.

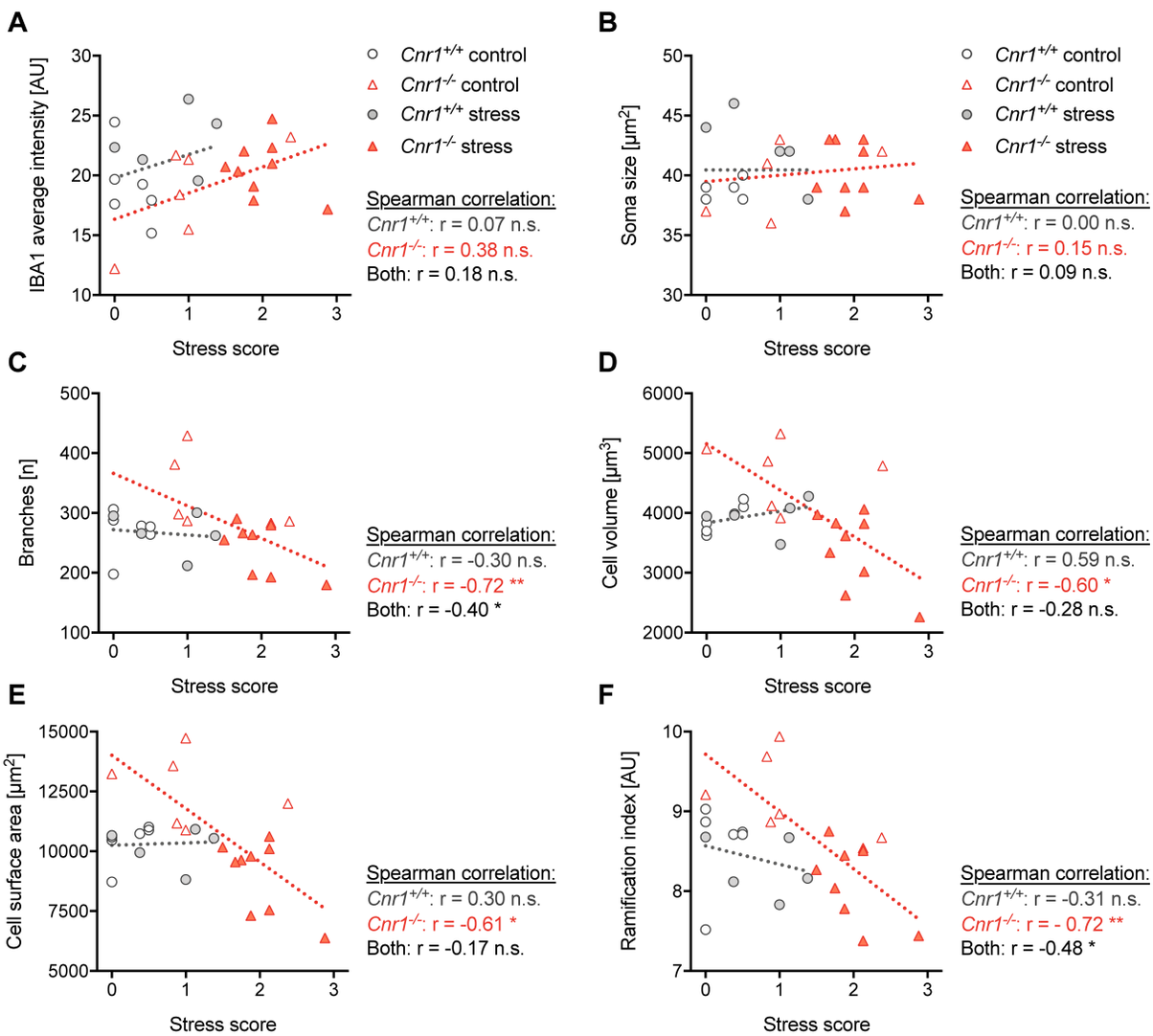

Figure 38. Microglia morphology changes in the dentate gyrus are correlated with stress-related behaviour in *Cnr1*$^{-/-}$ mice. Microglia morphology after mild CSDS was analysed in the inferior molecular layer of the dentate gyrus (DG) of the hippocampus using an ImageJ-based analysis tool (see Figure 37 for details). Spearman correlation analysis was performed for mean morphological values of each animal and the respective behavioural stress score. **(A)** IBA1 mean intensity (*Cnr1*$^{+/+}$: r = 0.07, p = 0.839; *Cnr1*$^{-/-}$: r = 0.38, p = 0.166; both genotypes: r= 0.18, p = 0.371). **(B)** Microglia soma size (*Cnr1*$^{+/+}$: r = -0.02, p = 0.959; *Cnr1*$^{-/-}$: r = 0.09, p = 0.739; both genotypes: r = 0.09, p = 0.667). **(C)** Number of branches per cell (*Cnr1*$^{+/+}$: r = -0.29, p = 0.38; *Cnr1*$^{-/-}$: r = -0.72, p = 0.003; both genotypes: r = -0.40, p = 0.044). **(D)** Cell volume (*Cnr1*$^{+/+}$: r = 0.59, p = 0.061; *Cnr1*$^{-/-}$: r = -0.60, p = 0.019; both genotypes: r = -0.28, p = 0.168). **(E)** Cell surface area (*Cnr1*$^{+/+}$: r = 0.30, p = 0.36; *Cnr1*$^{-/-}$: r = -0.61, p = 0.017; both genotypes: r = -0.35, p = 0.083). **(F)** Ramification index (*Cnr1*$^{+/+}$: r = -0.31, p = 0.357; *Cnr1*$^{-/-}$: r = -0.72, p = 0.004; both genotypes: r = -0.48, p = 0.012). AU = arbitrary unit.

3.2.13.2 Hippocampus: CA1 region

Analysis of microglial morphology in the stratum radiatum of the CA1 region revealed that compared to the DG, stress had a smaller effect on microglia morphology in this region (Figure 39). Generally, the direction of morphological changes was similar to those observed in the DG, but did not reach significance in most cases. In part, this might be due to lower numbers of cells analysed and thus lower statistical power. Only for the soma size, a significant stress effect was detected, due to a slight increase in soma size in stressed mice (Figure 39B). For IBA1 intensity on microglia, significant stress and genotype effects as well as a stress x genotype interaction was found (Figure 39A). In the CA1 region, IBA1 intensity was increased by stress only in *Cnr1*$^{+/+}$ mice.

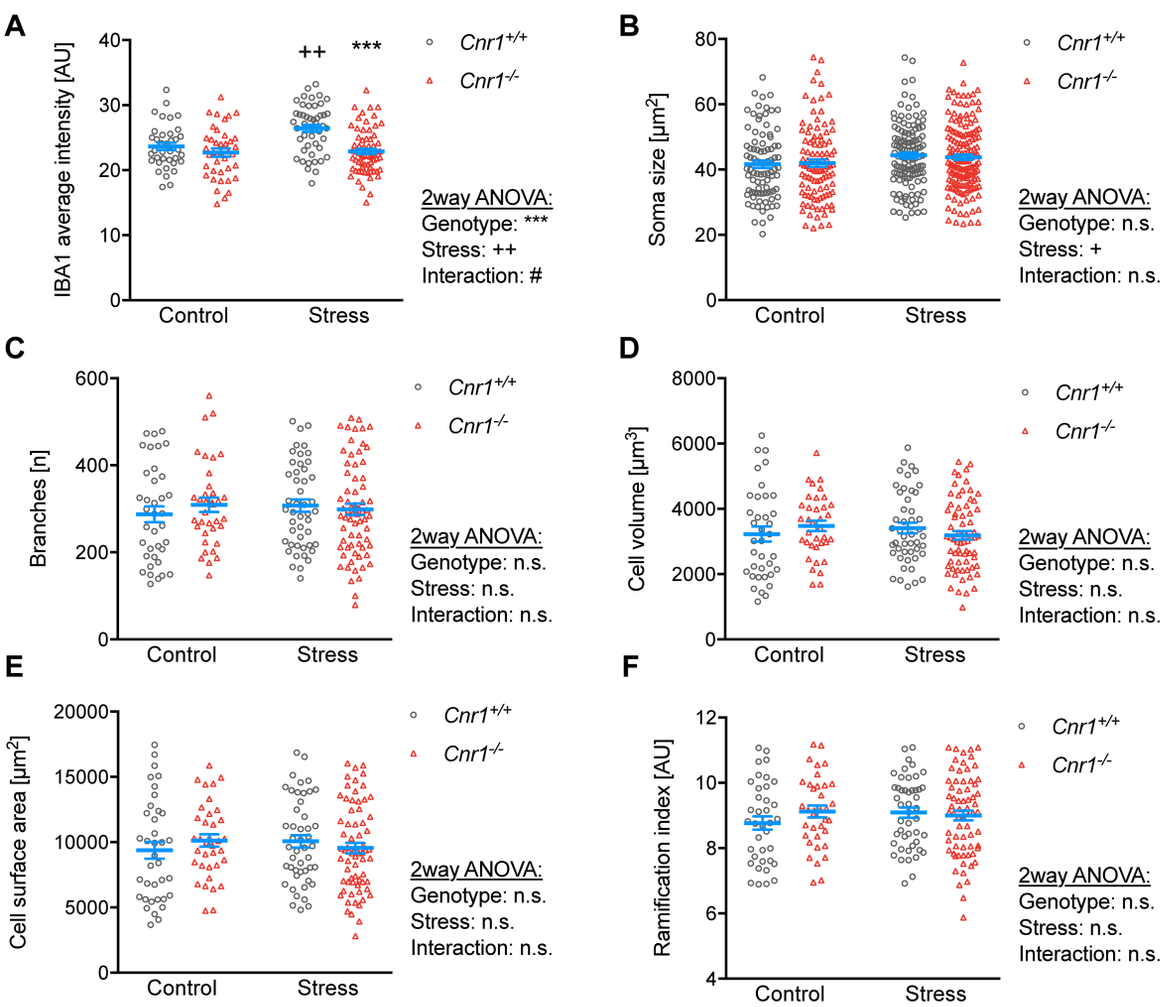

Figure 39. Mild CSDS does not significantly affect microglia morphology in the CA1 region of the hippocampus. Microglia morphology after mild CSDS was analysed in the stratum radiatum of the CA1 region of the hippocampus using an ImageJ-based analysis tool (see Figure 37 for details). A total of 37 - 68 cells were analysed per group. **(A)** Average intensity (mean grey) of IBA1 immunoreactivity on traced cells (stress: $F_{(1,187)} = 7.61$, $p < 0.006$; genotype: $F_{(1,187)} = 17.35$, $p < 0.0001$; stress x genotype interaction: $F_{(1,187)} = 5.78$, $p = 0.017$). **(B)** Cell soma size (stress: $F_{(1,465)} = 5.21$, $p = 0.023$). **(C)** Number of branches per cell (no significant main effects). **(D)** Cell volume (no significant main effects). **(E)** Cell surface area (no significant main effects). **(F)** Ramification index (no significant main effects). AU = arbitrary unit. Data was analysed by 2way ANOVA, followed by Bonferroni *post-hoc* comparisons. For genotype effects (compared to *Cnr1*$^{+/+}$ of the same group) * $p < 0.05$, ** $p < 0.01$, *** $p < 0.001$. For stress effects (compared to control of the same genotype) + $p < 0.05$, ++ $p < 0.01$, +++ $p < 0.001$.

3.2.13.3 Medial prefrontal cortex

Compared to changes observed in the hippocampus, mild CSDS had opposite effects on microglia morphology in the mPFC, although they were not as pronounced as those in the DG (Figure 40). It should also be noted that it was shown that microglia in different cortical layers show different cell sizes and morphologies (Kongsui et al., 2014). Since the analysis in the mPFC was not performed in a specific layer, it thus cannot be excluded that the effects observed here might be distorted by different microglia subtypes being analysed together. Changes in IBA1 intensity and soma size were similar to those observed in the hippocampus – stress significantly increased IBA1 expression (Figure 40A) and soma size (Figure 40B) of microglia in *Cnr1*$^{+/+}$, but not *Cnr1*$^{-/-}$ mice (significant stress x genotype interaction). Opposite to the stress-induced reduction of microglia branching seen in the DG, stress significantly reduced branch numbers only in *Cnr1*$^{+/+}$ mice (significant stress x genotype interaction) (Figure 40C). For cell volume and surface area, a tendency for a stress x genotype interaction and a significant interaction were detected, respectively (Figure 40D - E). However, the differences did not reach significance in *post-hoc* comparisons. Furthermore, microglia of control *Cnr1*$^{-/-}$ mice had a significantly lower ramification index than those of control *Cnr1*$^{+/+}$ mice (significant stress x genotype interaction) (Figure 40F).

Overall, morphological analysis of microglia indicates that stress effects on microglia are different between brain regions and are modulated by CB1 signalling. The strongest effects were observed in the DG of the hippocampus, suggesting that this region plays an important role during chronic stress exposure.

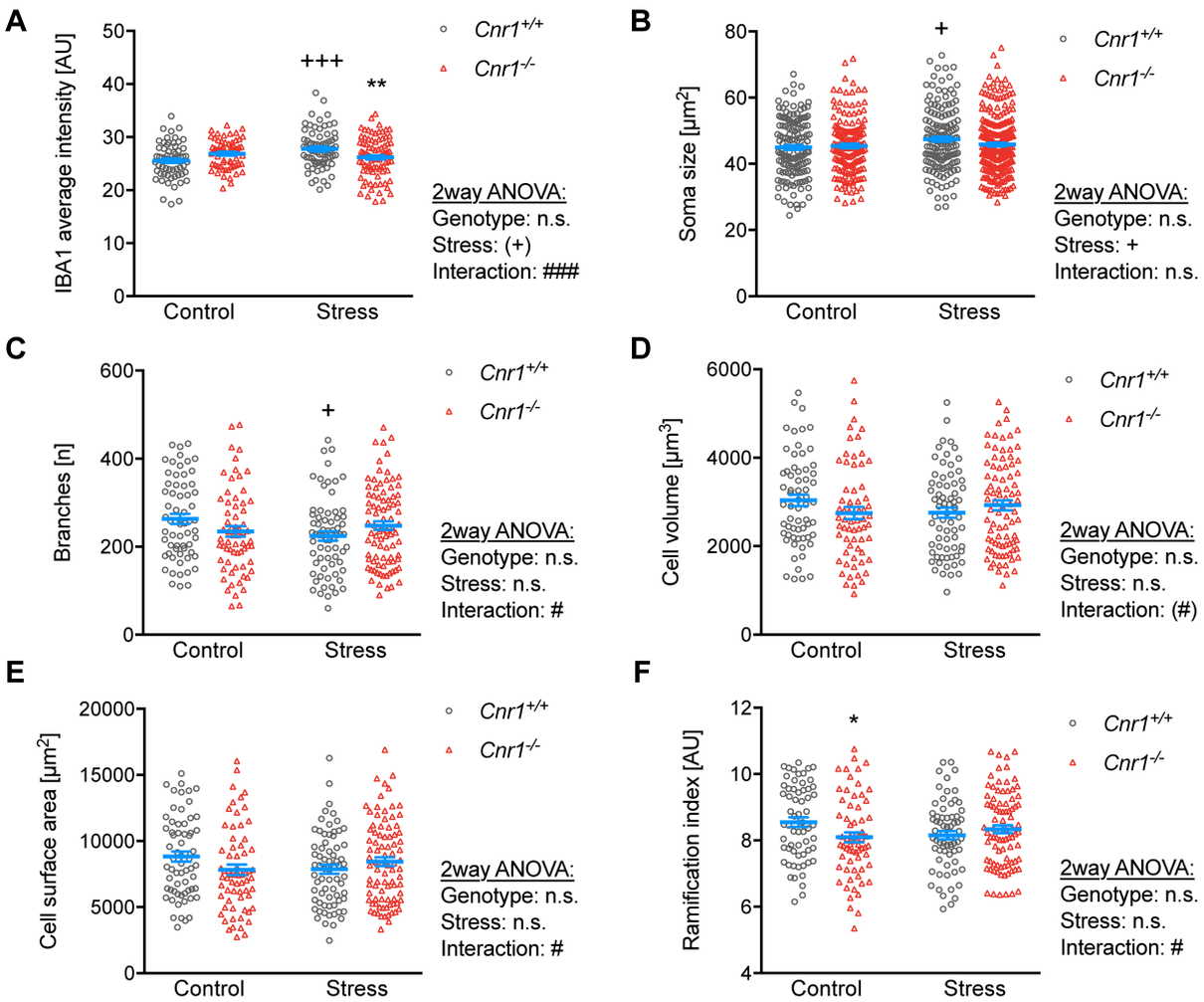

Figure 40. Mild CSDS slightly alters microglia morphology in the prefrontal cortex only in *Cnr1*$^{+/+}$ mice. Microglia morphology after mild CSDS was analysed in the mPFC using an ImageJ-based analysis tool (see Figure 37 for details). A total of 63 – 87 cells were analysed per group. **(A)** Average intensity (mean grey) of IBA1 immunoreactivity on traced cells (stress: $F_{(1,277)} = 3.33$, $p < 0.069$; stress x genotype interaction: $F_{(1,277)} = 12.17$, $p = 0.0006$). **(B)** Cell soma size (stress: $F_{(1,705)} = 4.65$, $p = 0.032$). **(C)** Number of branches per cell (stress x genotype interaction: $F_{(1,277)} = 5.55$, $p = 0.019$). **(D)** Cell volume (stress x genotype interaction: $F_{(1,277)} = 3.37$, $p = 0.067$). **(E)** Cell surface area (stress x genotype interaction: $F_{(1,277)} = 4.65$, $p = 0.032$). **(F)** Ramification index (stress x genotype interaction: $F_{(1,277)} = 5.43$, $p = 0.021$). AU = arbitrary unit. Data was analysed by 2way ANOVA, followed by Bonferroni *post-hoc* comparisons. For genotype effects (compared to *Cnr1*$^{+/+}$ of the same group) * $p < 0.05$, ** $p < 0.01$, *** $p < 0.001$. For stress effects (compared to control of the same genotype) + $p < 0.05$, ++ $p < 0.01$, +++ $p < 0.001$.

3.2.13.4 Brain regional differences in microglia morphology

In recent years, it has become evident that microglia within the brain are not a completely homogeneous population and show certain differences depending on their environment (Silvin and Ginhoux, 2018). Therefore, microglia morphology (using cell volume as an example) was compared between the different brain regions analysed in this study (Figure 41). Analysis of microglia from control mice revealed that microglia indeed show different volumes in different brain regions (significant brain region effect). In both *Cnr1*$^{+/+}$ and *Cnr1*$^{-/-}$ mice, microglia within the DG were the largest, being significantly larger than those in the CA1 region and the mPFC. Furthermore, a significant brain region x genotype interaction was detected. Microglia in the mPFC were generally the smallest and in *Cnr1*$^{-/-}$ mice, the difference between CA1 region and mPFC reached significance in *post-hoc* comparisons. The same pattern of cell volume (DG > CA1 > mPFC) and a significant brain region effect was also observed in microglia of stressed mice, with microglia within the DG being significantly larger than those in the mPFC for both genotypes. In *Cnr1*$^{+/+}$ mice, DG microglia were also significantly larger than those in the CA1 region, which in turn were larger than those in the mPFC.

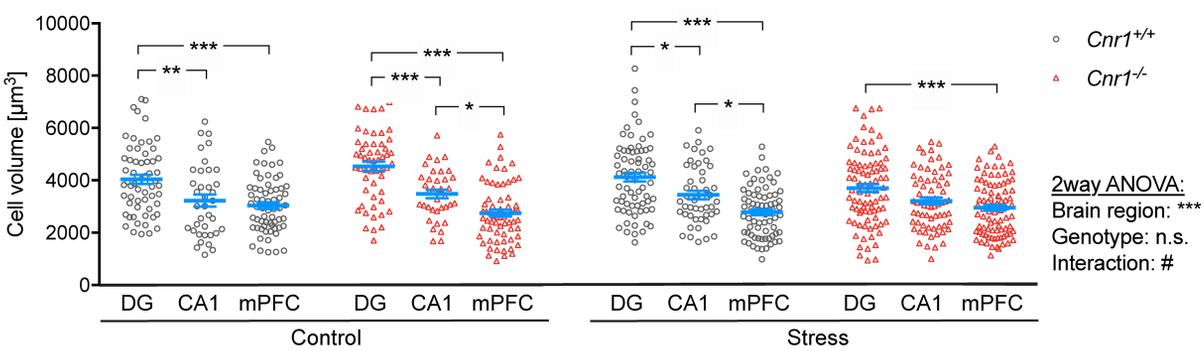

Figure 41. Microglia cell size shows brain-regional differences. Microglia morphology after mild CSDS was analysed in different hippocampal and cortical brain regions using an ImageJ-based analysis tool (see Figure 37 for details). Cell volume determined from 3D reconstructed cells (control group - brain region: $F_{(1,309)} = 41.43$, $p < 0.0001$; brain regions x genotype interaction: $F_{(1,309)} = 3.33$, $p = 0.037$; stress group - brain region: $F_{(1,419)} = 29.79$, $p < 0.0001$; brain regions x genotype interaction: $F_{(1,419)} = 2.44$, $p = 0.089$). Data was analysed by 2way ANOVA, followed by Bonferroni *post-hoc* comparisons. The analysis was performed separately for controls and for stressed mice. Significant differences between brain regions in *post-hoc* comparisons are indicated in the graph. * $p < 0.05$, ** $p < 0.01$, *** $p < 0.001$.

4 Discussion

The overall objective of this study was to analyse how CB1 signalling modulates behavioural, neuroendocrine, and immunological responses during chronic social stress. Furthermore, the aim was to analyse whether the increased stress-susceptibility observed in the absence of CB1 signalling is related to altered neuroimmune communication and altered myeloid cell function.

In summary, this study strongly supports the finding that CB1 signalling protects the organism from the physical and emotional harms of stress. Upon exposure to a mild stressor, it dampens the severity of the behavioural responses and modulates HPA axis activity and possibly its adaptation during chronic stress exposure. Overall, the lack of CB1 signalling during chronic stress seems to cause insufficient GC signalling. With respect to immunological responses to stress, CB1 signalling mainly modulates the function of brain-resident microglia, while effects on peripheral myeloid cells seem to be comparatively small. Finally, microglial parameter analysed in this study were correlated with the severity of the behavioural phenotype, thus implicating CB1-mediated modulation of microglia in the development of stress-related pathologies. The main findings of this study are further summarised in Figure 42.

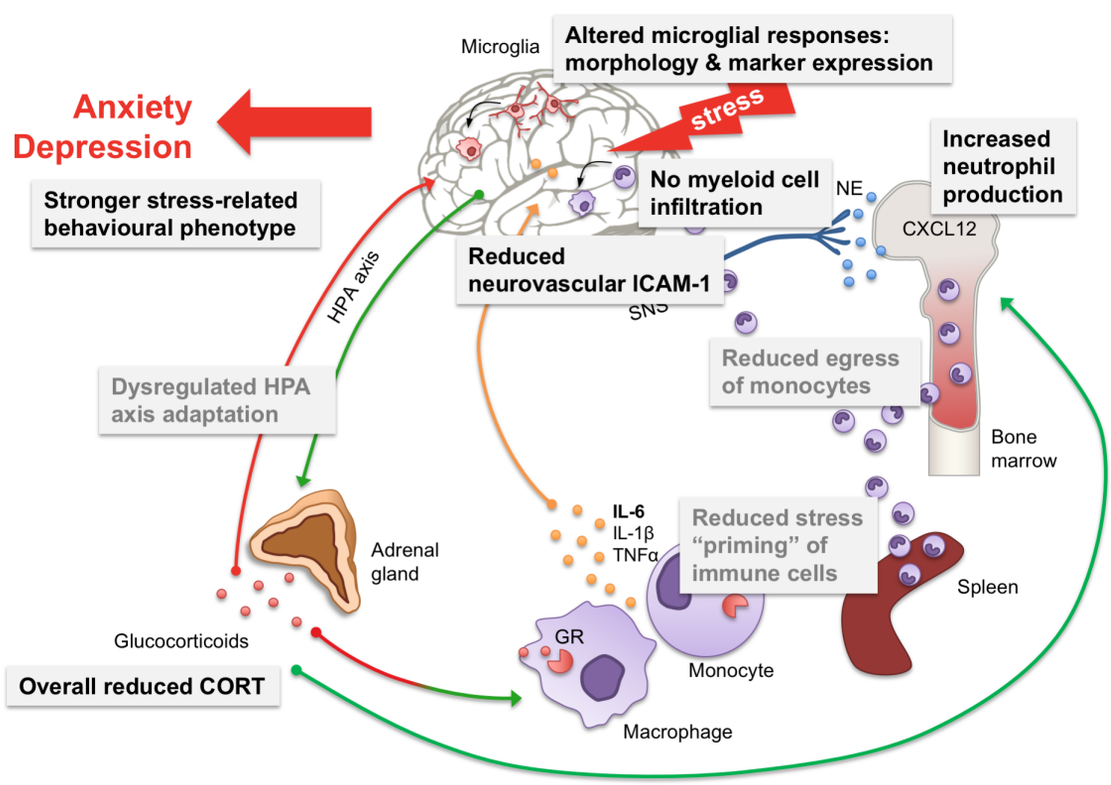

Figure 42. Summary of the effects of CB1 deficiency on neuroimmune communication systems after CSDS. Results of the present study are summarised in grey boxes, showing stress-induced changes observed in *Cnr1*$^{-/-}$ mice in comparison to stressed *Cnr1*$^{+/+}$ mice. Grey text indicates uncertain or speculative findings. Abbreviations: CXCL12 = C-X-C motif chemokine 12, GC = glucocorticoid, GR = glucocorticoid receptor, HPA axis = hypothalamic-pituitary-adrenal axis, ICAM-1 = intracellular adhesion molecule 1, IL = interleukin, NE = noradrenaline (norepinephrine), SNS = sympathetic nervous system, TNFα = tumor necrosis factor alpha.

4.1 Stress-induced mortality in the absence of CB1 signalling

Cnr1$^{-/-}$ mice are known to be highly stress-sensitive and prone to develop anxiety- and depressive-like behaviours (Valverde and Torrens, 2012). One aim of this study was to confirm that this increased stress-susceptibility is also observed in a standard model of CSDS, which consists of daily defeat sessions of 5 - 10 minutes (Golden et al., 2011). A very severe phenotype of *Cnr1*$^{-/-}$ mice was detected in this model, with *Cnr1*$^{-/-}$ mice showing mortality rates of approximately 50% – compared to 10% in *Cnr1*$^{+/+}$ mice. Similar, but slightly lower mortality rates (30%) were also observed during standard CSDS in mice that lack DAGLα, the main 2-AG synthesizing enzyme (Jenniches, 2016). This suggests that the protective effect of CB1 signalling during severe stress exposure is mainly, but not entirely, mediated by 2-AG. It is known that the *Cnr1*$^{-/-}$ line used in this study has an increased spontaneous mortality rate, however, the mechanisms are unknown (Zimmer et al., 1999). Based on the observations of the present study, it can be speculated that the increased spontaneous mortality is also linked to severe stress responses, for example during handling of the mice. Indeed, *Cnr1*$^{-/-}$ mice occasionally show handling-induced seizures or convulsions (unpublished observation) and have a lower threshold to develop chemically-induced epileptic seizures (Marsicano et al., 2003).

Since social defeat models are associated with high incidence of cardiac arrhythmias (Sgoifo and Papi, 1995) and the death of *Cnr1*$^{-/-}$ mice during standard CSDS was reminiscent of sudden cardiac death, heart activity was analysed during CSDS using ECG recordings. *Cnr1*$^{-/-}$ mice did not show signs of myocardial infarction or ventricular fibrillation (the most common cause of sudden cardiac death), but were bradycardic and did develop total AV-block before death. The ECG traces further implied that mice might have had seizures or convulsions concomitant with the AV-block, indicated by high amplitude disturbances of the signal, possibly caused by muscle contractions. In fact, cardiovascular comorbidities are common in epilepsy patients (Shmuely et al., 2017) and there are several case reports of patients that develop bradycardia and AV-block during seizures (Leung, 2006).

There are also several other possible explanations for the observed mortality under severe stress situations, that likely act in combination: direct cardiovascular effects of CB1 signalling via the SNS (Grzeda et al., 2015; Niederhoffer and Szabo, 1999; Varga et al., 1996); vagal over-activation in response to excessive SNS activity (“psycogenic death”), which has been associated with the occurence of AV-block (Alboni et al., 2013); or exacerbated inflammatory responses. Interestingly, stress-induced IL-6 levels were extremely high in one *Cnr1*$^{-/-}$ mouse that died shortly after the first defeat session. In humans, IL-6 is good predictor for mortality in cardiogenic shock patients (Andrié et al., 2012). IL-6 is released in response to stress (Zhou et al., 1993) and can further potentiate HPA axis activation by directly stimulating ACTH and GC production (Bethin et al., 2000). The extremely high levels could thus result from an uncontrolled cycle of HPA axis

activation and IL-6-production. Additionally, a study showed that macrophages are present in the AV node of the heart, where they directly regulate electrical conduction of cardiomyocytes (Hulsmans et al., 2017). Interestingly, lack of these resident cardiac macrophages could delay or abolish atrial conduction to the ventricles, thus inducing 2nd or 3rd degree AV block. While cardiac cells were not analysed here, there were some changes in myeloid cell populations in *Cnr1*$^{-/-}$ mice and it might be worthwhile to investigate whether this also applies to cardiac macrophages.

Overall, eCB signalling via CB1 appears to be extremely important for protecting the organism under severe stress exposure. In consequence, lack of CB1 signalling might impose a serious risk under these conditions, possibly related to cardiovascular complications. However, due to the substantial loss of *Cnr1*$^{-/-}$ mice during standard CSDS experiments, group sizes for subsequent behavioural and molecular analyses were very small and presumably the most stress-sensitive mice were underrepresented. Therefore, these results had to be interpreted with caution and will not be discussed in detail here.

4.2 Stress-related behaviour

Rodent models of social defeat stress are commonly used to model human psychiatric disorders, such as MDD or PTSD. The most common readout is the social avoidance test that is often used to differentiate between stress susceptible and resilient mice. In this test, typically two thirds of mice are classified as susceptible and the remaining one third is classified as resilient, meaning that they do not show reduced interaction with an unknown CD1 aggressor mouse (Golden et al., 2011). In the standard CSDS paradigm applied here (5 - 10 minutes defeat sessions), all mice that survived the procedure classified as stress susceptible, suggesting that the magnitude of stress exposure was very severe. When defeat sessions were reduced to a maximum of 5 minutes, *Cnr1*$^{+/+}$ mice showed the expected ratio of susceptible and resilient mice. However, this social avoidance behaviour was not correlated to any other behavioural readout, such as anxiety and anhedonia. This is in line with a study showing that mice can also be segregated into anxious and non-anxious groups after CSDS, independent from “stress susceptibility” (Bosch-Bouju et al., 2016; Krishnan et al., 2007). And even though there were clear effects on social avoidance in each standard CSDS experiment, the effect on other anxiety- or depressive-like behaviours was still comparably small and varied between the experiments. This demonstrates that behavioural responses to stress are very complex and a single behavioural trait, such as social avoidance behaviour after CSDS, cannot be used to generally classify mice into stress “susceptible” versus “resilient” groups. While traits like anxiety, anhedonia, and social behaviour surely have certain underlying mechanisms in common, they do not necessarily overlap in the context of chronic stress.

In later experiments with mild CSDS, we therefore developed an overall behavioural stress scoring system that incorporates the performance in each of the behavioural tests instead of using just one readout. First of all, this might be more comparable to the clinical diagnosis of mental disorders, where patients have to fulfil several criteria listed in the DSM-V to be diagnosed. Secondly, there often is considerable variability between individual mice and some controls also displayed stress-related behaviour – especially in *Cnr1*$^{-/-}$ mice. This can possibly be explained by the control housing conditions used in this study (two unfamiliar mice separated by a perforated wall). Together with daily handling for body weight measurements, these conditions likely already inflicted a certain level of stress. The stress score thus allowed correlation analysis of behaviour to molecular parameters based on the individual stress level, independent of the actual group.

Although *Cnr1*$^{-/-}$ mice already displayed symptoms of stress under control conditions, mild CSDS was still able to clearly increase stress-related behaviours in these mice. This was especially evident in the social avoidance and the nestlet test. In contrast, the stress effects in *Cnr1*$^{+/+}$ mice neither reached statistical significance for any individual test nor for the overall stress score. Generally, mild CSDS and even standard CSDS did not have a strong influence on anxiety and anhedonia. Similar findings were also seen in previous experiments with DAGL$\alpha^{-/-}$ mice, where standard CSDS only had minor effects on sucrose preference and anxiety in the open field or zero-maze (Jenniches, 2016). These findings are in contrast to several studies that report anxiogenic effects of repeated social defeat (McKim et al., 2016, 2017; Wohleb et al., 2011, 2014b). These discrepancies might be due to slightly different social defeat protocols and different control conditions. In these studies, control mice were left undisturbed in established groups of three mice, which presumably imposes less baseline stress than the control housing conditions in the experiments described here. Additionally, behavioural tests in these studies were performed during the inactive phase of mice (lights on), while our tests were performed during the dark phase under illuminated, aversive conditions. This likely affects exploratory behaviour of mice and thus the overall outcome of behavioural analyses. For example, it was also demonstrated that the behavioural effects of environmental enrichment on locomotion and exploration are only obvious when mice are tested in the light, but not in the dark phase (Loss et al., 2015).

In *Cnr1*$^{-/-}$ mice, the lack of a stress effect might further represent a ceiling effect, since they already showed increased anxiety and anhedonia at baseline. These results are in part inconsistent with another study using *Cnr1*$^{-/-}$ mice and a model of repeated social defeat (Dubreucq et al., 2012). In this study, pharmacologic blockade or constitutive deletion of CB1 did not affect anxiety or anhedonia, neither at baseline nor after social defeat. However, it should be noted that there are several differences in the experimental design that can explain the discrepancies. A different social defeat paradigm was applied, with seven days of stress, short-term sensory contact before and after the 10-minute defeat, and single-housing for the rest of the time. Stress exposure and

behavioural analysis was performed during the inactive phase of mice. Different behavioural tests were performed to evaluate emotional behaviour after stress (e.g. elevated plus maze for anxiety instead of open field in the current study). The authors further state that tests were performed under non-aversive conditions (dim illumination), in which the anxiogenic phenotype of *Cnr1*$^{-/-}$ mice is typically not detectable (Haller et al., 2004). Finally, a different *Cnr1*$^{-/-}$ mouse line was used (Marsicano et al., 2002), which was bred on a mixed, predominant C57BL/6N genetic background. There are several studies showing that different strains of mice and C57BL/6 sub-strains show different phenotypes and that certain phenotypes (e.g. anxiety) are highly dependent on the laboratory and sometimes difficult to reproduce in a different environment (Bothe et al., 2005; Crawley et al., 1997; Wahlsten et al., 2006). For example, it was shown that behavioural responses to chronic GC exposure are dependent on the genetic background and even vary between C57BL/6J and C57BL/6N sub-strains (Sturm et al., 2015).

4.3 HPA axis regulation

It is commonly assumed that persistently elevated GC signalling is detrimental and the cause of many chronic stress-related pathologies. However, stress-related neuropsychiatric disorders are in fact often associated with insufficient GC signalling (Raison and Miller, 2003). For example, patients suffering from PTSD often show low cortisol responses and overall blunted HPA axis activity (Miller et al., 2007). Chronically stressed subjects, such as caregivers of ill family members or victims or domestic violence, often display low cortisol output as well (Miller et al., 2002; Seedat et al., 2003; Vedhara et al., 2002). Another common observation in these chronically stressed populations is a flattening of diurnal cortisol patterns, with lower than normal morning secretion but higher levels during the rest of the day (Miller et al., 2007). Similar effects are also observed in rodent models of chronic stress, where CORT is consistently increased in the light but decreased in the dark phase (Bartlang et al., 2012; Koch et al., 2016; Reber et al., 2006, 2007). Results from *Cnr1*$^{+/+}$ mice after mild CSDS recapitulate this phenomenon. While plasma CORT levels taken during the dark phase were slightly lower than in control mice, cumulative 24-hour faecal CORT concentrations were elevated after stress, possibly caused by increased levels during the light phase. In contrast, *Cnr1*$^{-/-}$ mice did not show any stress-induced changes in CORT levels. This could suggest that the HPA axis does not show the normal adaptation pattern over the course of chronic stress exposure in these mice. Indeed, there is strong evidence that eCB signalling via CB1 regulates GC signalling and is necessary for both the fast feedback inhibition of the HPA axis and its habituation to repeated stress exposure (Hillard et al., 2017; Morena et al., 2016).

In several stress-responsive brain regions, GCs rapidly mobilise eCB/CB1 signalling, which contributes to the negative feedback inhibition of the HPA axis. In the PVN, acute stress or CORT administration induces 2-AG production by CRH neurons, which acts on CB1 receptors on

presynaptic glutamatergic neurons to suppress glutamate release and thereby inhibit the activity of CRH neurons (Di et al., 2003; Evanson et al., 2010). In contrast, CB1 receptors are mainly expressed on GABAergic interneurons in the mPFC and hippocampus. Thus, GC-induced 2-AG production in these regions would reduce GABA release and lead to disinhibition of excitatory projection neurons (Hill et al., 2011; Wang et al., 2012). These excitatory projections are thought to contribute to the cessation of the stress response via inhibitory relay neurons in the bed nucleus of the stria terminalis that in turn project to and inhibit CRH neurons in the PVN (Diorio et al., 1993; Forray and Gysling, 2004). Thus, CB1 signalling contributes to the negative feedback inhibition of the HPA axis at several levels, at least under acute stress situations. In line with this, increased or prolonged GC secretion has been repeatedly reported in *Cnr1*$^{-/-}$ mice after acute stress exposure (Aso et al., 2008b; Barna et al., 2004; Hill et al., 2011; Patel et al., 2004). In contrast, until now it has not been analysed how GC signalling is altered in *Cnr1*$^{-/-}$ mice after chronic stress exposure.

There is, however, evidence that CB1 signalling is involved in the habituation to repeated stress exposure, especially to homotypic stressors. Several studies showed that chronic stress alters CB1 expression and binding site density in a brain region-dependent manner. For example, chronic unpredictable stress increased gene expression and binding site densities of CB1 in the PFC (Hill et al., 2006, 2008), while both parameters were decreased in the hippocampus and hypothalamus (Hill et al., 2008). Chronic restraint stress decreased CB1 receptor binding in the DG, while there was no change in the CA1 region (Hill et al., 2009). In the present study, gene expression of *Cnr1* and other ECS-related genes in the brain was not significantly changed after mild CSDS, likely due to the mild level of stress exposure (see Appendix). Furthermore, repeated homotypic stress increases 2-AG concentrations in several brain regions, including the hippocampus, hypothalamus, PFC, and amygdala (Dubreucq et al., 2012; Patel et al., 2005; Rademacher et al., 2008; Sumislawski et al., 2011). Accordingly, amygdala-specific DAGLα deletion (and thus 2-AG reduction) impairs adaptation to repeated stress and increases stress-induced anxiety (Bluett et al., 2017). In contrast, brain AEA levels are consistently decreased in limbic brain regions after acute and repeated stress exposure (Hill et al., 2010a).

It is suggested that this differential regulation of eCBs mediates different processes during stress adaptation. While the progressive increase of amygdalar 2-AG seems to suppress CORT production in response to the reencountered stressor, reduced AEA levels likely induce basal hypersecretion of CORT during the light phase (Hill et al., 2010a). These findings are in line with observations of CORT levels in *Cnr1*$^{+/+}$ and *Cnr1*$^{-/-}$ mice after mild CSDS. Plasma CORT levels at the time point of expected stress exposure were higher in stressed *Cnr1*$^{-/-}$ mice compared to stressed *Cnr1*$^{+/+}$ mice, since stress caused a slight downregulation of CORT in *Cnr1*$^{+/+}$, but an upregulation in *Cnr1*$^{-/-}$ mice. The observed downregulation of plasma CORT in *Cnr1*$^{+/+}$ mice might

represent the 2-AG-mediated suppression of the HPA axis in anticipation of another defeat session. In contrast, cumulative daily CORT levels were increased by stress in *Cnr1*$^{+/+}$, but not in *Cnr1*$^{-/-}$ mice. This finding initially appears contrary to the common assumption that CB1 signalling inhibits the HPA axis. However, the overall increase in CORT in stressed *Cnr1*$^{+/+}$ mice might be caused by the above mentioned AEA-mediated hypersecretion of CORT during the light phase. These adaptive changes cannot take place in the absence of CB1 signalling, which would explain the higher plasma CORT levels at the expected time of stress exposure and the absence of a stress effect on cumulative CORT in stressed *Cnr1*$^{-/-}$ mice. Nonetheless, a thorough analysis of circadian CORT fluctuations over the time course of CSDS would be necessary to confirm this.

Another important factor that influences the outcome of GC signalling is the responsiveness of target organs. A consistent observation in depressed patients is GC resistance, meaning that the negative feedback inhibition of the HPA axis is not working properly, due to altered GR function in the brain (Anacker et al., 2011). The result is a hyperactive HPA axis and hypercorticolism. However, this does not necessarily translate into high downstream GC signalling. Since other GC targets (e.g. immune cells) can also develop GC resistance when repeatedly exposed to high levels of GCs during chronic stress, GCs do no longer provide their typical immunosuppressive function. Indeed, circulating monocytes of stressed humans show a transcriptional profile reminiscent of GC resistance (Miller et al., 2014). More precisely, expression of pro-inflammatory, NFκB-inducible genes is increased, while genes containing a glucocorticoid response element (GRE) are downregulated. Furthermore, the phenomenon of GC resistance has repeatedly been demonstrated in rodent models of chronic stress, where leukocytes isolated from stressed mice show exaggerated pro-inflammatory responses to subsequent stimulation and are less responsive to the suppressive effects of GCs (Avitsur et al., 2002; Stark et al., 2001, 2002; Wohleb et al., 2014a). The development of GC resistance and the priming of leukocytes by stress were shown to be dependent on GC production during repeated stress (Niraula et al., 2018). While the present study did not directly asses GC-responsiveness after CSDS, stimulation of splenocytes isolated after standard CSDS confirmed that prior stress exposure caused a stronger pro-inflammatory response to LPS. This priming effect of stress was less pronounced in *Cnr1*$^{-/-}$ mice, indirectly supporting the finding of lower GC levels in these mice when chronically stressed. But since the experiments were performed after standard CSDS, where a large fraction of *Cnr1*$^{-/-}$ mice was lost due to mortality, it is possible that these results do not properly represent the effect of CSDS on *Cnr1*$^{-/-}$ splenocyte function. Nonetheless, results from mild CSDS also indicate at different levels that stressed *Cnr1*$^{-/-}$ mice likely develop insufficient GC signalling over the course of chronic stress. In contrast, stimulation of splenocytes from naive, non-stressed *Cnr1*$^{+/+}$ and *Cnr1*$^{-/-}$ mice showed no difference in the anti-inflammatory effects of GCs on LPS-stimulated splenocytes (see Appendix). It can thus be excluded that splenocytes of *Cnr1*$^{-/-}$ mice already had an altered GC-responsiveness at baseline.

4.4 Effects of stress on peripheral myeloid cells

GCs produced during chronic stress are necessary for the egress of myeloid cells from the bone marrow into circulation, but are dispensable for increased myelopoiesis (Niraula et al., 2018). In contrast, the proliferation of HSCs and subsequent inflammatory monocyte and neutrophil production during chronic stress depends on adrenergic signalling (β3-adrenergic receptors) (Heidt et al., 2014). Both GCs and adrenergic signalling regulate expression of the chemokine retention factor CXCL12, which inhibits HSC proliferation and migration and retains cells within the bone marrow by interaction with its receptor CXCR4 (Ding and Morrison, 2013; Eash et al., 2010). Mild CSDS slightly reduced *Cxcl12* gene expression and this stress effect seemed a bit more pronounced in *Cnr1*$^{+/+}$ mice, which could be related to the higher levels of CORT in these mice. TH staining intensity (an indirect measure of noradrenaline synthesis) in the bone marrow was also slightly increased by mild CSDS in both genotypes. TH intensity further appeared marginally higher in *Cnr1*$^{-/-}$ mice, although this difference did not reach statistical significance, possibly due to the small group size available for that analysis. Increased noradrenaline levels, however, would be expected in *Cnr1*$^{-/-}$ mice, since CB1 activation is known to inhibit noradrenaline-release from sympathetic nerve terminals in the bone (Bab and Zimmer, 2008; Tam et al., 2008). Still, direct measurements of noradrenaline content in the bone marrow would be necessary to further validate the effect of mild CSDS and CB1 deficiency on adrenergic signalling.

The rather subtle effects on bone marrow CXCL12 and TH correspond well to the moderate changes in peripheral myeloid cell populations observed after mild CSDS. For example, mild CSDS generally did not cause increased monocyte frequencies in the bone marrow or circulation. In *Cnr1*$^{+/+}$ mice, circulating Ly6C^{hi} monocytes were increased by stress in one cohort of mice, but this was not consistently observed in the second cohort. Only in the spleen, a significant stress effect with respect to Ly6C^{hi} monocytes was observed. When looking at both bone marrow and circulating populations, it seemed like stressed *Cnr1*$^{-/-}$ mice showed higher Ly6C^{hi} monocyte frequencies in the bone marrow but lower frequencies in the blood, compared to stressed *Cnr1*$^{+/+}$ mice. Since monocyte egress during chronic stress is dependent on GCs, this could suggest that the lower GC levels in stressed *Cnr1*$^{-/-}$ mice prevented the release of these cells into circulation. Additionally, Ly6C^{hi} monocytes require CCR2 for their egress from the bone marrow (Shi and Pamer, 2011). *Cnr1*$^{-/-}$ mice generally had reduced expression of CCR2 on monocytes, which could further inhibit their release into circulation. In contrast, neutrophil frequencies were increased by mild CSDS in the bone marrow of *Cnr1*$^{-/-}$ mice, but not in the circulation, also suggesting reduced egress of myeloid cells from the bone marrow. Neutrophils are the most abundant myeloid cell type in mammals and are very short-lived (Manz and Boettcher, 2014). With a lifespan of only approximately 12 hours, they need to be continuously generated from precursors in the bone marrow (Basu et al., 2002). Under non-inflammatory conditions, aged neutrophils are eliminated by macrophages in the spleen, liver, and the bone marrow (Furze and Rankin, 2008; Suratt et al.,

2001). Aged neutrophils thus migrate back to the bone marrow to be phagocytosed by bone marrow macrophages. This elimination was shown to reduce CXCL12 expression and thereby regulate homeostatic release of new myeloid cells and HSCs (Casanova-Acebes et al., 2013). In peripheral blood macrophages, activation of CB1 receptors can induce phagocytosis (Mai et al., 2015), suggesting that phagocytic elimination of neutrophils might be impaired in *Cnr1*$^{-/-}$ mice. However, neutrophil populations were not analysed in more detail in the present study. It thus remains unclear whether the increased neutrophil frequencies in the bone marrow of *Cnr1*$^{-/-}$ mice after mild CSDS were caused by increased production, reduced egress, or reduced elimination of aged neutrophils.

According to the literature, peripheral monocytes are recruited to the brain neurovascular space after chronic stress and possibly enter into the brain parenchyma (Reader et al., 2015; Wohleb et al., 2015). This recruitment is mediated by interaction between integrins on monocytes and increased expression of cell adhesion molecules (CAMs) on brain endothelial cells. The increase of CAMs appears to be dependent on the number of social defeat cycles, since it was only detected after 6 days of social defeat – a time point that temporally correlated with the detection of peripheral monocytes in the brain (Sawicki et al., 2015). In *Cnr1*$^{+/+}$ mice, stress indeed caused an increase in neurovascular ICAM-1 in stress-related brain regions (hippocampus, mPFC, amygdala). Nonetheless, here we did not detect increased numbers of monocytes or other myeloid cells in the brain after mild CSDS, neither by flow cytometry nor by immunohistochemistry. Since monocyte frequencies were also not increased in peripheral tissues in these mice, it is likely that the mild version of CSDS was not sufficient to induce pronounced myelopoiesis and consequently no monocyte trafficking to the brain. The induction of reactive brain endothelium and peripheral myelopoiesis therefore seem to be mediated by independent pathways. Indeed, stress-induced myelopoiesis in the bone marrow depends on adrenergic signalling (Heidt et al., 2014; Ramirez et al., 2016). In contrast, expression of ICAM-1 is dependent on GCs released during chronic stress, since its induction could be prevented by adrenalectomy and by inhibiting GC synthesis over the course of social stress (Niraula et al., 2018). Interestingly, neurovascular ICAM-1 expression was only induced in *Cnr1*$^{+/+}$, but not in *Cnr1*$^{-/-}$ mice, which further supports the finding of overall reduced GC signalling after chronic stress in the absence of CB1 signalling.

The recruitment of inflammatory monocytes is suggested to play a causative role in the development of anxiety-like behaviour in response to chronic stress (Wohleb et al., 2015). In *Cnr1*$^{+/+}$ mice, mild CSDS neither induced monocyte trafficking, nor a clear anxiety-like phenotype. *Cnr1*$^{-/-}$ mice already displayed increased baseline open field-anxiety and anhedonia that was not further affected by stress. It thus cannot be entirely excluded that the mild CSDS paradigm was simply not as anxiogenic as the repeated social defeat protocols that revealed the link between peripheral monocytes and stress-induced anxiety. However, if the baseline anxiety of *Cnr1*$^{-/-}$ mice

is considered a consequence of the mildly stressful control housing conditions (see chapter 4.2), we would still expect to find increased monocyte trafficking in these mice. Furthermore, *Cnr1*$^{-/-}$ mice showed clear changes in other stress-related behaviours after mild CSDS, but did not show any infiltration of monocytes to the brain. If anything, they even had less monocytes in the brain than stressed *Cnr1*$^{+/+}$ mice. Thus, results from *Cnr1*$^{-/-}$ mice would argue against a crucial involvement of peripheral monocytes in mediating stress-related behaviour.

4.5 Microglial responses to stress

In contrast to the relatively weak effects on peripheral myeloid cell populations, mild CSDS did significantly affect brain-resident microglia and these changes were correlated to the degree of behavioural stress-susceptibility.

Similar to ICAM-1, stress increased microglial staining (IBA1+ area) in the hippocampus of *Cnr1*$^{+/+}$ mice, which has been reported in several other studies (Wohleb et al., 2011, 2014b). In contrast, this effect was not observed in *Cnr1*$^{-/-}$ mice. Again, these findings resemble those seen in mice treated with a GC antagonist during social defeat (Niraula et al., 2018). An increase in IBA1+ area is often considered a sign of microglial activation, although it can be the result of different factors, such as increased numbers of microglia, altered morphology, or increased IBA1 expression. Detailed analysis of hippocampal microglia after mild CSDS revealed that the different regulation of IBA1+ area between *Cnr1*$^{+/+}$ and *Cnr1*$^{-/-}$ mice was in fact caused by different mechanisms. In *Cnr1*$^{+/+}$ mice, the increase in IBA1+ area was a result of increased IBA1 expression and slightly enlarged cell bodies, which would be considered a sign of activation. In contrast, the absence of a stress-induced increase of IBA1+ area in *Cnr1*$^{-/-}$ mice was related to morphological rearrangements of microglia to a de-ramified state, which is also considered a sign of classical activation. Thus, analysis of IBA1+ area should always be complemented by a more detailed analysis of the underlying causes. Interestingly, only the morphological changes in *Cnr1*$^{-/-}$ mice (e.g. reduced number of branches) were correlated with the behavioural stress score. In contrast, stress-induced changes seen in *Cnr1*$^{+/+}$ mice (e.g. increased soma size) were not related to the behavioural phenotype.

In the literature, there is substantial controversy concerning the effects of stress on microglial morphology. Results range from either increased to decreased proliferation, IBA1 expression, cell size, and ramification (Bollinger et al., 2016; Hellwig et al., 2016; Hinwood et al., 2013; Kreisel et al., 2014; Lehmann et al., 2016; Wohleb et al., 2011, 2012). However, these discrepancies are not all together surprising when considering that different stress models, different brain regions, and different time points were analysed. For example, acute stress exposure (social or non-social) seems to induce proliferation of microglia in several brain regions, but this effect is no longer seen

or even reversed after prolonged stress (Kreisel et al., 2014; Lehmann et al., 2016). By now it is also recognised that microglia morphology and function show brain region-dependent heterogeneity (Ayata et al., 2018; Bollinger et al., 2016; De Biase et al., 2017; Masuda et al., 2019). Consistent with that, microglia displayed different morphologies under control conditions and in response to stress in the different regions analysed here. Microglia in the DG were generally larger and more ramified than those in the CA1 region and the mPFC. Furthermore, stress effects on microglia morphology were most pronounced in the DG.

The subgranular zone of the DG is one of the brain's neurogenic niches – a region where new neurons are generated from progenitor cells. Adult neurogenesis has been implicated in a range of psychiatric disorders and was also shown to be altered in several mouse models of chronic stress (Lucassen et al., 2016). Microglia can regulate neurogenesis via different mechanisms, including the release of substances that either stimulate or suppress neurogenesis (Sato, 2015; Sierra et al., 2014). For example, pro-inflammatory cytokines like IL-1β inhibit neural precursor cell proliferation and neuronal differentiation in the DG (Wu et al., 2013). On the other hand, microglia also produce BDNF, a neurotrophin that supports survival of newly generated neuronal cells (Ferrini and De Koninck, 2013). Microglia within the DG might therefore have a distinct function compared to other brain regions, which could also be reflected in their morphology. Since CB1 signalling is also known to regulate neurogenesis (Prenderville et al., 2015), it would be worthwhile to investigate whether the stress-induced microglial changes observed in the DG of *Cnr1*$^{-/-}$ mice are also related to changes in neurogenesis.

Control *Cnr1*$^{-/-}$ microglia in the DG were also slightly larger and hyper-ramified. Microglia hyper-ramification in the DG was previously shown to be induced by models of repeated stress (Hellwig et al., 2016). It therefore seems likely that the control housing conditions were indeed already stressful to highly sensitive *Cnr1*$^{-/-}$ mice. Microglia hyper-ramification is sometimes considered a first step in microglial responses to injury or a consequence of intense neuronal activity (Hinwood et al., 2012). For example, activation of neurons by NMDA and subsequent release of adenosine triphosphate (ATP) from neurons was shown to induce microglial process outgrowth via purinergic receptors in acute hippocampal slices (Dissing-Olesen et al., 2014). Similarly, blocking or stimulating glutamatergic signalling in an *ex vivo* retinal explant system induced a rapid retraction or outgrowth of microglial processes, respectively (Fontainhas et al., 2011). These morphological changes were also related to functional changes, since increased branching in response to glutamatergic signalling was also associated with increased motility of those branches. A role for neuronal activity in regulating microglia process dynamics was recently also demonstrated in longitudinal *in vivo* imaging studies the hippocampus, where motility of microglial processes was strongly influenced by the activity of local neurons (Nebeling et al., 2019). Furthermore, the study demonstrated a connection between microglia motility with the plasticity of dendritic spines, since

both the new formation and elimination of spines were associated with increased contact rates by microglia. So far, it is not known which signalling molecules mediate this interaction and what the functional role for the contacts are. Since CB1 receptor signalling limits excessive neuronal transmission, it will be important to analyse whether the differences in microglia morphology observed in *Cnr1*$^{-/-}$ mice are caused by altered neuronal activity at baseline and in response to stress. Importantly, it was also shown that the effects of GC signalling on monocyte trafficking and neurovascular ICAM-1 in response to repeated social defeat are active downstream of neuronal activation in stress-responsive brain regions (Niraula et al., 2018). Thus, dysregulated neuronal activity in response to stress could still directly and locally alter microglial function without the involvement of peripheral cells. The ECS is well-situated to provide an interaction pathway between microglia and neurons (and astrocytes), since eCBs are produced on-demand in response to high neuronal activity. While the typical retrograde feedback signalling of eCBs acts via CB1 receptors on presynaptic neurons, the eCBs released by an active synapse could also be sensed by nearby microglia – possibly by microglial CB2 receptors. By this, microglial processes could be attracted to the synapse, since 2-AG has been shown to induce microglial migration via CB2 *in vitro.* Additionally, ATP stimulation of microglia (simulating excessive neuronal activity or neuronal injury) induced the production of 2-AG, which in turn would limit synaptic activity via CB1 and thereby provide neuroprotection (Walter et al., 2003).

As a second readout for microglia function, surface expression of activation markers CD11b, CD40, and MHCII was analysed using flow cytometry and found upregulated after mild CSDS. Interestingly, expression of all three markers was positively correlated with behavioural stress scores and accordingly was highest on stressed *Cnr1*$^{-/-}$ mice. In comparison to microglial morphology changes – which were different between *Cnr1*$^{-/-}$ and *Cnr1*$^{+/+}$ mice – the direction of effects was similar in both genotypes, albeit more pronounced in *Cnr1*$^{-/-}$ mice. Since microglia were isolated from whole brain homogenates, it cannot be excluded that there are regional differences in these parameters as well. Together with CD18, CD11b forms the complement receptor 3 (CR3) – a pattern-recognition receptor and part of the complement cascade (Ehlers, 2000). In the brain, CR3 is expressed by microglia and is involved in microglia-mediated synaptic pruning (Schafer et al., 2012; Stevens et al., 2007). Synapses (e.g. immature or dysfunctional) are tagged by complement components C1q and C3, which targets them for elimination by microglia via C3-CR3 signalling. Mice deficient for either of the complement components have deficits in synaptic connectivity, pointing to a crucial role for this process during neuronal development. On the other hand, overexpression of complement components and increased or uncontrolled phagocytosis of synaptic terminals is observed in several neurodegenerative disorders (Morgan, 2018; Sekar et al., 2016). Increased CD11b expression, as observed in stressed *Cnr1*$^{-/-}$ mice, would thus point to an increased phagocytic activity of microglia. In line with this, a study using social defeat demonstrated that microglia of stress susceptible mice have an

increased capability of phagocyting neuronal debris (Lehmann et al., 2016, 2018). It was further demonstrated that acute stress causes a long-lasting increase in C1q in the hippocampus, that was associated with dendritic spine loss and microglial hyper-ramification (Smith et al., 2019). Similar to microglia morphology, also phagocytic activity of microglia shows great variability between brain regions and is especially high in regions with high neuronal death rates, such as the cerebellum. In brain regions with a rather stable neuronal population, like the striatum, microglial clearance activity seems to be inhibited via epigenetic suppression of clearance-related genes (Ayata et al., 2018). Intriguingly, induction of aberrant phagocytic activity in this region causes neuronal spine loss, thigmotaxis (reduced locomotion), increased anxiety, and the development of seizures with age – a phenotype very similar to that of *Cnr1*$^{-/-}$ mice. Notably, this clearance phenotype of microglia was not associated with an overall pro-inflammatory phenotype. These findings are supported by another study describing microglial heterogeneity in different basal ganglia nuclei with respect to morphology, metabolism, mitochondrial function, and phagocytic activity, but without substantial differences in typical immune functions (De Biase et al., 2017). Similarly, gene expression of pro-inflammatory cytokines in the brain was not affected by mild CSDS (see Appendix) and microglia did not show the very typical amoeboid morphology of classical pro-inflammatory activation. It is thus possible that mild CSDS did not induce profound neuroinflammation, but did affect other microglial functions.

In summary, while there were clear changes in microglia, there was no infiltration of peripheral myeloid cells into the brain after stress, which has been reported in several other studies (Lisboa et al., 2018; McKim et al., 2016, 2017; Niraula et al., 2018; Sawicki et al., 2015; Wohleb et al., 2013, 2014a, 2014b). On the one hand, this could be due to the very mild version of CSDS applied in this study. This would suggest that the response of microglia precedes the infiltration of monocytes, which is supported by the finding that activated microglia release CCL2 to recruit monocytes to the brain endothelium after chronic stress (McKim et al., 2017). On the other hand, also other groups reported that microglia activation alone was sufficient to induce depressive-like states after chronic stress, without the infiltration of peripheral cells (Lehmann et al., 2016, 2018) and that monocytes do not infiltrate into brain parenchyma, but only accumulate in brain vessels (Menard et al., 2017). Similar to the experiments described here, these studies performed stress exposure and tissue collection during the dark phase, while those that observed monocyte infiltration performed the experiments during the light phase or did not specify the time of day. It should also be noted that slightly different protocols were used in each study (e.g. setup of defeat sessions, control housing conditions). This suggests that the neuroinflammatory responses to chronic social stress are highly specific and probably time of day-dependent. Indeed, many of the aspects analysed in this context are under circadian control, prompting the need for clearly defined experimental setups. The following section will therefore discuss the possible influence of circadian rhythms and the time of stress exposure on some parameters analysed in this study.

4.6 Stress effects and their dependence on circadian rhythms

GCs follow a well-described circadian rhythm, peaking at the onset of the organism's active phase. Accordingly, the reactivity of the HPA axis (e.g. sensitivity of adrenal cells to ACTH) and the amplitude of a stress response to an acute stressor strongly depends on the time of stress exposure (Leliavski *et al*. 2014). Similarly, also responses to chronic stress and adaptation of the HPA axis to it depend on when the stressors are presented (Aslani et al., 2014; Koch et al., 2016). Furthermore, the ability of an organism to adapt to chronic stress exposure is not mediated by a universal mechanism, but seems to depend on the type of stressor (homotypic versus heterotypic stressors, social versus non-social stressors, etc.). This complexity is illustrated by several studies that analysed time of day effects in different rodent models of stress. In a model of acute predator scent stress, it was shown that rats are more vulnerable to the effects of traumatic stress when exposed at the beginning of the light phase – when baseline GCs levels are low (Cohen et al., 2015). The detrimental effects of chronic mild stress (heterotypic, non-social) on behaviour and neuronal structures were also more pronounced when animals were stressed during the light phase (Aslani et al., 2014). In contrast, it was shown that the effects of chronic social defeat (homotypic, social) on behaviour, immune function, and HPA axis adaption were more prominent when mice were stressed during the dark phase (Bartlang et al., 2012, 2014, 2015). In most cases, these time-dependent differences in susceptibility were mediated by altered responsiveness of adrenal cells to ACTH and thus altered circadian GC secretion (Bartlang et al., 2012; Reber et al., 2006, 2007; Ulrich-Lai et al., 2006).

Catecholamines show a diurnal pattern as well, which peaks at the beginning of an organism's active phase – similar to GCs. As described above, the bone marrow is one of the targets innervated by sympathetic nerves and accordingly, bone marrow noradrenaline also shows diurnal fluctuations with a peak during the active phase (Cosentino et al., 1998). The changes in noradrenaline are paralleled by fluctuations in the release of HSCs and myeloid cells into circulation (Méndez-Ferrer et al., 2008). Circulating and splenic Ly6C^{hi} monocytes peak during the inactive phase and also their recruitment to sites of inflammation is dependent on the time of day (Nguyen et al., 2013). In a model of virus-induced encephalitis, CCL2-mediated recruitment of Ly6C^{hi} monocytes to the CNS was higher when the infection was elicited at the beginning of the inactive phase (Gagnidze et al., 2016). It is thus possible that also stress-induced myeloid cell trafficking is different depending on the time of stress exposure and/or time point of the analysis.

Another factor that is likely influenced by the time of day is blood-brain-barrier integrity and endothelial cell function. It was shown that the blood-brain-barrier permeability is regulated by clock genes and thus different dependent on the time of day (Nakazato et al., 2017). Furthermore, ICAM-1 expression by vascular endothelial cells showed a rhythmic expression pattern in mouse bone marrow and skeletal muscle (Scheiermann et al., 2012). Consequently, leukocyte adhesion

to the tissue also showed a diurnal rhythm (high at night onset, low during the day). While this study did not analyse neurovascular ICAM-1 expression, it is possible that similar patterns are also observed in brain endothelial cells. Therefore, the ability to detect peripheral monocytes in the brain or brain vessels after chronic stress might also depend on the time point of analysis.

Microglia have an intrinsic circadian clock as well, which influences their response to inflammatory stimuli, both at baseline and in the context of acute stress (Fonken et al., 2015, 2016). Stress-induced inflammatory priming of microglia to a subsequent inflammatory stimulus was stronger when animals were stressed during the inactive phase, possibly mediated by different GC signalling in microglia (Fonken et al., 2016). This time-dependent microglial reactivity to stress might in turn also affect interaction of microglia with synapses and thereby affect stress-related neuronal function. Indeed, also synaptic plasticity, i.e. the formation and elimination of synapses, is dependent on the time-of-day. As such, it was demonstrated that circadian CORT oscillations promote learning-dependent synapse formation and maintenance (Liston et al., 2013). Formation of new spines after a motor-learning task was more frequent and spines were more stable when training was performed at the circadian CORT peak (beginning of dark phase). Although this study did not directly analyse stress effects, it can be assumed that the effect of stress-induced CORT on synapses is also dependent on the time of stress exposure. Adult neurogenesis, another form of neuronal plasticity, is regulated by the circadian rhythm as well. In the DG, the generation of newborn neurons increases during the dark phase (Tamai et al., 2008). It is thus also possible that those newly generated cells are differently affected by stress, depending on the time of stress exposure.

Finally, it is being recognised that the activity of the ECS follows a circadian rhythm as well. There is evidence that the number of CB1 receptors, eCB tissue content, and the activity of eCB synthesising and degrading enzymes show diurnal variations (Vaughn et al., 2010). For example, plasma levels of 2-AG show a nadir during sleep and a peak during the afternoon in healthy human adults (Hanlon et al., 2015). In the rodent brain, 2-AG levels are higher during the inactive phase in several brain regions, including PFC and hippocampus (Valenti et al., 2004). In the hippocampus, also CB1 receptor density is higher in the inactive phase (Rueda-Orozco et al., 2008). Interestingly, AEA exhibits an opposite diurnal pattern as 2-AG and CB1 in those regions, with higher levels measured during the active phase (Valenti et al., 2004). These results suggest that different phases of the day are accompanied by a different ECS tone, which will influence many downstream targets. Although speculative, this different ECS tone or different CB1 signalling might also contribute to the differences in stress-susceptibility observed at different times of the day.

4.7 Brain region- and cell type-specific effects of CB1 signalling

One limitation of this study is the use of constitutive *Cnr1*$^{-/-}$ mice, which lack CB1 receptors on all cells throughout development and might therefore show some adaptations in neuronal, endocrine and immune system activity. Although *Cnr1*$^{-/-}$ mice have no gross anatomical or neuronal defects, it is known that CB1 receptors are involved in embryonic neuronal development. CB1 signalling was shown to regulate neural progenitor proliferation, migration of pyramidal cortical neurons and interneurons, axonal guidance, and synaptogenesis (Berghuis et al., 2005, 2007; Díaz-Alonso et al., 2012; Mulder et al., 2008; Trazzi et al., 2010; Wu et al., 2010). It thus cannot be excluded that some of the phenotypes observed in *Cnr1*$^{-/-}$ mice are not due to the acute lack of CB1 signalling, but due to developmental adaptations (e.g. miswiring of neuronal circuits).

A second drawback of constitutive *Cnr1*$^{-/-}$ mice is the lack of CB1 on various cell types. CB1 receptors are expressed on virtually all neuronal subtypes, including glutamatergic, GABAergic, noradrenergic, dopaminergic, and serotonergic neurons (Marsicano and Kuner, 2008). The retrograde inhibition of synaptic activity of these neurons naturally has very different outcomes for the overall network activity and thus also the functional output (Busquets-Garcia et al., 2018). In a study using a slightly different repeated social defeat protocol, it was shown that CB1 receptors on different neuronal populations regulate different aspects of the behavioural consequences of stress (Dubreucq et al., 2012). CB1 receptors on cortical glutamatergic neurons were responsible for mediating fear responses after stress, while those on GABAergic neurons were involved in mediating stress-induced changes in locomotor activity, and CB1 on serotonergic neurons modulated hedonic behaviour. Additionally, CB1 receptors on adrenergic and noradrenergic cells in the hippocampus and the periphery were found necessary for mediating memory impairments induced by acute stress (Busquets-Garcia et al., 2016). Anxiogenic effects of central CB1 antagonism were also dependent on peripheral adrenergic transmission (Bellocchio et al., 2013), suggesting that CB1 signalling in the adrenergic system provides an essential communication pathway between the brain and periphery.

Furthermore, CB1 receptors and eCBs are differentially expressed between brain regions and accordingly can have different effects on stress-related brain circuits. For example, it was demonstrated that 2-AG signalling specifically in the BLA is both necessary and sufficient for promoting resilience to traumatic stress exposure in the form of foot shocks (Bluett et al., 2017). The resilient phenotype, determined by anxiety-related behaviour, was associated with higher 2-AG-mediated suppression of glutamate release from hippocampal projections to the BLA. In contrast, PFC-BLA synapses were not involved. Thus, CB1 receptors expressed by hippocampal glutamatergic projection neurons and their activation by amygdala-derived 2-AG might play an essential role in mediating stress resilience.

With respect to stress-related inflammation, there is generally not much information on the role of CB1 signalling, let alone CB1 signalling on different neuronal populations. In a model of repeated stress exposure (four days), constitutive *Cnr1*$^{-/-}$ mice showed exaggerated excitotoxicity and inflammation in the mPFC, but this was in part also already seen at baseline (Zoppi et al., 2011). Ageing is also associated with chronic low-grade neuroinflammation, which is aggravated in mice lacking CB1 on GABAergic, but not on glutamatergic neurons (Albayram et al., 2011). GABA-CB1 knockout mice further show some baseline changes in hippocampal microglial morphology and an altered microglial response to peripheral LPS injections (Ativie et al., 2018). Since these changes were also associated with altered expression of proteins involved in microglia-neuron communication (e.g. CX3CL1 on neurons), it is suggested that CB1 receptors on GABAergic neurons could play an important role in mediating neuronal control over microglial function. Whether this is also true for stress-related microglial responses, is however not known so far.

Finally, CB1 receptors are also expressed by non-neuronal cells both in the periphery and the brain, including adipocytes (Ruiz de Azua et al., 2017), pancreatic cells (Bermudez-Silva et al., 2008), astrocytes (Navarrete et al., 2014), oligodendrocytes (Molina-Holgado et al., 2002), and possibly microglia – albeit at very low levels (Walter et al., 2003). Another layer of complexity is added by the findings that CB1 receptors are not only located on the plasma membrane of cells, but also on intracellular membranes, for example on mitochondria (Bénard et al., 2012). So far, the presence of mtCB1 has been demonstrated on sperm and muscle cells (Aquila et al., 2010; Mendizabal-Zubiaga et al., 2016) as well as neurons and possibly astrocytes in the brain (Hebert-Chatelain et al., 2014, 2016), where it regulates mitochondrial respiration and thus cellular energy supply. In recent years, the concept of immunometabolism – the role of mitochondria and cellular metabolism in regulating immune cell function – has received a lot of interest (O'Neill et al., 2016). Although not analysed so far, the presence of mtCB1 in immune cells, including microglia, would provide an intriguing mechanism of how CB1 signalling could also directly regulate immune function.

It will therefore be important to clearly dissect the contribution of CB1 receptors on different cell types and in different brain regions to the increased stress-susceptibility that is clearly observed in constitutive *Cnr1*$^{-/-}$ mice. The availability of various cell type-specific CB1 knockout lines and viral vectors for site-specific manipulation of CB1 signalling provides a promising basis for accomplishing that.

4.8 Conclusions

In summary, this study provides clear evidence that CB1 signalling protects the body from the physical and emotional harms of social stress. CB1 signalling seems especially indispensable in situations of severe stress and lack of it may impose a serious risk, possibly related to cardiovascular complications. But even under mildly stressful conditions, which do not result in the development of maladaptive behaviours in most wild type mice, CB1 deficiency greatly increases the proportion of mice that do show a stress-related behavioural phenotype. This is in agreement with the view that the ECS generally acts as a buffering system and lack of its function reduces the capacity to cope with situations in which homeostasis is disturbed – as it is the case during stress. Differences in ECS signalling might thus also underlie some of the natural variance in stress-susceptibility/resilience observed in laboratory rodents and humans.

Surprisingly, the results described here indicate that the lack of CB1 signalling on the long run leads to insufficient GC signalling. Although this is in contradiction to the common believe that CB1 signalling mediates negative feedback of the HPA axis, it does support the idea that CB1 signalling is necessary for adaptation of the stress response under chronic stress conditions. In *Cnr1*$^{+/+}$ mice, this adaptation likely involves flattening of the circadian GC rhythm, which overall increases GC levels. Although GCs are often considered detrimental and the cause of stress-related pathologies, this shift in GC signalling might in fact be protective under chronic stress conditions.

Interestingly, the stress effects on myeloid cells and inflammatory signalling described in the literature (e.g. neurovascular ICAM-1, microglial IBA1, increase in circulating monocytes) were rather observed in *Cnr1*$^{+/+}$ mice, although these mice did not develop a clear behavioural phenotype after mild CSDS. It is thus possible that these changes are also somehow adaptive and not the cause for the development of behavioural deficits. Indeed, the fact that stressed *Cnr1*$^{-/-}$ mice showed a clear behavioural phenotype without strong changes in peripheral myeloid cells and no recruitment of monocytes to the brain argues against a crucial involvement of those cells. In contrast, different parameters of microglial function (morphology and surface marker expression) were changed after mild CSDS and correlated with the behavioural susceptibility – especially in *Cnr1*$^{-/-}$ mice. While this study cannot provide evidence for a causal relationship of microglial function to behaviour, it strongly suggests that microglia play an important role in stress-related pathologies. Whether microglia actively shape behaviour or rather respond to other (neuronal) changes that occur during chronic stress and how CB1 signalling can regulate microglial function remains to be analysed in future studies.

Bibliography

Aagaard, L. (2014). “Chapter 1 - Central nervous system stimulants and drugs that suppress appetite,” in *A worldwide yearly survey of new data in adverse drug reactions and interactions*, ed. J. K. B. T.-S. E. of D. A. Aronson (Elsevier), 1–25. doi:https://doi.org/10.1016/B978-0-444-62635-6.00001-2.

Albayram, O., Alferink, J., Pitsch, J., Piyanova, A., Neitzert, K., Poppensieker, K., et al. (2011). Role of CB1 cannabinoid receptors on GABAergic neurons in brain aging. *Proc. Natl. Acad. Sci.* 108, 11256–11261. doi:10.1073/pnas.1016442108.

Alboni, P., Holz, A., and Brignole, M. (2013). Vagally mediated atrioventricular block: pathophysiology and diagnosis. *Heart* 99, 904–8. doi:10.1136/heartjnl-2012-303220.

American Psychiatric Association (2013). *Diagnostic and Statistical Manual of Mental Disorders (5th edition)*. Washington, DC doi:10.1176/appi.pn.2016.7a7.

Anacker, C., Zunszain, P. A., Carvalho, L. A., and Pariante, C. M. (2011). The glucocorticoid receptor: Pivot of depression and of antidepressant treatment? *Psychoneuroendocrinology* 36, 415–425. doi:10.1016/j.psyneuen.2010.03.007.

Andrié, R. P., Becher, U. M., Frommold, R., Tiyerili, V., Schrickel, J. W., Nickenig, G., et al. (2012). Interleukin-6 is the strongest predictor of 30-day mortality in patients with cardiogenic shock due to myocardial infarction. *Crit. Care* 16, R152. doi:10.1186/cc11467.

Aquila, S., Guido, C., Santoro, A., Perrotta, I., Laezza, C., Bifulco, M., et al. (2010). Human Sperm Anatomy: Ultrastructural Localization of the Cannabinoid1 Receptor and a Potential Role of Anandamide in Sperm Survival and Acrosome Reaction. *Anat. Rec.* 293, 298–309. doi:10.1002/ar.21042.

Arganda-Carreras, I., Fernandez-Gonzalez, R., Munoz-Barrutia, A., and Ortiz-De-Solorzano, C. (2010). 3D reconstruction of histological sections: Application to mammary gland tissue. *Microsc. Res. Tech.* 73, 1019–1029. doi:10.1002/jemt.20829.

Askew, K., Li, K., Olmos-Alonso, A., Garcia-Moreno, F., Liang, Y., Richardson, P., et al. (2017). Coupled Proliferation and Apoptosis Maintain the Rapid Turnover of Microglia in the Adult Brain. *Cell Rep.* 18, 391–405. doi:10.1016/j.celrep.2016.12.041.

Aslani, S., Harb, M. R., Costa, P. S., Almeida, O. F. X., Sousa, N., and Palha, J. A. (2014). Day and night: diurnal phase influences the response to chronic mild stress. *Front. Behav. Neurosci.* 8, 82. doi:10.3389/fnbeh.2014.00082.

Aso, E., Ozaita, A., Valdizán, E. M., Ledent, C., Pazos, Á., Maldonado, R., et al. (2008a). BDNF impairment in the hippocampus is related to enhanced despair behavior in CB $_1$ knockout mice. *J. Neurochem.* 105, 565–572. doi:10.1111/j.1471-4159.2007.05149.x.

Aso, E., Renoir, T., Mengod, G., Ledent, C., Hamon, M., Maldonado, R., et al. (2009). Lack of CB $_1$ receptor activity impairs serotonergic negative feedback. *J. Neurochem.* 109, 935–944.

doi:10.1111/j.1471-4159.2009.06025.x.

Aso, E., Valdiza, E. M., Ledent, C., Maldonado, R., and Valverde, O. (2008b). BDNF impairment in the hippocampus is related to enhanced despair behavior in CB 1 knockout mice. 565–572. doi:10.1111/j.1471-4159.2007.05149.x.

Ativie, F., Komorowska, J. A., Beins, E., Albayram, Ö., Zimmer, T., Zimmer, A., et al. (2018). Cannabinoid 1 Receptor Signaling on Hippocampal GABAergic Neurons Influences Microglial Activity. *Front. Mol. Neurosci.* 11, 1–14. doi:10.3389/fnmol.2018.00295.

Avitsur, R., Stark, J. L., Dhabhar, F. S., Padgett, D. A., and Sheridan, J. F. (2002). Social disruption-induced glucocorticoid resistance: kinetics and site specificity. *J. Neuroimmunol.* 124, 54–61. Available at: http://www.ncbi.nlm.nih.gov/pubmed/11958822 [Accessed August 9, 2019].

Ayata, P., Badimon, A., Strasburger, H. J., Duff, M. K., Montgomery, S. E., Loh, Y.-H. E., et al. (2018). Epigenetic regulation of brain region-specific microglia clearance activity. *Nat. Neurosci.* 21, 1049–1060. doi:10.1038/s41593-018-0192-3.

Bab, I., and Zimmer, A. (2008). Cannabinoid receptors and the regulation of bone mass. *Br. J. Pharmacol.* 153, 182–8. doi:10.1038/sj.bjp.0707593.

Barna, I., Zelena, D., Arszovszki, A. C., and Ledent, C. (2004). The role of endogenous cannabinoids in the hypothalamo-pituitary-adrenal axis regulation: in vivo and in vitro studies in CB1 receptor knockout mice. *Life Sci.* 75, 2959–2970. doi:https://doi.org/10.1016/j.lfs.2004.06.006.

Bartlang, M. S., Neumann, I. D., Slattery, D. A., Uschold-Schmidt, N., Kraus, D., Helfrich-Forster, C., et al. (2012). Time matters: pathological effects of repeated psychosocial stress during the active, but not inactive, phase of male mice. *J. Endocrinol.* 215, 425–437. doi:10.1530/JOE-12-0267.

Bartlang, M. S., Oster, H., and Helfrich-Förster, C. (2015). Repeated psychosocial stress at night affects the circadian activity rhythm of male mice. *J. Biol. Rhythms* 30, 228–41. doi:10.1177/0748730415576192.

Bartlang, M. S., Savelyev, S. A., Johansson, A.-S., Reber, S. O., Helfrich-Förster, C., and Lundkvist, G. B. S. (2014). Repeated psychosocial stress at night, but not day, affects the central molecular clock. *Chronobiol. Int.* 31, 996–1007. doi:10.3109/07420528.2014.940085.

Basu, S., Hodgson, G., Katz, M., and Dunn, A. R. (2002). Evaluation of role of G-CSF in the production, survival, and release of neutrophils from bone marrow into circulation. *Blood* 100, 854–61. doi:10.1182/blood.v100.3.854.

Beins, E., Ulas, T., Ternes, S., Neumann, H., Schultze, J. L., and Zimmer, A. (2016). Characterization of inflammatory markers and transcriptome profiles of differentially activated embryonic stem cell-derived microglia. *Glia* 64, n/a-n/a. doi:10.1002/glia.22979.

Bekhbat, M., Rowson, S. A., and Neigh, G. N. (2017). Checks and balances: The glucocorticoid receptor and NFκB in good times and bad. *Front. Neuroendocrinol.* 46, 15–31.

doi:10.1016/j.yfrne.2017.05.001.

Bellocchio, L., Soria-Gomez, E., Quarta, C., Metna-Laurent, M., Cardinal, P., Binder, E., et al. (2013). Activation of the sympathetic nervous system mediates hypophagic and anxiety-like effects of CB1 receptor blockade. *Proc. Natl. Acad. Sci.* 110, 4786–4791. doi:10.1073/pnas.1218573110.

Bénard, G., Massa, F., Puente, N., Lourenço, J., Bellocchio, L., Soria-Gómez, E., et al. (2012). Mitochondrial CB1 receptors regulate neuronal energy metabolism. *Nat. Neurosci.* 15, 558. Available at: https://doi.org/10.1038/nn.3053.

Bennett, M. L., Bennett, F. C., Liddelow, S. A., Ajami, B., Zamanian, J. L., Fernhoff, N. B., et al. (2016). New tools for studying microglia in the mouse and human CNS. *Proc. Natl. Acad. Sci.* 113, E1738 LP-E1746. doi:10.1073/pnas.1525528113.

Berghuis, P., Dobszay, M. B., Wang, X., Spano, S., Ledda, F., Sousa, K. M., et al. (2005). Endocannabinoids regulate interneuron migration and morphogenesis by transactivating the TrkB receptor. *Proc. Natl. Acad. Sci.* 102, 19115–19120. doi:10.1073/pnas.0509494102.

Berghuis, P., Rajnicek, A. M., Morozov, Y. M., Ross, R. A., Mulder, J., Urbán, G. M., et al. (2007). Hardwiring the Brain: Endocannabinoids Shape Neuronal Connectivity. *Science (80-.).* 316, 1212 LP – 1216. doi:10.1126/science.1137406.

Bermudez-Silva, F. J., Suarez, J., Baixeras, E., Cobo, N., Bautista, D., Cuesta-Munoz, A. L., et al. (2008). Presence of functional cannabinoid receptors in human endocrine pancreas. *Diabetologia* 51, 476–487. doi:10.1007/s00125-007-0890-y.

Bethin, K. E., Vogt, S. K., and Muglia, L. J. (2000). Interleukin-6 is an essential , corticotropin-releasing hormone-independent stimulator of the adrenal axis during immune system activation. 97.

Bisogno, T., Howell, F., Williams, G., Minassi, A., Cascio, M. G., Ligresti, A., et al. (2003). Cloning of the first sn1-DAG lipases points to the spatial and temporal regulation of endocannabinoid signaling in the brain. *J. Cell Biol.* 163, 463–8. doi:10.1083/jcb.200305129.

Björkqvist, K. (2001). Social defeat as a stressor in humans. *Physiol. Behav.* 73, 435–42. doi:10.1016/s0031-9384(01)00490-5.

Blankman, J. L., Simon, G. M., and Cravatt, B. F. (2007). A comprehensive profile of brain enzymes that hydrolyze the endocannabinoid 2-arachidonoylglycerol. *Chem. Biol.* 14, 1347–56. doi:10.1016/j.chembiol.2007.11.006.

Bluett, R. J., Báldi, R., Haymer, A., Gaulden, A. D., Hartley, N. D., Parrish, W. P., et al. (2017). Endocannabinoid signalling modulates susceptibility to traumatic stress exposure. *Nat. Commun.* 8, 14782. doi:10.1038/ncomms14782.

Boche, D., Perry, V. H., and Nicoll, J. A. R. (2013). Review: Activation patterns of microglia and their identification in the human brain. *Neuropathol. Appl. Neurobiol.* 39, 3–18. doi:10.1111/nan.12011.

Bollinger, J. L., Bergeon Burns, C. M., and Wellman, C. L. (2016). Differential effects of stress on

microglial cell activation in male and female medial prefrontal cortex. *Brain. Behav. Immun.* 52, 88–97. doi:10.1016/j.bbi.2015.10.003.

Bosch-Bouju, C., Larrieu, T., Linders, L., Manzoni, O. J., and Layé, S. (2016). Endocannabinoid-Mediated Plasticity in Nucleus Accumbens Controls Vulnerability to Anxiety after Social Defeat Stress. *Cell Rep.* 16, 1237–1242. doi:10.1016/j.celrep.2016.06.082.

Bothe, G. W. M., Bolivar, V. J., Vedder, M. J., and Geistfeld, J. G. (2005). Behavioral differences among fourteen inbred mouse strains commonly used as disease models. *Comp. Med.* 55, 326–34. Available at: http://www.ncbi.nlm.nih.gov/pubmed/16158908 [Accessed August 9, 2019].

Brunetti, M., Martelli, N., Colasante, A., Piantelli, M., Musiani, P., and Aiello, F. B. (1995). Spontaneous and glucocorticoid-induced apoptosis in human mature T lymphocytes. *Blood* 86, 4199 LP – 4205. Available at: http://www.bloodjournal.org/content/86/11/4199.abstract.

Bult, A., and Lynch, C. B. (1997). Nesting and fitness: lifetime reproductive success in house mice bidirectionally selected for thermoregulatory nest-building behavior. *Behav. Genet.* 27, 231–240.

Busquets-Garcia, A., Bains, J., and Marsicano, G. (2018). CB1 Receptor Signaling in the Brain: Extracting Specificity from Ubiquity. *Neuropsychopharmacology* 43, 4–20. doi:10.1038/npp.2017.206.

Busquets-Garcia, A., Gomis-González, M., Srivastava, R. K., Cutando, L., Ortega-Alvaro, A., Ruehle, S., et al. (2016). Peripheral and central CB1 cannabinoid receptors control stress-induced impairment of memory consolidation. *Proc. Natl. Acad. Sci.* 113, 9904–9909. doi:10.1073/pnas.1525066113.

Carrier, E. J., Kearn, C. S., Barkmeier, A. J., Breese, N. M., Yang, W., Nithipatikom, K., et al. (2004). Cultured Rat Microglial Cells Synthesize the Endocannabinoid 2-Arachidonylglycerol, Which Increases Proliferation via a CB2 Receptor-Dependent Mechanism. *Mol. Pharmacol.* 65, 999–1007. doi:10.1124/mol.65.4.999.

Carvalho, L. A., Bergink, V., Sumaski, L., Wijkhuijs, J., Hoogendijk, W. J., Birkenhager, T. K., et al. (2014). Inflammatory activation is associated with a reduced glucocorticoid receptor alpha/beta expression ratio in monocytes of inpatients with melancholic major depressive disorder. *Transl. Psychiatry* 4, e344-8. doi:10.1038/tp.2013.118.

Carvalho, L. A., Garner, B. A., Dew, T., Fazakerley, H., and Pariante, C. M. (2010). Antidepressants, but not antipsychotics, modulate GR function in human whole blood: An insight into molecular mechanisms. *Eur. Neuropsychopharmacol.* 20, 379–387. doi:https://doi.org/10.1016/j.euroneuro.2010.02.006.

Casanova-Acebes, M., Pitaval, C., Weiss, L. A., Nombela-Arrieta, C., Chèvre, R., A-González, N., et al. (2013). Rhythmic Modulation of the Hematopoietic Niche through Neutrophil Clearance. *Cell* 153, 1025–1035. doi:10.1016/j.cell.2013.04.040.

Childs, E., White, T. L., and de Wit, H. (2014). Personality traits modulate emotional and physiological responses to stress. *Behav. Pharmacol.* 25, 493–502. doi:10.1097/FBP.0000000000000064.

Chiurchiu, V., Battistini, L., and Maccarrone, M. (2015). Endocannabinoid signalling in innate and adaptive immunity. *Immunology* 144, 352–364. doi:10.1111/imm.12441.

Christensen, R., Kristensen, P. K., Bartels, E. M., Bliddal, H., and Astrup, A. (2007). Efficacy and safety of the weight-loss drug rimonabant: a meta-analysis of randomised trials. *Lancet (London, England)* 370, 1706–1713. doi:10.1016/S0140-6736(07)61721-8.

Chrousos, G. P. (2009). Stress and disorders of the stress system. *Nat. Rev. Endocrinol.* 5, 374–381. doi:10.1038/nrendo.2009.106.

Cohen, S., Vainer, E., Matar, M. A., Kozlovsky, N., Kaplan, Z., Zohar, J., et al. (2015). Diurnal Fluctuations in HPA and Neuropeptide Y-ergic Systems Underlie Differences in Vulnerability to Traumatic Stress Responses at Different Zeitgeber Times. *Neuropsychopharmacology* 40, 774–790. doi:10.1038/npp.2014.257.

Colton, C. A., and Wilcock, D. M. (2010). Assessing Activation States in Microglia. *CNS Neurol. Disord. - Drug Targets* 9, 174–191. doi:10.2174/187152710791012053.

Coppen, A. (1967). The biochemistry of affective disorders. *Br. J. Psychiatry* 113, 1237–1264. doi:10.1192/bjp.113.504.1237.

Correa, F., Hernangómez, M., Mestre, L., Loría, F., Spagnolo, A., Docagne, F., et al. (2010). Anandamide enhances IL-10 production in activated microglia by targeting CB_2 receptors: Roles of ERK1/2, JNK, and NF-κB. *Glia* 58, 135–147. doi:10.1002/glia.20907.

Cosentino, M., Marino, F., Bombelli, R., Ferrari, M., Maestroni, G. J. M., Conti, A., et al. (1998). Association between the circadian course of endogenous noradrenaline and the hematopoietic cell cycle in mouse bone marrow. *J. Chemother.* 10, 179–181. doi:10.1179/joc.1998.10.2.179.

Cota, D., Marsicano, G., Tschop, M., Grubler, Y., Flachskamm, C., Schubert, M., et al. (2003). The endogenous cannabinoid system affects energy balance via central orexigenic drive and peripheral lipogenesis. *J. Clin. Invest.* 112, 423–431. doi:10.1172/JCI17725.

Cota, D., Steiner, M.-A., Marsicano, G., Cervino, C., Herman, J. P., Grübler, Y., et al. (2007). Requirement of Cannabinoid Receptor Type 1 for the Basal Modulation of Hypothalamic-Pituitary-Adrenal Axis Function. *Endocrinology* 148, 1574–1581. doi:10.1210/en.2005-1649.

Coutinho, A. E., and Chapman, K. E. (2011). The anti-inflammatory and immunosuppressive effects of glucocorticoids, recent developments and mechanistic insights. *Mol. Cell. Endocrinol.* 335, 2–13. doi:https://doi.org/10.1016/j.mce.2010.04.005.

Cravatt, B. F., Giang, D. K., Mayfield, S. P., Boger, D. L., Lerner, R. A., and Gilula, N. B. (1996). Molecular characterization of an enzyme that degrades neuromodulatory fatty-acid amides. *Nature* 384, 83–87. doi:10.1038/384083a0.

Crawley, J. N., Belknap, J. K., Collins, A., Crabbe, J. C., Frankel, W., Henderson, N., et al. (1997). Behavioral phenotypes of inbred mouse strains: implications and recommendations for molecular studies. *Psychopharmacology (Berl).* 132, 107–124. doi:10.1007/s002130050327.

Dantzer, R. (2009). Cytokine, sickness behavior, and depression. *Immunol. Allergy Clin. North Am.* 29, 247–264. doi:10.1016/j.iac.2009.02.002.

De Biase, L. M., Schuebel, K. E., Fusfeld, Z. H., Jair, K., Hawes, I. A., Cimbro, R., et al. (2017). Local Cues Establish and Maintain Region-Specific Phenotypes of Basal Ganglia Microglia. *Neuron* 95, 341-356.e6. doi:10.1016/j.neuron.2017.06.020.

De Kloet, E. R., Joëls, M., and Holsboer, F. (2005). Stress and the brain: from adaptation to disease. *Nat. Rev. Neurosci.* 6, 463–475. doi:10.1038/nrn1683.

Devane, W. A., Dysarz, F. A., Johnson, M. R., Melvin, L. S., and Howlett, A. C. (1988). Determination and characterization of a cannabinoid receptor in rat brain. *Mol. Pharmacol.* 34, 605–13. Available at: http://www.ncbi.nlm.nih.gov/pubmed/2848184 [Accessed August 8, 2019].

Devane, W., Hanus, L., Breuer, A., Pertwee, R., Stevenson, L., Griffin, G., et al. (1992). Isolation and structure of a brain constituent that binds to the cannabinoid receptor. *Science (80-.).* 258, 1946–1949. doi:10.1126/science.1470919.

Dhabhar, F. S., Malarkey, W. B., Neri, E., and McEwen, B. S. (2012). Stress-induced redistribution of immune cells--from barracks to boulevards to battlefields: a tale of three hormones--Curt Richter Award winner. *Psychoneuroendocrinology* 37, 1345–1368. doi:10.1016/j.psyneuen.2012.05.008.

Di, S., Malcher-Lopes, R., Halmos, K. C., and Tasker, J. G. (2003). Nongenomic Glucocorticoid Inhibition via Endocannabinoid Release in the Hypothalamus: A Fast Feedback Mechanism. *J. Neurosci.* 23, 4850 LP – 4857. Available at: http://www.jneurosci.org/content/23/12/4850.abstract.

Díaz-Alonso, J., Guzmán, M., and Galve-Roperh, I. (2012). Endocannabinoids via CB $_1$ receptors act as neurogenic niche cues during cortical development. *Philos. Trans. R. Soc. B Biol. Sci.* 367, 3229–3241. doi:10.1098/rstb.2011.0385.

Dibner, C., Schibler, U., and Albrecht, U. (2010). The mammalian circadian timing system: organization and coordination of central and peripheral clocks. *Annu. Rev. Physiol.* 72, 517–549. doi:10.1146/annurev-physiol-021909-135821.

Dieperink, E., Willenbring, M., and Ho, S. B. (2000). Neuropsychiatric symptoms associated with hepatitis C and interferon alpha: A review. *Am. J. Psychiatry* 157, 867–876. doi:10.1176/appi.ajp.157.6.867.

Dimsdale, J. E. (2008). Psychological stress and cardiovascular disease. *J. Am. Coll. Cardiol.* 51, 1237–1246. doi:10.1016/j.jacc.2007.12.024.

Ding, L., and Morrison, S. J. (2013). Haematopoietic stem cells and early lymphoid progenitors occupy distinct bone marrow niches. *Nature* 495, 231–235. doi:10.1038/nature11885.

Diorio, D., Viau, V., and Meaney, M. J. (1993). The role of the medial prefrontal cortex (cingulate gyrus) in the regulation of hypothalamic-pituitary-adrenal responses to stress. *J. Neurosci.* 13, 3839–47. Available at: http://www.ncbi.nlm.nih.gov/pubmed/8396170 [Accessed August 9, 2019].

Dissing-Olesen, L., LeDue, J. M., Rungta, R. L., Hefendehl, J. K., Choi, H. B., and MacVicar, B. A. (2014). Activation of neuronal NMDA receptors triggers transient ATP-mediated microglial process outgrowth. *J. Neurosci.* 34, 10511–10527. doi:10.1523/JNEUROSCI.0405-14.2014.

Dowlati, Y., Herrmann, N., Swardfager, W., Liu, H., Sham, L., Reim, E. K., et al. (2010). A meta-analysis of cytokines in major depression. *Biol. Psychiatry* 67, 446–457. doi:10.1016/j.biopsych.2009.09.033.

Dubreucq, S., Matias, I., Cardinal, P., Häring, M., Lutz, B., Marsicano, G., et al. (2012). Genetic Dissection of the Role of Cannabinoid Type-1 Receptors in the Emotional Consequences of Repeated Social Stress in Mice. *Neuropsychopharmacology* 37, 1885–1900. doi:10.1038/npp.2012.36.

Dunn, A. J. (2000). Cytokine activation of the HPA axis. *Ann. N. Y. Acad. Sci.* 917, 608–617. doi:10.1111/j.1749-6632.2000.tb05426.x.

Eash, K. J., Greenbaum, A. M., Gopalan, P. K., and Link, D. C. (2010). CXCR2 and CXCR4 antagonistically regulate neutrophil trafficking from murine bone marrow. *J. Clin. Invest.* 120, 2423–2431. doi:10.1172/JCI41649.

Ehlers, M. R. W. (2000). CR3 : a general purpose adhesion-recognition receptor essential for innate immunity. 18, 289–294.

Elgendi, M., Eskofier, B., Dokos, S., and Abbott, D. (2014). Revisiting QRS Detection Methodologies for Portable, Wearable, Battery-Operated, and Wireless ECG Systems. *PLoS One* 9, e84018. doi:10.1371/journal.pone.0084018.

Eljaschewitsch, E., Witting, A., Mawrin, C., Lee, T., Schmidt, P. M., Wolf, S., et al. (2006). The Endocannabinoid Anandamide Protects Neurons during CNS Inflammation by Induction of MKP-1 in Microglial Cells. *Neuron* 49, 67–79. doi:10.1016/j.neuron.2005.11.027.

Evanson, N. K., Tasker, J. G., Hill, M. N., Hillard, C. J., and Herman, J. P. (2010). Fast Feedback Inhibition of the HPA Axis by Glucocorticoids Is Mediated by Endocannabinoid Signaling. *Endocrinology* 151, 4811–4819. doi:10.1210/en.2010-0285.

Evers, A. W. M., Verhoeven, E. W. M., van Middendorp, H., Sweep, F. C. G. J., Kraaimaat, F. W., Donders, A. R. T., et al. (2014). Does stress affect the joints? Daily stressors, stress vulnerability, immune and HPA axis activity, and short-term disease and symptom fluctuations in rheumatoid arthritis. *Ann. Rheum. Dis.* 73, 1683–1688. doi:10.1136/annrheumdis-2012-203143.

Ferrini, F., and De Koninck, Y. (2013). Microglia Control Neuronal Network Excitability via BDNF Signalling. *Neural Plast.* 2013, 1–11. doi:10.1155/2013/429815.

Fonken, L. K., Frank, M. G., Kitt, M. M., Barrientos, R. M., Watkins, L. R., and Maier, S. F. (2015). Microglia inflammatory responses are controlled by an intrinsic circadian clock. *Brain. Behav. Immun.* 45, 171–179. doi:10.1016/j.bbi.2014.11.009.

Fonken, L. K., Weber, M. D., Daut, R. A., Kitt, M. M., Frank, M. G., Watkins, L. R., et al. (2016). Stress-induced neuroinflammatory priming is time of day dependent. *Psychoneuroendocrinology* 66, 82–90. doi:10.1016/j.psyneuen.2016.01.006.

Fontainhas, A. M., Wang, M., Liang, K. J., Chen, S., Mettu, P., Damani, M., et al. (2011). Microglial morphology and dynamic behavior is regulated by ionotropic glutamatergic and GABAergic neurotransmission. *PLoS One* 6, e15973. doi:10.1371/journal.pone.0015973.

Forray, M. I., and Gysling, K. (2004). Role of noradrenergic projections to the bed nucleus of the stria terminalis in the regulation of the hypothalamic-pituitary-adrenal axis. *Brain Res. Brain Res. Rev.* 47, 145–60. doi:10.1016/j.brainresrev.2004.07.011.

Frank, M. G., Miguel, Z. D., Watkins, L. R., and Maier, S. F. (2010). Prior exposure to glucocorticoids sensitizes the neuroinflammatory and peripheral inflammatory responses to E. coli lipopolysaccharide. *Brain. Behav. Immun.* 24, 19–30. doi:10.1016/j.bbi.2009.07.008.

Furze, R. C., and Rankin, S. M. (2008). The role of the bone marrow in neutrophil clearance under homeostatic conditions in the mouse. *FASEB J.* 22, 3111–3119. doi:10.1096/fj.08-109876.

Gagnidze, K., Hajdarovic, K. H., Moskalenko, M., Karatsoreos, I. N., McEwen, B. S., and Bulloch, K. (2016). Nuclear receptor REV-ERBα mediates circadian sensitivity to mortality in murine vesicular stomatitis virus-induced encephalitis. *Proc. Natl. Acad. Sci.* 113, 5730–5735. doi:10.1073/pnas.1520489113.

Galiegue, S., Mary, S., Marchand, J., Dussossoy, D., Carriere, D., Carayon, P., et al. (1995). Expression of Central and Peripheral Cannabinoid Receptors in Human Immune Tissues and Leukocyte Subpopulations. *Eur. J. Biochem.* 232, 54–61. doi:10.1111/j.1432-1033.1995.tb20780.x.

Gaoni, Y., and Mechoulam, R. (1964). Isolation, Structure, and Partial Synthesis of an Active Constituent of Hashish. *J. Am. Chem. Soc.* 86, 1646–1647. doi:10.1021/ja01062a046.

Geissmann, F., Manz, M. G., Jung, S., Sieweke, M. H., Merad, M., and Ley, K. (2010). Development of monocytes, macrophages, and dendritic cells. *Science* 327, 656–661. doi:10.1126/science.1178331.

Ginhoux, F., Lim, S., Hoeffel, G., Low, D., and Huber, T. (2013). Origin and differentiation of microglia. *Front. Cell. Neurosci.* 7, 1–14. doi:10.3389/fncel.2013.00045.

Godoy, L. D., Rossignoli, M. T., Delfino-Pereira, P., Garcia-Cairasco, N., and de Lima Umeoka, E. H. (2018). A Comprehensive Overview on Stress Neurobiology: Basic Concepts and Clinical Implications. *Front. Behav. Neurosci.* 12, 127. doi:10.3389/fnbeh.2018.00127.

Gola, H., Engler, H., Sommershof, A., Adenauer, H., Kolassa, S., Schedlowski, M., et al. (2013). Posttraumatic stress disorder is associated with an enhanced spontaneous production of

pro-inflammatory cytokines by peripheral blood mononuclear cells. *BMC Psychiatry* 13, 40. doi:10.1186/1471-244X-13-40.

Golden, S. A., Covington, H. E., Berton, O., Russo, S. J., and Covington III, H. (2011). A standardized protocol for repeated social defeat stress in mice. *Nat. Protoc.* 6, 1183–1191. doi:10.1038/nprot.2011.361.A.

Goldstein, D. S., and Kopin, I. J. (2007). Evolution of concepts of stress. *Stress* 10, 109–120. doi:10.1080/10253890701288935.

Gomez-Nicola, D., and Perry, V. H. (2015). Microglial dynamics and role in the healthy and diseased brain: a paradigm of functional plasticity. *Neuroscientist* 21, 169–184. doi:10.1177/1073858414530512.

Gordon, S., and Taylor, P. R. (2005). Monocyte and macrophage heterogeneity. *Nat. Rev. Immunol.* 5, 953–964. doi:10.1038/nri1733.

Grzeda, E., Schlicker, E., Luczaj, W., Harasim, E., Baranowska-Kuczko, M., and Malinowska, B. (2015). Bi-directional CB1 receptor-mediated cardiovascular effects of cannabinoids in anaesthetized rats: role of the paraventricular nucleus. *J. Physiol. Pharmacol.* 66, 343–53. Available at: http://www.ncbi.nlm.nih.gov/pubmed/26084216 [Accessed August 9, 2019].

Haller, J., Varga, B., Ledent, C., Barna, I., and Freund, T. F. (2004). Context-dependent effects of CB1 cannabinoid gene disruption on anxiety-like and social behaviour in mice. *Eur. J. Neurosci.* 19, 1906–1912. doi:10.1111/j.1460-9568.2004.03293.x.

Hanlon, E. C., Tasali, E., Leproult, R., Stuhr, K. L., Doncheck, E., de Wit, H., et al. (2015). Circadian Rhythm of Circulating Levels of the Endocannabinoid 2-Arachidonoylglycerol. *J. Clin. Endocrinol. Metab.* 100, 220–226. doi:10.1210/jc.2014-3455.

Hansen, H. S., Moesgaard, B., Hansen, H. H., and Petersen, G. (2000). N-Acylethanolamines and precursor phospholipids - relation to cell injury. *Chem. Phys. Lipids* 108, 135–50. Available at: http://www.ncbi.nlm.nih.gov/pubmed/11106787 [Accessed August 8, 2019].

Hebert-Chatelain, E., Desprez, T., Serrat, R., Bellocchio, L., Soria-Gomez, E., Busquets-Garcia, A., et al. (2016). A cannabinoid link between mitochondria and memory. *Nature* 539, 555–559. doi:10.1038/nature20127.

Hebert-Chatelain, E., Reguero, L., Puente, N., Lutz, B., Chaouloff, F., Rossignol, R., et al. (2014). Cannabinoid control of brain bioenergetics: Exploring the subcellular localization of the CB1 receptor. *Mol. Metab.* 3, 495–504. doi:10.1016/j.molmet.2014.03.007.

Heidt, T., Sager, H. B., Courties, G., Dutta, P., Iwamoto, Y., Zaltsman, A., et al. (2014). Chronic variable stress activates hematopoietic stem cells. *Nat. Med.* 20, 754–758. doi:10.1038/nm.3589.

Hellwig, S., Brioschi, S., Dieni, S., Frings, L., Masuch, A., Blank, T., et al. (2016). Altered microglia morphology and higher resilience to stress-induced depression-like behavior in CX3CR1-deficient mice. *Brain. Behav. Immun.* 55, 126–137. doi:10.1016/j.bbi.2015.11.008.

Herkenham, M., Lynn, A. B., Johnson, M. R., Melvin, L. S., de Costa, B. R., and Rice, K. C. (1991).

Characterization and localization of cannabinoid receptors in rat brain: a quantitative in vitro autoradiographic study. *J. Neurosci.* 11, 563–83. Available at: http://www.ncbi.nlm.nih.gov/pubmed/1992016 [Accessed August 8, 2019].

Hill, M. N., Carrier, E. J., McLaughlin, R. J., Morrish, A. C., Meier, S. E., Hillard, C. J., et al. (2008). Regional alterations in the endocannabinoid system in an animal model of depression: effects of concurrent antidepressant treatment. *J. Neurochem.* 106, 2322–2336. doi:10.1111/j.1471-4159.2008.05567.x.

Hill, M. N., Ho, W.-S. V., Sinopoli, K. J., Viau, V., Hillard, C. J., and Gorzalka, B. B. (2006). Involvement of the endocannabinoid system in the ability of long-term tricyclic antidepressant treatment to suppress stress-induced activation of the hypothalamic-pituitary-adrenal axis. *Neuropsychopharmacology* 31, 2591–9. doi:10.1038/sj.npp.1301092.

Hill, M. N., Hunter, R. G., and McEwen, B. S. (2009). Chronic stress differentially regulates cannabinoid CB1 receptor binding in distinct hippocampal subfields. *Eur. J. Pharmacol.* 614, 66–9. doi:10.1016/j.ejphar.2009.04.048.

Hill, M. N., McLaughlin, R. J., Bingham, B., Shrestha, L., Lee, T. T. Y., Gray, J. M., et al. (2010a). Endogenous cannabinoid signaling is essential for stress adaptation. *Proc. Natl. Acad. Sci. U. S. A.* 107, 9406–9411. doi:10.1073/pnas.0914661107.

Hill, M. N., McLaughlin, R. J., Pan, B., Fitzgerald, M. L., Roberts, C. J., Lee, T. T.-Y., et al. (2011). Recruitment of Prefrontal Cortical Endocannabinoid Signaling by Glucocorticoids Contributes to Termination of the Stress Response. *J. Neurosci.* 31, 10506–10515. doi:10.1523/JNEUROSCI.0496-11.2011.

Hill, M. N., Patel, S., Campolongo, P., Tasker, J. G., Wotjak, C. T., and Bains, J. S. (2010b). Functional Interactions between Stress and the Endocannabinoid System: From Synaptic Signaling to Behavioral Output. *J. Neurosci.* 30, 14980–14986. doi:10.1523/JNEUROSCI.4283-10.2010.

Hillard, C. J., Beatka, M., and Sarvaideo, J. (2017). Endocannabinoid Signaling and the Hypothalamic-Pituitary-Adrenal Axis Introduction to the Components and Paradigms of CNS Endocannabinoid Signaling. *Compr Physiol* 7, 1–15. doi:10.1002/cphy.c160005.

Hinwood, M., Morandini, J., Day, T. A., and Walker, F. R. (2012). Evidence that microglia mediate the neurobiological effects of chronic psychological stress on the medial prefrontal cortex. *Cereb. Cortex* 22, 1442–54. doi:10.1093/cercor/bhr229.

Hinwood, M., Tynan, R. J., Charnley, J. L., Beynon, S. B., Day, T. A., and Walker, F. R. (2013). Chronic stress induced remodeling of the prefrontal cortex: structural re-organization of microglia and the inhibitory effect of minocycline. *Cereb. Cortex* 23, 1784–97. doi:10.1093/cercor/bhs151.

Hodes, G. E., Pfau, M. L., Leboeuf, M., Golden, S. A., Christoffel, D. J., Bregman, D., et al. (2014). Individual differences in the peripheral immune system promote resilience versus

susceptibility to social stress. *Proc. Natl. Acad. Sci.* 111, 16136–16141. doi:10.1073/pnas.1415191111.

Hoeffel, G., and Ginhoux, F. (2015). Ontogeny of Tissue-Resident Macrophages. *Front. Immunol.* 6, 486. doi:10.3389/fimmu.2015.00486.

Hulsmans, M., Clauss, S., Xiao, L., Aguirre, A. D., King, K. R., Hanley, A., et al. (2017). Macrophages Facilitate Electrical Conduction in the Heart. *Cell* 169, 510-522.e20. doi:10.1016/j.cell.2017.03.050.

Idris, A. I., and Ralston, S. H. (2012). Role of cannabinoids in the regulation of bone remodeling. *Front. Endocrinol. (Lausanne).* 3, 136. doi:10.3389/fendo.2012.00136.

Ishac, E. J., Jiang, L., Lake, K. D., Varga, K., Abood, M. E., and Kunos, G. (1996). Inhibition of exocytotic noradrenaline release by presynaptic cannabinoid CB1 receptors on peripheral sympathetic nerves. *Br. J. Pharmacol.* 118, 2023–2028. Available at: http://www.ncbi.nlm.nih.gov/pmc/articles/PMC1909901/.

Izzo, A. A., and Sharkey, K. A. (2010). Cannabinoids and the gut: New developments and emerging concepts. *Pharmacol. Ther.* 126, 21–38. doi:10.1016/j.pharmthera.2009.12.005.

Jenniches, I. (2016). The importance of endogenous cannabinoids in stress-related disorders and depression.

Kadmiel, M., and Cidlowski, J. A. (2013). Glucocorticoid receptor signaling in health and disease. *Trends Pharmacol. Sci.* 34, 518–30. doi:10.1016/j.tips.2013.07.003.

Kano, M., Ohno-Shosaku, T., Hashimotodani, Y., Uchigashima, M., and Watanabe, M. (2009). Endocannabinoid-Mediated Control of Synaptic Transmission. *Physiol. Rev.* 89, 309–380. doi:10.1152/physrev.00019.2008.

Katayama, Y., Battista, M., Kao, W. M., Hidalgo, A., Peired, A. J., Thomas, S. A., et al. (2006). Signals from the sympathetic nervous system regulate hematopoietic stem cell egress from bone marrow. *Cell* 124, 407–421. doi:10.1016/j.cell.2005.10.041.

Katona, I., Sperlágh, B., Sík, A., Käfalvi, A., Vizi, E. S., Mackie, K., et al. (1999). Presynaptically located CB1 cannabinoid receptors regulate GABA release from axon terminals of specific hippocampal interneurons. *J. Neurosci.* 19, 4544–58. Available at: http://www.ncbi.nlm.nih.gov/pubmed/10341254 [Accessed August 8, 2019].

Katona, I., Urbán, G. M., Wallace, M., Ledent, C., Jung, K.-M., Piomelli, D., et al. (2006). Molecular composition of the endocannabinoid system at glutamatergic synapses. *J. Neurosci.* 26, 5628–37. doi:10.1523/JNEUROSCI.0309-06.2006.

Katz, R. J. (1981). Animal models and human depressive disorders. *Neurosci. Biobehav. Rev.* 5, 231–46. Available at: http://www.ncbi.nlm.nih.gov/pubmed/7022272 [Accessed August 8, 2019].

Kettenmann, H., Kirchhoff, F., and Verkhratsky, A. (2013). Microglia: new roles for the synaptic stripper. *Neuron* 77, 10–18. doi:10.1016/j.neuron.2012.12.023.

Kierdorf, K., and Prinz, M. (2013). Factors regulating microglia activation. *Front. Cell. Neurosci.* 7,

1–8. doi:10.3389/fncel.2013.00044.

Kivimaki, M., and Steptoe, A. (2018). Effects of stress on the development and progression of cardiovascular disease. *Nat. Rev. Cardiol.* 15, 215–229. doi:10.1038/nrcardio.2017.189.

Koch, C. E., Bartlang, M. S., Kiehn, J. T., Lucke, L., Naujokat, N., Helfrich-Forster, C., et al. (2016). Time-of-day-dependent adaptation of the HPA axis to predictable social defeat stress. *J. Endocrinol.* 231, 209–221. doi:10.1530/JOE-16-0163.

Kongsui, R., Beynon, S. B., Johnson, S. J., and Walker, F. R. (2014). Quantitative assessment of microglial morphology and density reveals remarkable consistency in the distribution and morphology of cells within the healthy prefrontal cortex of the rat. *J. Neuroinflammation* 11, 182. doi:10.1186/s12974-014-0182-7.

Kreisel, T., Frank, M. G., Licht, T., Reshef, R., Ben-Menachem-Zidon, O., Baratta, M. V, et al. (2014). Dynamic microglial alterations underlie stress-induced depressive-like behavior and suppressed neurogenesis. *Mol. Psychiatry* 19, 699–709. doi:10.1038/mp.2013.155.

Kreitzer, A. C., and Regehr, W. G. (2001a). Cerebellar depolarization-induced suppression of inhibition is mediated by endogenous cannabinoids. *J. Neurosci.* 21, RC174. Available at: http://www.ncbi.nlm.nih.gov/pubmed/11588204 [Accessed August 8, 2019].

Kreitzer, A. C., and Regehr, W. G. (2001b). Retrograde inhibition of presynaptic calcium influx by endogenous cannabinoids at excitatory synapses onto Purkinje cells. *Neuron* 29, 717–27. Available at: http://www.ncbi.nlm.nih.gov/pubmed/11301030 [Accessed August 8, 2019].

Krishnan, V., Han, M., Graham, D. L., Berton, O., Renthal, W., Russo, S. J., et al. (2007). Molecular Adaptations Underlying Susceptibility and Resistance to Social Defeat in Brain Reward Regions. 1, 391–404. doi:10.1016/j.cell.2007.09.018.

Lehmann, M. L., Cooper, H. A., Maric, D., and Herkenham, M. (2016). Social defeat induces depressive-like states and microglial activation without involvement of peripheral macrophages. *J. Neuroinflammation* 13, 1–19. doi:10.1186/s12974-016-0672-x.

Lehmann, M. L., Weigel, T. K., Cooper, H. A., Elkahloun, A. G., Kigar, S. L., and Herkenham, M. (2018). Decoding microglia responses to psychosocial stress reveals blood- brain barrier breakdown that may drive stress susceptibility. *Sci. Rep.*, 1–19. doi:10.1038/s41598-018-28737-8.

Lesch, K. P. (2004). Gene-environment interaction and the genetics of depression. *J. Psychiatry Neurosci.* 29, 174–184. Available at: https://www.ncbi.nlm.nih.gov/pubmed/15173894.

Leung, H. (2006). Finding the missing link between ictal bradyarrhythmia , ictal asystole , and sudden unexpected death in epilepsy. 9, 19–30. doi:10.1016/j.yebeh.2006.05.009.

Li, Y., and Kim, J. (2015). Neuronal expression of CB2 cannabinoid receptor mRNAs in the mouse hippocampus. *Neuroscience* 311, 253–267. doi:10.1016/j.neuroscience.2015.10.041.

Liles, W. C., Dale, D. C., and Klebanoff, S. J. (1995). Glucocorticoids inhibit apoptosis of human neutrophils. *Blood* 86, 3181 LP – 3188. Available at: http://www.bloodjournal.org/content/86/8/3181.abstract.

Lisboa, S. F., Niraula, A., Resstel, L. B., Guimaraes, F. S., Godbout, J. P., and Sheridan, J. F. (2018). Repeated social defeat-induced neuroin fl ammation , anxiety- like behavior and resistance to fear extinction were attenuated by the cannabinoid receptor agonist WIN55 , 212-2. *Neuropsychopharmacology* 2. doi:10.1038/s41386-018-0064-2.

Liston, C., Cichon, J. M., Jeanneteau, F., Jia, Z., Chao, M. V, and Gan, W.-B. (2013). Circadian glucocorticoid oscillations promote learning-dependent synapse formation and maintenance. *Nat. Neurosci.* 16, 698–705. doi:10.1038/nn.3387.

Liu, Y., Ho, R. C.-M., and Mak, A. (2012). Interleukin (IL)-6, tumour necrosis factor alpha (TNF-alpha) and soluble interleukin-2 receptors (sIL-2R) are elevated in patients with major depressive disorder: a meta-analysis and meta-regression. *J. Affect. Disord.* 139, 230–239. doi:10.1016/j.jad.2011.08.003.

Livak, K. J., and Schmittgen, T. D. (2001). Analysis of relative gene expression data using real-time quantitative PCR and the 2(-Delta Delta C(T)) Method. *Methods* 25, 402–8. doi:10.1006/meth.2001.1262.

Loeper, M., and Crouzon, O. (1904). *L'action de l'adrenaline sur le sang*.

Loss, C. M., Binder, L. B., Muccini, E., Martins, W. C., de Oliveira, P. A., Vandresen-Filho, S., et al. (2015). Influence of environmental enrichment vs. time-of-day on behavioral repertoire of male albino Swiss mice. *Neurobiol. Learn. Mem.* 125, 63–72. doi:10.1016/j.nlm.2015.07.016.

Lowin, T., and Straub, R. H. (2015). Cannabinoid-based drugs targeting CB<inf>1</inf> and TRPV1, the sympathetic nervous system, and arthritis. *Arthritis Res. Ther.* 17, 1–13. doi:10.1186/s13075-015-0743-x.

Lucassen, P. J., Oomen, C. A., Schouten, M., Encinas, J. M., and Fitzsimons, C. P. (2016). "Chapter 8 - Adult Neurogenesis, Chronic Stress and Depression," in, ed. J. J. B. T.-A. N. in the H. Canales (San Diego: Academic Press), 177–206. doi:https://doi.org/10.1016/B978-0-12-801977-1.00008-8.

Lupien, S. J., McEwen, B. S., Gunnar, M. R., and Heim, C. (2009). Effects of stress throughout the lifespan on the brain, behaviour and cognition. *Nat. Rev. Neurosci.* 10, 434–445. doi:10.1038/nrn2639.

Mackie, K. (2005). Distribution of cannabinoid receptors in the central and peripheral nervous system. *Handb. Exp. Pharmacol.*, 299–325. Available at: http://www.ncbi.nlm.nih.gov/pubmed/16596779 [Accessed August 8, 2019].

Maes, M. (1995). Evidence for an immune response in major depression: a review and hypothesis. *Prog. Neuropsychopharmacol. Biol. Psychiatry* 19, 11–38.

Mai, P., Yang, L., Tian, L., Wang, L., Jia, S., Zhang, Y., et al. (2015). Endocannabinoid System Contributes to Liver Injury and Inflammation by Activation of Bone Marrow–Derived Monocytes/Macrophages in a CB1-Dependent Manner. *J. Immunol.* 195, 3390–3401. doi:10.4049/jimmunol.1403205.

Manz, M. G., and Boettcher, S. (2014). Emergency granulopoiesis. *Nat. Rev. Immunol.* 14, 302–314. doi:10.1038/nri3660.

Marrie, R. A., Walld, R., Bolton, J. M., Sareen, J., Walker, J. R., Patten, S. B., et al. (2017). Increased incidence of psychiatric disorders in immune-mediated inflammatory disease. *J. Psychosom. Res.* 101, 17–23. doi:https://doi.org/10.1016/j.jpsychores.2017.07.015.

Marsicano, G., Goodenough, S., Monory, K., Hermann, H., Eder, M., Cannich, A., et al. (2003). CB1 Cannabinoid Receptors and On-Demand Defense Against Excitotoxicity. *Science (80-.).* 302, 84–88. doi:10.1126/science.1088208.

Marsicano, G., and Kuner, R. (2008). "Anatomical Distribution of Receptors, Ligands and Enzymes in the Brain and in the Spinal Cord: Circuitries and Neurochemistry BT - Cannabinoids and the Brain," in, ed. A. Köfalvi (Boston, MA: Springer US), 161–201. doi:10.1007/978-0-387-74349-3_10.

Marsicano, G., Wotjak, C. T., Azad, S. C., Bisogno, T., Rammes, G., Cascio, M. G., et al. (2002). The endogenous cannabinoid system controls extinction of aversive memories. *Nature* 418, 530–4. doi:10.1038/nature00839.

Martinez, F. O., and Gordon, S. (2014). The M1 and M2 paradigm of macrophage activation: time for reassessment. *F1000Prime Rep.* 6, 13. doi:10.12703/P6-13.

Masuda, T., Sankowski, R., Staszewski, O., Böttcher, C., Amann, L., Sagar, et al. (2019). Spatial and temporal heterogeneity of mouse and human microglia at single-cell resolution. *Nature* 566, 388–392. doi:10.1038/s41586-019-0924-x.

Matsuda, L. A., Lolait, S. J., Brownstein, M. J., Young, A. C., and Bonner, T. I. (1990). Structure of a cannabinoid receptor and functional expression of the cloned cDNA. *Nature* 346, 561–564. doi:10.1038/346561a0.

Mawdsley, J. E., and Rampton, D. S. (2005). Psychological stress in IBD: new insights into pathogenic and therapeutic implications. *Gut* 54, 1481–1491. doi:10.1136/gut.2005.064261.

McCorry, L. K. (2007). Physiology of the autonomic nervous system. *Am. J. Pharm. Educ.* 71, 78. doi:10.5688/aj710478.

McHugh, D. (2012). GPR18 in microglia: Implications for the CNS and endocannabinoid system signalling. *Br. J. Pharmacol.* 167, 1575–1582. doi:10.1111/j.1476-5381.2012.02019.x.

McKim, D. B., Patterson, J. M., Wohleb, E. S., Jarrett, B. L., Reader, B. F., Godbout, J. P., et al. (2016). Sympathetic Release of Splenic Monocytes Promotes Recurring Anxiety Following Repeated Social Defeat. *Biol. Psychiatry* 79, 803–813. doi:10.1016/j.biopsych.2015.07.010.

McKim, D. B., Weber, M. D., Niraula, A., Sawicki, C. M., Liu, X., Jarrett, B. L., et al. (2017). Microglial recruitment of IL-1β-producing monocytes to brain endothelium causes stress-induced anxiety. *Mol. Psychiatry*, 1–11. doi:10.1038/mp.2017.64.

Mckim, D. B., Yin, W., Wang, Y., Cole, S. W., Godbout, J. P., Sheridan, J. F., et al. (2018). Social

Stress Mobilizes Hematopoietic Stem Cells to Establish Persistent Splenic Myelopoiesis Article Social Stress Mobilizes Hematopoietic Stem Cells to Establish Persistent Splenic Myelopoiesis. *CellReports* 25, 2552-2562.e3. doi:10.1016/j.celrep.2018.10.102.

Meccariello, R., Battista, N., Bradshaw, H. B., and Wang, H. (2014). Updates in reproduction coming from the endocannabinoid system. *Int. J. Endocrinol.* 2014, 412354. doi:10.1155/2014/412354.

Mechoulam, R., Ben-Shabat, S., Hanus, L., Ligumsky, M., Kaminski, N. E., Schatz, A. R., et al. (1995). Identification of an endogenous 2-monoglyceride, present in canine gut, that binds to cannabinoid receptors. *Biochem. Pharmacol.* 50, 83–90. doi:10.1016/0006-2952(95)00109-d.

Menard, C., Pfau, M. L., Hodes, G. E., Kana, V., Wang, V. X., Bouchard, S., et al. (2017). Social stress induces neurovascular pathology promoting depression. *Nat. Neurosci.* 20, 1752–1760. doi:10.1038/s41593-017-0010-3.

Méndez-Ferrer, S., Lucas, D., Battista, M., and Frenette, P. S. (2008). Haematopoietic stem cell release is regulated by circadian oscillations. *Nature* 452, 442–447. doi:10.1038/nature06685.

Mendizabal-Zubiaga, J., Melser, S., Bénard, G., Ramos, A., Reguero, L., Arrabal, S., et al. (2016). Cannabinoid CB(1) Receptors Are Localized in Striated Muscle Mitochondria and Regulate Mitochondrial Respiration. *Front. Physiol.* 7, 476. doi:10.3389/fphys.2016.00476.

Metna-Laurent, M., and Marsicano, G. (2015). Rising stars: Modulation of brain functions by astroglial type-1 cannabinoid receptors. *Glia* 63, 353–364. doi:10.1002/glia.22773.

Miller, A. H., Spencer, R. L., Pearce, B. D., Pisell, T. L., Azrieli, Y., Tanapat, P., et al. (1998). Glucocorticoid Receptors Are Differentially Expressed in the Cells and Tissues of the Immune System. *Cell. Immunol.* 186, 45–54. doi:https://doi.org/10.1006/cimm.1998.1293.

Miller, G. E., Chen, E., and Zhou, E. S. (2007). If it goes up, must it come down? Chronic stress and the hypothalamic-pituitary-adrenocortical axis in humans. *Psychol. Bull.* 133, 25–45. doi:10.1037/0033-2909.133.1.25.

Miller, G. E., Cohen, S., and Ritchey, A. K. (2002). Chronic psychological stress and the regulation of pro-inflammatory cytokines: a glucocorticoid-resistance model. *Health Psychol.* 21, 531–541.

Miller, G. E., Murphy, M. L. M., Cashman, R., Ma, R., Ma, J., Arevalo, J. M. G., et al. (2014). Greater inflammatory activity and blunted glucocorticoid signaling in monocytes of chronically stressed caregivers. *Brain. Behav. Immun.* 41, 191–199. doi:10.1016/j.bbi.2014.05.016.

Mnich, S. J., Hiebsch, R. R., Huff, R. M., and Muthian, S. (2010). Anti-Inflammatory Properties of CB₁-Receptor Antagonist Involves β₂ Adrenoceptors. *J. Pharmacol. Exp. Ther.* 333, 445 LP – 453. doi:10.1124/jpet.109.163998.

Molina-Holgado, E., Vela, J. M., Arévalo-Martín, A., Almazán, G., Molina-Holgado, F., Borrell, J., et al. (2002). Cannabinoids Promote Oligodendrocyte Progenitor Survival: Involvement of

Cannabinoid Receptors and Phosphatidylinositol-3 Kinase/Akt Signaling. *J. Neurosci.* 22, 9742 LP – 9753. doi:10.1523/JNEUROSCI.22-22-09742.2002.

Montecucco, F., and Di Marzo, V. (2012). At the heart of the matter: the endocannabinoid system in cardiovascular function and dysfunction. *Trends Pharmacol. Sci.* 33, 331–340. doi:10.1016/j.tips.2012.03.002.

Morena, M., Patel, S., Bains, J. S., and Hill, M. N. (2016). Neurobiological Interactions Between Stress and the Endocannabinoid System. *Neuropsychopharmacology* 41, 80–102. doi:10.1038/npp.2015.166.

Moretti, P., Bouwknecht, J. A., Teague, R., Paylor, R., and Zoghbi, H. Y. (2005). Abnormalities of social interactions and home-cage behavior in a mouse model of Rett syndrome. *Hum. Mol. Genet.* 14, 205–220. doi:10.1093/hmg/ddi016.

Morgan, B. P. (2018). Complement in the pathogenesis of Alzheimer's disease. *Semin. Immunopathol.* 40, 113–124. doi:10.1007/s00281-017-0662-9.

Mulder, J., Aguado, T., Keimpema, E., Barabas, K., Ballester Rosado, C. J., Nguyen, L., et al. (2008). Endocannabinoid signaling controls pyramidal cell specification and long-range axon patterning. *Proc. Natl. Acad. Sci.* 105, 8760–8765. doi:10.1073/pnas.0803545105.

Munro, S., Thomas, K. L., and Abu-Shaar, M. (1993). Molecular characterization of a peripheral receptor for cannabinoids. *Nature* 365, 61–65. doi:10.1038/365061a0.

Murataeva, N., Straiker, A., and Mackie, K. (2014). Parsing the players: 2-arachidonoylglycerol synthesis and degradation in the CNS. *Br. J. Pharmacol.* 171, 1379–1391. doi:10.1111/bph.12411.

Murray, P. J., Allen, J. E., Biswas, S. K., Fisher, E. A., Gilroy, D. W., Goerdt, S., et al. (2014). Macrophage activation and polarization: nomenclature and experimental guidelines. *Immunity* 41, 14–20. doi:10.1016/j.immuni.2014.06.008.

Murray, R. M., Morrison, P. D., Henquet, C., and Di Forti, M. (2007). Cannabis, the mind and society: the hash realities. *Nat. Rev. Neurosci.* 8, 885–895. doi:10.1038/nrn2253.

Nakazato, R., Kawabe, K., Yamada, D., Ikeno, S., Mieda, M., Shimba, S., et al. (2017). Disruption of Bmal1 Impairs Blood–Brain Barrier Integrity via Pericyte Dysfunction. *J. Neurosci.* 37, 10052–10062. doi:10.1523/JNEUROSCI.3639-16.2017.

Natelson, B. H., Ottenweller, J. E., Cook, J. A., Pitman, D., McCarty, R., and Tapp, W. N. (1988). Effect of stressor intensity on habituation of the adrenocortical stress response. *Physiol. Behav.* 43, 41–46. doi:10.1016/0031-9384(88)90096-0.

Navarrete, M., Díez, A., and Araque, A. (2014). Astrocytes in endocannabinoid signalling. *Philos. Trans. R. Soc. Lond. B. Biol. Sci.* 369, 20130599. doi:10.1098/rstb.2013.0599.

Nebeling, F. C., Poll, S., Schmid, L. C., Mittag, M., Steffen, J., Keppler, K., et al. (2019). Microglia motility depends on neuronal activity and promotes structural plasticity in the hippocampus. *bioRxiv*, 515759. doi:10.1101/515759.

Nemeroff, C. B. (2007). Prevalence and management of treatment-resistant depression. *J. Clin.*

Psychiatry 68 Suppl 8, 17–25.

Ng, A. P., and Alexander, W. S. (2017). Haematopoietic stem cells: past, present and future. *Cell Death Discov.* 3, 17002. Available at: https://doi.org/10.1038/cddiscovery.2017.2.

Nguyen, K. D., Fentress, S. J., Qiu, Y., Yun, K., Cox, J. S., and Chawla, A. (2013). Circadian Gene Bmal1 Regulates Diurnal Oscillations of Ly6Chi Inflammatory Monocytes. *Science (80-.).* 341, 1483–1488. doi:10.1126/science.1240636.

Niederhoffer, N., and Szabo, B. (1999). Effect of the cannabinoid receptor agonist WIN55212-2 on sympathetic cardiovascular regulation. *Br. J. Pharmacol.* 126, 457–466. doi:10.1038/sj.bjp.0702337.

Nimmerjahn, A., Kirchhoff, F., and Helmchen, F. (2005). Resting microglial cells are highly dynamic surveillants of brain parenchyma in vivo. *Science* 308, 1314–1318. doi:10.1126/science.1110647.

Niraula, A., Wang, Y., Godbout, J. P., and Sheridan, J. F. (2018). Corticosterone Production during Repeated Social Defeat Causes Monocyte Mobilization from the Bone Marrow, Glucocorticoid Resistance and Neurovascular Adhesion Molecule Expression. *J. Neurosci.* 38, 2568–17. doi:10.1523/JNEUROSCI.2568-17.2018.

O'Neill, L. A. J., Kishton, R. J., and Rathmell, J. (2016). A guide to immunometabolism for immunologists. *Nat. Rev. Immunol.* 16, 553–565. doi:10.1038/nri.2016.70.

Ohno-Shosaku, T., Maejima, T., and Kano, M. (2001). Endogenous cannabinoids mediate retrograde signals from depolarized postsynaptic neurons to presynaptic terminals. *Neuron* 29, 729–38. Available at: http://www.ncbi.nlm.nih.gov/pubmed/11301031 [Accessed August 8, 2019].

Okamoto, Y., Wang, J., Morishita, J., and Ueda, N. (2007). Biosynthetic Pathways of the Endocannabinoid Anandamide. *Chem. Biodivers.* 4, 1842–1857. doi:10.1002/cbdv.200790155.

Onaivi, E. S., Ishiguro, H., Gong, J., Mora, Z., Tagliaferro, P., Gardner, E., et al. (2006). Discovery of the Presence and Functional Expression of Cannabinoid CB2 Receptors in Brain. 536, 514–536. doi:10.1196/annals.1369.052.

Oppong, E., and Cato, A. C. B. (2015). "Effects of Glucocorticoids in the Immune System BT - Glucocorticoid Signaling: From Molecules to Mice to Man," in, eds. J.-C. Wang and C. Harris (New York, NY: Springer New York), 217–233. doi:10.1007/978-1-4939-2895-8_9.

Oropeza, V. C., Mackie, K., and Van Bockstaele, E. J. (2007). Cannabinoid receptors are localized to noradrenergic axon terminals in the rat frontal cortex. *Brain Res.* 1127, 36–44. doi:10.1016/j.brainres.2006.09.110.

Pace, T. W. W., Hu, F., and Miller, A. H. (2007). Cytokine-effects on glucocorticoid receptor function: relevance to glucocorticoid resistance and the pathophysiology and treatment of major depression. *Brain. Behav. Immun.* 21, 9–19. doi:10.1016/j.bbi.2006.08.009.

Pacher, P., Batkai, S., and Kunos, G. (2006). The endocannabinoid system as an emerging target

of pharmacotherapy. *Pharmacol. Rev.* 58, 389–462. doi:10.1124/pr.58.3.2.

Pariante, C. M. (2017). Why are depressed patients inflamed? A reflection on 20 years of research on depression, glucocorticoid resistance and inflammation. *Eur. Neuropsychopharmacol.* 27, 554–559. doi:10.1016/j.euroneuro.2017.04.001.

Parkin, J., and Cohen, B. (2001). An overview of the immune system. *Lancet* 357, 1777–1789. doi:https://doi.org/10.1016/S0140-6736(00)04904-7.

Patel, S., Roelke, C. T., Rademacher, D. J., Cullinan, W. E., Hillard, C. J., and College, M. (2004). Endocannabinoid Signaling Negatively Modulates Stress- Induced Activation of the Hypothalamic-Pituitary-. 145, 5431–5438. doi:10.1210/en.2004-0638.

Patel, S., Roelke, C. T., Rademacher, D. J., and Hillard, C. J. (2005). Inhibition of restraint stress-induced neural and behavioural activation by endogenous cannabinoid signalling. *Eur. J. Neurosci.* 21, 1057–1069. doi:10.1111/j.1460-9568.2005.03916.x.

Pfitzer, T., Niederhoffer, N., and Szabo, B. (2005). Search for an endogenous cannabinoid-mediated effect in the sympathetic nervous system. *Naunyn. Schmiedebergs. Arch. Pharmacol.* 371, 9–17. doi:10.1007/s00210-004-1003-9.

Plescher, M., Seifert, G., Hansen, J. N., Bedner, P., Steinhauser, C., and Halle, A. (2018). Plaque-dependent morphological and electrophysiological heterogeneity of microglia in an Alzheimer's disease mouse model. *Glia* 66, 1464–1480. doi:10.1002/glia.23318.

Porsolt, R. D., Bertin, A., and Jalfre, M. (1977). Behavioral despair in mice: a primary screening test for antidepressants. *Arch. Int. Pharmacodyn. Ther.* 229, 327–336.

Pothion, S., Bizot, J.-C., Trovero, F., and Belzung, C. (2004). Strain differences in sucrose preference and in the consequences of unpredictable chronic mild stress. *Behav. Brain Res.* 155, 135–46. doi:10.1016/j.bbr.2004.04.008.

Prenderville, J. A., Kelly, Á. M., and Downer, E. J. (2015). The role of cannabinoids in adult neurogenesis. *Br. J. Pharmacol.* 172, 3950–3963. doi:10.1111/bph.13186.

Prescott, S. M., and Majerus, P. W. (1983). Characterization of 1,2-diacylglycerol hydrolysis in human platelets. Demonstration of an arachidonoyl-monoacylglycerol intermediate. *J. Biol. Chem.* 258, 764–9. Available at: http://www.ncbi.nlm.nih.gov/pubmed/6822511 [Accessed August 8, 2019].

Puffenbarger, R. A., Boothe, A. C., and Cabral, G. A. (2000). Cannabinoids inhibit LPS-inducible cytokine mRNA expression in rat microglial cells. *Glia* 29, 58–69. Available at: http://www.ncbi.nlm.nih.gov/pubmed/10594923 [Accessed August 8, 2019].

Rademacher, D. J., Meier, S. E., Shi, L., Ho, W.-S. V., Jarrahian, A., and Hillard, C. J. (2008). Effects of acute and repeated restraint stress on endocannabinoid content in the amygdala, ventral striatum, and medial prefrontal cortex in mice. *Neuropharmacology* 54, 108–116. doi:10.1016/j.neuropharm.2007.06.012.

Raison, C. L., and Miller, A. H. (2003). When Not Enough Is Too Much: The Role of Insufficient Glucocorticoid Signaling in the Pathophysiology of. *Am. J. Psychiatry* IX, 1554–1565.

doi:10.1176/appi.ajp.160.9.1554.

Ramirez, K., Niraula, A., and Sheridan, J. F. (2016). GABAergic modulation with classical benzodiazepines prevent stress-induced neuro-immune dysregulation and behavioral alterations. *Brain. Behav. Immun.* 51, 154–168. doi:10.1016/j.bbi.2015.08.011.

Reader, B. F., Jarrett, B. L., McKim, D. B., Wohleb, E. S., Godbout, J. P., and Sheridan, J. F. (2015). Peripheral and central effects of repeated social defeat stress: Monocyte trafficking, microglial activation, and anxiety. *Neuroscience* 289, 429–442. doi:10.1016/j.neuroscience.2015.01.001.

Reber, S. O., Birkeneder, L., Veenema, A. H., Obermeier, F., Falk, W., Straub, R. H., et al. (2007). Adrenal insufficiency and colonic inflammation after a novel chronic psycho-social stress paradigm in mice: Implications and mechanisms. *Endocrinology* 148, 670–682. doi:10.1210/en.2006-0983.

Reber, S. O., Obermeier, F., Straub, R. H., Falk, W., and Neumann, I. D. (2006). Chronic intermittent psychosocial stress (social defeat/overcrowding) in mice increases the severity of an acute DSS-induced colitis and impairs regeneration. *Endocrinology* 147, 4968–4976. doi:10.1210/en.2006-0347.

Rinaldi-Carmona, M., Barth, F., Héaulme, M., Shire, D., Calandra, B., Congy, C., et al. (1994). SR141716A, a potent and selective antagonist of the brain cannabinoid receptor. *FEBS Lett.* 350, 240–4. doi:10.1016/0014-5793(94)00773-x.

Rueda-Orozco, P. E., Soria-Gomez, E., Montes-Rodriguez, C. J., Martínez-Vargas, M., Galicia, O., Navarro, L., et al. (2008). A potential function of endocannabinoids in the selection of a navigation strategy by rats. *Psychopharmacology (Berl).* 198, 565–576. doi:10.1007/s00213-007-0911-z.

Ruiz de Azua, I., Mancini, G., Srivastava, R. K., Rey, A. A., Cardinal, P., Tedesco, L., et al. (2017). Adipocyte cannabinoid receptor CB1 regulates energy homeostasis and alternatively activated macrophages. *J. Clin. Invest.* 127, 4148–4162. doi:10.1172/JCI83626.

Ryan, K. K. (2014). "Stress and Metabolic Disease," in *Sociality, Hierarchy, Health: Comparative Biodemography: A Collection of Papers*, eds. M. Weintein and M. A. Lane (Washington (DC): National Academies Press (US)), 247–267. Available at: https://www.ncbi.nlm.nih.gov/books/NBK242443/?report=reader [Accessed August 12, 2019].

Sanudo-Pena, M. C., Strangman, N. M., Mackie, K., Walker, J. M., and Tsou, K. (1999). CB1 receptor localization in rat spinal cord and roots, dorsal root ganglion, and peripheral nerve. *Zhongguo Yao Li Xue Bao* 20, 1115–1120.

Sato, K. (2015). Effects of Microglia on Neurogenesis. *Glia* 63, 1394–1405. doi:10.1002/glia.22858.

Sawicki, C. M., McKim, D. B., Wohleb, E. S., Jarrett, B. L., Reader, B. F., Norden, D. M., et al. (2015). Social defeat promotes a reactive endothelium in a brain region-dependent manner with

increased expression of key adhesion molecules, selectins and chemokines associated with the recruitment of myeloid cells to the brain. *Neuroscience* 302, 151–164. doi:10.1016/j.neuroscience.2014.10.004.

Scanzano, A., and Cosentino, M. (2015). Adrenergic regulation of innate immunity: a review. *Front. Pharmacol.* 6, 171. doi:10.3389/fphar.2015.00171.

Schafer, D. P., Lehrman, E. K., Kautzman, A. G., Koyama, R., Mardinly, A. R., Yamasaki, R., et al. (2012). Microglia Sculpt Postnatal Neural Circuits in an Activity and Complement-Dependent Manner. *Neuron* 74, 691–705. doi:10.1016/j.neuron.2012.03.026.

Scheiermann, C., Kunisaki, Y., Lucas, D., Chow, A., Jang, J.-E., Zhang, D., et al. (2012). Adrenergic Nerves Govern Circadian Leukocyte Recruitment to Tissues. *Immunity* 37, 290–301. doi:10.1016/j.immuni.2012.05.021.

Schildkraut, J. J. (1995). The catecholamine hypothesis of affective disorders: a review of supporting evidence. 1965. *J. Neuropsychiatry Clin. Neurosci.* 7, 524. doi:10.1176/jnp.7.4.524.

Seedat, S., Stein, M. B., Kennedy, C. M., and Hauger, R. L. (2003). Plasma cortisol and neuropeptide Y in female victims of intimate partner violence. *Psychoneuroendocrinology* 28, 796–808.

Sekar, A., Bialas, A. R., de Rivera, H., Davis, A., Hammond, T. R., Kamitaki, N., et al. (2016). Schizophrenia risk from complex variation of complement component 4. *Nature* 530, 177. Available at: https://doi.org/10.1038/nature16549.

Sgoifo, A., and Papi, F. (1995). Effects of social and non-social acute Stressors on plasma levels of cate-cholamines and corticosterone in wild rats. *Rend. Lincei* 6, 289. doi:10.1007/BF03001690.

Shi, C., and Pamer, E. G. (2011). Monocyte recruitment during infection and inflammation. *Nat. Rev. Immunol.* 11, 762–774. doi:10.1038/nri3070.

Shmuely, S., Lende, M. Van Der, Lamberts, R. J., Sander, J. W., and Thijs, R. D. (2017). The heart of epilepsy : Current views and future concepts. *Seizure Eur. J. Epilepsy* 44, 176–183. doi:10.1016/j.seizure.2016.10.001.

Sierra, A., Beccari, S., Diaz-Aparicio, I., Encinas, J. M., Comeau, S., and Tremblay, M. È. (2014). Surveillance, phagocytosis, and inflammation: How never-resting microglia influence adult hippocampal neurogenesis. *Neural Plast.* 2014. doi:10.1155/2014/610343.

Sierra, A., Encinas, J. M., Deudero, J. J. P., Chancey, J. H., Enikolopov, G., Overstreet-Wadiche, L. S., et al. (2010). Microglia shape adult hippocampal neurogenesis through apoptosis-coupled phagocytosis. *Cell Stem Cell* 7, 483–495. doi:10.1016/j.stem.2010.08.014.

Silvin, A., and Ginhoux, F. (2018). Microglia heterogeneity along a spatio-temporal axis: More questions than answers. *Glia* 66, 2045–2057. doi:10.1002/glia.23458.

Smith, K. L., Kassem, M. S., Clarke, D. J., Kuligowski, M. P., Bedoya-Pérez, M. A., Todd, S. M., et al. (2019). Microglial cell hyper-ramification and neuronal dendritic spine loss in the

hippocampus and medial prefrontal cortex in a mouse model of PTSD. *Brain. Behav. Immun.* 80, 889–899. doi:10.1016/j.bbi.2019.05.042.

Son, G. H., Chung, S., and Kim, K. (2011). The adrenal peripheral clock: glucocorticoid and the circadian timing system. *Front. Neuroendocrinol.* 32, 451–465. doi:10.1016/j.yfrne.2011.07.003.

Stark, J. L., Avitsur, R., Hunzeker, J., Padgett, D. A., and Sheridan, J. F. (2002). Interleukin-6 and the development of social disruption-induced glucocorticoid resistance. *J. Neuroimmunol.* 124, 9–15. Available at: http://www.ncbi.nlm.nih.gov/pubmed/11958817 [Accessed August 9, 2019].

Stark, J. L., Avitsur, R., Padgett, D. A., Campbell, K. A., Beck, F. M., and Sheridan, J. F. (2001). Social stress induces glucocorticoid resistance in macrophages. *Am. J. Physiol. Integr. Comp. Physiol.* 280, R1799–R1805. doi:10.1152/ajpregu.2001.280.6.R1799.

Stein, D. J., Vasconcelos, M. F., Albrechet-souza, L., and Benedetto, B. Di (2017). Microglial Over-Activation by Social Defeat Stress Contributes to Anxiety- and Depressive-Like Behaviors. *Front. Behav. Neurosci.* 11. doi:10.3389/fnbeh.2017.00207.

Steiner, M. A., Wanisch, K., Monory, K., Marsicano, G., Borroni, E., Bächli, H., et al. (2008). Impaired cannabinoid receptor type 1 signaling interferes with stress-coping behavior in mice. *Pharmacogenomics J.* 8, 196–208. doi:10.1038/sj.tpj.6500466.

Stella, N. (2010). Cannabinoid and cannabinoid-like receptors in microglia, astrocytes, and astrocytomas. *Glia* 58, 1017–1030. doi:10.1002/glia.20983.

Stempel, A. V., Stumpf, A., Zhang, H.-Y., Ozdogan, T., Pannasch, U., Theis, A.-K., et al. (2016). Cannabinoid Type 2 Receptors Mediate a Cell Type-Specific Plasticity in the Hippocampus. *Neuron* 90, 795–809. doi:10.1016/j.neuron.2016.03.034.

Stevens, B., Allen, N. J., Vazquez, L. E., Howell, G. R., Christopherson, K. S., Nouri, N., et al. (2007). The Classical Complement Cascade Mediates CNS Synapse Elimination. *Cell* 131, 1164–1178. doi:10.1016/j.cell.2007.10.036.

Sturm, M., Becker, A., Schroeder, A., Bilkei-Gorzo, A., and Zimmer, A. (2015). Effect of chronic corticosterone application on depression-like behavior in C57BL/6N and C57BL/6J mice. *Genes, Brain Behav.* 14, 292–300. doi:10.1111/gbb.12208.

Sugiura, T., Kishimoto, S., Oka, S., and Gokoh, M. (2006). Biochemistry, pharmacology and physiology of 2-arachidonoylglycerol, an endogenous cannabinoid receptor ligand. *Prog. Lipid Res.* 45, 405–446. doi:10.1016/j.plipres.2006.03.003.

Sugiura, T., Kondo, S., Sukagawa, A., Nakane, S., Shinoda, A., Itoh, K., et al. (1995). 2-Arachidonoylgylcerol: A Possible Endogenous Cannabinoid Receptor Ligand in Brain. *Biochem. Biophys. Res. Commun.* 215, 89–97. doi:10.1006/bbrc.1995.2437.

Sumislawski, J. J., Ramikie, T. S., and Patel, S. (2011). Reversible gating of endocannabinoid plasticity in the amygdala by chronic stress: a potential role for monoacylglycerol lipase inhibition in the prevention of stress-induced behavioral adaptation.

Neuropsychopharmacology 36, 2750–2761. doi:10.1038/npp.2011.166.

Suratt, B. T., Young, S. K., Lieber, J., Nick, J. A., Henson, P. M., and Worthen, G. S. (2001). Neutrophil maturation and activation determine anatomic site of clearance from circulation. *Am. J. Physiol. Cell. Mol. Physiol.* 281, L913–L921. doi:10.1152/ajplung.2001.281.4.L913.

Swirski, F. K., Nahrendorf, M., Etzrodt, M., Wildgruber, M., Panizzi, P., Figueiredo, J., et al. (2009). Identification Monocytes Inflammatory of Splenic Reservoir and Their Deployment Sites. *Science (80-.).* 325, 612–616. doi:10.1126/science.1175202.Identification.

Szabo, B., Nordheim, U., and Niederhoffer, N. (2001). Effects of cannabinoids on sympathetic and parasympathetic neuroeffector transmission in the rabbit heart. *J. Pharmacol. Exp. Ther.* 297, 819–826.

Tam, J., Trembovler, V., Di Marzo, V., Petrosino, S., Leo, G., Alexandrovich, A., et al. (2008). The cannabinoid CB1 receptor regulates bone formation by modulating adrenergic signaling. *FASEB J. Off. Publ. Fed. Am. Soc. Exp. Biol.* 22, 285–294. doi:10.1096/fj.06-7957com.

Tamai, S., Sanada, K., and Fukada, Y. (2008). Time-of-day-dependent enhancement of adult neurogenesis in the hippocampus. *PLoS One* 3, e3835. doi:10.1371/journal.pone.0003835.

Tamashiro, K. L., Sakai, R. R., Shively, C. A., Karatsoreos, I. N., and Reagan, L. P. (2011). Chronic stress, metabolism, and metabolic syndrome. *Stress* 14, 468–474. doi:10.3109/10253890.2011.606341.

Teixeira-Clerc, F., Julien, B., Grenard, P., Tran Van Nhieu, J., Deveaux, V., Li, L., et al. (2006). CB1 cannabinoid receptor antagonism: a new strategy for the treatment of liver fibrosis. *Nat. Med.* 12, 671–676. doi:10.1038/nm1421.

Tian, L., Li, W., Yang, L., Chang, N., Fan, X., Ji, X., et al. (2017). Cannabinoid receptor 1 participates in liver inflammation by promoting M1 macrophage polarization via RhoA/NF-κB p65 and ERK1/2 pathways, respectively, in mouse liver fibrogenesis. *Front. Immunol.* 8, 1–18. doi:10.3389/fimmu.2017.01214.

Trazzi, S., Steger, M., Mitrugno, V. M., Bartesaghi, R., and Ciani, E. (2010). CB1 cannabinoid receptors increase neuronal precursor proliferation through AKT/glycogen synthase kinase-3beta/beta-catenin signaling. *J. Biol. Chem.* 285, 10098–109. doi:10.1074/jbc.M109.043711.

Tremblay, M.-E. (2011). The role of microglia at synapses in the healthy CNS: novel insights from recent imaging studies. *Neuron Glia Biol.* 7, 67–76. doi:10.1017/S1740925X12000038.

Turu, G., and Hunyady, L. (2010). Signal transduction of the CB1 cannabinoid receptor. *J. Mol. Endocrinol.* 44, 75–85. doi:10.1677/JME-08-0190.

Ulrich-Lai, Y. M., Arnhold, M. M., and Engeland, W. C. (2006). Adrenal splanchnic innervation contributes to the diurnal rhythm of plasma corticosterone in rats by modulating adrenal sensitivity to ACTH. *Am. J. Physiol. Integr. Comp. Physiol.* 290, R1128–R1135. doi:10.1152/ajpregu.00042.2003.

Valenti, M., Vigan□, D., Casico, M. G., Rubino, T., Steardo, L., Parolaro, D., et al. (2004). Differential diurnal variations of anandamide and 2-arachidonoyl-glycerol levels in rat brain. *Cell. Mol. Life Sci.* 61, 945–950. doi:10.1007/s00018-003-3453-5.

Valverde, O., and Torrens, M. (2012). CB1 receptor-deficient mice as a model for depression. *Neuroscience* 204, 193–206. doi:10.1016/j.neuroscience.2011.09.031.

Varga, K., Lake, K. D., Huangfu, D., Guyenet, P. G., and Kunos, G. (1996). Mechanism of the hypotensive action of anandamide in anesthetized rats. *Hypertens. (Dallas, Tex. 1979)* 28, 682–6. doi:10.1161/01.hyp.28.4.682.

Vaughn, L. K., Denning, G., Stuhr, K. L., de Wit, H., Hill, M. N., and Hillard, C. J. (2010). Endocannabinoid signalling: has it got rhythm? *Br. J. Pharmacol.* 160, 530–543. doi:10.1111/j.1476-5381.2010.00790.x.

Vedhara, K., McDermott, M. P., Evans, T. G., Treanor, J. J., Plummer, S., Tallon, D., et al. (2002). Chronic stress in nonelderly caregivers: psychological, endocrine and immune implications. *J. Psychosom. Res.* 53, 1153–1161.

Wahlsten, D., Bachmanov, A., Finn, D. A., and Crabbe, J. C. (2006). Stability of inbred mouse strain differences in behavior and brain size between laboratories and across decades. *Proc. Natl. Acad. Sci.* 103, 16364–16369. doi:10.1073/pnas.0605342103.

Wake, H., Moorhouse, A. J., Miyamoto, A., and Nabekura, J. (2013). Microglia: actively surveying and shaping neuronal circuit structure and function. *Trends Neurosci.* 36, 209–217. doi:10.1016/j.tins.2012.11.007.

Walter, L., Franklin, A., Witting, A., Wade, C., Xie, Y., Kunos, G., et al. (2003). Nonpsychotropic cannabinoid receptors regulate microglial cell migration. *J. Neurosci.* 23, 1398–405. Available at: http://www.ncbi.nlm.nih.gov/pubmed/12598628 [Accessed August 8, 2019].

Wang, M., Hill, M. N., Zhang, L., Gorzalka, B. B., Hillard, C. J., and Alger, B. E. (2012). Acute restraint stress enhances hippocampal endocannabinoid function via glucocorticoid receptor activation. *J. Psychopharmacol.* 26, 56–70. doi:10.1177/0269881111409606.

Weber, M. D., Godbout, J. P., and Sheridan, J. F. (2017). Repeated Social Defeat, Neuroinflammation, and Behavior: Monocytes Carry the Signal. *Neuropsychopharmacology* 42, 46–61. doi:10.1038/npp.2016.102.

Wilson, R. I., Kunos, G., and Nicoll, R. A. (2001). Presynaptic specificity of endocannabinoid signaling in the hippocampus. *Neuron* 31, 453–62. Available at: http://www.ncbi.nlm.nih.gov/pubmed/11516401 [Accessed August 8, 2019].

Wohleb, E. S., Fenn, A. M., Pacenta, A. M., Powell, N. D., Sheridan, J. F., and Godbout, J. P. (2012). Peripheral innate immune challenge exaggerated microglia activation, increased the number of inflammatory CNS macrophages, and prolonged social withdrawal in socially defeated mice. *Psychoneuroendocrinology* 37, 1491–505. doi:10.1016/j.psyneuen.2012.02.003.

Wohleb, E. S., Hanke, M. L., Corona, A. W., Powell, N. D., Stiner, L. M., Bailey, M. T., et al. (2011). beta-Adrenergic receptor antagonism prevents anxiety-like behavior and microglial reactivity

induced by repeated social defeat. *J. Neurosci.* 31, 6277–6288. doi:10.1523/JNEUROSCI.0450-11.2011.

Wohleb, E. S., McKim, D. B., Shea, D. T., Powell, N. D., Tarr, A. J., Sheridan, J. F., et al. (2014a). Re-establishment of Anxiety in Stress-Sensitized Mice Is Caused by Monocyte Trafficking from the Spleen to the Brain. *Biol. Psychiatry* 75, 970–981. doi:10.1016/j.biopsych.2013.11.029.

Wohleb, E. S., McKim, D. B., Sheridan, J. F., and Godbout, J. P. (2015). Monocyte trafficking to the brain with stress and inflammation: a novel axis of immune-to-brain communication that influences mood and behavior. *Front. Neurosci.* 8, 447. doi:10.3389/fnins.2014.00447.

Wohleb, E. S., Patterson, J. M., Sharma, V., Quan, N., Godbout, J. P., and Sheridan, J. F. (2014b). Knockdown of Interleukin-1 Receptor Type-1 on Endothelial Cells Attenuated Stress-Induced Neuroinflammation and Prevented Anxiety-Like Behavior. *J. Neurosci.* 34, 2583–2591. doi:10.1523/JNEUROSCI.3723-13.2014.

Wohleb, E. S., Powell, N. D., Godbout, J. P., and Sheridan, J. F. (2013). Stress-Induced Recruitment of Bone Marrow-Derived Monocytes to the Brain Promotes Anxiety-Like Behavior. *J. Neurosci.* 33, 13820–13833. doi:10.1523/JNEUROSCI.1671-13.2013.

World Health Organization (WHO) (2018). Fact sheet - Depression - 22 March 2018. Available at: https://www.who.int/news-room/fact-sheets/detail/depression [Accessed August 13, 2019].

Wright, R. J. (2005). Stress and atopic disorders. *J. Allergy Clin. Immunol.* 116, 1301–1306. doi:10.1016/j.jaci.2005.09.050.

Wu, C.-S., Zhu, J., Wager-Miller, J., Wang, S., O'Leary, D., Monory, K., et al. (2010). Requirement of cannabinoid CB1 receptors in cortical pyramidal neurons for appropriate development of corticothalamic and thalamocortical projections. *Eur. J. Neurosci.* 32, 693–706. doi:10.1111/j.1460-9568.2010.07337.x.

Wu, M. D., Montgomery, S. L., Rivera-Escalera, F., Olschowka, J. A., and O'Banion, M. K. (2013). Sustained IL-1β expression impairs adult hippocampal neurogenesis independent of IL-1 signaling in nestin+ neural precursor cells. *Brain. Behav. Immun.* 32, 9–18. doi:10.1016/j.bbi.2013.03.003.

Yamazaki, K., and Allen, T. D. (1990). Ultrastructural morphometric study of efferent nerve terminals on murine bone marrow stromal cells, and the recognition of a novel anatomical unit: the "neuro-reticular complex". *Am. J. Anat.* 187, 261–276. doi:10.1002/aja.1001870306.

Yang, J., Zhang, L., Yu, C., Yang, X. F., and Wang, H. (2014). Monocyte and macrophage differentiation: Circulation inflammatory monocyte as biomarker for inflammatory diseases. *Biomark. Res.* 2, 1–9. doi:10.1186/2050-7771-2-1.

Yaribeygi, H., Panahi, Y., Sahraei, H., Johnston, T. P., and Sahebkar, A. (2017). The impact of stress on body function: A review. *EXCLI J.* 16, 1057–1072. doi:10.17179/excli2017-480.

Zelasko, S., Arnold, W. R., and Das, A. (2015). Endocannabinoid metabolism by cytochrome P450 monooxygenases. *Prostaglandins Other Lipid Mediat.* 116–117, 112–123. doi:10.1016/j.prostaglandins.2014.11.002.

Zhou, D., Kusnecov, A. W., Shurin, M. R., DePaoli, M., and Rabin, B. S. (1993). Exposure to physical and psychological stressors elevates plasma interleukin 6: relationship to the activation of hypothalamic-pituitary-adrenal axis. *Endocrinology* 133, 2523–2530. Available at: http://dx.doi.org/10.1210/endo.133.6.8243274.

Ziegler, M. G. (2004). "50 - Psychological Stress and the Autonomic Nervous System," in, eds. D. Robertson, I. Biaggioni, G. Burnstock, and P. A. B. T.-P. on the A. N. S. (Second E. Low (San Diego: Academic Press), 189–190. doi:https://doi.org/10.1016/B978-012589762-4/50051-7.

Zimmer, A., Zimmer, A. M., Hohmann, A. G., Herkenham, M., and Bonner, T. I. (1999). Increased mortality , hypoactivity , and hypoalgesia in cannabinoid CB1 receptor knockout mice. *Proc. Natl. Acad. Sci.* 96, 5780–5785.

Zoppi, S., Pérez Nievas, B. G., Madrigal, J. L. M., Manzanares, J., Leza, J. C., and García-Bueno, B. (2011). Regulatory role of cannabinoid receptor 1 in stress-induced excitotoxicity and neuroinflammation. *Neuropsychopharmacology* 36, 805–818. doi:10.1038/npp.2010.214.

Appendix

A1. Behavioural analysis after standard CSDS (first cohort)

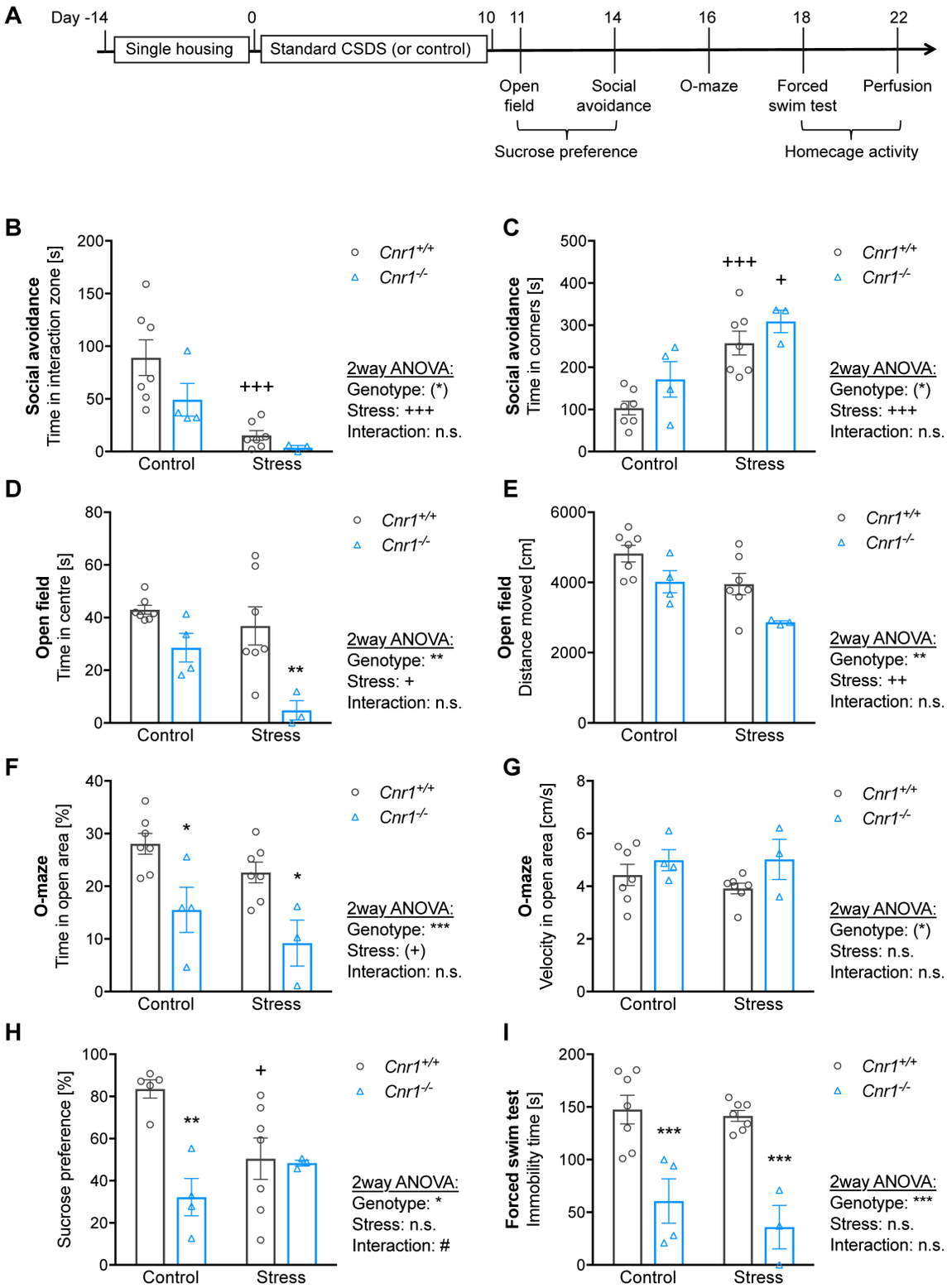

Supplementary Figure 1. Detailed behavioural analysis of *Cnr1*$^{+/+}$ and *Cnr1*$^{-/-}$ mice after standard CSDS (first cohort).
See next page for continuation of figure and figure legend.

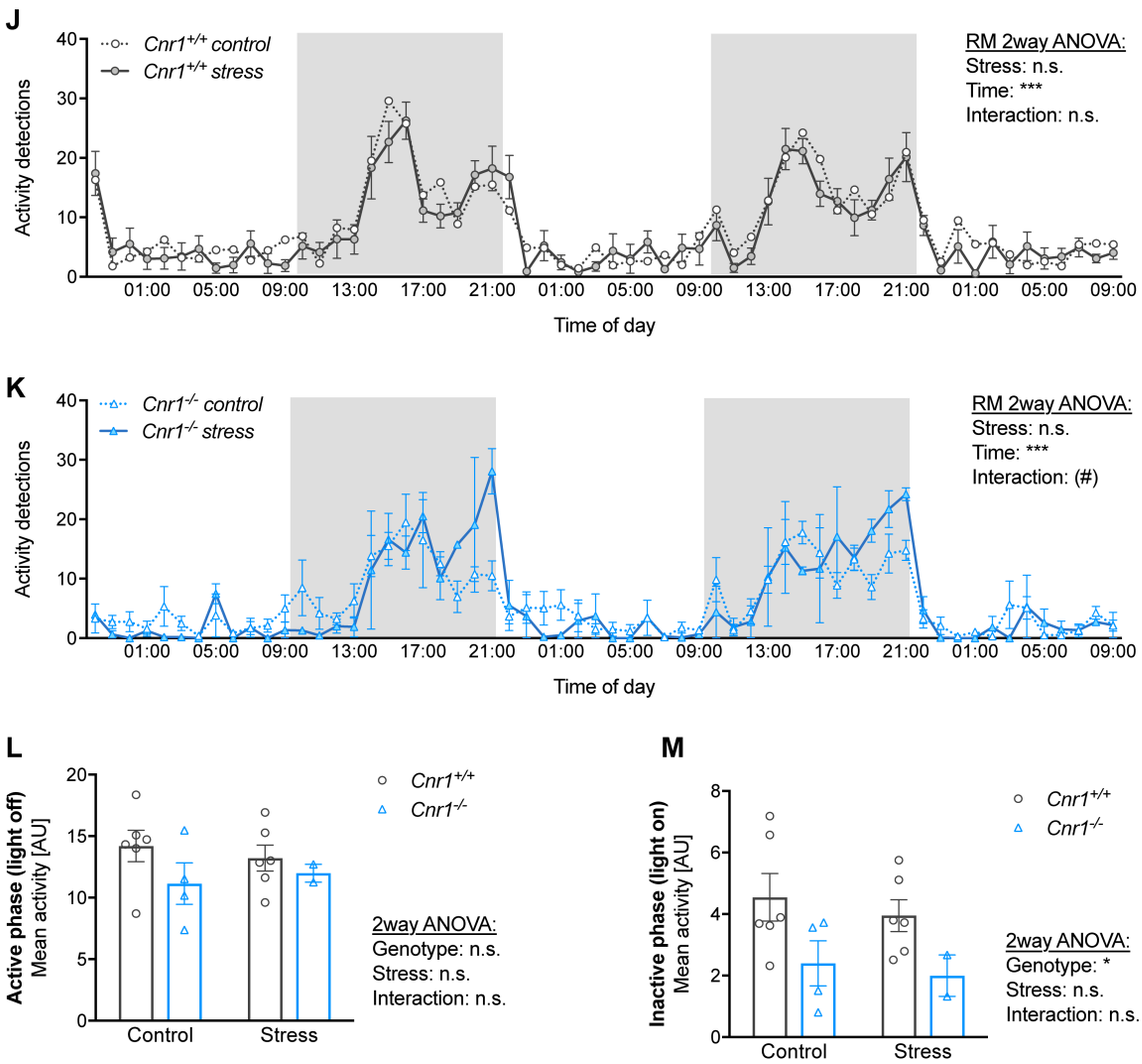

Supplementary Figure 1. Detailed behavioural analysis of *Cnr1*$^{+/+}$ and *Cnr1*$^{-/-}$ mice after standard CSDS (first cohort). **(A)** Experimental timeline of standard CSDS and subsequent behavioural tests. **(B - C)** Standard CSDS induced strong social avoidance, indicated by reduced interaction with a novel CD1 mouse **(D)** and increased time spent in corner areas **(C)** in both genotypes. In *Cnr1*$^{-/-}$ mice, stress effects on interaction time did not reach significance in *post-hoc* comparisons, due to low baseline interaction in control mice and small group sizes. **(D - E)** CB1 deficiency (and stress) increases anxiety in the open field test. **(D)** Time spent in the centre of the open field was reduced in *Cnr1*$^{-/-}$ mice, especially in stressed mice. **(E)** Both stress and CB1-deficiency reduced locomotion in the open field. **(F - G)** CB1 deficiency increases anxiety in the elevated zero-maze (O-maze). **(F)** Time spent in the open (brightly illuminated) area of the O-maze was reduced in *Cnr1*$^{-/-}$ mice. **(G)** Velocity in the open area was slightly increased in *Cnr1*$^{-/-}$ mice. **(H)** Stress reduced sucrose preference (thus induced anhedonia) in *Cnr1*$^{+/+}$ mice. In contrast, *Cnr1*$^{-/-}$ mice showed reduced sucrose preference in control conditions, which was not further affected by stress. **(I)** *Cnr1*$^{-/-}$ mice showed reduced immobility time in the Porsolt forced swim test, usually a sign for lower depressive-like behaviour. However, in this test *Cnr1*$^{-/-}$ mice appeared very nervous and hyperactive. Stress had no effect on immobility time. **(J - K)** Home cage activity was not significantly affected by stress in neither *Cnr1*$^{+/+}$ **(J)**, nor in *Cnr1*$^{-/-}$ mice **(K)**. **(L)** Mean activity during the active phase was not affected by stress or CB1 deficiency. **(M)** Mean activity in the inactive phase was slightly lower in *Cnr1*$^{-/-}$ mice, independent from stress. Home cage activity data was analysed separately for *Cnr1*$^{+/+}$ and *Cnr1*$^{-/-}$ mice by repeated measure (RM) 2way ANOVA, followed by Bonferroni *post-hoc* comparisons. Data was analysed by 2way ANOVA, followed by Bonferroni *post-hoc* comparisons. For genotype effects (compared to *Cnr1*$^{+/+}$ of the same group) * $p < 0.05$, ** $p < 0.01$, *** $p < 0.001$. For stress effects (compared to control of the same genotype) + $p < 0.05$, ++ $p < 0.01$, +++ $p < 0.001$.

A2. Behavioural analysis after standard CSDS (second cohort)

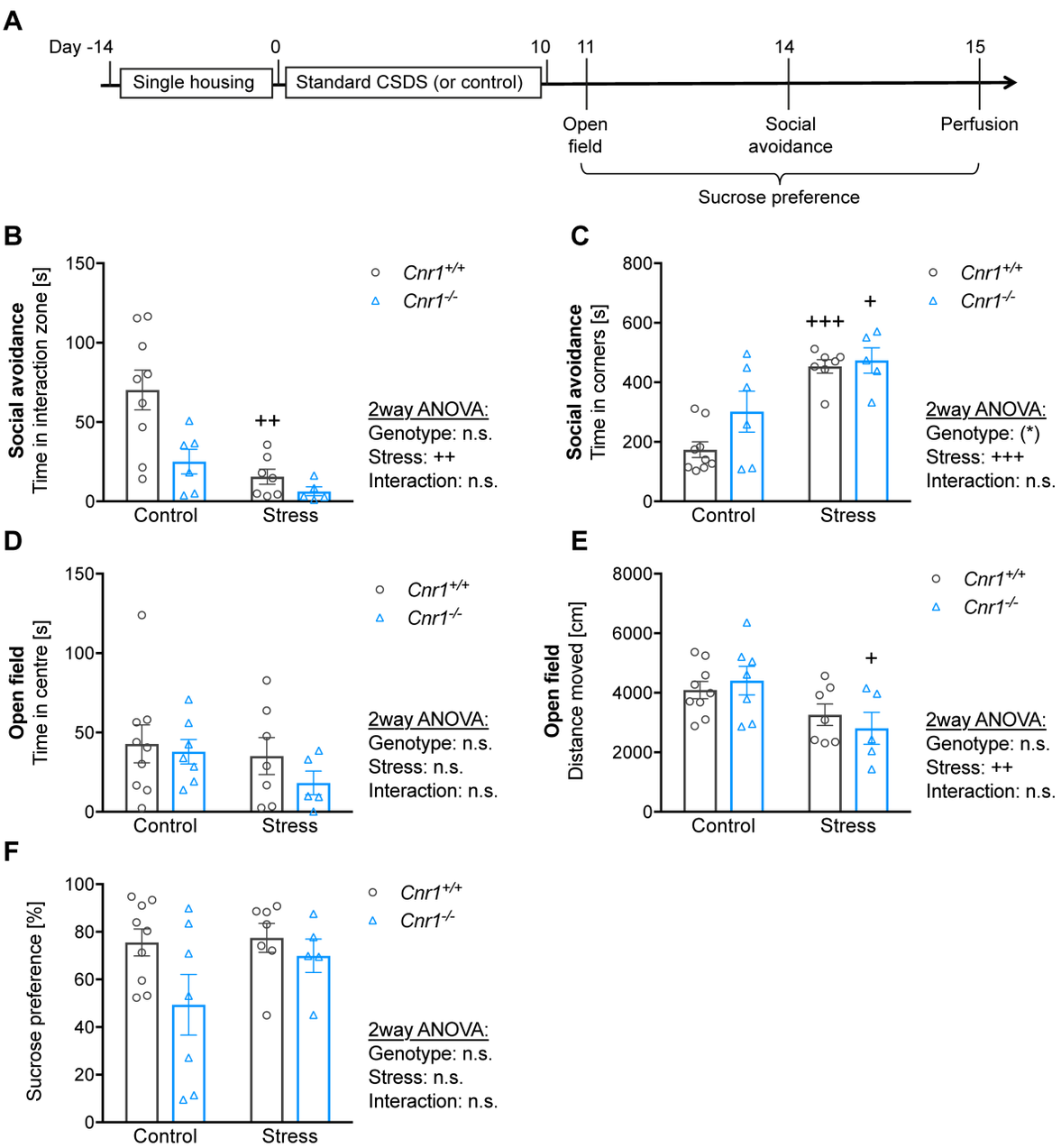

Supplementary Figure 2. Behavioural analysis of *Cnr1*$^{+/+}$ and *Cnr1*$^{-/-}$ mice after standard CSDS (second cohort). **(A)** Experimental timeline of standard CSDS and subsequent behavioural tests. **(B - C)** Standard CSDS induced strong social avoidance, indicated by reduced interaction with a novel CD1 mouse **(D)** and increased time spent in corner areas **(C).** In *Cnr1*$^{-/-}$ mice, stress effects on interaction time did not reach significance in *post-hoc* comparisons, due to low baseline interaction in control mice and small group sizes. **(D - E)** CB1 deficiency and stress did not affect anxiety in the open field test in this cohort. **(D)** Time spent in the centre of the open field was not significantly different between the groups. **(E)** Stress reduced locomotion in the open field in *Cnr1*$^{-/-}$ mice. **(F)** Sucrose preference was not affected by stress or genotype in this cohort. Data was analysed by 2way ANOVA, followed by Bonferroni *post-hoc* comparisons. For genotype effects (compared to *Cnr1*$^{+/+}$ of the same group) * $p < 0.05$, ** $p < 0.01$, *** $p < 0.001$. For stress effects (compared to control of the same genotype) + $p < 0.05$, ++ $p < 0.01$, +++ $p < 0.001$.

A3. Immunosuppressive function of CORT in LPS-treated splenocytes

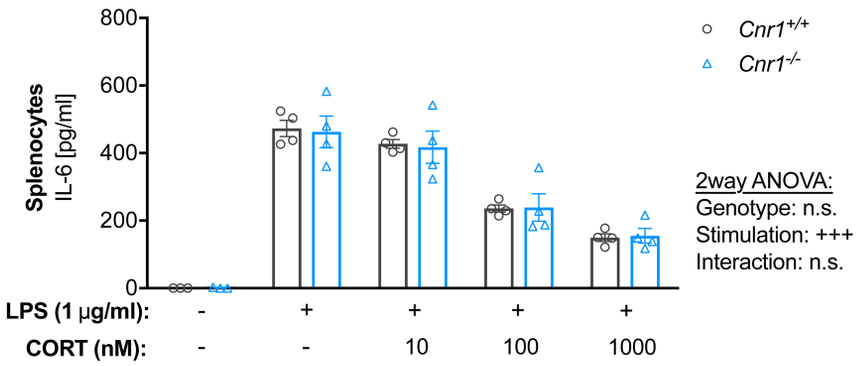

Supplementary Figure 3. ***In vitro*** **analysis of immunosuppressive function of CORT in LPS-stimulated splenocytes.** Splenocytes were isolated from naive, non-stressed male *Cnr1*$^{+/+}$ and *Cnr1*$^{-/-}$ mice and cultured overnight. Cells were stimulated with LPS from *E. coli 0127:B8,* with or without co-treatment with different concentrations of CORT. After stimulation, IL-6 secretion was analysed in the supernatant using ELISA. LPS treatment alone induced secretion of IL-6, which was dose-dependently reduced by increasing concentrations of CORT. Neither the pro-inflammatory response to LPS, nor the immunosuppressive action of CORT was affected by the genotype. Data was analysed by 2way ANOVA, followed by Bonferroni *post-hoc* comparisons.

A4. Expression of ECS-related genes after mild CSDS

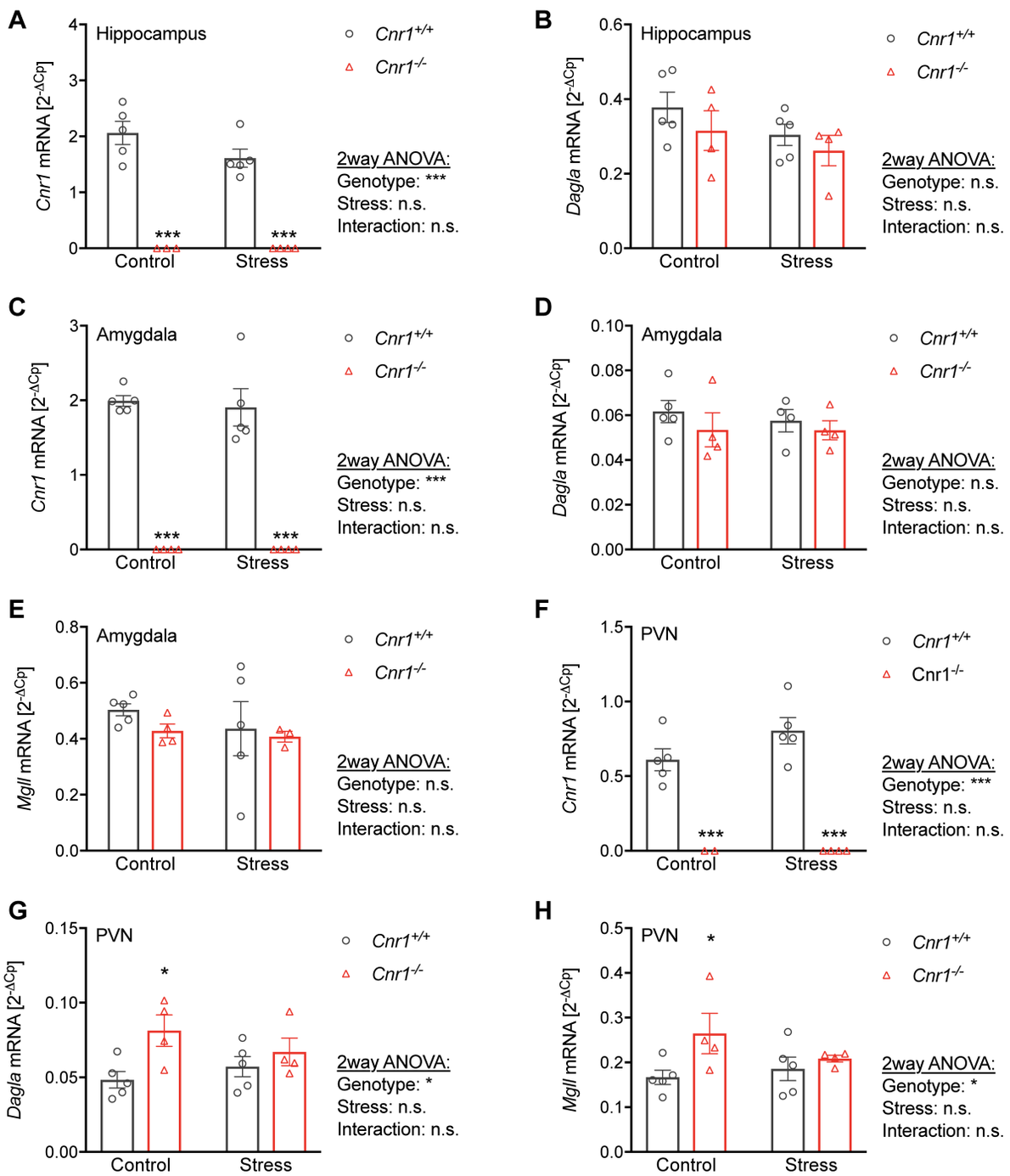

Supplementary Figure 4. Gene expression analysis of ECS-related genes after mild CSDS. Brain regions were isolated approximately 24 h after the last stress exposure in one cohort of mice. RNA was isolated, reverse transcribed into cDNA and gene expression analysed by qPCR. Expression of target genes was normalised to the expression of reference gene *Hprt* and is presented as $2^{-\Delta Cp}$. **(A - B)** Hippocampus: mild CSDS had no effect on *Cnr1* or *Dagla* gene expression. **(C - E)** Amygdala: stress had no effect on *Cnr1*, DAGLα (*Dagla*), or MAGL (*Mgll*) gene expression. **(F - H)** PVN: stress had no effect on *Cnr1*, DAGLα (*Dagla*), or MAGL (*Mgll*) gene expression. Control *Cnr1*$^{-/-}$ mice showed slightly higher *Dagla* and *Mgll* expression. **(A, C, F)** Analysis of *Cnr1* expression confirms the absence of *Cnr1* mRNA in *Cnr1*$^{-/-}$ mice. Data was analysed by 2way ANOVA, followed by Bonferroni *post-hoc* comparisons. For genotype effects (compared to *Cnr1*$^{+/+}$ of the same group) * $p < 0.05$, ** $p < 0.01$, *** $p < 0.001$. For stress effects (compared to control of the same genotype) + $p < 0.05$, ++ $p < 0.01$, +++ $p < 0.001$.

A5. Expression of inflammatory genes after mild CSDS

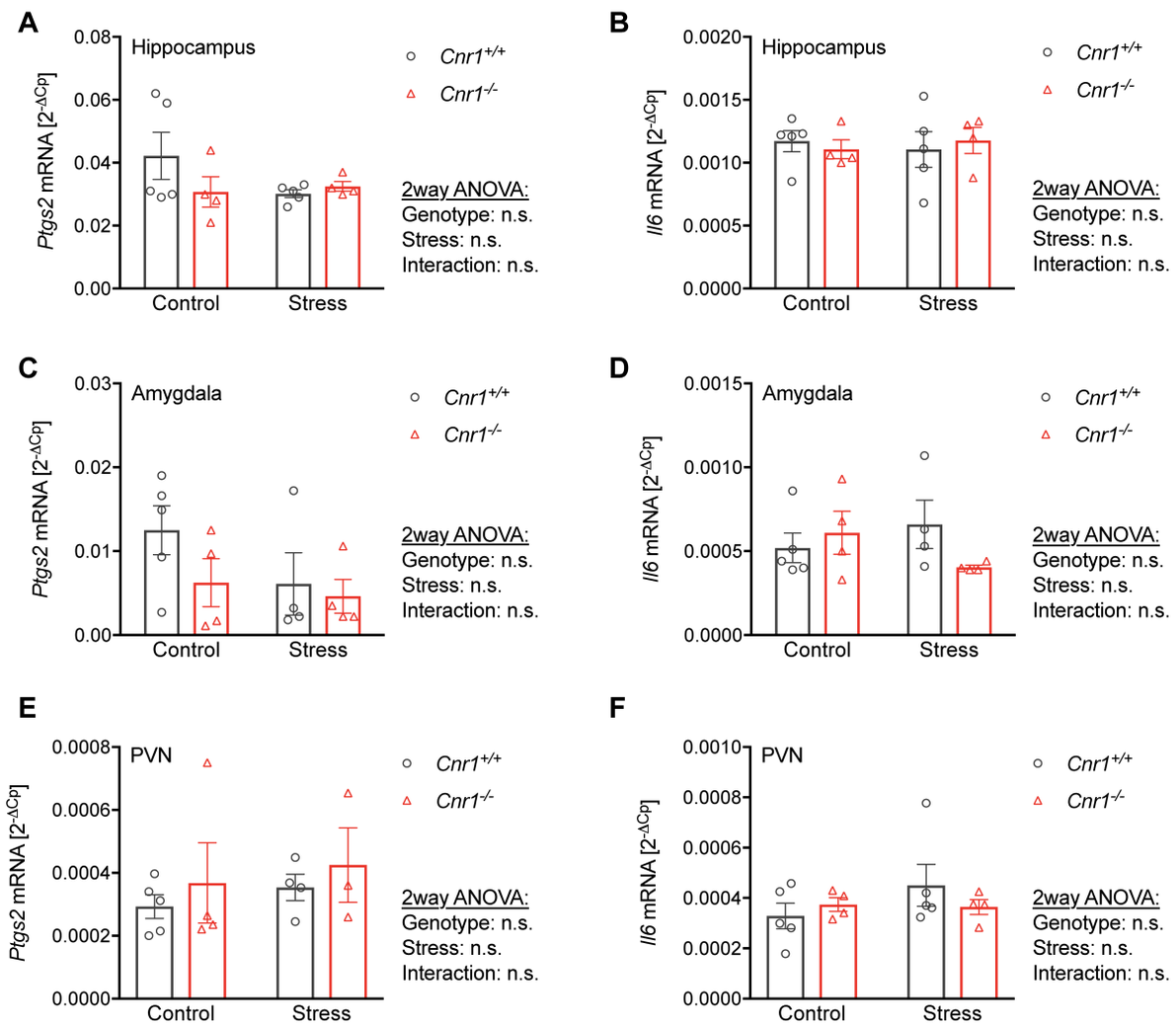

Supplementary Figure 5. Gene expression analysis of immune-related genes after mild CSDS. Brain regions were isolated approximately 24 h after the last stress exposure in one cohort of mice. RNA was isolated, reverse transcribed into cDNA and gene expression analysed by qPCR. Expression of target genes was normalised to the expression of reference gene *Hprt* and is presented as $2^{-\Delta Cp}$. **(A - B)** Hippocampus: mild CSDS had no effect on COX-2 (*Ptgs2*) or IL-6 (*Il6*) gene expression. **(C - D)** Amygdala: mild CSDS had no effect on COX-2 (*Ptgs2*) or IL-6 (*Il6*) gene expression. **(E - F)** PVN: mild CSDS had no effect on COX-2 (*Ptgs2*) or IL-6 (*Il6*) gene expression. In all regions, expression of IL-1β (*Il1b*) and TNFα (*Tnf*) were below the detection limit of the qPCR (all Cp values > 35). Data was analysed by 2way ANOVA, followed by Bonferroni *post-hoc* comparisons. For genotype effects (compared to *Cnr1*$^{+/+}$ of the same group) * $p < 0.05$, ** $p < 0.01$, *** $p < 0.001$. For stress effects (compared to control of the same genotype) + $p < 0.05$, ++ $p < 0.01$, +++ $p < 0.001$.

A6. Microglia morphology after mild CSDS

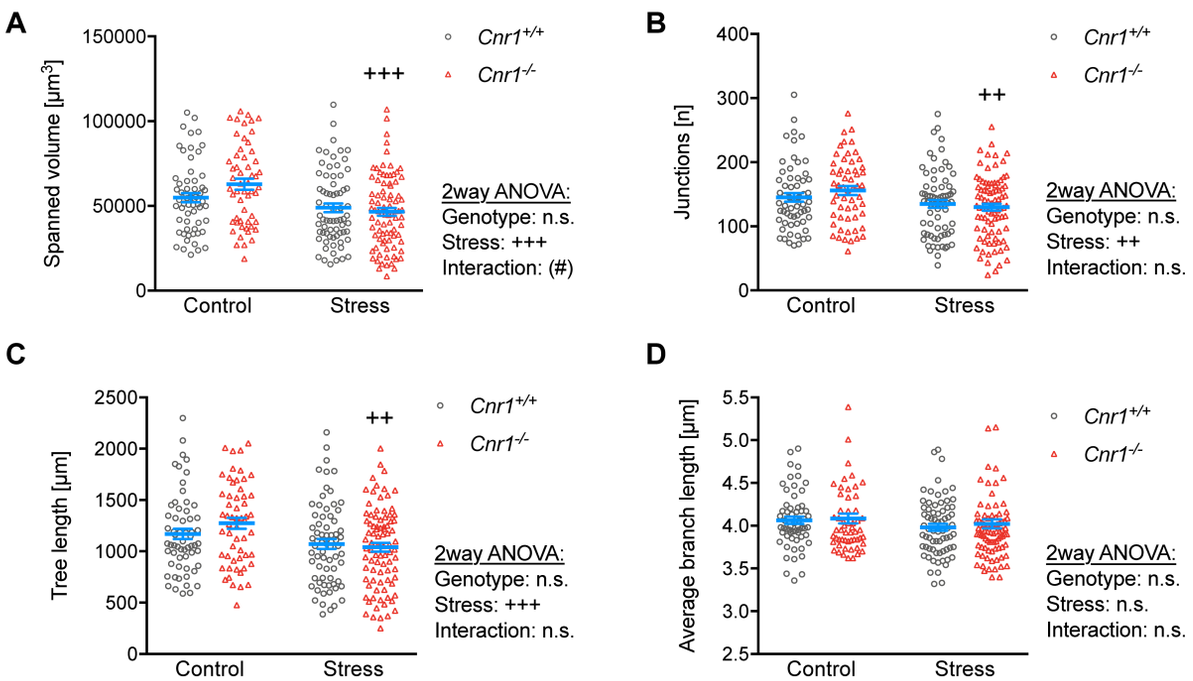

Supplementary Figure 6. Extended data on microglia morphology in the dentate gyrus after mild CSDS. Microglia morphology was analysed in the inferior molecular layer of the dentate gyrus (DG) of the hippocampus after mild CSDS. Coronal brain sections of 60 µm were stained for IBA1 and images acquired using confocal microscopy. Z-stack images were analysed using an automated ImageJ-based analysis tool that traces cells through the z-stack to generate 3D reconstructions and cell skeletons. A total of 56 – 87 cells were analysed per group. **(A)** Stress reduced the spanned volume (determined from the convex hull of the reconstructed cell) of *Cnr1*$^{-/-}$ microglia. **(B)** Stress reduced the number of junctions (determined from the skeleton of the reconstructed cell) of *Cnr1*$^{-/-}$ microglia. **(C)** Stress reduced the tree length, i.e. the total length of all branches (determined from the skeleton) of *Cnr1*$^{-/-}$ microglia. **(D)** The average branch length was not affected by stress or genotype. Data was analysed by 2way ANOVA, followed by Bonferroni *post-hoc* comparisons. For genotype effects (compared to *Cnr1*$^{+/+}$ of the same group) * $p < 0.05$, ** $p < 0.01$, *** $p < 0.001$. For stress effects (compared to control of the same genotype) + $p < 0.05$, ++ $p < 0.01$, +++ $p < 0.001$.

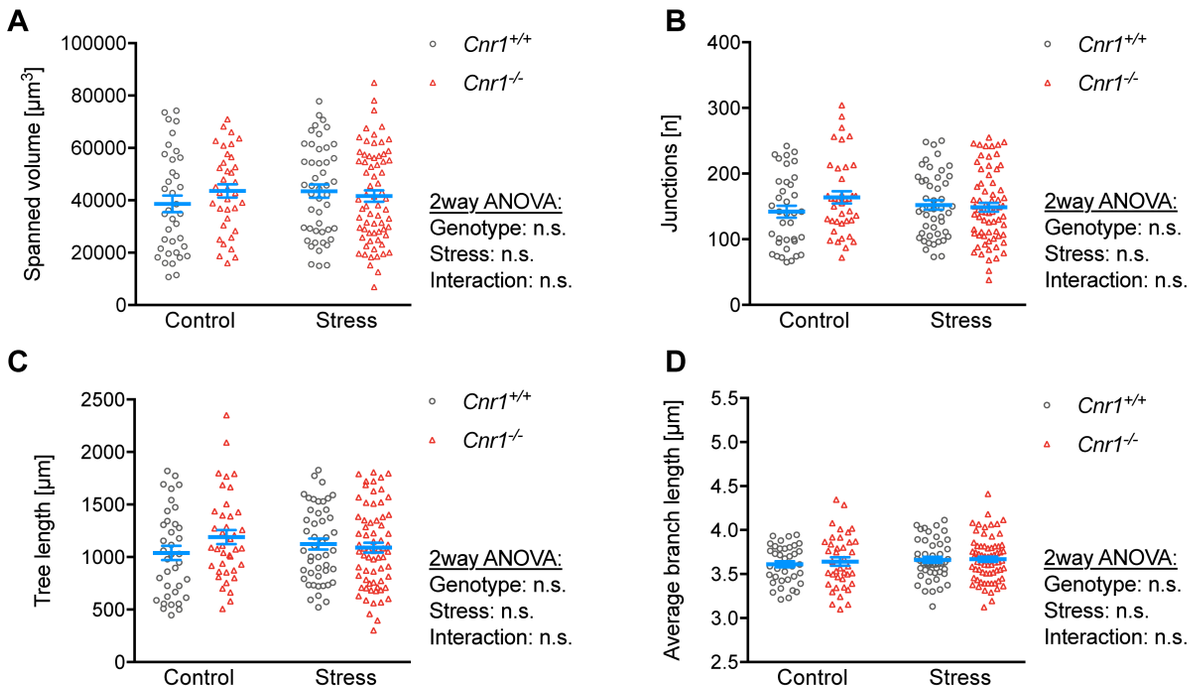

Supplementary Figure 7. Extended data on microglia morphology in the CA1 region after mild CSDS. Microglia morphology was analysed in the stratum radiatum of the CA1 region of the hippocampus after mild CSDS. A total of 37 - 68 cells were analysed per group. **(A - D)** Stress or genotype did not significantly affect microglia morphology in this region. Data was analysed by 2way ANOVA, followed by Bonferroni *post-hoc* comparisons.

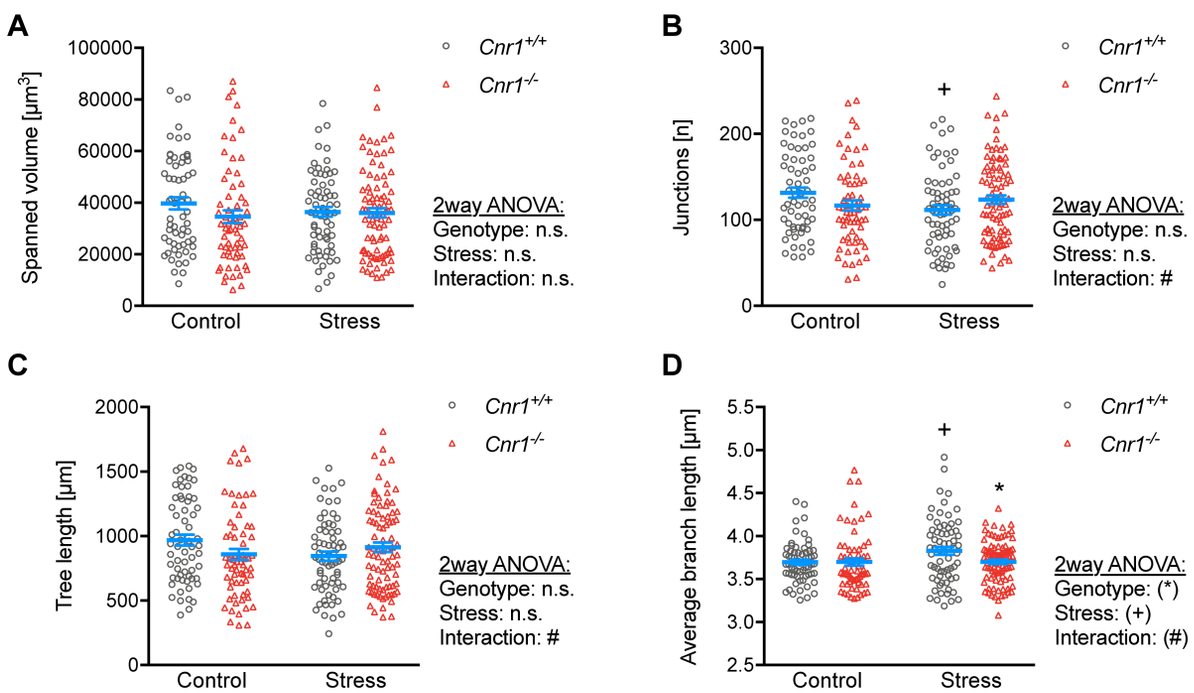

Supplementary Figure 8. Extended data on microglia morphology in the prefrontal cortex after mild CSDS. Microglia morphology was analysed in the medial prefrontal cortex (mPFC) after mild CSDS. A total of 63 – 87 cells were analysed per group. **(A)** Stress or genotype did not affect the spanned volume of microglia. **(B)** Stress reduced the number of junctions of *Cnr1*$^{+/+}$ microglia. **(C)** Stress or genotype did not affect the total tree length of microglia. **(D)** Stress increased the number of junctions of *Cnr1*$^{+/+}$, but not *Cnr1*$^{-/-}$ microglia. Data was analysed by 2way ANOVA, followed by Bonferroni *post-hoc* comparisons. For genotype effects (compared to *Cnr1*$^{+/+}$ of the same group) * $p < 0.05$, ** $p < 0.01$, *** $p < 0.001$. For stress effects (compared to control of the same genotype) + $p < 0.05$, ++ $p < 0.01$, +++ $p < 0.001$

A7. Publications

Parts of this work have been submitted for publication:

Beins E.C., Beiert T., Jenniches I., Hansen J.N., Leidmaa E., Schrickel J.W. & Zimmer A. (2020) Cannabinoid receptor 1 signalling modulates microglial responses in a mouse model of chronic social defeat stress.

Other publications:

Ativie, F., Komorowska, J. A., **Beins, E.**, Albayram, Ö., Zimmer, T., Zimmer, A., et al. (2018). Cannabinoid 1 Receptor Signaling on Hippocampal GABAergic Neurons Influences Microglial Activity. *Front. Mol. Neurosci.* 11, 295. doi:10.3389/fnmol.2018.00295.

Beins, E., Ulas, T., Ternes, S., Neumann, H., Schultze, J. L., and Zimmer, A. (2016). Characterization of inflammatory markers and transcriptome profiles of differentially activated embryonic stem cell-derived microglia. *Glia,* n/a-n/a. doi:10.1002/glia.22979.

Beins, E., and Zimmer, A. (2016). Zinc homoeostasis: Basic research indicates therapeutic risks and opportunities. *Eur. Neuropsychopharmacol.* 26, 1083–4. doi:10.1016/j.euroneuro.2016.02.014.

Schmöle, A.-C., Lundt, R., Gennequin, B., Schrage, H., **Beins, E.**, Krämer, A., et al. (2015). Expression Analysis of CB2-GFP BAC Transgenic Mice. *PLoS One* 10, e0138986. doi:10.1371/journal.pone.0138986.

Schmöle, A.-C., Lundt, R., Toporowski, G., Hansen, J. N., **Beins, E.**, Halle, A., et al. (2018). Cannabinoid Receptor 2-Deficiency Ameliorates Disease Symptoms in a Mouse Model with Alzheimer's Disease-Like Pathology. *J. Alzheimers. Dis.* 64, 379–392. doi:10.3233/JAD-180230.

Acknowledgements

An erster Stelle möchte ich mich bei Prof. Dr. Andreas Zimmer bedanken, für die Möglichkeit in seinem Institut zu arbeiten und seine konstante Unterstützung während der letzten Jahre. Besonders bedanken möchte ich mich auch für sein Vertrauen und die Freiheit, die er mir bei der Entwicklung dieses Projektes gewährt hat. Ich hätte mir keinen besseren Mentor wünschen können.

Ebenfalls bedanke ich mich bei Prof. Joachim Schultze für die bereitwillige Übernahme der Funktion als Zweitgutachter, sowie bei den anderen Mitgliedern der Promotionskommission Prof. Frank Bradke und Prof. Ulrike Thoma.

Ich danke meinem Biologielehrer Herr Diesing, der mich mit seinem Unterricht für die Biologie begeistert hat und ohne den ich diesen Weg vermutlich niemals eingeschlagen hätte.

Danke auch an alle Kooperationspartner für die gute Zusammenarbeit und die Bereitstellung ihrer Zeit und Expertise. Besonderen Dank an Dr. med. Thomas Beiert und Jan Niklas Hansen.

Ein ganz großes Dankeschön gilt allen Mitarbeiten des Instituts für Molekulare Psychiatrie. Danke für Eure tatkräftige Hilfe im Labor und die sehr positive und entspannte Arbeitsatmosphäre. Ihr alle habt die letzten Jahre zu einer unglaublich schönen Zeit gemacht und es wird mir sehr schwerfallen, das Labor zu verlassen. Besonders erwähnen möchte ich Hanna, Kerstin, Imke, Ramona, Britta, Este und Balint, die neben der Arbeit auch gute Freunde geworden sind. Ein extra großes Dankeschön an Hanna, die mir bei unzähligen Experimenten geholfen hat und die beste Büronachbarin war!

Zuallerletzt gilt ein besonderer Dank natürlich meinen Freunden und meiner Familie, die mich die letzten Jahre und mein gesamtes Leben lang unterstützt haben. Ohne Euch wäre das alles nicht möglich gewesen. DANKE!